Role of FoxO3a in Osteoblast Differentiation and Matrix Calcification

by

Kathy Cheng-Chia Tang

A thesis submitted in partial fulfillment of the requirements for the degree of

Doctor of Philosophy

in
Pharmaceutical Sciences

Faculty of Pharmacy and Pharmaceutical Sciences
University of Alberta

ABSTRACT

Forkhead Box O transcription factors play important roles in bone metabolism via defending against oxidative stress and apoptosis (Almeida, 2011; Ambrogini et al., 2010). FoxO3a is of special interest as it is the predominant isoform in bone cells (Ambrogini et al., 2010). In osteoblasts, the administration of 1,25 dihydroxyvitamin D_3 ($1,25D_3$) increases FoxO3a expression, and alters calcium handling. We therefore queried whether FoxO3a participates in vitamin D-mediated calcium regulation or osteoblast differentiation and matrix calcification, independent of reactive oxygen species (ROS) formation. This dissertation investigates the regulating role of Forkhead Box O3 transcription factors (FoxO3) in osteoblast differentiation and matrix mineralization. FoxO3a expression increased throughout differentiation. At day 3 and 7, FoxO3a mRNA and protein expression levels were significantly higher than pre-differentiation. $1,25D_3$ further enhanced both FoxO3a mRNA and protein expression levels in the 7-day differentiated osteoblast cells. Immunocytofluorescence localization of FoxO3a demonstrated the addition of $1,25D_3$ led to nuclear localization. 7-day differentiated osteoblast cells incubated with H_2O_2 showed no obvious difference from control, however, increased FoxO3a expression was attenuated when H_2O_2 was added with $1,25D_3$. In order to study the effect of $1,25D_3$ on calcium regulation in osteoblasts, expression of calcium homeostasis mediators were assessed. Increased expression of the calcium channel $Ca_v3.1$ and plasma membrane Ca^{2+} ATPase (PMCA-1b) was observed throughout osteoblast differentiation. Addition of $1,25D_3$ enhanced expression of Calbindin-D_{9K} and the sodium-calcium exchanger (NCX). $1,25D_3$ increased calcium uptake and calcium deposition in differentiated osteoblasts as demonstrated by ratiometric live cell calcium imaging and alizarin red staining, respectively. FoxO3a overexpression led to a reduction in calcium uptake and calcium deposition, resulting in

uncalcified matrix. When FoxO3a was over-expressed in MC3T3-E1 cells, pre-osteoblasts failed to differentiate into osteoblasts and unmineralized osteoid failed to calcify its matrix, as assessed by the biomarkers Runx2 and osteocalcin, respectively. Based on expression and functional data, the results suggest that high levels of FoxO3a inversely regulate osteoblast differentiation and matrix calcification, with a role in the repression of both processes.

PREFACE

This thesis is an original work by Kathy Cheng-Chia Tang. No part of this thesis has been previously published.

ACKNOWLEDGEMENTS

In full gratitude, I would like to thank my academic supervisors Dr. R. Todd Alexander and Dr. Michael R. Doschak for their intelligent guidance and support. It has been an incredible privilege to work under the direction of Dr. Alexander, I am sincerely thankful for his insights, motivation, enthusiasm and patience. I would also like to thank Dr. Doschak for the insightful input and commitment of time. This journey of learning has been one of the most important chapters of my life.

I would like to thank my committee members, Dr. Arno Siraki, and Dr. Tam for providing invaluable feedback and expertise during my studies.

I thank all the lab members of the Alexander laboratory both past and present for creating a positive environment that stimulates discussions and ideas. Thank you for sharing your technical expertise and knowledge. More importantly, fun personalities that made long hours of work more enjoyable.

Finally, I am deeply grateful for my family, mom, dad and my brother Robin, who have supported me unconditionally and provided me with endless encouragement and motivation.

This work was supported by grants from the Women and Children Health Research Institute (WCHRI), which is supported by the Stollery Children's Hospital Foundation and the Canadian Institutes of Health Research (CIHR, MOP 136891).

TABLE OF CONTENTS

List of Tables

List of

List of Abbreviations

1,25D3	1,25-dihydroxyviamin D, 1,25-dihydroxycholecalciferol
1-OHase	25-hydroxyvitamin D-1alpha-hydroxylase
24-OHase	25-hydroxyvitamin D-24-hydroxylase
25(OH)D3	25-hydroxyvitamin D3
25-OHase	Vitamin D-25-hydroxylase
ALP	Alkaline phosphatase
AA	Ascorbic acid
APS	Ammonium persulfate
ARS	Alizarin Red S
ATP	Adenosine triphosphate
B-GP	Beta-glycerophosphate
BMD	Bone mineral density
BP	Bisphosphonate
BMD	Bone mineral density
BMP	Bone morphogenetic proteins
BMU	Bone multicellular unit
BSA	Bovine serum albumin
BSP	Bone sialoprotein
Ca2+	Calcium
(Ca10(PO4)6OH)2	hydroxyapatite
CaSR	Calcium-sensing receptor
COL I	Type I collagen
CYP24	25(OH)D-24-hydroxylase
CYP27A1	Cytochrome P450 family 27 subfamily A member 1
CYP27B1	Cytochrome P450 family 27 subfamily B member 1
CD	Crohn's disease
CT	Calcitonin
DAPI	4', 6'-Diamidino-2-Phenylindole, Dihydrochloride
DBP	Vitamin D binding protein
DCF	2',7'-dichlorofluorescin
DCFDA	2',7'-dichlorofluorescin diacetate
DMSO	Dimethyl Sulfoxide
DR3	Direct repeat 3
ECL	enhanced chemiluminescence
ECM	Extracellular matrix
EDTA	Ethylenediaminetetraacetic acid
EGF	Epidermal transforming growth factors
ER	Endoplasmic reticulum
FBS	Fetal calf serum
FGF23	Fibroblast growth factor 23
GH	Growth hormone
GIOP	Glucocorticoid-induced osteoporosis

H_2O_2	Hydrogen peroxide
HRP	Horseradish phosphatase
$LaCl_3$	Lanthanum Chloride
IBD	Inflammatory bowel disease
IL-6	Interleukin-6
IU	International units
mAb	Monoclonal antibody
M-CSF	Macrophage colony-stimulating factor
MEM	Minimum essential medium eagle
MTT	Thiazolyl blue tetrazolium bromide
MV	Matrix vesicles
NCP	Noncollagenous proteins
NCX	Sodium-calcium exchanger
OB	Osteoblast
OCN	Osteocalcin
Osf2	Osteoblast-specific factor 2
OP	Osteoporosis
OPN	Osteopontin
OPG	Osteoprotegerin
OI	Osteogenesis Imperfecta
pOB	Pre-osteoblast
PBS	Phosphate buffer saline
PFA	paraformaldehyde
PG	Prostaglandins
PGE2	Prostaglandin E2
PMCA	Plasma membrane calcium ATPase pump
PMSF	Phenylmethane sulfonyl fluoride
PSG	Penicillin-streptomycin-glutamine
PTH	Parathyroid hormone
PTHrP	Parathyroid hormone-related protein
PVDF	Polyvinylidene fluoride
qRT-PCR	Real-time polymerase chain reaction
RT-PCR	Real time-chain reaction
RA	Rheumatoid Arthritis
RANKL	Receptor activator of NFkB ligand
RIPA	Radioimmunoprecipitation assay
RPM	Revolutions per minute
ROS	Reactive oxygen species
RT	Room temperature
RXR	Retimoid X receptor
SD	Standard deviation
SDS-PAGE	Sodium dodecyl sulfate polyacrylamide gel electrophoresis
TEMED	Tetramethylethylenediamine
TGF-β	Transforming growth factor-β

TNF	Tumor Necrosis factors
TNF-α	Tumor Necrosis factor-α
TRAP	Tartrate resistant acid phosphatase
Trpv5	Transient receptor potential 5
Trpv6	Transient receptor potential 6
UC	Ulcerative Colitis
UVB	Ultraviolet B
VDRE	Vitamin D response elements
VD	Vitamin D
VDR	Vitamin D Receptor
VDRE	Vitamin D response element
VSCCs	Voltage-activated channels

CHAPTER 1: INTRODUCTION

1.1 Bone structure and function

The skeleton serves a multifunctional complex system. Bones provide mechanical support, protect vital organs, allow body movement, facilitate muscle action, and locomotion. Bones also function as a reservoir of growth factors and cytokines, and bone marrow is important for circulatory and immune system (Clarke, 2008; Massaro and Rogers, 2004). Most importantly, bone maintains mineral homeostasis, especially elemental calcium, which is critical for bone formation and intracellular signaling pathways (Clarke, 2008; Flynn, 2003).

The adult human skeleton has a total of 213 bones excluding the sesamoid bones, and can be divided into four major types: long bones, short bones, flat bones and irregular bones (Clarke, 2008). Long bones include the clavicles, humeri, radii, ulnae, metacarpals, femurs, tibiae, fibulae, metatarsals, and phalanges. Short bones include carpal and tarsal bones, patellae, and sesamoid bones. Flat bones include the skull, mandible, scapulae, sternum, and ribs. Irregular bones include the vertebrae, sacrum, coccyx and hyoid bone. Long bones are formed by a combination of endochondral and membranous bone formation, where a mineralized cartilaginous precursor is first formed and later replaced by mineralized bone matrix (Clarke, 2008; Mahamid et al., 2011). Flat bones are formed by intramembranous bone formation, involving direct mineralization of type-I collagen matrix (Clarke, 2008; Mahamid et al., 2011). Long bones contain diaphysis, a hollow shaft, which is composed mainly of cortical bone. The epiphyses above the growth plate and metaphyses below it are both composed of trabecular with a thin shell of cortical bone (Clarke, 2008). Cortical and trabecular bones are the two major bone types that make up the skeleton, accounting for 80% and 20%, respectively (Eriksen et al., 1994). Cortical bone, or compact bone, is dense and hard. Cortical bone forms the outer layer of bone,

surrounding the marrow space. Trabecular or spongy bone is present inside the cortical bone, providing the skeleton with flexibility (Burr and Akkus, 2014; Clarke, 2008).

1.1.1 Bone Remodeling: Bone Resorption and Bone Formation

Bone is a dynamic tissue that is constantly undergoing remodeling throughout lifetime. Bone remodeling involves the continuous removal of old mineralized bone by osteoclasts, followed by replacement with newly synthesized extracellular matrix by osteoblasts and the subsequent mineralization of the matrix to form new bone (**Error: Reference source not found**) (Clarke, 2008). In humans, the initiation process of lengthening long bone starts from birth to when skeletal matures at approximately 18 years of age. Cortical thickness and bone diameter occurs from birth to adulthood (Duren et al., 2013; Garn, 1970a). Bone mass in regards to bone mineral density (BMD) and bone mineral content (BMC) are also constantly changing over the course of a lifetime. BMD reaches the peak in adulthood and remains relatively stable for a period of approximately 40 years before declining dramatically after menopause in women (Duren et al., 2013; Henrik et al., 2003). Other factors, environmental and genetic influences also have an impact on skeletal development (Duren et al., 2013). Imbalance between bone resorption and formation may lead to bone-related pathologies such as osteoporosis (Burr and Akkus, 2014).

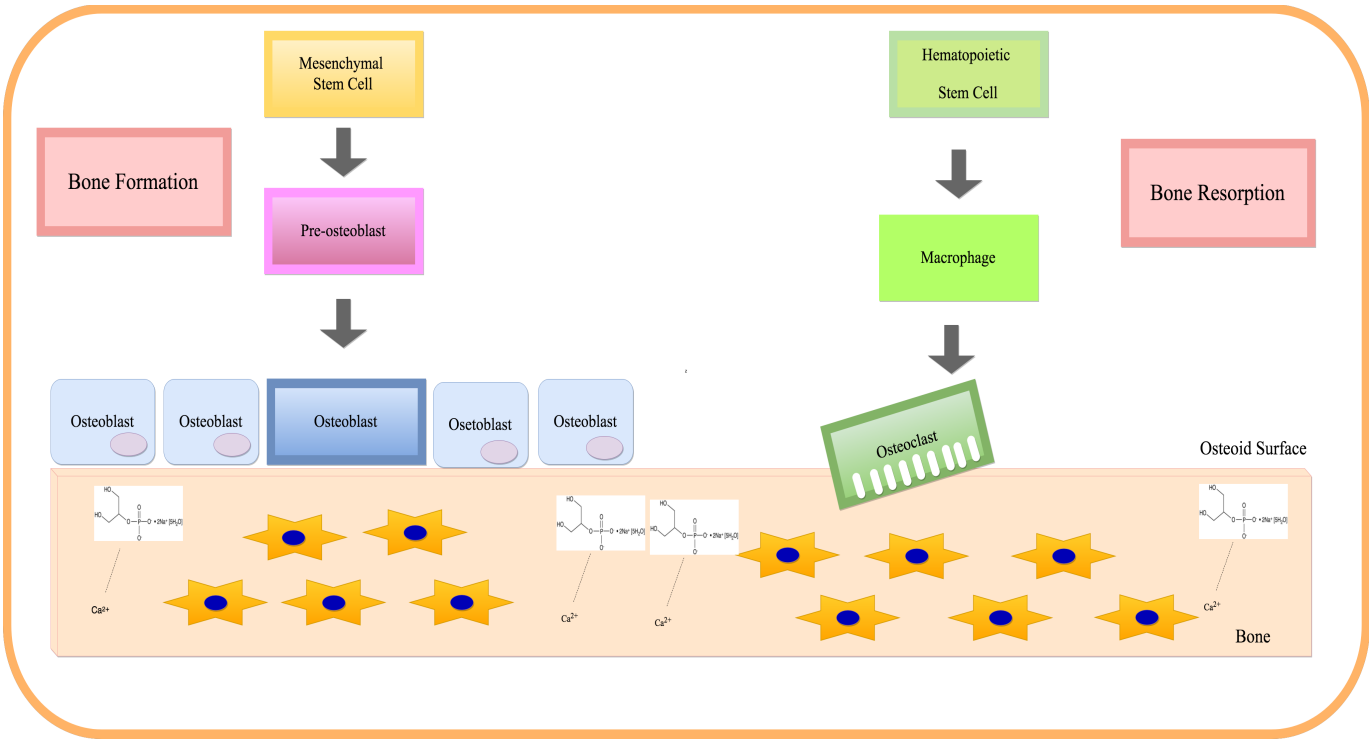

Figure 1. 1 **Bone Remodeling Process**

Osteoclasts resorb bone by secreting protons thus creating a lacunae on the bone surface. Then osteoblasts lay down collagen on the same site, forming an extracellular matrix, which is later mineralized during bone formation. Osteoblasts that become embedded in the matrix become osteocytes.

1.1.2 Osteoporosis

Osteoporosis (OP) is a medical condition characterized by low bone mass and deterioration of micro-architecture, leading to bone fragility and a consequent increase in fracture risk (Dennison et al., 2006; Riggs and Melton III, 1995). Osteoporosis is a world-wide health problem impacting 200 million people and causing significant morbidity and mortality (Cooper and Melton III, 1999). According to the World Health Organization (WHO) rankings of causes for years lived with disability worldwide in 2013 osteoporosis-related "back pain" and "other musculoskeletal" categories ranked among the top 20 causes, with lower back pain from osteoporosis causing the most significant morbidity. Worldwide, 200 million women are affected and more than 8.9 million fractures occur annually, that is an osteoporotic fracture every 3 seconds. Osteoporosis-related fractures cost the US around $17.9 billion annually, the EU €37 billion and 3.9 billion in Canada (Hopkins et al., 2016). According to Osteoporosis Canada, both men and women are at high risks of developing an osteoporotic fracture in their lifetime, thus osteoporosis is a significant public health concern that should be taken seriously.

The World Health Organization (WHO) Fracture Risk Assessment tool is used to calculate the risk of osteoporotic-fractures. It uses the following parameters: sex, age, body mass index, prior fracture, parental hip fracture, prolonged glucocorticoid use, rheumatoid arthritis (or secondary causes of osteoporosis), current smoking, alcohol intake (three or more unis daily) and bone mineral density (BMD) of femoral neck to do so. WHO Bone mineral density (BMD) provides a standardized score, known as a T-score. It is used to identify individuals at high risk of fragility fractures. The WHO T-scores can be divided in to 4 categories. A T score of -1.0 and above indicates individuals have normal BMD, T-score between -1.0 and -2.5 indicates osteopenia, a T-score of -2.5 and below indicates osteoporosis and T-score of -2.5 and below

with a history of fracture indicates severe osteoporosis (Lentle et al, 2011). Osteoporosis can be classified into primary (idiopathic) or secondary osteoporosis (Dennison et al., 2006). Causes of secondary osteoporosis include hypogonadism, hyperthyroidism, skeletal metastases, multiple myeloma, anticonvulsant or corticosteroid use and excessive alcohol use (Wheater et al, 2013). The occurrence of osteoporosis increases with age, especially in the first few years post-menopause in women, when they experience rapid bone deterioration due to a rapid decline in estrogen levels (Weitzmann and Pacifici, 2006; Wheater et al, 2013).

1.1.2.1. Osteoporosis in Canadians

According to the International Osteoporosis Foundation, both men and women are at high risk of hip fractures in Canada, with post-menopausal Canadian women at the highest risk (Kanis et al, 2012). The Canadian healthcare system spent over 2.3 billion dollars in 2010 on Osteoporosis, including acute care, outpatient care, prescription drugs and indirect costs. This cost goes up to 3.9 billion dollars annually when combined with Canadians who were assumed to be living in long-care facilities due to osteoporotic fractures (Tarride et al, 2012). Patients suffering from osteoporotic hip fractures take up more hospital admission days than stroke patients, patients with diabetes or heart attack. Of individuals who suffer from an osteoporotic fracture, only 44% were able to return home, 27% went into rehabilitation care, 10% went to another hospital, leaving 17% in long-term care facilities (Ioannidis et al, 2009). Individuals with hip or vertebral fractures have increased risk of mortality after their first fracture (Ioannidis et al, 2009).

According to 2010 Canada clinical practice guidelines, men and women over the age of 50 should be assessed annually for their risk of osteoporosis-related fractures (Papaioannou et al, 2010). This should include a detailed medical history and focused physical examination. In

selected individuals, BMD should be measured with dual-energy x-ray absorptiometry (Papaioannou et al, 2010). Markers for bone turnover can also be assessed for selected patients, including alkaline phosphatase, thyroid-stimulating hormone, calcium levels corrected for albumin, 25-hydroxyvitamin D, complete blood count, and creatinine (Papaioannou et al, 2010).

1.1.2.2. Risk Factors for Osteoporosis

Common osteoporotic fractures include wrist, vertebra, and femoral neck fractures. Risk factors for this include loss of estrogen in postmenopausal women, resulting in increased bone turnover and an imbalance between bone resorption and bone formation (Weitzmann and Pacifici, 2006). An imbalance between the two processes leads to decreased trabecular bone mass and ultimately osteoporosis (OP). OP bone loss affects both cortical and trabecular bone. Cortical thickness and number and size of trabeculae are significantly reduced, leading to higher porosity in bone density (Bala et al., 2014). Trabecular bone loss occurs more rapidly than cortical bone loss due to its porous density and higher bone turnover. Hormones that regulate bone remodeling include parathyroid hormone (PTH), calcitonin, estrogen, vitamin D, cytokines and local factors including prostaglandins. Loss of estrogen in postmenopausal women leads to an imbalance between RANKL and OPG, which in turn increases osteoclast differentiation and activation (Imel et al, 2014). Aging is another risk factor for developing OP. Aging results in reduced calcium absorption, reduced circulating vitamin D metabolites in plasma and a lower stem cell population that can be differentiated into functional osteoblasts (Imel et al, 2014). Other risk factors for OP include race, female gender, small body size, use of glucocorticoids, calcium or vitamin D deficiency (Imel et al, 2014).

1.1.2.3 Currently available treatment options for osteoporosis

There are many FDA-approved antiresorptive and anabolic medications available for osteoporosis treatment. Bisphosphonates are the most common anti-resorptive treatment and include Alendronate (Fosamax), Risedronate (Actonel), Ibandronate (Boniva), and zoledronic acid (Reclast). Other antiresorptive treatment options include estrogen replacement therapy such as raloxifene (Evista) or Denosumab (Prolia), which is a humanized monoclonal antibody that binds to RANKL to inhibit its action (Patel et al., 1999; McClung et al., 2006). Romosozumab, a humanized monoclonal antibody targeting sclerostin, is currently under phase III clinical trials (Winkler et al., 2003). The anabolic medication, Teriparatide (Forteo), is a biosynthestic humn parathyroid hormone (PTH) which is also under investigation from the treatment of osteoporosis (Brixen et al., 2004).

1.1.3. Pathophysiology of osteoporosis

Osteoporosis results from imbalanced bone remodeling cycle; excessive osteoclast activity during bone resorption while osteoblast activity during bone formation is unable to keep up (Jilka, 2003). Osteoclast differentiation and maturation are described in detail in **1.2.2**. **Figure 1. 2** shows that differentiated and multi-nucleated osteoclasts form a sealing zone by attaching to the bone surface via $\alpha_V\beta3$ integrin. Once attached, these polarized osteoclasts form a ruffled border inside where vacuolar H^+-ATPase, a proton pump lowers internal pH to approximately 3-4 and therefore create a suitable environment to dissolve bone minerals, aiding the acidification process (Baron et al., 1985, Manolagas, 2015). Multiple factors contribute to enhanced osteoclast activity therefore increasing bone resorption. In post-menopausal women, bone reduction rate increases to 10-fold compared to the 0.3 to 0.5% annual reduction in both men and women (Riggs and Melton III. 1992). Estrogen reduces RANKL and M-CSF expression directly, thereby

inhibiting RANKL-induced osteoclast activation. Estrogen also negatively regulates osteoclastogenesis cytokines including IL-1, IL-6 and tumour necrosis factors (Shevde et al., 2000). Thus, estrogen deficiency increases osteoclastogenesis and bone resorption, resulting in osteoporosis (Nirupama et al., 2000; Riggs et al., 1998; Suda et al., 1995).

Many other factors also contribute to the accelerated rate of boss loss, such as vitamin D deficiency, hyperthyroidism, hyperparathyroidism, Paget's disease, Cushing's syndrome, Hypogonadism, inflammation that increases cytokine release or induced by tumor. Hyperthyroidism and inflammation-induced release of cytokine lead to increased bone resorption while low estrogen levels result in decreased osteoprotegerin levels binding to RANK. Other causes of secondary osteoporosis include prolong use glucocorticoids, anti-convulsants, aromatase inhibitors which result in estrogen depletion, and methotrexate (Holick, 2007). Glucocorticoids are commonly used to treat inflammatory conditions such as rheumatoid arthritis (RA), inflammatory bowel disease (IBD) including ulcerative colitis (UC) and Crohn's diseases (CD). Individuals who may be put on glucocorticoids for treating inflammation are therefore more at risk of developing osteoporosis. In fact, glucocorticoid-induced osteoporosis (GIOP) is the most common form of secondary osteoporosis (Briot and Roux, 2015).

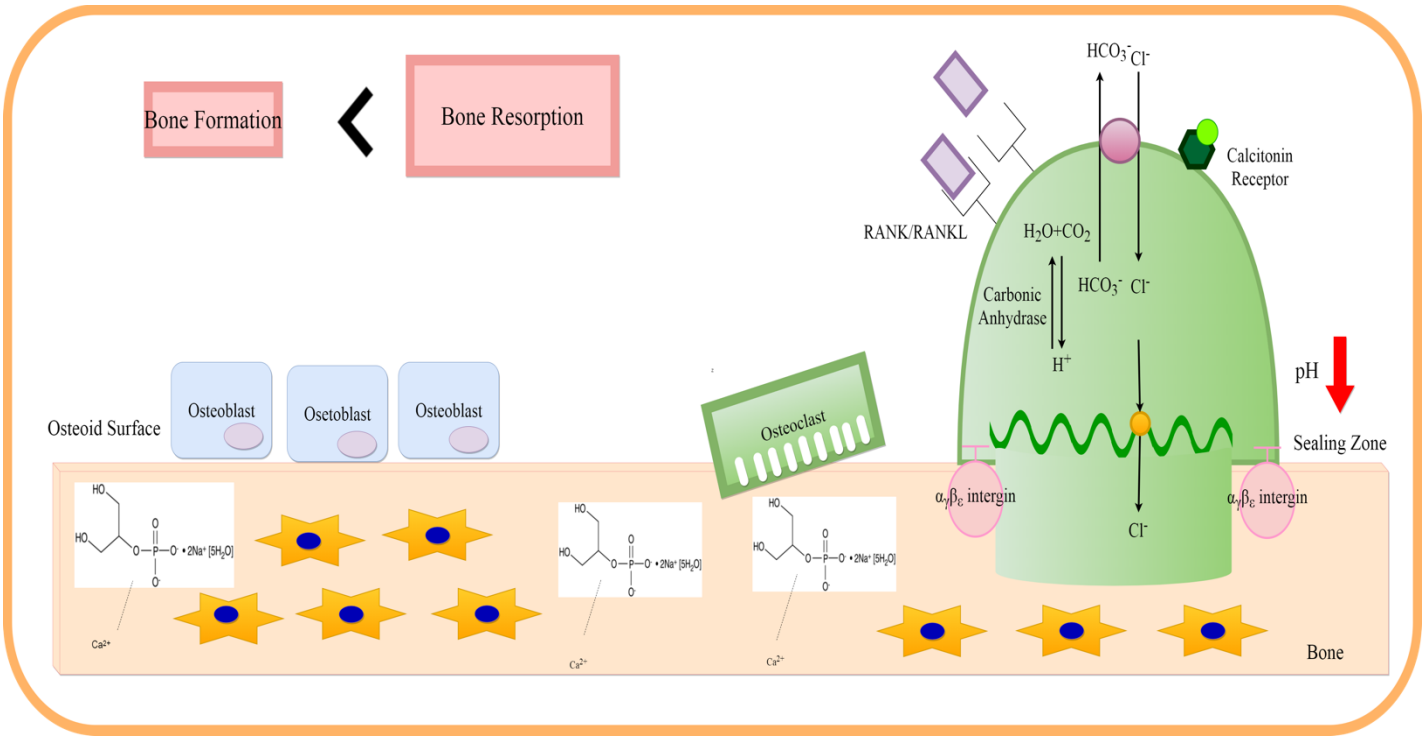

Figure 1. 2 Osteoporosis caused by imbalance between Bone Resorption and Bone Formation

Imbalanced bone remodeling cycle where bone resorption exceeds bone formation results in osteoporosis. Osteoclasts are activated upon RANK/RANKL binding and activated osteoclasts start pumping in protons thus lowering internal pH.

Stars embedded in the bone are to represent osteocytes and the white molecules are to represent hydroxyapatite $Ca_{10}(PO_4)_6(OH)_2$.

1.2 Bone cells

Four different types of cells line and reside inside the bone: osteoblasts, osteoclasts, osteocytes and bone lining cells. Osteoblast, osteocytes and bone lining cells originate from mesenchymal stem cells. Osteoclasts originate from hematopoietic stem cells (Buckwalter et al., 1996;Clarke, 2008). During the bone remodeling process, bone is resorbed continuously by the osteoclasts and new bone is laid down by osteoblasts. Osteocytes are embedded in the interior of the bone important for mechanosensors, signaling transduction and respond to the external stimuli (Bonewald, 2011; Clarke,2008). Functions of bone lining cells are still under investigation and studies have suggested their involvement in coupling bone resorption to bone formation (Everts et al., 2002).

1.2.1. Osteoblasts

Osteoblast cells, originate from pluripotential mesenchymal cells, are capable of synthesizing new bone matrix during bone formation. Pluripotential mesenchymal stem cells have the ability to differentiate into osteoblasts and other lineages, including chondroblasts, fibroblasts, adipocytes, and myoblasts shown in **Figure 1. 3** (Kartsogiannis and Ng., 2004; Nijweide et al., 1986; Friedenstein et al., 1987; Aubin et al., 1995). Committed osteoprogenitors from stem cells can undergo differentiation to pre-osteoblasts. Pre-osteoblasts can undergo further differentiation to become osteoblasts. Osteoblasts go through osteoblastogenesis, series of developmental stages from proliferation to extracellular matrix development and maturation, mineralization and finally apoptosis (Bukka et al., 2004; Burr and Akkus, 2014). During the proliferation period, osteoblasts synthesize genes required for activation of proliferation and cell cycle progression as well as genes encoding adhesion proteins such as fibronectin. Osteoblasts then enter the phase of

development and maturation of extracellular matrix (ECM) where genes such as alkaline phosphatase (ALP), Runx2, type I collagen associated with ECM organization are up-regulated, forming the unmineralized organic matrix, known as osteoid. Followed by ECM mineralization which involves genes acts on the deposition of hydroxyapatite including osteocalcin and osteopontin while calcium and phosphate ions are incorporated into the matrix (Meyer et al., 2014; Rodan and Noda, 1991; Stein et al., 1996). At the same time, mature osteoblasts become wider and flatter, losing most of the Golgi apparatus and become elongated with extensions. These terminally differentiated osteocytes become embedded in the mineralized matrix. Some will become bone lining cells that cover the quiescent surface of the bone while others undergo apoptosis (Bellido et al., 2014; Burr and Akkus., 2014).

Osteoblasts display multiple receptors and respond to 1,25-dihydroxyvitamin D_3 [$1,25D_3$], parathyroid hormone (PTH), prostaglandins (PGs), tumor necrosis factors (TNFs), epidermal and transforming growth factors (EGFs, TGFs) which can influence the differentiation process (Kartsogiannis and Ng., 2004; Chen et al., 2012; Heath and Reynolds., 1990). Several lines of literature show $1,25D_3$ enhanced mineral deposition and genes associated for the process in osteoblasts (Prince et al., 2001; Maehata et al., 2006). However, varying observations on $1,25D_3$-mediated effects on mineralization have been reported and will be discussed later in this dissertation.

Osteoblast lineage cells are capable of secreting RANKL and M-CSF, which bind with RANK and c-fms on osteoclasts to activate osteoclastogenesis. RANKL is a membrane bound protein belonging to the TNF superfamily. In addition to RANKL, osteoblast lineage cells produce osteoprotegerin (OPG), which is a soluble decoy receptor that binds RANKL, thus inhibiting

interaction with RANK. The RANKL-to-OPG ratio is crucial to maintain healthy bone formation (Hofbauer and Heufelder, 2001).

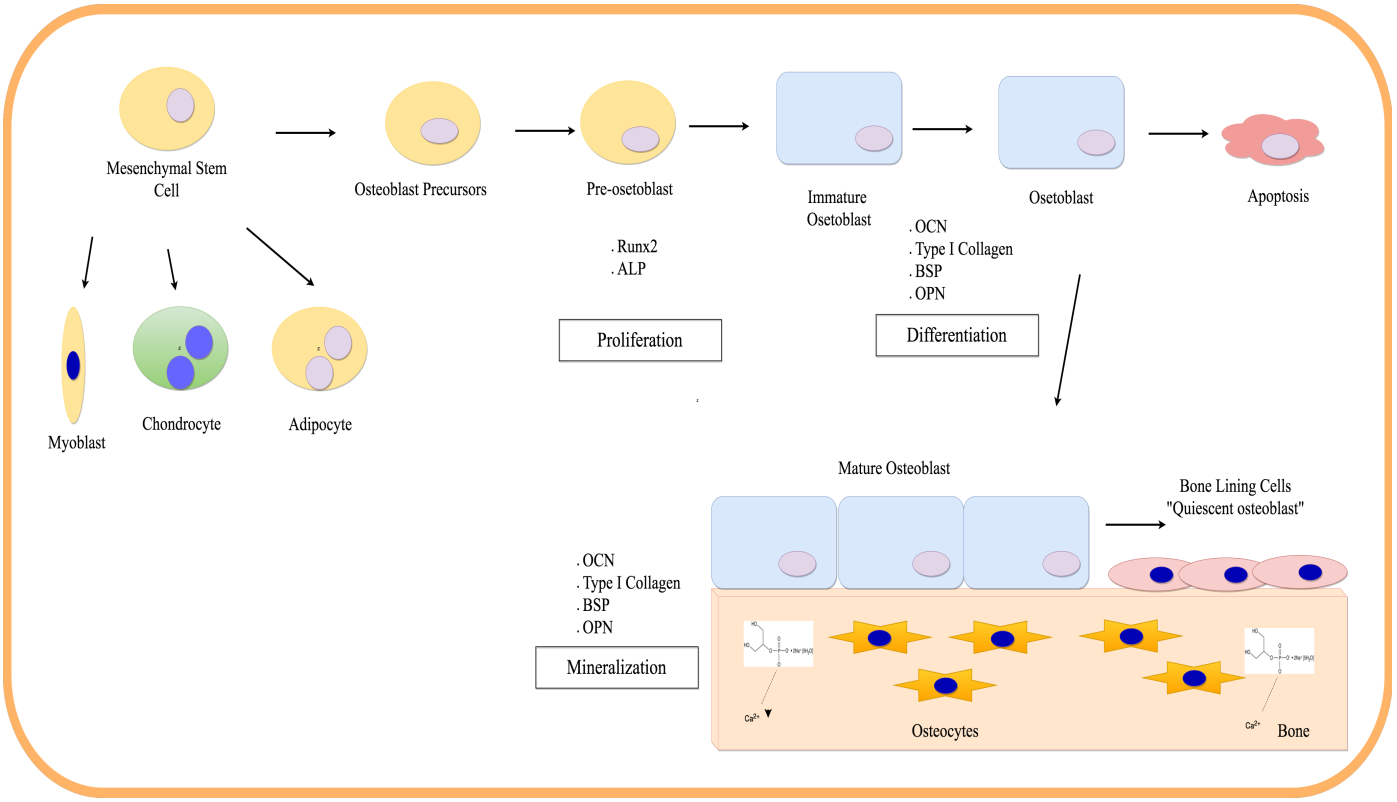

Figure 1. 3 Osteoblast Differentiation

Osteoblast precursors originate from mesenchymal stem cells and give rise to pre-osteoblasts which can then undergo differentiation to immature osteoblasts, osteoblasts and finally mature osteoblasts. Mature osteoblasts have two fates, some become bone lining cells while others undergo apoptosis.

1.2.1.1 Model of osteoblast differentiation and matrix calcification: MC3T3-E1 cells

In order to understand the osteoblast developmental sequence, extracellular matrix (ECM) secretion and mineralization, immortalized *in vitro* cell lines were used. They provide a convenient means to study these processes. They retain key features of the osteoblast phenotype and offer the advantage of stability, relative homogeneity, ready maintenance and reproducibility (Karin and Farach-Carson., 2004).

The murine MC3T3-E1 cell line is a clonal non-transformed cell line established from fetal murine calvaria (Kodama et al., 1981; Sudo et al., 1983; Kartsogiannis and Ng., 2004). MC3T3-E1 cells display features and a phenotype similar to *in vivo* conditions, for example, this cell line can synthesize type I collagen, form matrix vesicles which can then be deposited on collagen fibrils and eventually nodular extracellular matrix mineralization, resembling woven bone *in vivo* (Sudo et al., 1983; Karin and Farach-Carson., 2004; Kartsogiannis and Ng., 2004; Quarles et al., 1992). MC3T3-E1 cells also offer the advantage of greater uniformity and homogeneity than primary osteoblast cultures (Quarles et al., 1992). In comparison with primary cell lines, MC3T3-E1 cells require less preparation and can undergo several passages (Quarles et al., 1992).

Cells undergo three stages in osteoblast differentiation *in vitro* as described by Lian and Stein (1992). Pre-osteoblasts first undergo a proliferative stage where the cells divide and grow rapidly before reaching growth arrest. During this phase, osteoblasts secrete and synthesize type I collagen and fibronectin. Cells then enter the second stage, or the matrix maturation stage. Cells at this stage express high levels of alkaline phosphatase (ALP), bone-matrix proteins including Runx2, low levels of osteocalcin, osteopontin, bone sialoprotein, and osteonectin. The final

phase is osteoblast mineralization. The cells express less ALP levels but increasing OCN levels. Ca^{2+} is actively deposited into the extracellular matrix during this stage, marking the terminal phase in bone formation (Sudo et al., 1983). Differentiation of MC3T3-E1 cells into differentiated osteoblasts can be initiated by addition of 50 μg/mL ascorbic acid and 10 mM β-glycerophosphate to the cell culture media. Addition of ascorbic acid stimulates alkaline phosphatase and osteocalcin production during accumulation of collagenous extracellular matrix (Franceschi et al., 1994; Quarles et al., 1992). β-glycerol phosphate supplies inorganic phosphate for the formation of extracellular matrix (Franceschi et al., 1994; Quarles et al., 1992). This cell model is also capable of type I collagen and alkaline phosphatase synthesis, formation of matrix vesicles which can then be deposited on collagen fibrils and eventual nodular extracellular matrix mineralization, resembling woven bone (Sudo et al., 1983; Kartsogiannis and Ng., 2004; Quarles et al., 1992; Wang et al., 1999).

MC3T3-E1 cells can be regulated by $1,25D_3$, PGE_2 and PTH (Kartsogiannis and Ng., 2004). Treatment with $1,25D_3$ has been reported to increase ALP and type I collagen production (Sudo et al., 1983). 10 different subclones of the original MC3T3-E1 cells have been isolated with various phenotypic properties (Wang et al., 1999). Clone 4, which is used in this thesis has been reported to express high levels pf osteocalcin and type I collagen which correlate with high mineralizing potential (Wang et al., 1999). Although ALP expression is absent in clone 4, this clone is capable of synthesizing mineral fibrils in the ECM. These similarities in developmental stages support the biological relevance of the MC3T3-E1 cell model system to *in vivo* bone formation, and can thus can serve as a suitable model to study osteoblast differentiation and mineralization (Quarles et al., 1992).

1.2.2 Osteoclasts

Osteoclasts are the primary cells mediating bone resorption, they are capable of degrading organic and inorganic components of bone (Jilka, 2003). Osteoclasts originate from hematopoietic progenitors that give rise to macrophages (Bellido et al., 2014). Osteoclast precursors are recruited to the bone surface where they respond to signals from cytokines to initiate bone resorption. Osteoclast precursors then undergo differentiation where they fuse together to become functional multinucleated osteoclasts. Mature osteoclasts then line up on the mineralized surface where bone lining cells have retracted. Resorption is initiated when osteoclasts start pumping out protons thereby creating an acidic environment to dissolve mineral and release collagen fragments. During this process, newly mature multinucleated osteoclasts are constantly recruited to the site to maintain the resorption process (Allen and Burr, 2013; Bellido et al., 2014; Jilka, 2003). Key features of osteoclasts include a ruffled membrane and actin rings. The ruffled membrane is a result of intracellular acidified vesicles and the actin ring surrounds the ruffled membrane creating a microenvironment for acidification. The mature osteoclast is a polarized cell that attaches its apical side to the surface of the mineralized bone thus creating a sealing zone. Integrins, adhesion molecules responsible for attaching osteoclasts to the mineralized surface (Allen and Burr, 2013; Suda et al., 1992). Osteoclasts contain high levels of carbonic anhydrase which generates protons and bicarbonate from carbon dioxide and water. Protons are pumped out via the H^+ ATPase pumps and this process is tightly regulated by channels, and ion exchangers on the basolateral side of the osteoclast cell to maintain intracellular pH (Allen and Burr, 2013).

1.2.3 Osteocyte

Osteocytes are mature osteoblasts that become embedded in their own osteoid. The main function of osteocytes is to produce calcified matrix by regulating initiation and control of bone matrix mineralization. Osteocytes have long extensions embedded in the lacunocanalicular bone network. This morphology is important for signal transduction via gap junctions. Gap junctions connect with neighbouring cells, regulating the passage of molecules. Osteocytes are able to sense mechanical loads, coordinate signals by releasing molecules which control osteoblast and osteoclast activity, thereby contributing to osteoblast differentiation and bone turnover (Klein-Nulend et al., 2003; Manalogas., 2000; Wheater et al, 2013).

When osteoid begins to undergo mineralization a process known as osteocytogenesis, biomarkers including osteocalcin, bone sialoprotein, collagen type I, and ALP expression are down-regulated or diminished. During osteocytogenesis, notable morphological changes can be observed, such as reduced ER and Golgi apparatus sizes (these morphological changes are due to less protein synthesis and secretion). Lamellipodia and pseudopodia are then produced with osteocyte dendrite formation. These dendrites are organized in a polarized manner on the mineralizing front, and the dendrites extend in the direction of either the vascular space or bone surface. Directionality of the dendirites are crucial for mineral formation (Dallas and Bonewald, 2010). Osteocytes can influence osteoblasts to secrete type I collagen in preparation for mineralization.

1.2.4 Bone matrix and mineralization

Bone is made up of 65% inorganic mineral component, 25% of organic component and 10% of water. Hydroxyapatite [$Ca_{10}(PO_4)_6(OH)_2$] is the major content of the mineral component, with

small amounts of carbonate, magnesium and acid phosphate (Clarke, 2008). Type I collagen is the major component in of the organic component, with small traces of type III and V and FACIT collagens for fibril diameter determination (Clarke, 2008). The other 10% is composed of noncollagenous proteins (NCPs), including proteoglycans, glycosylated proteins and γ-carboxylated (gla) proteins. These matrix proteins have been reported to have multiple roles including collagen formation regulation, mineralization and cell attachment (Burr and Akkus, 2014; Clarke, 2008; McLean and Olsen, 2004). Matrix calcification occurs in three processes: initiation of mineralization followed by partial transformation to hydroxyapatite crystals and the continued growth of mineral crystal (Puzas, 2004). To start mineralization, optimal Ca^{2+} and PO_4 must be achieved. This process is under active investigation, and there are different theories proposed on how calcium is delivered into the ECM (Boonrungsiman et al., 2012). The initial theory posits that calcium reaches the ECM directly from the capillary lumen without crossing through the intracellular space of the osteoblast. However, evidence of calcium passing through the cytosol of the osteoblast and then being released into the ECM started to emerge in 1971 and this latter theory has become more widely accepted (Howell et al., 1968; Howell, 1971). The extracellular matrix mineralization is a complex process that is poorly understood. Some suggested formation of nucleation pores where Ca^{2+} bind to lipids of glycosaminoglycans associated with gap zones between collagen fibrils to reach optimal concentrations in order to precipitate out. Glycosaminoglycans are highly negative, thus they display high binding affinity to cationic ions such as calcium. Binding triggers mineral nucleation from other ions in the solution thereby facilitating calcification (Glimcher, 1984; Fratzl et al., 1991). Another hypothesis describes a cell-dependent mechanisms involving matrix vesicles (MVs) budding from the plasma membrane to be directly deposited on the osteoid. MVs are approximately 30

nm to100 nm in diameter and have high content of Ca^{2+}, ALP and calcium-binding molecules to attract Ca^{2+} and thus increase [Ca^{2+}] in the MVs (Anderson et al., 2005). These molecules include calbndin-D_{9K}, annexin II, annexin V, annexin VI calcium-binding acidic phospholipids (Anderson, 1995; Anderson, 2003; Peress et al., 1974). ALP enzymes are for initiation of crystal deposition then crystals growth occurs it fills the matrix which then spread to cover large area of ECM. Involvement of MVs in intramembranous bone formation is still under active investigation. Presences of MVs have been detected *in vitro* human and murine osteoblastic cells including MC3T3-E1 cells (Ringbom-Anderson et al., 1994; Ecarot-Charrier et al., 1983; Ecarot-Charrier et al., 1988; Sudo et al., 1983).

1.3. Calcium Homeostasis

Bone plays an important role in calcium homeostasis by serving as a major reservoir for calcium. The adult human body contains approximately 1200 g of Ca^{2+} which accounts for 1-2% of total body weight, and 99% of calcium is stored in the hydroxyapatite $Ca_{10}(PO_4)_6(OH)_2$ (Kopic and Geibel, 2013). Serum calcium concentration is maintained at 9 - 10 mg/dL under tight regulation by the intestine, kidneys and bones through the action of PTH, $1,25D_3$ and calcitonin (Garabedian et al., 1972).

1.3.1 Calcium transport machinery in bone

Calcium is under tight regulation by specialized channels, transports and mediators in bone. In resting osteoblasts, cytoplasmic [Ca^{2+}] ranges between 50 nM and 150 nM and can be stimulated by pharmacological treatment or fluctuation in external [Ca^{2+}] rising cytoplasmic [Ca^{2+}] to 200 nM to 400 nM. Calcium permeability is mediated by voltage-sensitive channels (VSCCs) present on the plasma membrane. Ca^{2+} serves many roles in the bone, for example, as an signaling molecule in regulating hormone and cytokine actions, regulator of cell attachment and proliferation (Blair et al., 2007). Increase in intracellular [Ca^{2+}] can then return to resting levels via efflux mechanism and movement of Ca^{2+} into stores, processes primarily driven by ATP-driven Ca^{2+} pumps (**Figure 1. 4**) (Duncan et al., 1998; Jung et al., 2007; Tsien and Tsien, 1990).

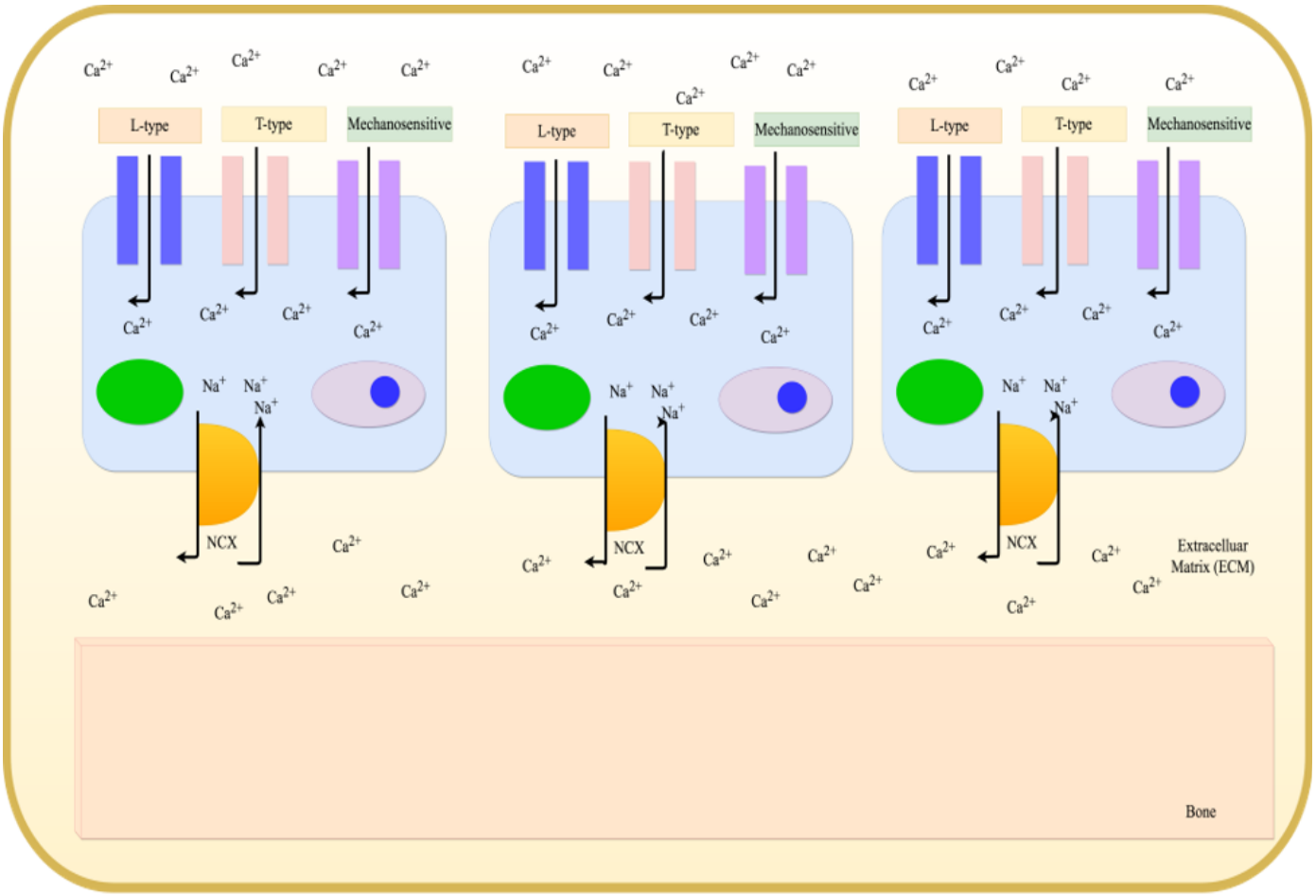

Figure 1. 4 Voltage-sensitive calcium channels (VSCCs) maintain calcium homeostasis in bone

L-type or high voltage-sensitive T-type or low voltage-sensitive channels and channels that respond to external mechanosensitive stimuli allow Ca2+ entry into osteoblasts which can then be translocated to the opposite side of the cell allowing it to be deposited in the osteoid via efflux through the NCX transporter or PMCA-1b pump calcium pump.

1.3.1.1 Calcium influx mechanism

Ca^{2+} enters osteoblasts via a plasma membrane channels, including voltage-sensitive Ca^{2+} channels (VSCCs) shown in **Figure 1. 4**. VSCCs serve important roles in cellular signaling, stimulation coupling and regulating cell growth and differentiation. Furthermore, VSCCs influence local bone remodeling by involving in paracrine signaling between osteoblasts and osteoclasts (Farach-Carson., 1996). Major classes of VSCCs include high-voltage activate, such as L-, P/Q-, N and R-type and low-voltage activated of T-type channels. L-type Ca^{2+} channels consist of four protein subunits (α1, α2δ and β), where α1 forms the pore that permits Ca^{2+} entry. Currently, more than ten α-subunits have been identified in osteoblasts. L-type consisting of $Ca_v1.1\alpha_{1s}$-, $Ca_v1.2$ α_{1c}-, $Ca_v1.3$ α_{1D}-, and $Ca_v1.4$ α_{1F}- subunits. P/Q-type of $Ca_v2.1$ (α_{1A}), N-type of $Ca_v2.2$ (α_{1B}), and R-type of $Ca_v2.3$ (α1E) subunits. Low-voltage activated T-type VSCCs include $Ca_v3.1$ (α_{1G}), $Ca_v3.2$ (α_{1H}), and $Ca_v3.3$ (α_{1I}). In particular, L-type $Ca_v1.2$ Ca^{2+} channel was reported to regulate majority of Ca^{2+} influx into osteoblasts (Liu et al., 2000). Treatment of $1,25D_3$ was found to increase Ca^{2+} permeability by shifting threshold of activation toward resting potential, thus prolonging gate-opening time (Bergh et al., 2006). This raise in cytosolic [Ca^{2+}] can bind to calcium-binding proteins such as Calbindin-D_{9K} or Calbindin-D_{28K} and permitting translocation to the other side of the osteoblast to be deposited into ECM (Bergh et al., 2006).

1.3.1.2 Calcium efflux mechanism

Ca^{2+} efflux mechanism is critical for calcium deposition into mineralizing matrix during bone formation.

1.3.1.2.1 Plasma membrane calcium ATPase pumps (PMCA)

The plasma membrane calcium ATPase pump (PMCA) is an ATP-driven pump that is present on the plasma membrane of the osteoblast, facing the bone marrow. It is responsible for the extrusion of one Ca^{2+} -ion per one ATP molecule hydrolysed (Akisaka et al., 1988; Nakano et al., 2007; Nakano et al., 2004). Four different genes encode the tissue-specific expression of isoforms, PMCA1, PMCA2, PMCA3 and PMCA4. PMCA1 and PMCA4 are found in human osteoblasts; however, PMCA1, PMCA2 and PMCA4 have been identified in mouse osteoblasts, including UMR 106-01 and ROS17/2.8 cells. PMCA-1b expression was identified in mouse and rat calvarial osteoblasts. Localization of PMCA and its role in delivering Ca^{2+} into the extracelluar matrix during bone mineralization is under active investigation (Nakano et al., 2004). Transgenic animals negative for PMCA1 display a significant reduction in BMD and, over-expression of PMCA results in an increase in bone mass, confirming its role in bone formation and consistent with it secreting calcium into the ECM. However, its localization suggests PMCA may not be involved in ECM mineralization directly but rather indirectly involved in calcium signaling thus maintaining calcium homeostasis.

1.3.1.2.2 Sodium Calcium Exchanger (NCX)

The sodium-calcium exchanger (NCX) is a bi-directional Na^{+}-dependent calcium transporter. In exchange for one Ca^{2+} ion exported, NCX transfers three Na^{+} ion into the cell and this action can be reversed depending on membrane potential and ion concentrations (Brini et al., 2011;

Sosnoski et al., 2008). NCX1, NCX2 and NCX3 are three isoforms found in mammals, only NCX1 and NCX3 are present in osteoblasts (Stains et al., 2002). During osteoblasts differentiation, NCX3 is the predominant expressed isoform, with low levels of NCX1. Both NCX isoforms are expressed at nearly static levels throughout differentiation (Stains et al., 2002). Both NCX isoforms reside on the osteoid-facing side of osteoblasts, supporting its role in regulating calcium efflux from osteoblast for bone mineralization (Stains and Gay, 1998). NCX exhibits low Ca^{2+}-binding affinity, further supporting its role in calcium efflux. Inhibition of NCX in osteoblasts prevents mineralization *in vitro* (Stains and Gay, 2001).

1.4 Vitamin D metabolism and function

Vitamin D serves as an important nutritional supplement for bone health and has been used to prevent rickets, osteomalacia, osteoporosis and fragility fractures (Holick and Chen, 2008). Health Canada recommends daily intake of 400-1000 IU vitamin D for young and individuals at low risk, and 800- 2000 IU vitamin D for older adults and individuals with high risks (Hanley et al., 2010). Vitamin D and its metabolites are crucial in calcium homeostasis, bone mineralization and formation (Bouillon and Reid., 2008; Christakos et al., 2011; Haussler et al., 2011; Jones, 2010; Pike and Meyer, 2010; Pike et al., 2011; Rochel and Moras, 2011; Souberbielle et al., 2006)

Metabolism of vitamin D is illustrated in **Figure 1. 5**. Vitamin D can be obtained from two sources, one is from the exposure to sunlight as ultraviolet B radiation (UVB) converts 7-dehydrocholesterol to previtamin D_3, which is then converted to vitamin D by heat-dependent process (Chen et al., 2010; Holick and Chen, 2008; Plum and DeLuca, 2010). Another source is from dietary sources, such as fish oil, fortified milk or juice, and supplements of vitamin D_3 (Chen et al., 2010; Holick and Chen, 2008; Plum and DeLuca, 2010; Prentice et al., 2008). Vitamin D obtained from both sources is converted in the liver by the vitamin D-25-hydroxylase (25-OHase) or CYP27A1 to 25- hydroxyvitamin D [25(OH)D]. The most important conversion then occurs in the kidneys where 25(OH)D is converted by the 25-hydroxyvitamin D-1α-hydroxylase (1-OHase) or CYP27B1 to its biologically active form 1,25-dihydroxyvitamin D [$1,25(OH)_2D$] or $1,25D_3$ (Bikle, 2012; Chen et al., 2010; Christakos et al., 2011; Erben, 2001; Holick and Chen, 2008; Haussler et al., 2008; Lanteri et al., 2013; Sakaki et al., 2011). During vitamin D degradation, this active form of vitamin D can then be hydroxylated at the C-24

position to 24,25-(OH_2)D_3 by 25-hydroxyvitamin D-24-hydroxylase (24-OHase) or CYP 24A1 to biologically inactive calcitroic acid which is excreted in the bile (van Leeuwen et al., 2001).

A circulating concentration lower <50 nmol/L of 25(OH)D is considered vitamin D deficient. 51-74 nmol/L is vitamin D insufficient and >75nmol/L is the optimal concentration, which provides beneficial values for bone health (Holick and Chen, 2008). Vitamin D receptor, VDR, a member of a large family of nuclear hormone receptors, including other receptors for glucocorticoids, mineralocorticoids, sex hormones and thyroid hormone (Binkley, 2010; Dowd and MacDonald, 2010). VDR can be activated by binding with $1,25D_3$ and form a heterodimer with other nuclear hormone receptors, particularly family of retinoid x receptors (RXRs). This VDR-RXR heterodimer can then bind to vitamin D response elements (VDRE) in the promoter region of

target genes to regulate transcription (Meyer et al., 2010; Peppel, 2014).

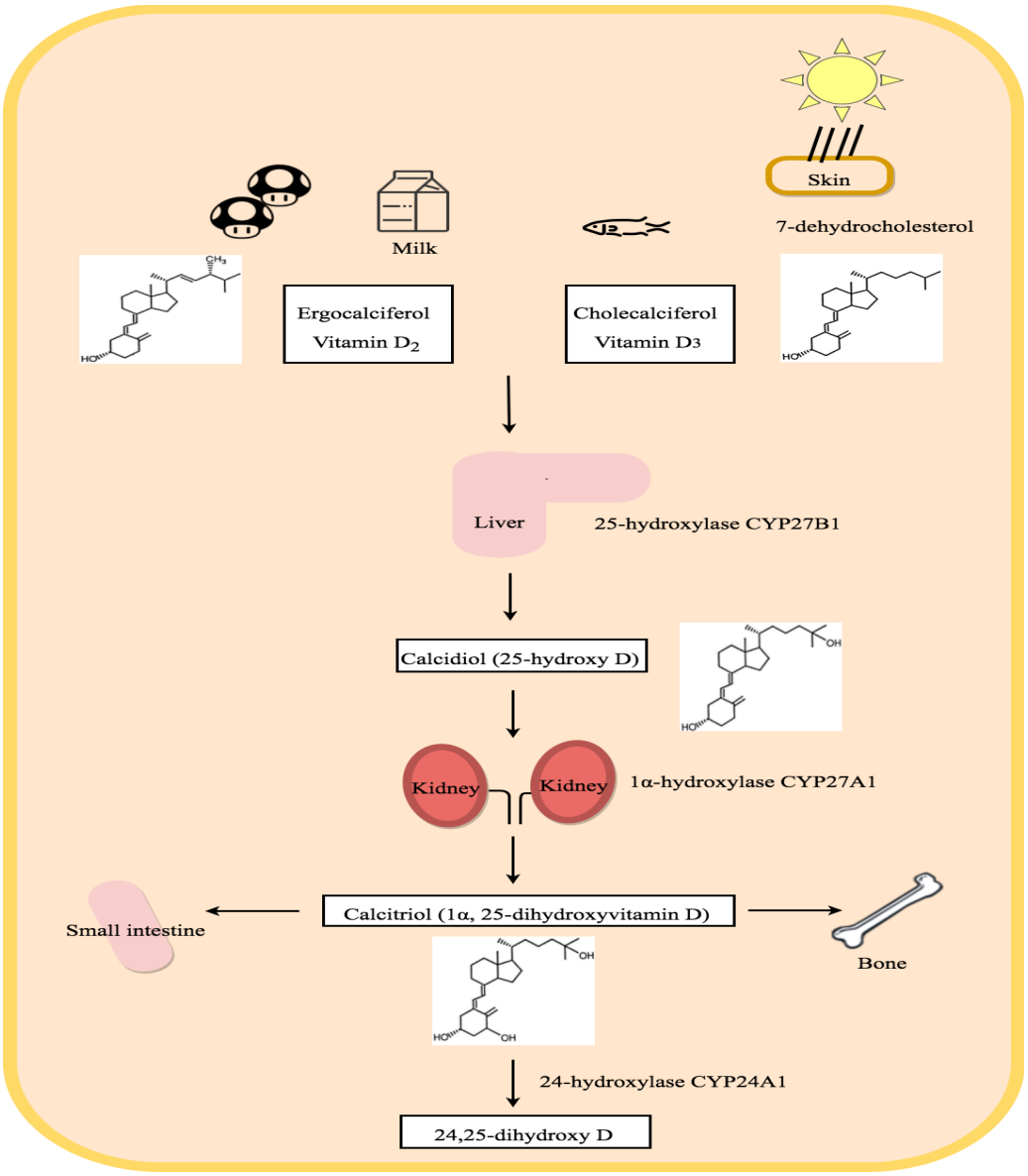
Skin
7-dehydrocholesterol
Milk
Ergocalciferol
Vitamin D2
Cholecalciferol
Vitamin D3
Liver
25-hydroxylase CYP27B1
Calcidiol (25-hydroxy D)
Kidney
Kidney
1α-hydroxylase CYP27A1
Small intestine
Calcitriol (1α, 25-dihydroxyvitamin D)
Bone
24-hydroxylase CYP24A1
24,25-dihydroxy D

Figure 1. 5 Vitamin D Metabolism

Vitamin D obtained as ergocalciferol and cholecalciferol undergo two steps of hydroxylation, first in the liver by 25-hydroxylase to calcidiol, which then undergoes the rate-limiting step in the kidneys by 1 α-hydroxylase to the biological active calcitriol. Calcitriol acts on calcium regulation via small intestine and bone before it gets degraded by the 24-hydroxylase to 24,25-dihydroxy vitamin D.

1.4.1 Vitamin D and Calcium Homeostasis

Vitamin D is important in maintaining adequate levels of calcium ions in the serum (Christakos et al., 2014; Lieben et al., 2012; Rodriguez-Martinez and Garcia-Cohen., 2002). A decrease in serum calcium concentration sensed by the calcium-sensing receptor on the parathyroid gland stimulates parathyroid hormone (PTH) secretion (**Figure 1. 6**). Production of PTH then causes an up-regulation of 1α-hydroxylase activity, resulting in increased production of $1,25D_3$ to enhance intestinal calcium absorption (Ajibade et al., 2010; Christakos et al., 2014; Feldman et al., 2008). PTH also acts on the kidneys to reduce urinary Ca^{2+} excretion and on the bone to further release Ca^{2+}. This forms the negative feedback loop that blocks PTH secretion, thus synthesis of $1,25D_3$ can be inhibited (Feldman et al., 2008; Lieberherrs, 1987; Prentice et al., 2003). Furthermore, $1,25D_3$ reduces gene expression of 1α-hydroxylase and promoting activity of 24-hydroxylase, causing a reduction on synthesis of $1,25D_3$ (Christakos et al., 2011). Calcitonin secreted by the thyroid gland then inhibits osteoclast activity and thereby reducing bone resorption and maintaining a positive calcium balance.

1.4.2 Effects of Vitamin D on Bone

Vitamin D prevents rickets in children and reduces risks of osteomalacia and osteoporosis in adults, thus is indispensable for maintaining normal calcium and bone homeostasis (Eisman and Bouillon, 2014). There has been extensive ongoing effort to understand the direct effects of $1,25D_3$ on bone mineralization in addition to indirect effects via intestinal and renal Ca^{2+} and phosphate regulation.

1.4.2.1. Vitamin D on Bone Formation

Rats receiving chronic and short-term treatment with $1,25D_3$ resulted in increased bone formation and osteoblast precursor cells (Erben et al., 1998). *In vivo* VDR over-expression murine models displayed enhancement in bone mass (Gardiner et al., 2000). Similarly, *in vivo* VDR knock out mice (Vdr -/-) exhibited conditions similar to osteoporosis (Eisman and Bouillon, 2014; Erben et al., 2002; Lieben and Carmeliet. 2013). Influences of $1,25D_3$ on bone mineralization is still actively under debate and detail explanation for the variation in differences in species is still convoluted. Thus far, available studies in human osteoblasts all demonstrated $1,25D_3$ to stimulate bone formation and mineralization via stimulation on osteogenic differentiation. $1,25D_3$ stimulates ALP activity during osteoblast differentiation and production of bone matrix proteins including collagen, osteocalcin, osteopontin and matrix Gla proteins during osteoblast mineralization (Murshed et al., 2004; van Leeuwen et al., 2014). Furthermore, $1,25D_3$ stimulates production of ALP in matrix vesicles and during bone mineralization. During matrix calcification, $1,25D_3$ has been shown to stimulate Calbindin-D_{9K} synthesis in rats. Calbindin-D_{9K} is responsible for translocating calcium across osteoblasts (Balmain et al., 1989). Woeckel and colleagues demonstrated cultured human osteoblasts treated with $1,25D_3$ prior to

the onset of mineralization enhanced mineralization while $1,25D_3$ treatment during mineralization did not further stimulate the process. Further, gene chip expression profiling demonstrated that $1,25D_3$ treatment up-regulated genes involved in the pre-mineralization phase significantly, suggesting $1,25D_3$ is not directly involved in the process of mineralization, but rather in the process of preparing the environment for mineralization (Woeckel et al., 2010; Woeckel et al., 2012). Transgenic mice over-expressing VDR under control of an osteoblast-specific promoter had increased bone mass and strength (Gardiner et al., 2000). *in vivo* studies involving ovariectomized rats showed an increase in bone formation and mineralization when fed $1,25D_3$ and $1,25D_3$ analog (Matsumoto et al., 1985; Shevde et al., 2002). However conflicting observations have been reported in rat and murine osteoblasts (Leeuwen et al., 2001). $1,25D_3$ has been shown to inhibit osteoblast differentiation and mineralization in murine models including MC3T3-E1 cells. $1,25D_3$ treatment has been reported to inhibit Runx2 expression in murine models while it increases it in human osteoblasts. Inhibition on collagen I and osteocalcin production in murine models by $1,25D_3$ has been reported. Furthermore, expression of osteopontin, an inhibitor of bone mineralization has been shown to increase by $1,25D_3$ treatment (Staal et al., 1996). A detailed explanation for the variation among species is absent and still under active investigation.

1.4.2.2. Vitamin D on Bone Resorption

Carlsson first noted vitamin D enhances calcium mobilization from bone in 1952. Vitamin D deficient rats were fed a low calcium diet for weeks and developed hypocalcemia. He then dosed these animals with 100 IU of vitamin D and noticed plasma $[Ca^{2+}]$ increased significantly. These animals had no external Ca^{2+} source since they were fed a low calcium diet, thus he proposed this increase in Ca^{2+} did not come from intestinal regulation but from bone resorption (Carlsso,

1952). This hypothesis was confirmed later in organ cultures when $1,25D_3$ induced ^{45}Ca release from the pre-labeled bone (Raisz et al., 1972). Suda and colleagues showed $1,25D_3$ enhanced osteoclast precursor differentiation and further activation (Boyce and Weisbrode, 1985; Erben, 2001; Holtrop et al., 1981; Roodman, 1996; Suda et al., 1992; 1992). Suda and colleagues then developed a co-culture system with primary osteoblast cells and spleen cells under the treatment of $1,25D_3$. They perform TRAP assay to determine osteoclast activity and found positive TRAP activity in the co-cultures with primary osteoblast cells, suggesting combined effort of both osteoclast and osteoblasts (Takahashi et al., 1988). This was later confirmed that $1,25D_3$-induced RANKL secreted by osteoblasts would facilitate activation of osteoclasts by binding to RANK (Takahashi et al., 2014). Osteoclasts also exhibit VDR and Cyp27B1, permitting $1,25D_3$ direct actions (Kogawa et al., 2010). *In vivo* studies also demonstrated elevated levels of $1,25D_3$ inhibit PTH production and increase bone resorption by increasing osteoclast differentiation and activity (Suda et al., 1992; Takahashi e al., 2014; Eisman and Bouillon, 2014).

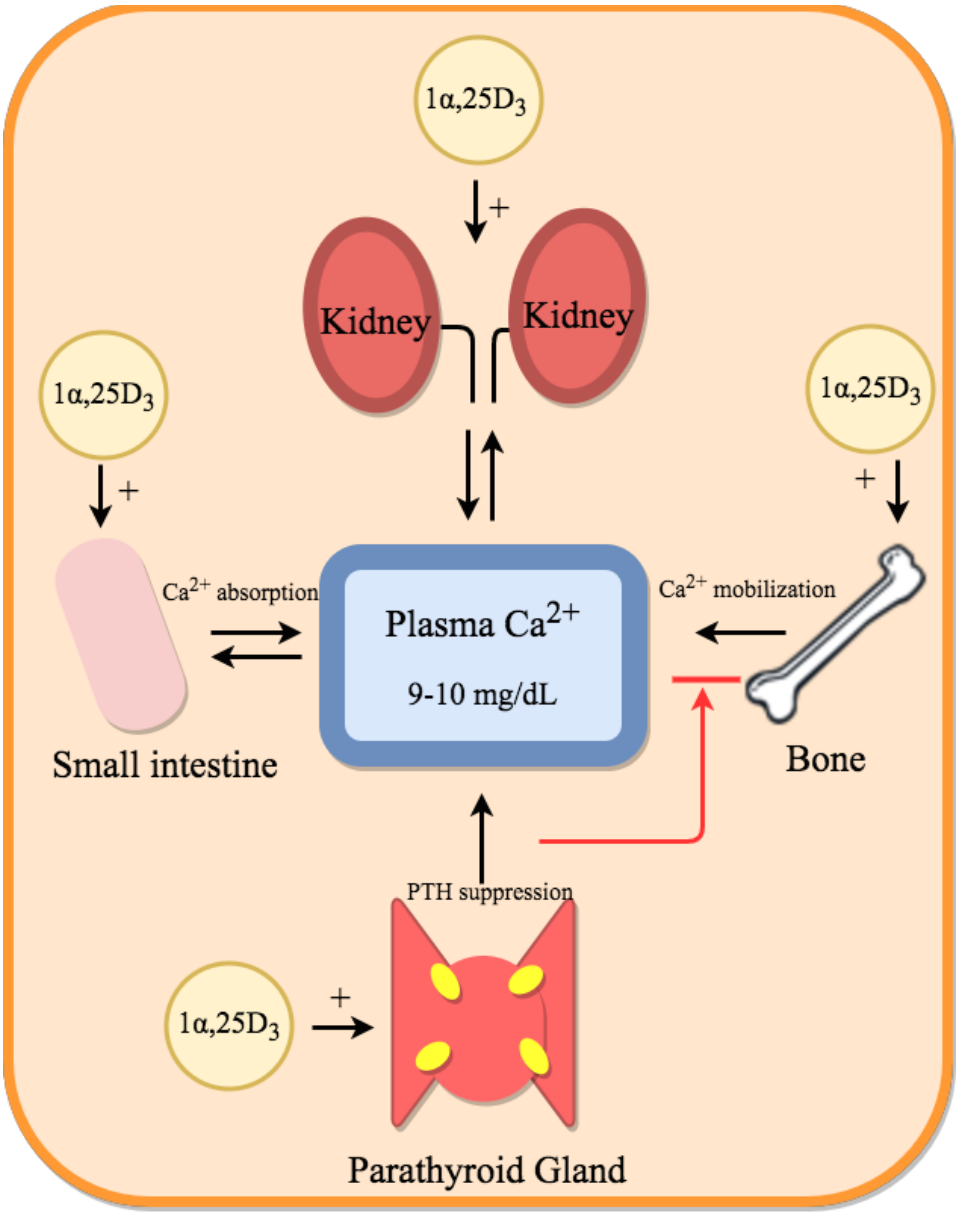

Figure 1. 6 Vitamin D is important in maintaining calcium homeostasis

1α, 25-dihydroxyvitamin D, the biological active form of vitamin D made in the kidneys plays an important role in calcium regulation. Active vitamin D enhances intestinal calcium absorption, calcium re-absorption in the kidneys and calcium mobilization from the bone to raise serum calcium levels. Active vitamin D has also been shown to have direct effects on osteoblasts and osteoclasts.

1.5 Forkhead Transcription Factors (FOX)

The Forkhead gene was first discovered in Drosophila melanogaster in 1989, since then more than 100 forkhead genes and 19 human subgroups have been identified; from FOXA to FOXS based on sequence homology (Weigel et al., 1989; Kaestner et al., 2000; Maiese et al., 2008). FOX transcription factors characterized by a conserved DNA-binding domain (DBD) - TTGTTTAC originally identified as being conserved from Caenorhabditis elegans to mammals. This motif was termed a "forkhead box" or winged helix domain due to its resemblance to a butterfly-like appearance (Calnan and Brunet., 2008; Clark et al.,1993; Maiese et al., 2007; Wang et al., 2009). FOX transcription factors are important for a variety of biological processes including development, differentiation, proliferation, metabolism and apoptosis (Myatt and Lam, 2007). Since the discovery of FOX transcription factors in mammals and with the technology to manipulate FOX in genetic animal models, FOX transcription factors have gained wide interest as therapeutic potentials for conditions such as tumorigenesis, diabetes and cardiac functions (Eijkelenboom and Burgering, 2013; Maiese et al., 2008Rommebaum and Patterson, 2010).

1.5.1. Forkhead Transcription Factors Box O (FoxO)

The Forkhead box, class O (FoxO) subfamily has been extensively studied among all FOX subfamilies for their roles involved in cell proliferation and survival in the hopes to find answers in extending longevity and promoting stress resistance (Arden, 2008; Lan et al., 2013; Myatt and Lam, 2007l; Puig and Mattila, 2011; Sahin and DePinho, 2010). The FoxO group has four mammalian members, including FoxO1 (FKHR), FoxO3a (FKHRL1), FoxO4 (AFX) and FoxO6 (Calnan and Brunet, 2008; Wang et al., 2009). These members play important roles in cellular processes including regulating stress resistance, cell cycle arrest, metabolism and apoptosis

(Martins et al., 2016). FoxO 1, 3, and 4 expression have been detected in various tissues in the human body including the bone and implicate in many diseases including cardiovascular, diabetes and cancer (Calnan and Brunet, 2008; Ronnebaum and Patterson, 2010). FoxO 6 is one exception which is predominately expressed in the brain (Furuyama et al., Jacobs et al., 2003; Lam et al., 2013; Maiese et al., 2008). Deletion of FoxO1 resulted in pre-mature death due to defects in angiogenesis and vessel formation. On the other hand, deletion in FoxO3 and FoxO4 result in normal development, however, female mice with FoxO3 deletion resulted in age-dependent infertility due to abnormal ovarian follicular development later (Nakae et al., 2003; Richards et al., 2002; Wang et al., 2009).

FoxO transcription factors are regulated by external stimuli including insulin, growth factors and oxidative stress. This regulation is achieved by sub-cellular localization through post-transcriptional modifications (PTMs) including phosphorylation and mono-ubiquitination (Brunet et al., 1999). In the absence of external stimuli, the majority of FoxO transcription factors remain unphosphorylated and reside in the nucleus. In the presence of insulin or growth factors, PI3K-AKT pathway is activated and phosphorylation occurs at three conserved sites by the protein kinases Akt and SGK (serum and glucocorticoid-induced kinase) (Brunet et al., 1999; Kops et al., 1999)f. **Figure 1. 7** illustrates FoxO transcription factors regulated by AKT pathway discovered by Brunet et al in 1999 (Brunet et al., 1999). FoxOs participate in the signaling pathways inside the cell. Un-phosphorylated FoxOs can bind to the promoter region of the target genes to enhance downstream transcription and eventual translation. Induction with external stimuli including insulin, insulin-like growth factor (IGF-1), cytokines and oxidative stress control FoxO subcellular localization, DNA-binding and activity ability and therefore resulting in FoxO protein levels (Brunet et al., 1999; Calnan and Brunet, 2008). Insulin induction leads to

phosphorylation of FoxO transcription factors at T32 and S253, resulting in binding to the adapter protein 14-3-3z to facilitate FoxO3 nuclear export to the cytoplasm. In the cytoplasm, phosphorlayed FoxO transcription factors are degraded in proteasome (Calnan and Brunet, 2008; Tzivion et al., 2011).

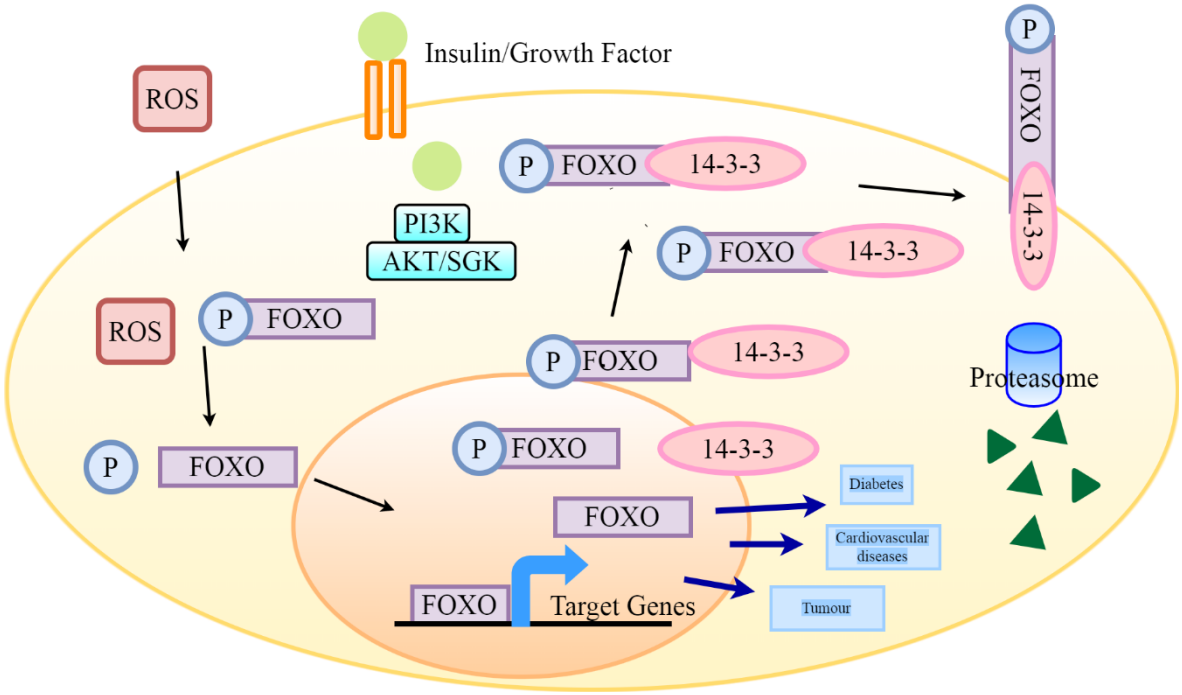

Figure 1. 7 Localization of Forkhead Box O (FoxO) transcription factors regulated by external stimuli

External stimuli such as insulin and growth factors cause FoxOs to be phosphorylated which then bind to adapter protein 14-3-3z designated for nuclear export to the cytoplasm. Oxidative stress, on the other hand, un-phosphorylates FoxOs and leads to nuclear import, up-regulating expression of Catalase and MnSOD.

1.5.2. Roles of FoxOs in Bone

The focus on FoxOs in skeletal homeostasis started when FoxOs have been identified to play a protective role and reduce tissue damage in age-related pathologies (Almeida, 2011; Partridge and Bruning, 2008). Oxidative stress damage results from excess reactive oxygen species (ROS) is a common pathology in age-related diseases (Chen et al., 2004). ROS such as superoxide and hydrogen peroxide are generated through aerobic metabolism (Burdon, 1995). They can cause adverse effects including lipid peroxidation, protein damage and DNA lesions and have been associated with aging and age-related diseases including osteoporosis (Ambrogini et al., 2010; Bai et al, 2004; Banfi et al., 2008). Growing evidence indicate that ROS-induced oxidative stress increases with aging and it can have damaging effects on bone homeostasis (Altindag et al., 2008; Almeida et al., 2007; Callaway and Jiang, 2015; Ozgocmen et al., 2007). This observation has also been reported in animal models. Aging mice demonstrate a decline in bone mass and high levels of oxidative stress (Almeida et al., 2007). High levels of oxidative stress can increase osteoclastogenesis, including osteoclast differentiation and maturation, and inhibit osteoblast differentiation and increases osteoblast apoptosis, resulting in reduced bone mass (Almeida et al., 2007; Bai et al., 2004; Garrett et al., 1990). Ovariectomy or the removal of the ovaries is a common surgery in animal models to mimic post-menopausal women with reduced estrogen levels (Almeida et al., 2007). Ovariectomized mice exhibit high levels of oxidative stress and increased loss of bone mass and osteoblast numbers. Treatment with antioxidants inhibit the increased osteoclastogenesis, osteoblast and osteocyte apoptosis and loss in bone mass, further confirming that oxidative stress plays an important role in maintaining bone homeostasis (Ambrogini et al., 2010; Lean et al., 2003; Almeida et al., 2007). FoxOs have been reported to up-regulate key detoxification enzymes including MnSOD (manganese superoxide dismutase),

catalase, and GADD45, thus preventing pathological conditions (Ambrogini et al., 2010; Salih and Brunet, 2008; van der Horst and Burgering,. 2007; Kops et al*.,* 2002; Nemoto and Finkel, 2002).

1.5.2.1 FoxO3a: Defender against oxidative stress in bone

Ambrogini and colleagues demonstrated deletion of FoxO 1, FoxO 3 and FoxO 4 in transgenic mice resulted in significant reduction in bone mass with high levels of reactive oxygen species (ROS) evident by increased phosphorylation of $p66^{shc}$, which is a biomarker for oxidative stress (Ambrogini et al., 2010). They generated transgenic mice with deletion of FoxO 1, FoxO 3 and FoxO 4 in differentiated osteoblasts and these animals exhibited a 60%-75% decrease in calvaria, vertebrae bone mass, rate of bone formation and significantly higher apoptosis of osteoblasts and osteocytes (Ambrognini et al., 2010). In contrast, *in vivo* transgenic female mice with FoxO3a over-expression in mature osteoblasts demonstrated decreased oxidative stress, osteoblast apoptosis, and increased osteoblast number, bone formation rate and mass. These observations support FoxOs is critical for defending oxidative stress and maintaining skeletal homeostasis (Ambrogini et al., 2010).

On the other hand, transgenic mice with deletion of FoxO 1, FoxO 3 and FoxO 4 in osteoblast progenitor cells displayed significant increase in bone mass and cortical thickness in both female and male (Iyer et al., 2013). In a longitudinal study, three FoxOs were deleted in mice at 3 months of age and BMD was measured at 24 months of age. These animals exhibited significant increase in bone mass at spine and femur, suggesting ability of FoxOs to defend against oxidative stress may not be directly involved in age-related bone loss. These authors suggested interplay between FoxOs and Wnt signaling pathway (Iyer et al., 2013). Iyer and colleagues

proposed that FoxOs bind to β-catenin, and this FoxO/β-catenin association decreases the available β-catenin for Wnt signaling. Wnt/β-catenin pathway is important for osteoblastogenesis and promotes proliferation and differentiation of osteoblasts by regulating Runx2, osteocalcin and osteorix (Day et al., 2005). Therefore, by deleting FoxO in mice, Wnt/β-catenin would not be diverted from Wnt/β-catenin activation, and leading to higher bone mass (Iyer et al., 2013).

1.6 Aim of the study

The aim of this thesis is to investigate the role of FoxO3a in osteoblast differentiation and matrix calcification. FoxO3a is the most abundant isoform in bone cells, exhibiting 2-3 fold higher in expression than FoxO1 and FoxO4 assessed by qRT-PCR (Ambrogini et al, 2010). Therefore, we focused on role of FoxO3a in our studies. Several lines of literature reported that FoxO3a plays an important role in maintaining redox balance in bone. Disturbance of the redox balance leads to adverse effects on bone homeostasis, resulting in pathological conditions. However vitamin D regulates Foxo3 expression in bone inferring a potential role in calcium homeostasis independent of oxidative stress. We therefore set out to determine if FoxOs play a role in calcium regulation in bone independent of ROS during osteoblastogenesis.

Hypothesis

We hypothesized that FoxO3a is involved in the regulation of osteoblast differentiation and matrix calcification.

In order to test our hypothesis, the first objective was to develop an *in vitro* cell culture model in MC3T3-E1 to study the process of osteoblast differentiation. Second objective was to characterize important transcription factors and genes including FoxO3a, RXRα, VDR during osteoblast differentiation. Third objective was to identify expression of calcium channels, including L-type ($Ca_v1.2$ and $Ca_v1.3$), and T-type ($Ca_v3.1$), calcium mediators and transporters involved in calcium transport machinery in the current *in vitro* model. Finally, FoxO3a over-expression was generated in MC3T3-E1 cells to study the effects of FoxO3a on differentiation and matrix calcification. We developed specific aims to answer these objectives.

1.6.1 Specific Aim #1

To characterize an *in vitro cell* culture model, MC3T3-E1 cells, during osteoblast differentiation.

1.6.2 Specific Aim #2

To determine the effects of ROS and vitamin D signaling on the expression of genes important for osteoblast calcium handling.

1.6.3 Specific Aim #3

To understand the role of FoxO3a in osteoblast differentiation and calcium handling.

CHAPTER 2: MATERIALS AND METHODS

2.1 Materials

2.1.1 Cell culture

Minimum Essential Medium Eagle (MEM) alpha modification (Gibco Life Technologies, MA, USA) and Hyclone MEM Alpha modification 1x (GE Healthcare Life Sciences, IL, USA) was supplemented with 10% fetal calf serum (FBS) and 1% Penicillin-Streptomycin-Glutamine (PSG) purchased from Thermo Fisher Scientific (MA, USA). Ascorbic acid and β-glycerophosphate were purchased from Sigma-Aldrich (MO, USA). Falcon 15mL and 50 mL Conical Centrifuge tubes (Catalog #352098) were purchased from Corning (Corning Life Sciences, NY, USA). 25 cm^2 rectangular canted neck cell culture flasks with vent cap (Catalog# 430639) and 75 cm^2 rectangular canted neck cell culture flasks with vent cap (Catalog# 430720) were purchased from Corning Life Sciences (NY, USA). 100 mm culture dishes were purchased from Gibco Life Technologies (MA, USA). 6, 12, 24, 48 and 96-well Corning Costar flat bottom cell culture plates were purchased from Sigma-Aldrich (MO, USA). Fisherbrand premium microcentrifuge tubes in 1.5 mL and 2.0 mL were purchased from Fisher Scientific (MA, USA). Pipeman and T.C filters (Catalog# 3-000-051) were purchased from Drummond (PA, USA). Fisherbrand sterile polystyrene disposable serological pipets with magnifier stripe were purchased in 2 mL (Catalog# 13-675-3C; 13-675-2C), 5 mL (Catalog# 13-678-11D; 13-676-10H; 13-676-10C), 10 mL (Catalog# 13-676-10F; 13-678-11E; 13-676-10J) and 25 mL (Catalog# 13-676-10M; 13-678-11; 13-676-10K; 13-678-11PM). Fisherbrand Pasteur pipets (Catalog# 22-042817) were purchased from Thermo Fisher scientific (MA, USA). Protein G Mag Sepharose (Catalog# 28-9440-08) were purchased from GE Healthcare Life Sciences (IL, USA). 6-tube magnetic separation rack (Catalog# S1506S) was purchased from Biolabs Inc, (New England, UK). Cryo vials for frozen cell stocks were purchased from Thermo Fisher

Scientific (MA, USA). Cell scrapers (Catalog#08-771-1A, Fisher Scientific, USA). Microscopic coverslips were 25 mm in diameter, and 0.13 to 0.17 mm in thickness (Catalog# 12-545-102 25CIR-1), Fisherbrand™ Frosted Microscope slides 25 mm in length, 75 mm in width and 1 mm in thickness (Catalog# 12-552) and 18 mm Fisherbrand cover glasses (Catalog# 12-546) were purchased from Fisher Scientific (MA, USA). Mouse FoxO3a cDNA Myc-DDK-tagged (Catalog# MR226631), and pCMV6-Entry Mammalian vector with C-terminal Myc-DDK Tang (Catalog # PS100001) were purchased from Origene (MD, USA).

2.1.2 Laboratory chemicals

Hydrogen peroxide (Catalog #H1009) and 1α, 25-Dihydroxyvitamin D_3 (Catalog# D1530) were purchased from Sigma-Aldrich (MO, USA). Trizol Reagent, random primers and SuperScipt II reverse transcriptase were purchased from Invitrogen (Carlsbad, USA). Protease inhibitor cocktail was purchased from calbiochem (Millipore, USA), and PMSF was purchased from Santa Cruz (USA). Bovine serum albumin (BSA, Sigma-Aldrich A-4503) standard curve. Pierce microBCA kit (Catalog# 23235, ThermoFisher Scientific, USA). 2x Lameli sample buffer (Catalog# 1610737, Bio-Rad). Protein marker excel/band (SMOBIO, Taiwan), precision all plus protein standards (Biorad, USA), and PageRuler prestained protein ladder (Thermo, USA). Reagents for making SDS-PAGE include Tris-HCl, 30% Acrylamide/Bis Solution 37.5:1 2.6% crosslinker, 10% Ammonium Persulfate (APS) were purchased from *Bio-Rad* Laboratories (Hercules, CA). SDS was purchased from Thermo Scientific and TEMED was purchased from Fisher Bioreagents (USA). Immobilon PVDF membrane (Catalog# IPVH00010) was purchased from Millipore (MA, USA). Amersham ECL Western Blotting Detection Reagent (Catalog#45-000-875) was purchased from GE Healthcare Life Sciences (IL, USA) Amersham ECL Prime

Western Blotting Detection Reagent (Catalog# 45-002-401) was purchased from GE Healthcare Life Sciences (IL, USA) and Laminata Crescendo Western HRP Substrate was purchased from Millipore (MA, USA). Restore Western Blot Stripping Buffer (Catalog #21059) was purchased from Thermo Fisher Scientific (MA, USA). 4% PFA was purchased from Canemco (Catalog# 0173). Fluorescence mounting medium DAKO (Catalog# S3023) was purchased from VWR (PA, USA). Fura-2AM (Catalog # F1221) was purchased from Molecular Probes (OR, USA). DMSO was purchased from Sigma-Aldrich and Pluronic F-125 (Catalog# P3000MP) was purchased from Molecular Probes (OR, USA). Ionomycin from *Streptomyces conglobatus* ≥n98% (HPLC) (Catalog# I9657) was purchased from Sigma-Aldrich Canada (Oakville, ON). Alexa Fluor phalloidin (Catalog#A12379 3000) and DAPI (Catalog# D1306) were purchased from Invitrogen Molecular probes (CA, USA). 2',7'-dichlorodihydrofluorescein diacetate (DCFH-DA) was purchased from Sigma-Aldrich Canada (ON, Canada).

2.1.3 Antibodies

Primary antibodies: anti-FoxO3a (D19A7) rabbit mAb (Catalog# 12829), phospho-FoxO3a (Ser318/321) rabbit mAb (Catalog# 9465), phospho-FoxO1 (Thr24)/FoxO3a (Thr32) rabbit mAb (Catalog# 9464), anti-myc-tag (9B11) mouse mAb (Catalog# 2276) and β-Actin (13E5) rabbit mAb (Catalog# 4970) were all from Cell Signaling (MA, USA). Anti-FoxO3a antibody-ChIP Grade (Catalog# ab12162), Anti-retinoid receptor alpha, anti-RXRα (Catalog# ab125001), anti-vitamin D receptor, VDR (Catalog# ab3508) and anti-c-Myc (Y69) rabbit mAb (Catalog# ab32072) were purchased from abcam (MA, USA). Anti-calbindin D_{9K} rabbit mAb and anti-calbindin D_{-28K} rabbit mAb were purchased from Swant Inc. (*Marly 1* ,Switzerland). Secondary antibodies: Immun-star goat anti-rabbit (GAR)-HRP Conjugate (Catalog# 170-5046) from Bio-

Rad Laboratories (ON, Canada), and goat anti-rabbit IgG-HRP linked (Catalog# 7074S) from Cell Signaling (MA, USA). Cy3 donkey anti-rabbit monoclonal antibodies (Catalog# 703-165-155) was purchased from Jackson ImmunoResearch Laboratories Inc (PA, USA).

2.1.4 Ca^{2+} channel antagonists

Felodipine (Catalog# F9677), Benzamil hydrochloride hydrate (Catalog# B2417), (1S,2S)-2-(2-(N-[(3-Benzimidazol-2-yl)propyl]-N-methylamino)ethyl)-6-fluoro-1,2,3,4-tetrahydro-1-isopropyl-2-naphtyl cyclopropanecarboxylate dihydrochloride hydrate, NNC 55-0396 hydrate (Catalog# N0287), Ruthenium Red (Catalog# R275-1) and Lanthanum chloride were all purchased from Sigma-Aldrich Canada (ON, Canada).

2.1.5 Laboratory equipment and software

Thermo Forma 3110 CO_2 water jacketed incubator and HEPA filter (Catalog# 760175) purchased from Thermo Fisher Scientific (MA, USA). Eppendorf 5810 R refrigerated centrifuge used to spin down cells equipped with rotor model Eppendorf A-4-62 and Sorvall Legend XT centrifuge were both purchased from Thermo Fisher Scientific (MA, USA). Microfuge 22R centrifuge and microfuge 18 centrifuge were purchased from Beckman Coulter (CA, USA). ManSci mini centrifuge was purchased from ManScin Inc (FL, USA). Microplate shaker and tube rotator were purchased from VWR (PA, USA). Fixed speed vortex mixer was purchased from Fisher Scientific (MA, USA). Cell handling was performed in Canadian cabinets model number BM6-2A purchased from Johns Scientific Services (ON, Canada). Metallized haemacytometer hausser bright-line was purchased from Hausser Scientific (PA, USA). ABI Prism 7900 HT Sequence Detection System was purchased from Applied Biosystensm (CA,

USA). Casting stand, gel cassette assembly, casting frames and 10 wells 1.5 mm and 15 wells 1.5 mm combs were all purchased from Bio-Rad Laboratories (Mississauga, ON). Vertical gel electrophoresis equipment, PowerPac™ HC High-Current Power Supply was purchased from Bio-Rad Laboratories (Mississauga, ON). Nanodrop 2000C Spectrophotometer (Catalog# ND-2000C) was purchased from Thermo Fisher Scientific (MA, USA). Isotemp digital-control water bath models 210 was purchased from Fisher Scientific (MA, USA). Beckman Coulter pH meter model pHi 510 was purchased from Beckman Coulter (CA, USA). Fisher Scientific accumet AB15 basic and biobasic pH/mV/ °C meter was purchased from Fisher Scientific (MA, USA). ImageQuant LAS 4000 mini purchased GE Healthcare Life Sciences (IL, USA) and ChemiDoc MP Imaging System with Image Lab™ Software (Catalog# 17001402) was purchased from Bio-Rad Laboratories (Mississauga, ON). Spectrophotometric measurements were made with Bio-Tek Synergy H1 Hybrid Multi-Mode Microplate Readers purchased from Bio-Tek Instruments (VT, USA), ELx808 Absorbance Reader from BioTek (VT, USA) and Leica DMI6000B was purchased from Leica Microsystems (Wetzlar, Germany). Angstrom Illumination system was purchased from Quorum Technologies Inc (ON, Canada), OptiGrid structured illumination was purchased from Qioptiq (ON, Canada), excitation and emission filter wheels were purchased from Ludl Electronic Products (NY, USA) and a Flash 4.0 camera was purchased from Hamamatsu, (Hamamatsu, Japan). Metamorph software was purchased from Molecular Devices (CA, USA). GraphPad Prism version 7.00 for Mac was purchased from GraphPad Software (CA, USA, www.graphpad.com).

2.2 Methods

2.2.1 Cell culture

MC3T3-E1 cells were cultured in α-MEM culture medium supplemented with 10% fetal calf serum (FBS) and 1% Penicillin-Streptomycin-Glutamine (PSG). Pre-osteoblasts underwent differentiation to osteoblasts by adding 50 μg/ml ascorbic acid and 10 mM β-glycerophosphate to the culture media. RNA and protein lysates were harvested from cell culture under incubation for 1 day, 3 days or 7 days (**Figure 2. 1**). Both ascorbic acid and β-glycerophosphate, or β -GP were dissolved in autoclaved deionized water to make 5 mg/ml ascorbic acid and 1M β –GP stocks which were kept in aliquots and frozen until the day of experiment. 0.25% Trypsin-1 mM EDTA was used to detach adherent cells for passaging and a hemocytometer was used to count cells for seeding at 0.5-2x10,000 cells/cm^2. Once cells were detached, they were transferred to a Falcon 50 mL Conical Centrifuge tube and spun down at 1000 rpm for 5 minutes at 22°C. Old culture media was discarded and replaced with fresh culture media. Cells were pipetted up and down gently and transfer to 25 cm^2 or 75 cm^2 rectangular canted neck cell culture flasks. Cell cultures were maintained at 37°C in the presence of 5% CO_2 in an incubator. Aliquots of cells were kept frozen at a cell density of 1 x 10^6 cells/ml in cryo vials in liquid nitrogen tanks.

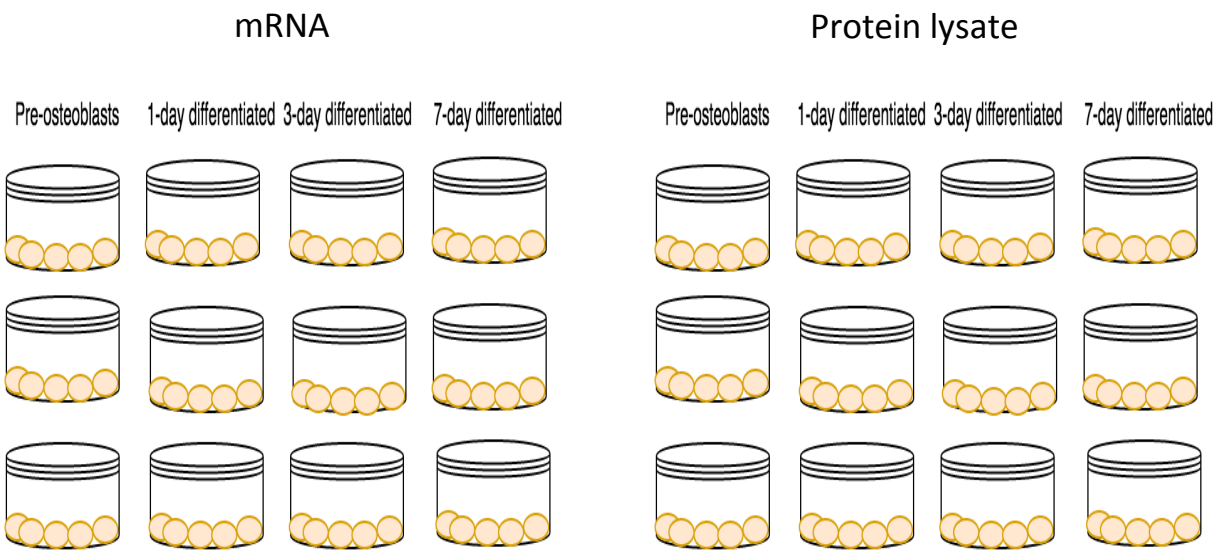

Figure 2.11 MC3T3-E1 cell culture scheme

MC3T3-E1 cells were grown on dishes as pre-osteoblasts without differentiating medium, immature osteoblasts and osteoblasts grown in differentiating medium for 3 and 7 days, respectively. mRNA was harvested with TRIzol and protein lysates collected with RIPA buffer to assess gene expression in pre-osteoblasts, 1-day, 3-day, and 7-day differentiated osteoblasts.

2.2.1.1 Drug treatment matrix

7-day differentiated osteoblasts were given various drug treatment shown in **Figure 2. 1**. First well served as control, next well of cells were treated with 10^{-7} M $1,25D_3$ for 24 hours with a dose change every 12 hours. Next well was treated with 250 μM H_2O_2 for an hour and last well was treated with combination of $1,25D_3$ with H_2O_2.

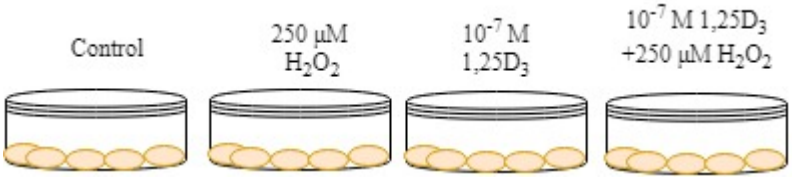

Figure 2. 1 Drug treatment matrix in 7-day differentiated MC3T3-E1 cells

Cells were treated with freshly prepared $1,25D_3$ and H_2O_2 were treated.

2.2.1.2 Measurement of intracellular reactive oxygen species (ROS)

Various concentrations of H2O2 were added to pre-osteoblasts and 7-day differentiated osteoblasts to induce reactive oxygen species (ROS). ROS levels were measured with 2',7' – dichlorofluorescin diacetate (DCFDA). DCFDA is a cell-permeant fluorescent dye that measures hydroxyl, peroxyl and other ROS activity within the cell (**Figure 2. 2**). After diffusion into the cell, DCFDA was deacetylated by cellular esterases to a non-fluorescent compound, which was then oxidized by ROS into 2', 7' –dichlorofluorescein (DCF). DCF is a highly fluorescent compound with a maximum excitation and emission spectra of 495 nm and 529 nm respectively to be quantified by by Bio-Tek Synergy H1 Hybrid Multi-Mode Microplate Reader (**Figure 2. 2**).

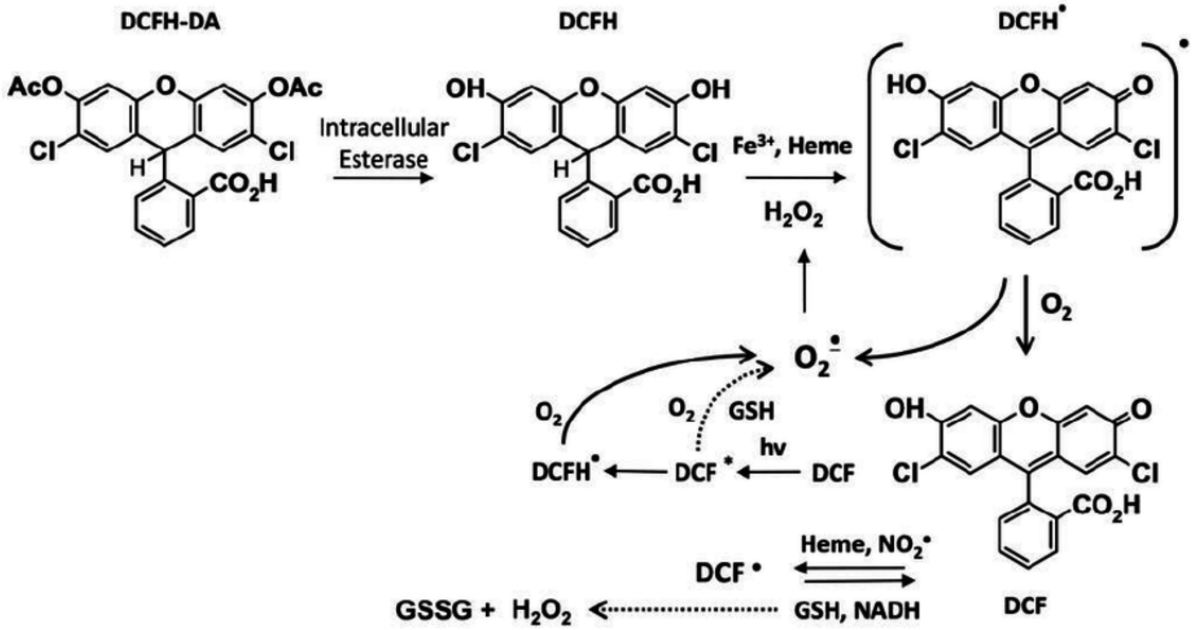

Figure 2. 2 3 2',7'-dichlorodihydrofluorescein diacetate (DCFDA) to assess formation of reactive oxygen species (ROS)

DCFH-DA, non-fluorescent compound, is deacetylated by intracellular esterase to DCFH and it reacts with ROS to DCF, a highly fluorescent compound that can be detected by fluorescence spectroscopy (Chen et al., 2010).

2.2.1.3 Cell viability assay

Cell viability was determined by Thiazolyl Blue Tetrazolium Bromide, MTT, a colometric assay used to measure cell proliferation (Berridge and Tan, 1993). Spectrophotometric measurements were made with ELx808 Absorbance Reader.

2.2.2 Real-time quantitative PCR

Total RNA was isolated with Trizol Reagent according to the manufacturer's instructions. Protocol was adopted from the Alexander lab with modifications (Pan et al., 2012). RNA was quantified by UV spectroscopy at 260 nm on a nanoPhotometer and purity was determined at 260/280 nm ratio. 1 μg of RNA was reverse transcribed using random primers and SuperScipt II reverse transcriptase. Subsequence cDNA was used to determine FoxO3a, RXRα, VDR, Runx2, OCN (bglap), L-type calcium channel $Ca_v1.2$ (cacna1c), $Ca_v1.3$ (cacna1d), T-type calcium channel $Ca_v3.1$ (cacna1g), calcium-sensing receptor (casr), calbin-D_{9K} (S100g), calbindin-D_{28K} (calb1), the plasma membrane Ca^{2+}-ATPase (PMCA1b), the sodium/calcium exchanger, member 1 (NCX1, Slc8a1), transient receptor potential 5 (Trpv5), transient receptor potential (Trpv6), claudin-2, claudin-12, claudin-14 mRNA levels. Housekeeping gene 18s mRNA levels were used as internal control. Primers and probes used to evaluate gene expression are listed in **Table 2.1.** For statistical analysis, One-way ANOVA followed by Tukey multiple comparisons test or student t-test as appropriate were performed using GraphPad Prism version 7.00 for Mac, (GraphPad Software, La Jolla California USA, www.graphpad.com).

Table 2.1 Primers and probe sequences

FoxO3a	Forward: CGTTGTTGGTTTGAATGTGGG
	Reverse: GGTTTTCTCTGTAGGTCTTCCG
	Probe: TGCCCATTTCCCCTTTCCTCAGT
RXRα	Forward: GCCCAAGACTGAGACATACG
	Reverse: AGCTCAGAAAAGTGTGGGATC
	Probe: AGCTCACCAAATGACCCTGTTACCAA
VDR	Forward: GTCAGTTACAGCATCCAAAAGG
	Reverse: AGGTAAAAGACTGGTTGGAGC
	Probe: TGGCACTTGACTTAAGCAGGACAATCT
Runx2	Forward: GCTATTAAAGTGACAGTGGACGG
	Reverse: GGCGATCAGAGAACAAACTAGG
	Probe: CGGGAAACCAAGAAGGCACAGACA
OCN (bglap)	Forward: CACCTAGCAGACACCATGAG
	Reverse: GTTCACTACCTTATTGCCCTCC
	Probe: ACCTCACAGATGCCAAGCCCA
$Ca_v1.2$	Forward: AGCGACAAAAGGATCAAGGG
	Reverse: GGGAATGTGGTAGGAGAATGG
	Probe: CATTGGCAGTGGCAGGVTTGAG
$Ca_v1.3$	Forward: AGTCAACCAGATAGCCAACAG
	Reverse: TCCTCTTCCTCTTCACCTACTG
	Probe: CCCTTACCCGCCCTGTGATGT
$Ca_v3.1$	Forward: TGGTGACAACTGGAATGGTATTA
	Reverse: CACGAAGTAGATGGGTGAGATG
	Probe: ACGGTGTTGTAGCAGGTGGACTC
Calcium-sensing receptor (casr) exon 3	Forward: GGAGTAGCAGCCAAAGATCAA
	Reverse: GGAAGGACTTGAACTGGTTCTTA
	Probe: CGTAGCTCACCTGATGCACTCCAC
Calcium-sensing receptor (casr) exon 6-7	Forward: TTTGAGTGTGTGGAGTGTCC
	Reverse: GGTTCTCATTGGACCAGAAGT
	Probe: AGTGGTGAGACAGATGCGAGTGC
Calcium-sensing receptor (casr) exon 5	Forward: GGTCCTGTGCAGACATCAA
	Reverse: CAATGATGCCCTTCCTGGT
	Probe: CTGGCAGGTGCCCTTCTCCAA
Calbin-D9K (S100g)	Forward: TGGATAAGAATGGCGATGGAG
	Reverse: GCTAGAGCTTCAGGATTGGAG
	Probe: ACAGCACCTACTGATTGAACGCACG
Calbindin-D28K (calb1)	Forward: AGAACTTGATCCAGGAGCTTC
	Reverse: CTTCTGTGGGTAAGACGTGAG

	Probe: AGGCTGGATTGGAGCTATCACCG
PMCA1b	Forward: CGCCATCTTCTGCACCATT
	Reverse: CAGCCATTGCTCTATTGAAAGTTC
	Probe: CAGCTGAAAGGCTTCCCGCCAAA
NCX (slc8a1)	Forward: TGGTCTGAAAGATTCCGTGAC
	Reverse: AGTGACATTGCCTATAGACGC
	Probe: AGCTACCCAGGACCAGTATGCAGA
Trpv5	Forward: : CGCTCTGGTATCTGTGGTTG
	Reverse: TGCTCTTGTACTTCCTCTTTGTC
	Probe: CGTAAGAACCAACGGTCTCCCAGG
Trpv6	Forward: ATGGCTGTGGTAATTCTGGG
	Reverse: AGGAAGAGTTCAAAGGTGCTG
	Probe: AGAGGATCCCGTGAGCTGGGTC
Trpv 6 (set 2)	Forward: CTGTCTCCTCC
	Reverse: TCACACACCTTCCCACAATC
	Probe: CACAGAACTCTTCCCAGGGTGCTC
Caludin-2	Forward: GCTTGTGACCCCTTGGAC
	Reverse: CTCCTTACAAGTATCTGTGGGTG
	Probe: CGTTCGCCTTTCTCTGGACCTAGT
Claudin-12	Forward: TCGCCAGAACGCACTTC
	Reverse: TGAACTCAGATGCAACAGGAG
	Probe: ATCCCGCTCACCCACTCCG
Claudin-14	Forward: TGGCATGAAGTTTGAAATCGG
	Reverse: CGGGTAGGGTCTGTAGGG
	Probe: TGAGAGACAGGGATGAGGAGATGAAGC
18s	Forward: GAGACTCTGGCATGCTAACTAG
	Reverse: GGACATCTAAGGGCATCACAG
	Probe: TGCTCAATCTCGGGTGGCTGAA

Primers purchased from Integrated DNA Technologies (IDT): mCaSr Exon6-7 RT primers, N009789.1.pt.mS100g(Calb9K), mCa$_v$1.2, mCa$_v$1.3, mCa$_v$3.1, Casr exon 3 our RT primer, Casr exon 5 out RT primer, Casr exon 6-7 full RT primer, mCldn12 real-time, mCLDN14-TmRT, N019740.1.pt.Foxo3, N011406.1.pt.mSlc8a1(NCX), mPMCA 1, Rxra, mouseTrpv5 qPCR, N022413.1.pt.mTrpv6, Trpv6 (set2), Runx2, mBglp2 (OCN).

Primers purchased from Applied Biosystems (AB): Rn18s (m-18s), and Vdr.

2.2.3 Immunoblotting

2.2.3.1 Protein Preparation

Protocol was adopted from the Alexander lab with modifications (Pan et al., 2012). Cells were washed three times with 1x Phosphate-buffered saline (PBS) and total protein was harvested freshly with radioimmunoprecipitation assay (RIPA) buffer pH7.4 (50mM Tris Base, 150mM NaCl, 1mM EDTA, 1% Triton X-100, 0.1% SDS, 1% NP-40, 1% protease inhibitor and phenylmethane sulfonyl fluoride (PMSF). Protease inhibitor cocktail and PMSF were added freshly to RIPA buffer on the day of the experiment. Protein lysate was scraped from the plate with cell scrapers, collected and sonicated with a mixer. Protein lysate was then centrifuged at 13,000 revolutions per minute (RPM) for 5 minutes at 4°C. Supernatant containing protein was collected and the pellet then discarded. Protein concentration was determined with a Nanodrop 2000C Spectrophotometer at 280nm absorbance with a bovine serum albumin (BSA) standard curve. Pierce microBCA kit was also used to determine protein concentrations following manufacturer's instructions. 2x Lameli sample buffer was used in 1:1 ratio with reducing agent 2-Mercaptoethanol, and samples were heated to 95°C for 5 minutes for FoxO3a, RXR immunoblotting. Other samples, including the calbidin-D_{9K} and vitamin D receptor (VDR) were incubated at 37°C for 10 minutes.

2.2.3.2 Sodium dodecyl sulfate polyacrylamide gel electrophoresis (SDS-PAGE)

SDS-PAGE was performed with 12% separating gel and 4% stacking gel for all proteins. Calbidin-D_{9k} immunoblotting was performed with a 15% separating gel and 4% stacking gel. Gels were made with 1.5M Tris-HCl pH 8.8, 1.5 M Tris-HCl pH 6.8, 30% Acrylamide/Bis Solution 37.5:1 2.6% crosslinker, 10% Ammonium Persulfate (APS), 20% SDS and TEMED.

pH was measured with a Beckman Coulter pH meter model pHi 510. Gels were run with ladders including Protein marker excel/band, precision all plus protein standards, and PageRuler prestained protein ladder were used.

PowerPac™ HC High-Current Power Supply, a vertical gel electrophoresis equipment was used to run gels. A casting stand secured the gel cassette assembly, casting frames were used hold gel cassettes together and 10 wells 1.5 mm and 15 wells 1.5mm combs were used to make wells in the polymerized gel. Electrode assembly holding gel cassette sandwich was filled with 1x running buffer inside and an anode banana plug (red) and cathode banana plug (black) on the lid were set in place to ensure current flowing through in the appropriate direction. 10x running buffer was made up of the following ingredients in 1L: Tris 30.3 g, glycine 144 g, SDS 10 g. SDS-PAGE gels were run at 80 V for an hour and a half and then immediately proceeded to be transferred. Protein was transferred onto an Immobilon PVDF membrane activated prior with methanol.

Transfer occurred at 80 V for an hour and fifteen minutes at 4 °C in 1X transfer buffer with methanol. 1x transfer buffer was made up of the following ingredients in 1L: Tris 3.03 g, glycine 14.4 g and 200 mL methanol. Once the transfer was complete, membranes were washed three times with deionized water for 5 minutes each, and membranes stained with 0.1% ponceau R to confirm successful transfer of proteins to the PVDF membranes. Once the transfer was confirmed to be successful, membranes were then incubated in 5% non-fat milk for either an hour at room temperature or overnight at 4 °C in order to reduce non-specific binding. Membrane blots were then washed three times with 1x TBS-Tween for 5 minutes each at RT and then immediately proceeded to incubation with primary antibody at 1/1000 dilution at RT for an hour or 4°C overnight on a rotator. Membranes were then washed three times with 1x TBS-

Tween for 5 minutes each at RT before putting into 5% non-fat milk containing secondary antibody. Membranes were incubated with secondary antibody for an hour on a rotator at RT. Membranes were then washed three times with 1x TBS-Tween for 5 minutes each at RT before imaging. Proteins on membranes were visualized via chemiluminescence detection method with ImageQuant LAS 4000 mini and ChemiDoc. Restore Western Blot Stripping Buffer was used to strip membranes for re-probing. Membranes were incubated with the stripping buffer for 10 minutes at RT with gentle shaking followed by washing in 1x TBS-Tween for 10 minutes at RT with gentle shaking. Membranes were then blocked with 5% non-fat milk and re-probed with antibodies. Quantification of relative band intensity was performed with Image J Software and Image Lab™ software. For statistical analysis, One-way ANOVA followed by Tukey multiple comparisons test or a student t-test were performed using GraphPad Prism version 7.00 for Mac.

2.2.4 Immunofluorescence

Protocol was adopted from the Alexander lab with modification (Dimke et al., 2013). Cells were seeded on 25 mm glass coverslips which were plated in 6-well plates. Cells were first washed three times with cold 1x PBS with 1mM $CaCl_2$ and 1mM $MgCl_2$, pH 7.4. Cells were then fixed with 4% paraformaldehyde (PFA) for 20 minutes at room temperature with gentle shaking followed by a 5% glycine quenching. The cells were next blocked with 5% milk with 0.2% Triton X-100 with gentle shaking for an hour at RT. Triton X-100 was used to permeabilize the membrane. Blocking solution was then removed, and followed by an incubation with primary antibodies at 1/1000 dilution for an hour with gentle shaking at RT. Primary antibodies employed were: anti-FoxO3a (D19A7) rabbit mAb, and anti-FOXO3A rabbit polyclonal antibody. At the end of incubation, cells were washed three times with 1x PBS. Secondary

antibody Cyanine Cy3 donkey anti-rabbit monoclonal antibodies was applied at a dilution of 1/1000 for an hour at RT with gentle shaking. Actin was stained with Alexa Fluor phalloidin and nucleus was stained with 4', 6'-Diamidino-2-Phenylindole, Dihydrochloride (DAPI). After incubation, cells were washed three times with 1x PBS. Coverslips were mounted on a microscope slide with DAKO. Cells were analyzed 24 hours after mounting on Leica DMI6000. This system is equipped features including OptiGrid structured illumination excitation and emission filter wheels, a Flash 4.0 camera and operated by Angstrom Illumination system.

2.2.5 Ratiometric Calcium Imaging

2.2.5.1. Fura-2AM

The rate of calcium uptake into MC3T3-E1 cells was determined with Fura-2AM, a ratiometric fluorescent dye. Cellular esterases would cleave off acetohexyomethal upon entering the cell, liberating a fluorescent compound remains in the cytosol (**Figure 2. 3A**). When Fura-2 binds with Ca^{2+}, there is an absorption shift from 380 nm (Ca^{2+}–free) to 340 nm (Ca^{2+} –bound) while fluorescence emission maximum stays relatively unchanged. Ratios of fluorescence at 340/380 correspond directly to calcium levels intracellularly (**Figure 2. 3B**). Fura-2 AM was dissolved in DMSO with 0.1% Pluronic F-125, which was used to enhance Fura-2 AM uptake into the cells.

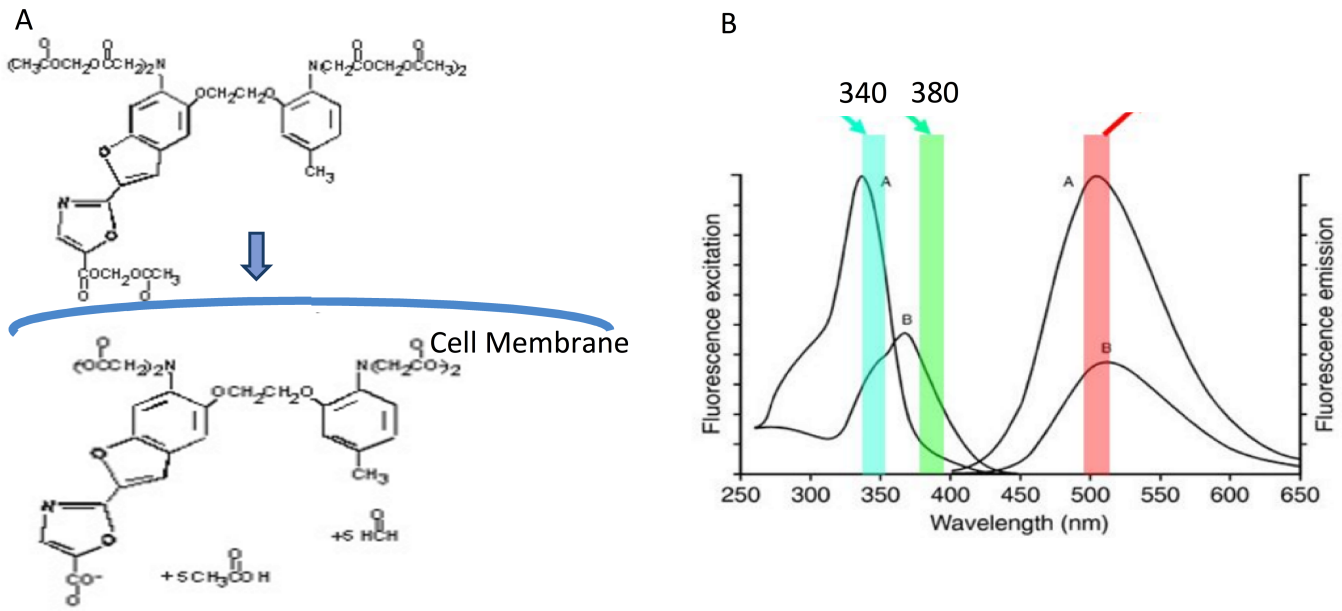

Figure 2. 3 Chemical structure of Fura-2 AM and excitation/emission spectrum

(A). Fura-2 AM undergoes de-esterification as it enters cell membrane. (B) Excitation at 340/380 nm, emission at 510 nm. Image taken from European molecular biology laboratory https://www.embl.de/eamnet/html/calcium/ratio.htm with minor modifications.

2.2.5.2 Ratiometric calcium imaging set-up

Ratiometric calcium imaging set-up is shown in **Figure 2. 4**. Fluorescent microscope Leica DMI6000B is placed in the middle, excitation filters (340/380 nm) are placed on the left platform (**Figure 2. 5A**), emission filters and Flash 4.0 camera are placed next to the microscope. Buffers were maintained at 37°C on the hotplate and perfusion tubes were maintained at 37°C. Real-time measurements were conducted on the computer on the table.

Figure 2. 4 Ratiometric calcium imaging set-up

Fluorescent microscope Lecia DMI6000B is placed in the middle, perfusion tubes were maintained at 37°C. Measurements were done live on the computer attached to the microscope.

2.2.5.3 Preparation for imaging

Pre-osteoblast MC3T3-E1 cells were seeded onto 25 mm coverslips as pre-osteoblast cells, and these coverslips were placed in 6-well plates. Confluent cells underwent differentiation with ascorbic acid and β-glycerophosphate for 7 days. On the day of the experiment, coverslips with cells attached on the surface were moved gently with tweezers to a small culture dish (**Figure 2. 5B**) followed by three washes with 1x PBS. Fura-2 AM at 1/1000 dilution was then added and incubated for 30 min with gentle shaking, protected from light. After incubation with FURA-2AM, coverslip was moved gently with tweezer to the apparatus (**Figure 2. 5C**) and placed on the microscope. Changes in ratio intensities of 340/380 nm can be directly visualized on the computer screen (**Figure 2. 5D**).

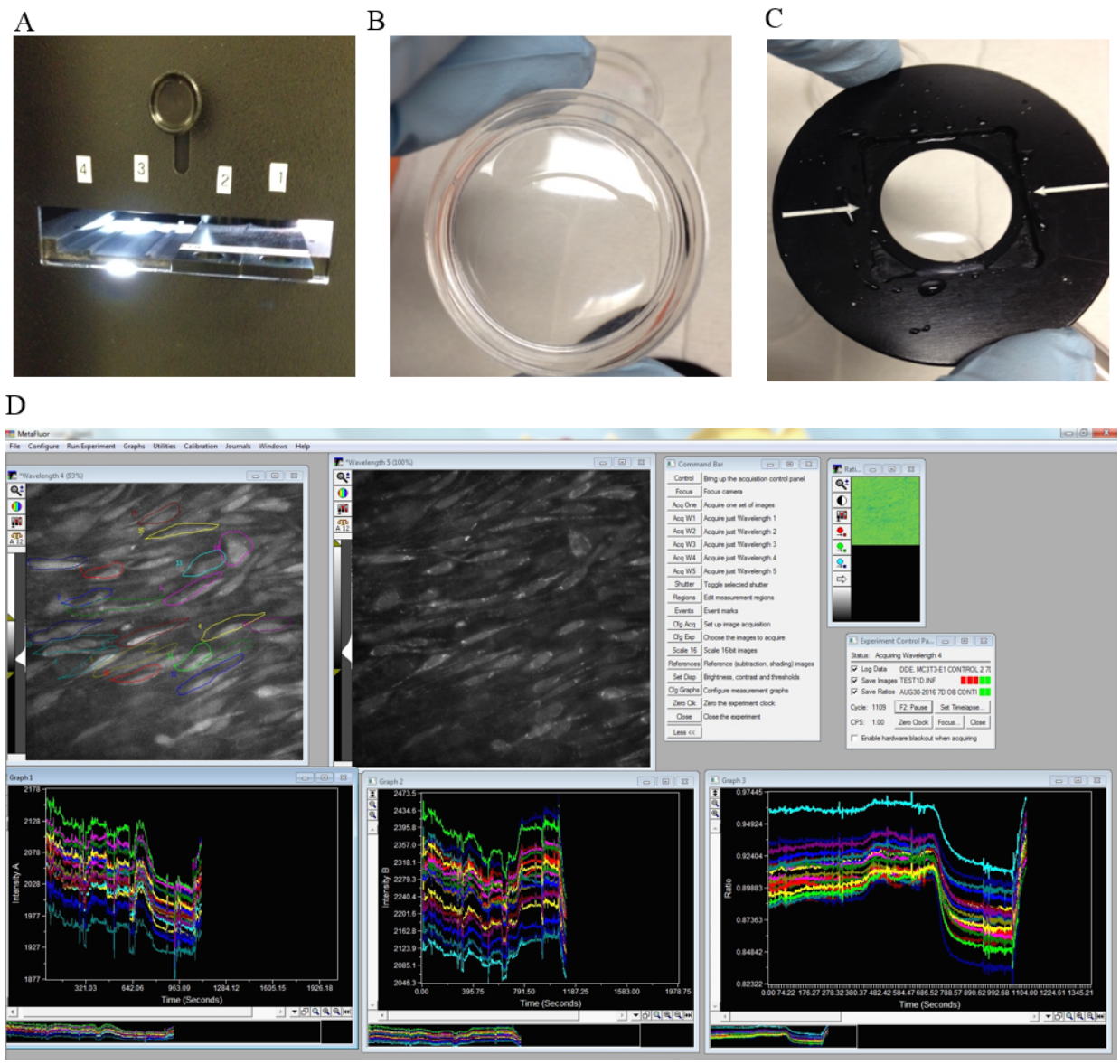

Figure 2. 5 Fura-2AM calcium imaging in 7-day differentiated MC3T3-E1 cells

(A). Excitation filters at 340 nm and 380 nm.

(B). Cells grown on coverslips were incubated with Fura-2AM at room temperature for half an hour with gentle shaking protected from light.

(C). Coverslips were moved onto the apparatus and ready for imaging.

(D). Live monitor of real-time changes in intracellular calcium levels.

2.2.5.4 Ca^{2+} uptake protocol

Protocol we followed was a modified version from Miederer and colleagues (Miederer et al., 2015) shown in **Figure 2. 6**. This protocol first goes through three steps of Ca^{2+} perfusion followed by three steps of calibration. Cells were first perfused in 0.5 mM $CaCl_2$ with 140 mM NaCl, 3 mM KCl, 1 mM $MgCl_2$, 5 mM Hepes for 5 minutes until a stable ratio signal was reached, then external calcium concentration was raised to 3.0 mM $CaCl_2$ with 140 mM NaCl, 3 mM KCl, 1 mM $MgCl_2$, 5 mM Hepes for 5 minutes, and then cells were switched to Ca^{2+}-free buffer containing140 mM NaCl, 3 mM KCl, 3 mM $MgCl_2$, 5 mM Hepes, 1mM EGTA for 5 minutes before switching back to first buffer of 0.5 mM $CaCl_2$. Calcium uptake was measured in the first 30 seconds after cells were switched back to 0.5 mM $CaCl_2$. Calcium channel antagonists were applied during this step, indicated by red arrow in **Figure 2. 6**. Followed by three steps of calibration with ionomycin from *Streptomyces conglobatus* ≥ 98% (HPLC) in Ca^{2+}-free, 10 mM $CaCl_2$, and 2.0 mM $CaCl_2$ with $MnCl_2$ to quench the reaction. Ionomycin was used to permeabilize cells to equalize internal and external calcium concentrations. Ionomycin was prepared by dissolving in acetonitrile as 10 mM stocks and stored at -20°C. Fresh ionomycin was used fresh on the day of the experiment for all measurements. All above buffers were adjusted to pH 7.4 with 2M Tris with a pH meter. Absolute [Ca^{2+}] was quantified from 340/380 ratio intensity with the conversion equation in **Figure 2. 7** developed by Grynkiewicz and colleagues (Grynkiewicz et al., 1985).

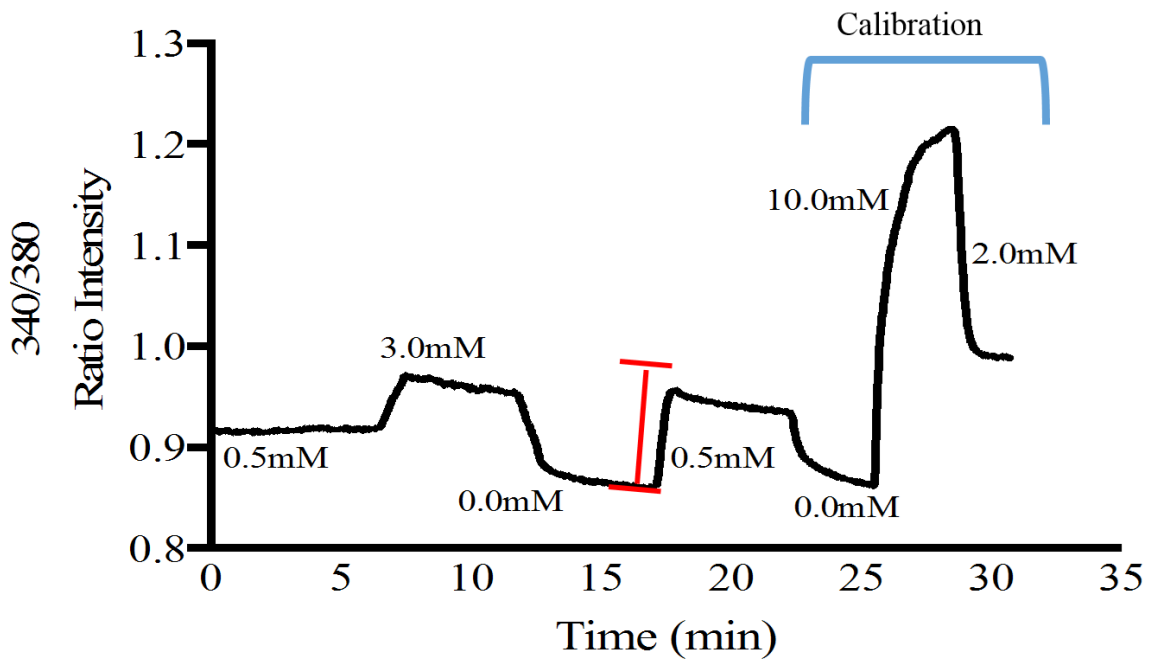

Figure 2. 6 Protocol for measuring Ca^{2+} uptake in MC3T3-E1 cells

$$[Ca^{2+}] = K_d \frac{(R - R_{min})}{(R_{max} - R)} \text{ (Sf2/Sb2)}$$

Figure 2. 7 Grynkiewicz equation for measuring intracellular Ca^{2+}

K_d: Disassociation constant of indicator (for Ca^{2+} binding to Fura-2 at 37°C) = 225 nM, R= 340/380 ratio, R_{max}= 340/380 ratio under Ca^{2+}-saturating conditions, R_{min} = 340/380 ratio under Ca^{2+}-free conditions, and sfb = ratio of baseline fluorescence (380 nm) under Ca^{2+}-free and –bound conditions.

2.2.5.5 Calcium channel antagonists

Felodipine was used to inhibit L-type calcium channels and was prepared by dissolving in DMSO as 10 mM stocks. On the day of the experiment, 10 μM was prepared from a10 mM stock, making the final DMSO concentration in solution 0.001 % , which was applied to 7-day differentiated MC3T3-E1 cells. (1S,2S)-2-(2-(N-[(3-Benzimidazol-2-yl)propyl]-N-methylamino)ethyl)-6-fluoro-1,2,3,4-tetrahydro-1-isopropyl-2-naphtyl cyclopropanecarboxylate dihydrochloride hydrate, NNC 55-0396 hydrate, used to inhibit $Ca_v3.1$, a T-type calcium channel was dissolved in autoclave deionized water as 10 mM stocks. On the day of the experiment, a 10 μM solution was prepared fresh from the stock and applied to the 7-day differentiated MC3T3-E1 cells. Ruthenium Red, a TRPV channel blocker was dissolved in autoclaved deionized water as 10 mM stocks and prepared fresh on the day of experiment as a 100 μM solution. Lanthanum chloride ($LaCl_3$), a non-specific cationic blocker was dissolved in autoclave deionized water as 1 M stock and prepared freshly on the day of experiment as 100 μM solution. All of the above channel inhibitors were stored at -20°C, except NNC 55-0396 hydrate, which was stored at 4°C. All antagonists were added fresh to the buffer on the day of the experiment.

2.2.6 Calcium deposition assay by Alizarin Red Staining

Ability of MC3T3-E1 cells to deposit calcium *in vitro* was assessed by Alizarin red staining (ARS). Sodium 1,2-dihydroxyanthraquinone-3-sulfonate, known as Alizarin Red S (ARS) is a widely used histological method of mineralization to detect calcium compounds in culture. Protocol was adopted from Wu and Frosling, 1992 and Gregory et al., 2004 (Wu and Frosling, 1992; Gregory et al., 2004). Cells were grown in 6-well plates to confluency and underwent drug treatment described previously in section **2.2.1.1**. Cell layers were washed three times with

1x PBS and stained with ARS, resulting in a copper colour (**Figure 2. 8A**). This stained monolayer was gently scraped off with a cell-scraper and transferred to an Eppendorf tube (**Figure 2. 8B**). Tube was centrifuged and the stained cell layer was discarded (**Figure 2. 8C**). Finally, 150 μM of each sample was loaded on a 96 well-plate along with standard prepared from serial dilutions (**Figure 2. 8D**). A standard curve with absorbance 405 nm on the y-axis and calcium concentration in units of μg/ml on the x-axis was generated to determine [Ca^{2+}] in the samples (**Figure 2. 8E**).

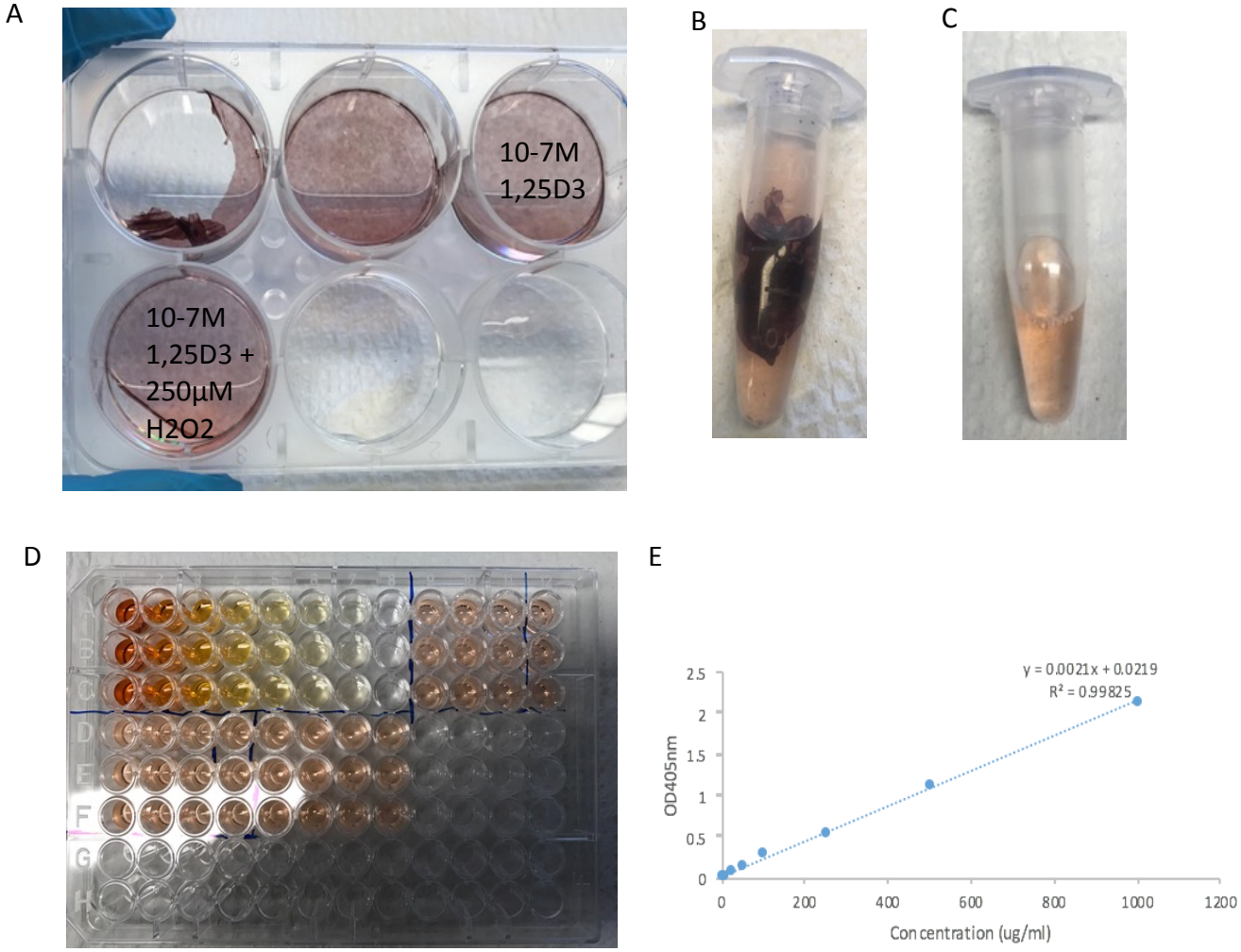

Figure 2. 8 Alizarin Red S (ARS) staining in 7-day differentiated MC3T3-E1 cells

(A). ARS was performed for three treatment groups with one control was performed. ARS stained the monolayer of osteoblasts that can be scrapped off with a cell scraper

(B). Monolayer was scrapped-off and 10% acetic acid was used to liberate calcium from the matrix

(C). Monolayer was eliminated, leaving only calcium ions in acetic acid

(D). Treatment groups were loaded on a 96-well plate along with standards and read at 405 nm

(E). A standard curve was plotted for calculating calcium levels in treatment groups

2.2.7 Co-Immunoprecipitation (Co-IP)

Protein G Mag Sepharose, magnetic beads, were used to pull down FoxO3a or RXRα antibodies. These magnetic beads were placed in Eppendorf tubes with FoxO3a or RXRα antibodies and placed on a 6-tube magnetic separation rack. Anti-FoxO3a (D19A7) rabbit mAb was used to pull down RXRα proteins and anti-RXR α antibodies were used to pull down FoxO3a proteins. After pull-down, lysate was washed three times with 1x PBS and proceeded to immunoblotting. Potential interaction was verified with both anti-FoxO3a and anti RXRα antibodies, followed by secondary antibodies including donkey anti-rabbit IgG-HRP and goat anti-rabbit IgG-HRP linked. Detection of interaction proceeded as described above in immunoblotting.

2.2.8 Transfection/generation of stable cell line.

Transfection protocol was adopted from the Alexander lab (Pan et al., 2010).
Pre-osteoblast MC3T3-E1 cells were stably transfected with a mouse FOXO3A construct containing a Myc-DDK-tag in the C-terminus (**Figure 2. 9A**). FoxO3a was inserted between Mlu I and Sgf I restriction sites (**Figure 2. 9B**). Stable cell lines were selected in the presence of 500μM G418 and screened by immunoblotting and immunofluorescence of Myc-tagged FoxO3a. Controls were generated by cells stably expressing empty vector pCMV 6 followed the same protocol. 500 μM G418 was chosen from the dose-response kill curve with eight different concentrations of Geneticin G418 including 0 μM (control), 500 μM, 750 μm, 1 mM, 1.5 mM, 2 mM, 2.5 mM, 3 mM (**Figure 2. 10**).

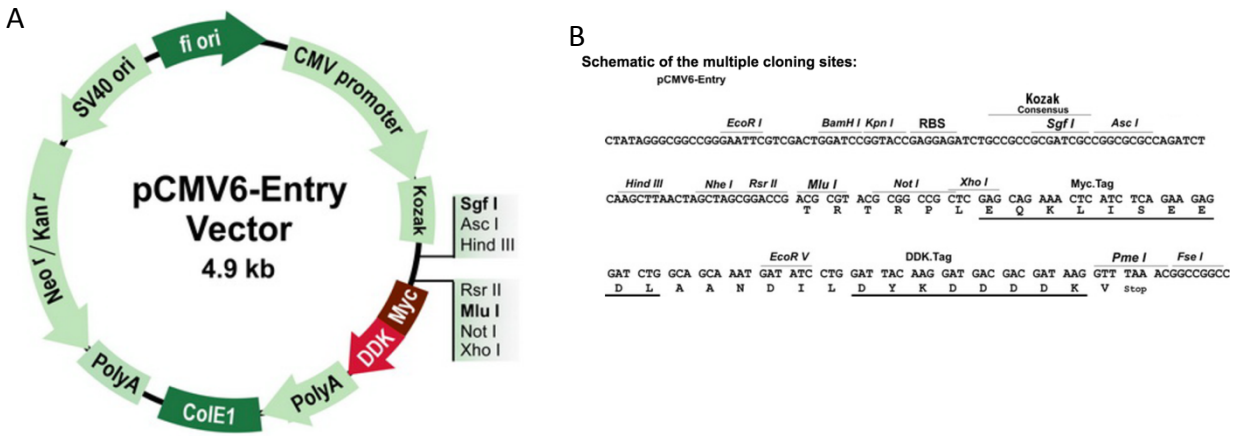

Figure 2. 9 Map and sequence of pCMV6-Entry vector carrying FoxO3a cDNA

(A). Map of pCMV6-entry vector with SgfI and Mlu I cleaved to insert FoxO3a

(B). Sequence of pCMV6-entry vector with two restriction sites.

Image taken from OriGene

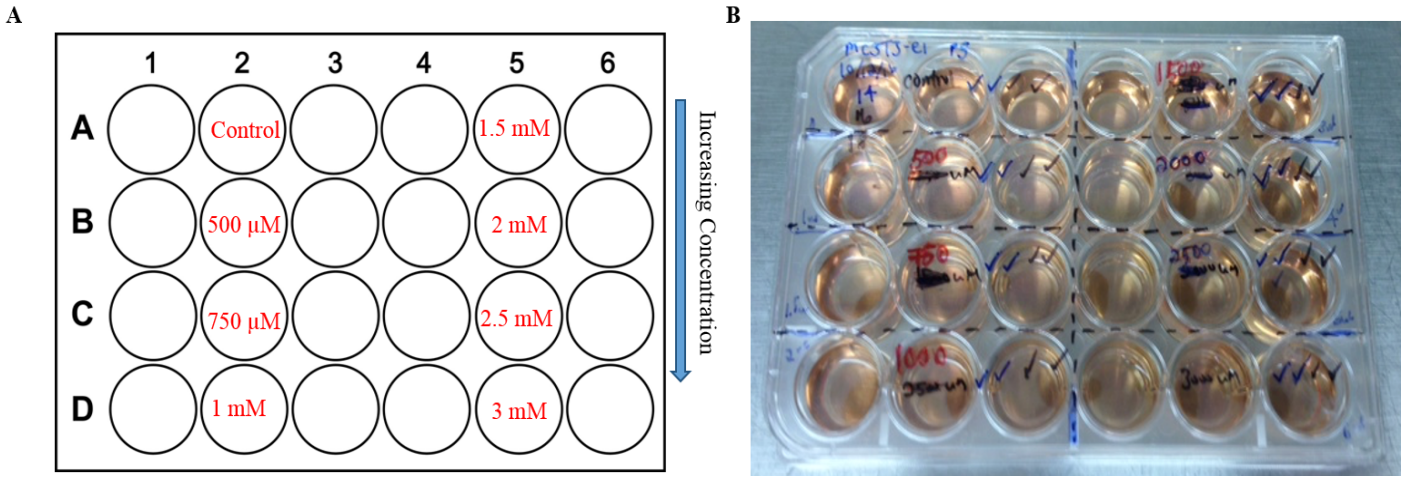

Figure 2. 10 Kill curve in MC3T3-E1 cells

(A). Cells were incubated with seven concentrations of Geneticin and in the absence of antibiotic to generate a kill curve, 500 µM was determined to be the most suitable concentration to use.

(B). MC3T3-E1 cells in 24-well plate with a media change every other day.

Data are presented as means ± SEM. n=3 each.

2.3 Statistical analysis

All results on figures are presented as the mean ± standard error of the sample group. The statistics for values used in figures and tables were generated with GraphPad Prism7. Unpaired two-tail t-tests were employed and significance between groups was reported as p-value was below 0.05. For multiple group comparison analysis, One-way ANOVA followed by Tukey multiple comparisons test was performed using GraphPad Prism version 7.00 for Mac.

CHAPTER 3: EXAMINATION OF A PHYSICAL INTERACTION BETWEEN FOXO3a AND RXRα

3.1. Characterization of murine pre-osteoblast MC3T3-E1 cells: an in vitro model of osteoblasts differentiation and mineralization

FoxO3a is the most abundant FoxO in bone, having 2-3 fold higher expression in osteoblasts and osteoclasts than FoxO1 and FoxO4 (Ambrogini et al, 2010). We seek to determine the role of FoxO3a in osteoblasts during differentiation and subsequent mineralization. We hypothesized that FoxO3a is essential for osteoblast differentiation and matrix calcification. To this end, an *in vitro* model of osteoblast-lineage was characterized. We choose to use Murine MC3T3-E1 pre-osteoblast cells from calvaria for many reasons. MC3T3-E1 cells are a transformed cell line that are adherent to flasks, and offers the advantage of osteoblast origin. They differ from *in vivo* primary cell culture models that are made up of a mixed pool of cell populations including osteoblasts, osteoclasts and osteocytes. Furthermore, MC3T3-E1 cells can be differentiated into osteoblasts by the addition of 50 μg/ml ascorbic acid and 10 mM β-glycerophosphate. This enables studying osteoblast differentiation. MC3T3-E1 cells exhibit a developmental sequence similar to osteoblasts of bone tissue *in vivo*, they undergo proliferation of undifferentiated osteoblast precursors, differentiation of pre-osteoblasts to osteoblasts, extracellular matrix formation and mineralization of matrix production (Quarles et al., 1992). MC3T3-E1 cells demonstrate differentiated state specific gene expression that can be used as biomarkers to assess developmental sequence. For instance, pre-differentiation they express Runx2, an early differential stage biomarker and once differentiated osteocalcin, which is a later stage biomarker. MC3T3-E1 cells are also able to secrete collagen fibrils, and form extracellular matrix. This extracellular matrix can then be mineralized and calcified similar to *in vivo* osteoblasts. They are thus a suitable model to study osteoblast mineralization. Lastly, genes involved in osteoblast differentiation and extracellular matrix mineralization can be stimulated by active vitamin D in

MC3T3-E1 cells (van Leeuwen, 2001). MC3T3-E1 cells are thus an ideal model to study osteoblast differentiation and matrix calcification based on these characteristics.

3.1.1. Examining cell morphology of pre-osteoblast MC3T3-E1 cells in culture

MC3T3-E1 cells were seeded sparsely in cell culture dishes at a cell density of 0.5-2 x 10,000 cells/cm^2 (**Figure 3. 1A**). During their initial proliferation stage, undifferentiated pre-osteoblasts actively replicate and maintain a fusiform appearance and display minimal collagen production. Cells reach confluency after 48h to 72h of seeding (**Figure 3. 1B**). Once cells reach confluency, differentiation was initiated with 50 μg/ml ascorbic acid and 10 mM β-glycerophosphate. MC3T3-E1 cells exhibit basal levels of collagen secretion at this stage and maintain fusiform morphology (**Figure 3. 2A**). As cells undergo differentiation, they exhibit changes in morphology, from fusiform to an elongated appearance and some extracellular collagenous matrix is produced (**Figure 3. 2B**). Significant changes in appearance are observed in 7-day differentiated MC3T3-E1 cells. They exhibit a long and thin morphology (**Figure 3. 2C**). Production of collagen is significantly increased and cells become embedded in a white multi-layered extracellular matrix similar to woven bone (**Figure 3. 2D**).

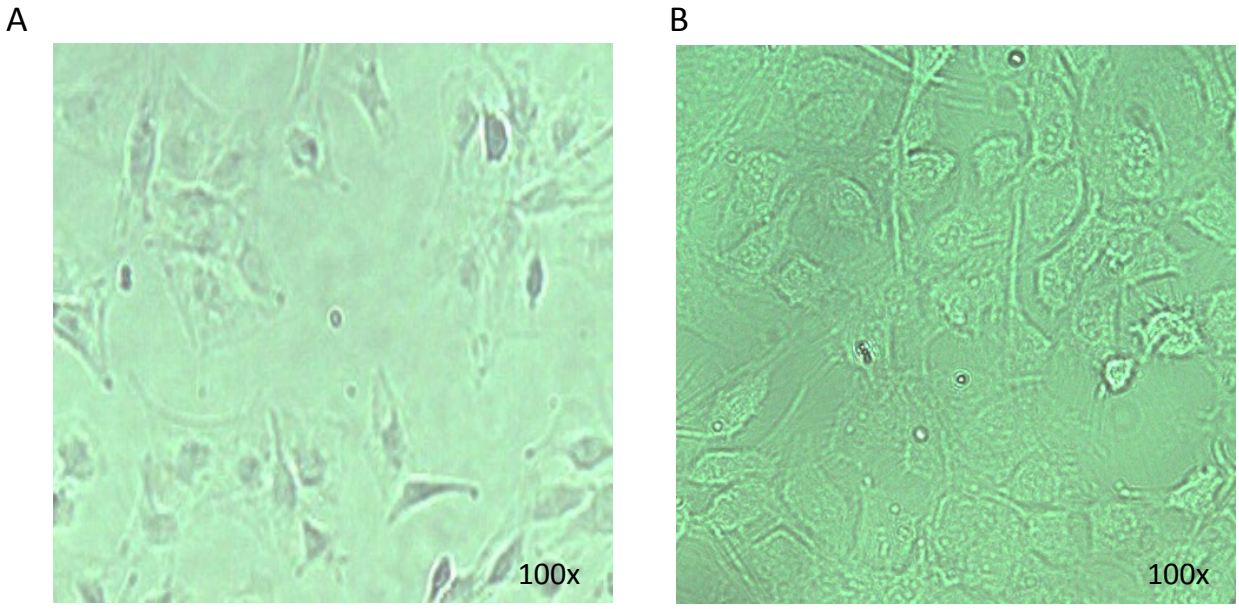

Figure 3. 1 **Morphology of pre-osteoblast MC3T3-E1 cells**

(A) When cells are seeded sparsely and (B) once cells reach confluency after 48 h-72 h.

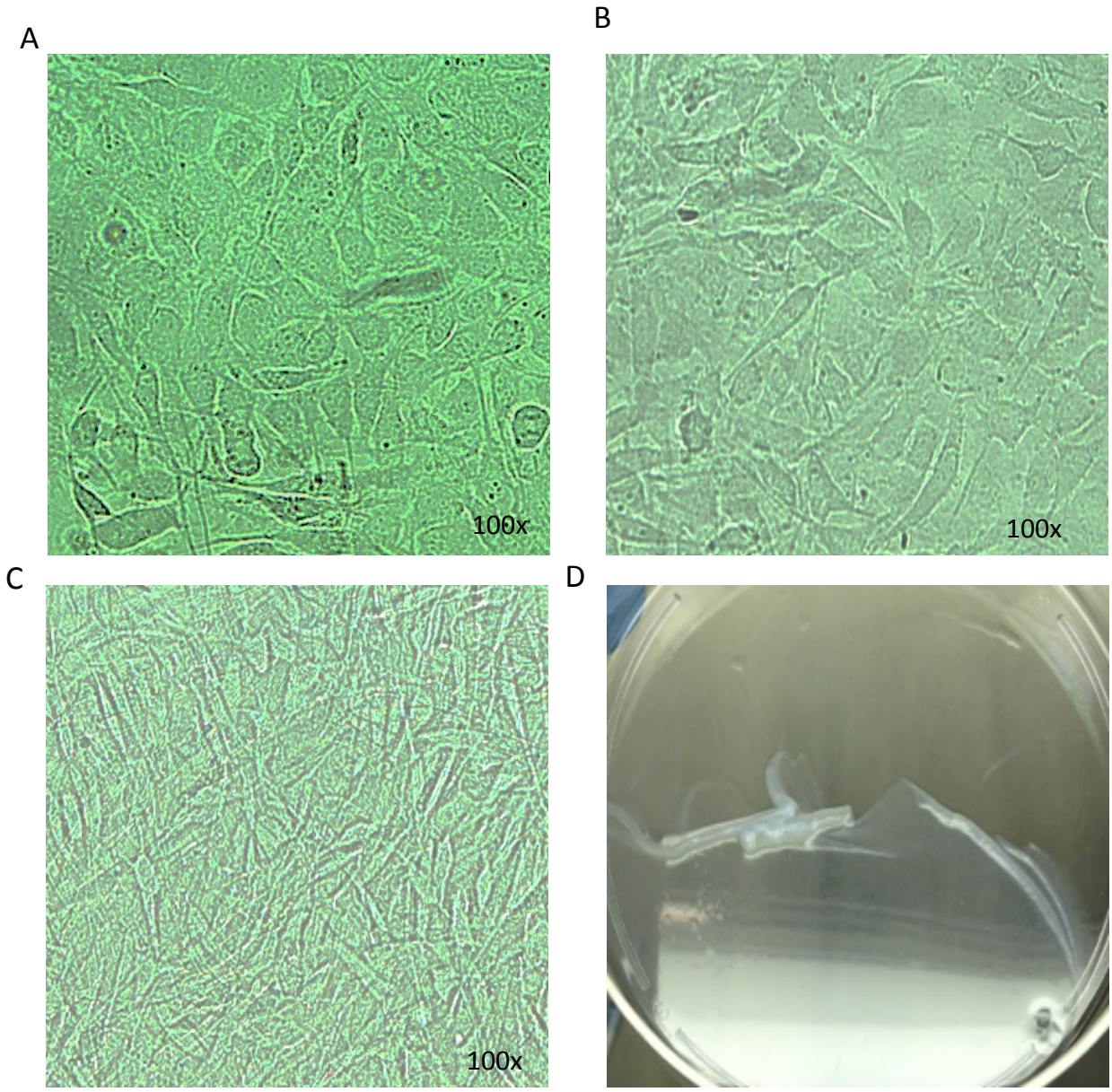

Figure 3. 2 Morphology of MC3T3-E1 cells post differentiation

(A) 1 day into differentiation (B) 3 days into differentiation (C) 7 days into differentiation. (D) Accumulation of collagenous matrix in 7-day differentiated osteoblasts grown on a cell culture dish is evident.

3.1.2. Assessment of osteoblast differentiation and mineralization in MC3T3-E1 cells

The ability of MC3T3-E1 cells to differentiate and mineralize *in vitro* was confirmed via assessment of two biomarkers, Runx2 and osteocalcin (OCN). Runx2 is the protein product of the CBFA1 gene. It is an early stage transcription regulator of osteoblast differentiation (**Figure 3. 3**) (Komori et al., 1997; Otto et al., 1997; Stein et al., 2004 ; Zhang et al., 2006). Runx2 mRNA expression was detected in pre-osteoblasts, and increased significantly in 1-day differentiated MC3T3-E1 cells, indicating pre-osteoblasts have differentiated into immature osteoblasts. As immature osteoblasts began to further differentiate into mature osteoblasts, a gradual decrease in Runx2 expression is observed by 3-days differentiated osteoblasts and reached the lowest levels in 7-day differentiated osteoblasts, indicating cells are mature osteoblasts (**Figure 3. 4A**). This observation is consistent with the suggested role of Runx2 to orchestrate the formation of immature bone and inhibits osteoblast maturation (Komori., 2010).

Osteocalcin (OCN) is also known as bone gamma-carboxyglutamic acid-containing protein (BGLAP). It is a non-collagenous protein secreted by osteoblasts during the middle to late stage of differentiation (Desbois et al., 1994; Tsao et al., 2017). Minimal levels of OCN were observed in pre-osteoblasts and a gradual increase found as cells underwent differentiation, reaching the highest levels in 7-day differentiated MC3T3-E1 cells (**Figure 3. 4B**). This is consistent with the cells becoming differentiated into mature osteoblasts. This observation is consistent with the reported ability or OCN to regulate maturation of bone mineral (Rathore et al., 2016). OCN is also used clinically as a measure of osteoblast mineralization and calcium-binding affinity (Rathore et al., 2016). Higher expression is associated with higher bone mineral density *in vivo*. Thus OCN expression is consistent with MC3T3-E1 cells mineralizing and calcifying matrix *in vitro*. The expression of RUNX2 and OCN provides evidence that MC3T3-E1 cells differentiate

in vitro and suggest they can mineralize matrix *in vitro*. They are thus an ideal model to study osteogenesis.

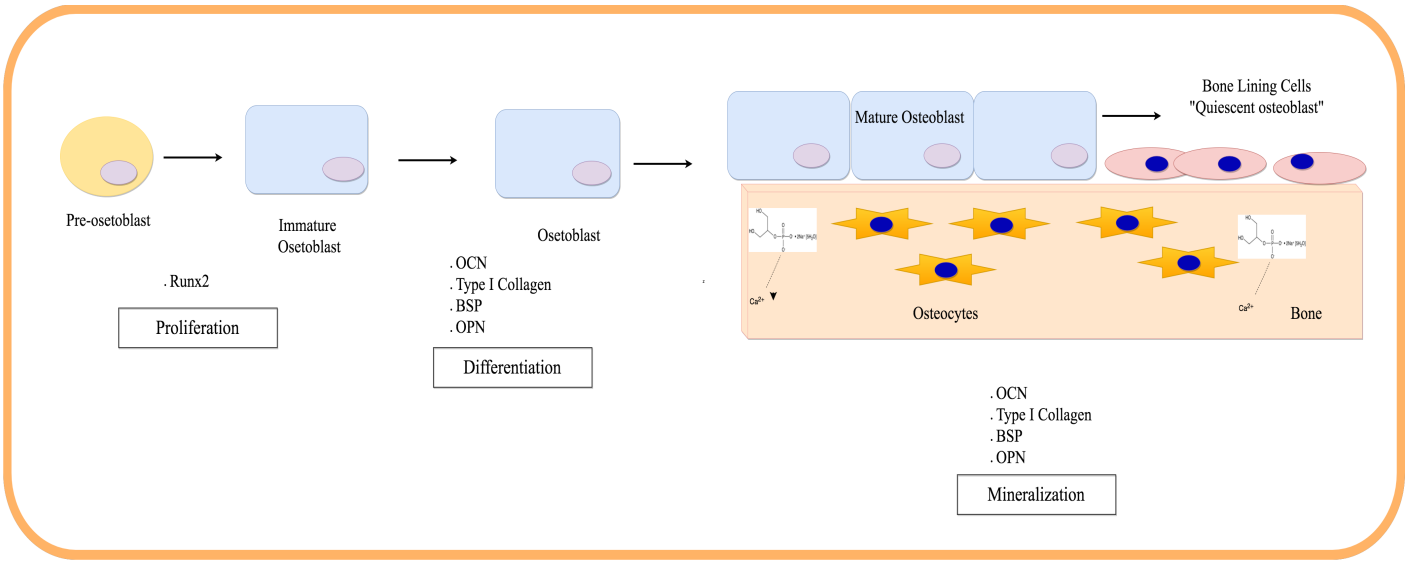

Figure 3. 3 **Assessment of osteoblast differentiation in MC3T3-E1 cells**

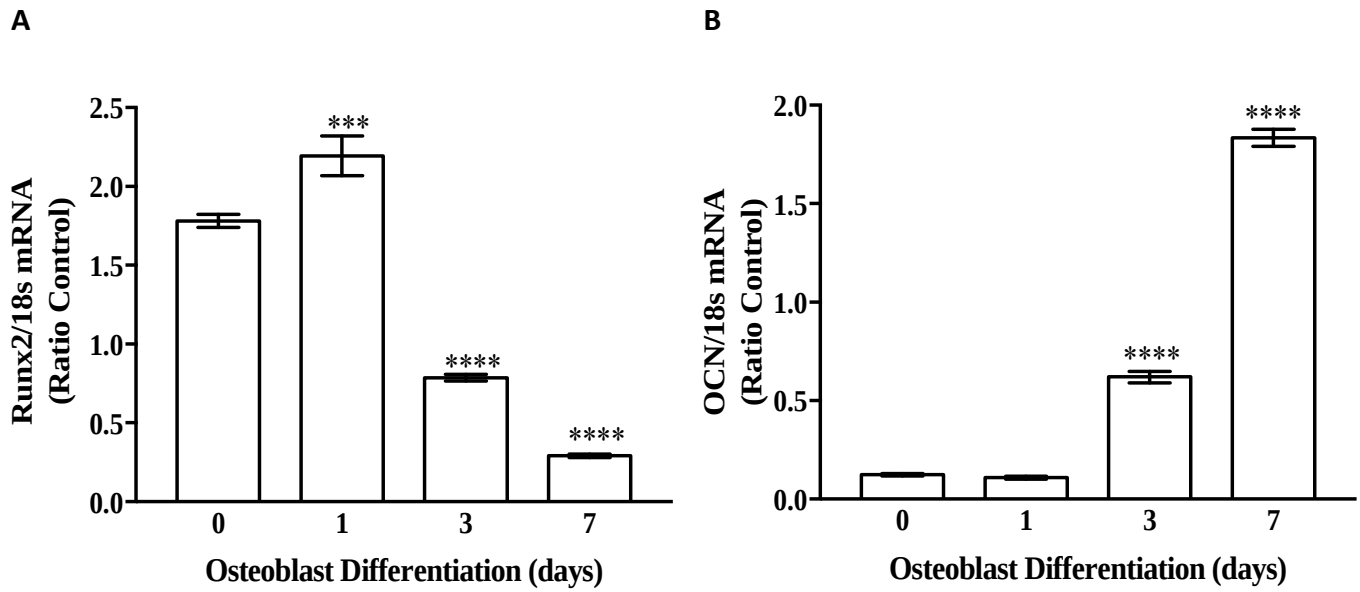

Figure 3. 4 Assessment of differentiation biomarkers

(A). Runx2 is expressed in pre-osteoblasts, up-regulated in immature osteoblasts, but then down-regulated in mature osteoblasts. (B). Osteocalcin (OCN) shows minimal expression in pre-osteoblasts, increases during differentiation and displays the highest expression in mature osteoblasts.

3.2. Identify expression of important transcription factors and genes during osteoblast differentiation and mineralization

The gene expression of FoxO3a, RXRα and VDR was assessed during osteoblast differentiation using the *in vitro* model. RNA and protein lysates were collected from pre-osteoblasts, 1-day, 3-day and 7-day differentiated osteoblasts and gene expression assessed via qPCR and protein expression by immunoblotting.

3.2.1. FoxO3a expression levels increase during osteoblast differentiation and mineralization

Pre-osteoblast cells displayed minimal expression of FoxO3a both at the mRNA (**Figure 3. 5A**) and protein (**Figure 3. 5B**) level. A gradual increase was observed as differentiation was initiated, reaching a significantly higher level in 7-days differentiated osteoblasts. Immunofluorescence indirectly labeled FoxO3a with Cyanine 3-conjugated secondary antibody bound to rabbit anti-FoxO3a antibodies. **Figure 3. 6A** shows 1-day post differentiated MC3T3-E1 cells with minimal FoxO3a expression, **Figure 3. 6B** demonstrates higher expression of FoxO3a in 3-day differentiated osteoblasts and **Figure 3. 6C** reveals the highest level of FoxO3a expression in 7-day differentiated osteoblasts. Immunofluorescence also provided information with regards to FoxO3a localization. Although the majority of FoxO3a resides in the nucleus, there is still approximately 10% of FoxO3a expressed in the cytoplasm in pre-osteoblasts (**Figure 3. 6A**). As FoxO3a expression increases, there is an increase of FoxO3a localization in the nucleus in the 3-day differentiated osteoblasts (**Figure 3. 6B**) and the highest expression with close to 95% of FoxO3a being expressed in the nucleus of the 7-day differentiated osteoblasts (**Figure 3. 6C**). DAPI was used to stain the nucleus, and this allowed us to measure the co-localization between FoxO3a and DAPI. This was quantified using the Pearson's correlation

coefficient (**Figure 3. 7**). Pearson's correlation coefficient was 0.002 in pre-osteoblats, 0.068 in 1-day differentiated osteoblasts, 0.316 in 3-day differentiated osteoblasts, and 0.368 in 7-day differentiated osteoblasts consistent with an increase in FoxO3a nuclear localizing as the cells undergo differentiation (**Table 3.2**).

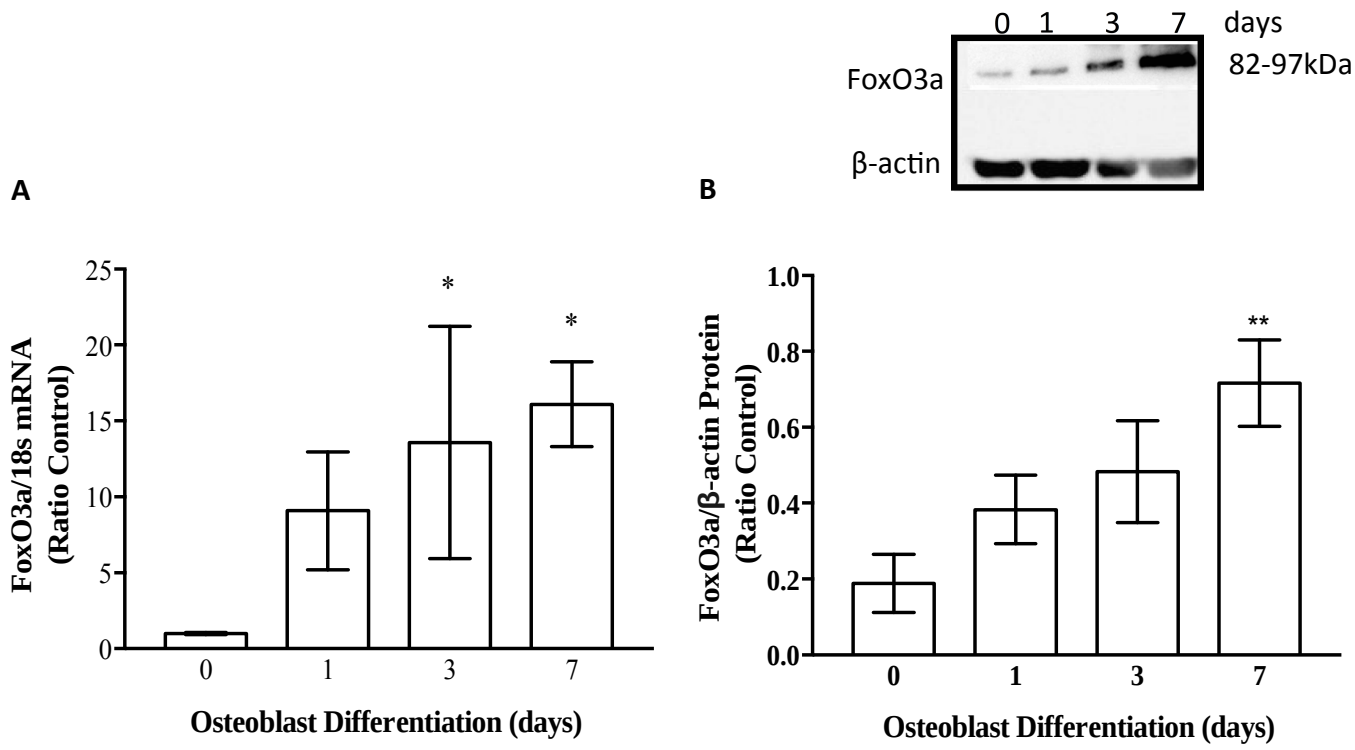

Figure 3. 5 FoxO3a expression is highest in 7-day differentiated osteoblasts

FoxO3a expression was determined in MC3T3-E1 cells at various differentiation stage. 0 day are pre-osteoblasts and other differentiated cells are identified as 1-day into differentiation, 3-day and 7-day into differentiation. (A) FoxO3a mRNA expression normalized to 18s as expression (B) FoxO3a protein expression normalized to β-actin expression. n=6 for each group. Data are presented as means ± SEM. * $p \leq 0.05$, ** $p \leq 0.01$.

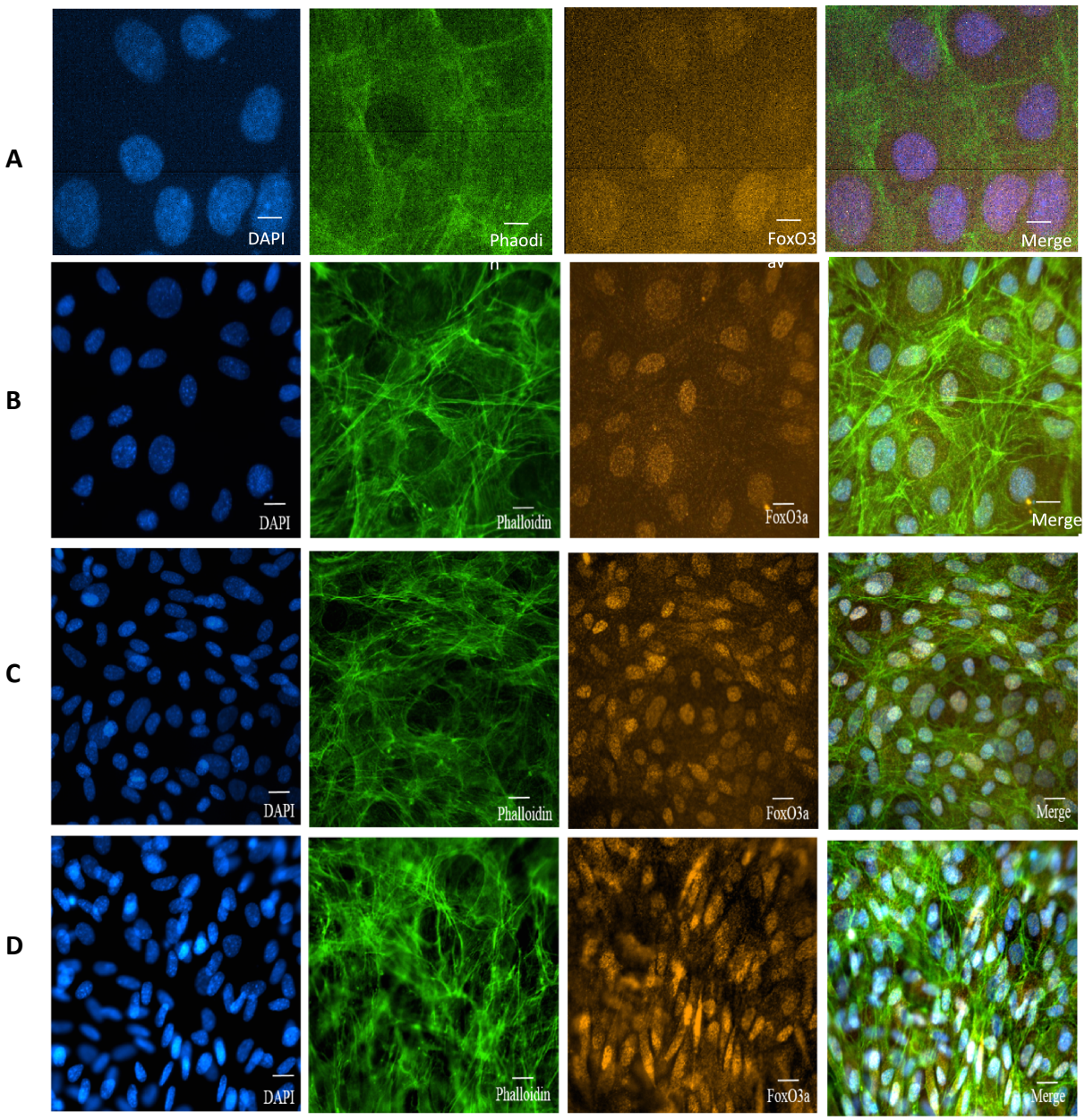

Figure 3. 6 **Immunofluorescence confirms significance FoxO3a nuclear localization**

MC3T3-E1 cells at various differentiation stage were stained with DAPI to identify the nucleus, Alexa Fluor 488 phalloidin to stain actin and FoxO3a rabbit monoclonal antibodies, which were then bound to donkey anti-rabbit Cy3 antibodies. (A) Pre-osteoblasts. (B). 1-day differentiated osteoblasts. (C) 3-day differentiated osteoblasts. (D) 7-day differentiated osteoblasts. Scale bar = 20 μM

Table 3.2 Measurement of FoxO3a nuclear localization during osteoblast differentiation

Stage of differentiation	Pearson's correlation coefficient ± SEM	P-value
Pre-osteoblasts	0.002 ± 0.007996	-
1-day differentiated	0.068 ± 0.009682	<0.0001
3-day differentiated	0.316 ± 0.01574	<0.0001
7-day differentiated	0.368 ± 0.007162	<0.0001

FoxO3a in the nucleus was assessed by co-staining with DAPI and quantified with Pearson's correlation coefficient in pre-osteoblasts, 1-day, 3-day, and 7-day differentiated osteoblasts. n=25 in each group.

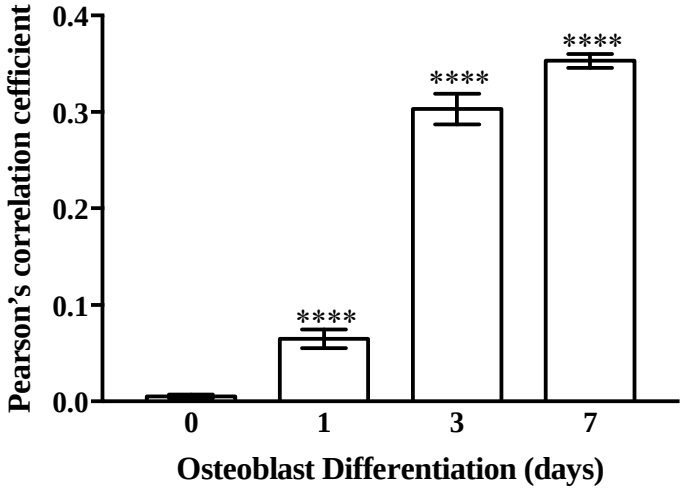

Figure 3. 7 **Increasing FoxO3a nuclear localization during cell differentiation**

Very little co-localization between FoxO3a and DAPI was detected in pre-osteoblasts by Pearson's correlation coefficient (PCC). PCC increased in a time-dependent manner from 1-day differentiated MC3T3-E1 cells to the highest levels in 7-day differentiated MC3T3-E1 cells. Data are presented as means ±SEM. n=25 each. ****p ≤0.0001

3.2.2 Vitamin D signaling during osteoblast differentiation and mineralization

To examine vitamin D participation during osteoblast differentiation and mineralization, expression of VDR and RXRα was assessed. $1,25D_3$-activated VDR would form a heterodimer

with RXR and it would then translocate to the nucleus where it binds with vitamin D response element (VDRE) to initiate transcription in target genes, including FoxO3a and osteocalcin (Dowd and MacDonald, 2010; Eelen et al., 2013; Lian et al., 1998).

RXRα mRNA and protein expression is at basal levels in pre-osteoblasts, and displays a progressive increase from 1-day to 3-day differentiated osteoblasts reaching the highest level in 7-day differentiated osteoblasts (**Figure 3. 8A and B**).

VDR mRNA and protein expression is at lowest levels in pre-osteoblasts, increases from 1-day to 3-day differentiated osteoblasts and reaches the highest level in 7-day differentiated osteoblasts (**Figure 3. 9A and B**).

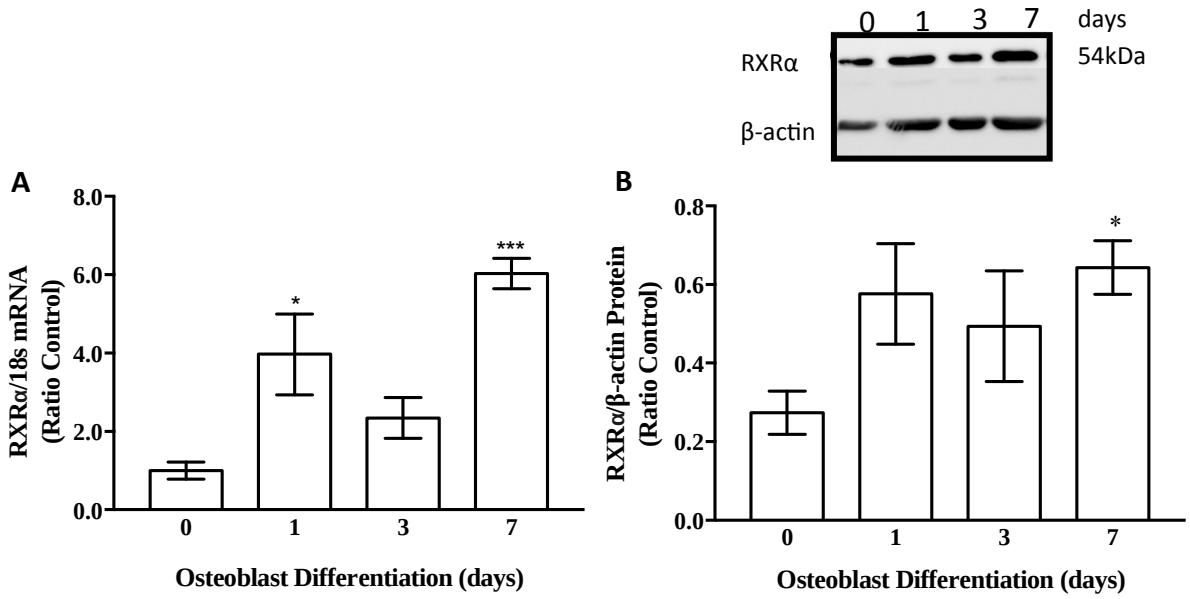

Figure 3. 8 RXRα expression increase as cells undergo differentiation, reaching its highest level in 7-day differentiated osteoblasts

(A) RXRα mRNA expression with normalized to18s (B) RXRα protein expression normalized to β-actin. n=6 each. Data are presented as means ± SEM. *p≤0.05, ***p ≤0.001

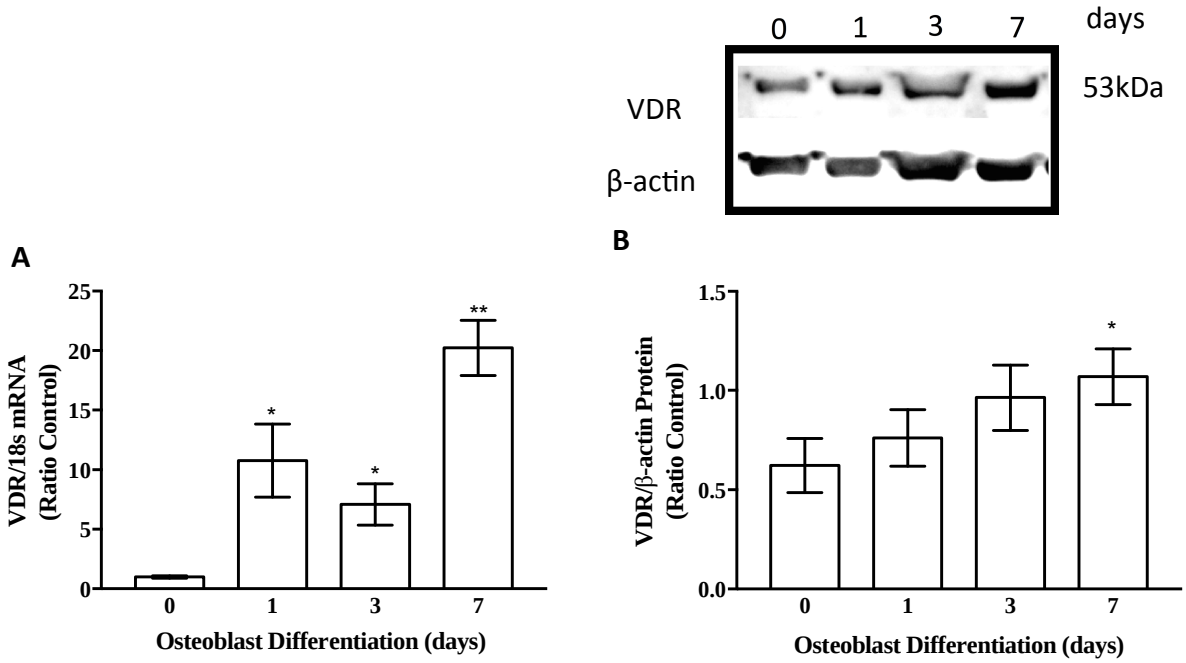

Figure 3. 9 **Vitamin D Receptor (VDR) expression shows a gradual increase as cells undergo differentiation, reaching its highest level in 7-day differentiated osteoblasts**

(A) VDR mRNA expression normalized to 18s (B) VDR protein expression normalized to β-actin. n=6 each. Data are presented as means ± SEM. *p≤0.05, **p ≤0.01

3.3 Characterization of calcium transport genes during osteoblast differentiation

Calcium homeostasis is critical for osteoblast function and bone formation (Imai et al., 1992). Calcium influx is regulated through a variety of membrane channels including voltage-sensitive calcium channels (VSCCs), voltage-insensitive calcium channels (VICCs), mechanosensitive divalent cation channels (MDCCs) and receptor-operated calcium channels (ROCs) (Thompson et al., 2011) VSCCs including L-type calcium channels, $Ca_v1.2(\alpha_{1C})$, $Ca_v1.3$ (α_{1D}), and low-threshold T-type calcium channel, $Ca_v3.1(\alpha_{1G})$ are the major Ca^{2+} channels expressed in the plasma membrane of osteoblasts accounting for the majority of Ca^{2+} permeability (Thompson et al., 2011). We thus determined the expression of these and other calcium mediators in our *in vitro* model.

3.3.1 Plasma membrane Ca^{2+} channels in MC3T3-E1 cells

Expression of calcium influx through channels on the plasma membrane such as $Ca_v1.2$, $Ca_v1.3$, and $Ca_v3.1$ were examined. $Ca_v1.2$ mRNA expression was detected at the highest levels in pre-osteoblasts, and displayed a gradual decrease in 1-day and 3-day osteoblasts and reached the lowest levels in 7-day differentiated osteoblasts (**Figure 3. 10A**). $Ca_v1.3$ expression levels remained constant in pre-osteoblasts, 1-day and 3-day differentiated osteoblasts. $Ca_v1.3$ showed the lowest expression levels in 7-day differentiated osteoblasts (**Figure 3. 10B**). $Ca_v3.1$ showed the opposite pattern of expression. $Ca_v3.1$ was detected at low levels in pre-osteoblasts, and increased gradually from 1-day, 3-day to the highest levels in 7-day differentiated osteoblasts (**Figure 3. 10C**). The expression of calcium-binding protein, Calbindin-D_{9K} is detected in pre-osteoblasts and remained the same levels in 1-day differentiated osteoblasts. Calbindin-D_{9K} expression gradually decreases in levels in 3-day differentiated osteoblasts and reached the lowest levels in 7-day differentiated osteoblasts (Figure 3. 10**D**).

Expression of other calcium mediators and transporters was assessed, including Calbindin-D_{28K}, calcium sensing receptor (CaSR), TRPV5 and TRPV6. All of above were not detected in the current model of MC3T3-E1 cells.

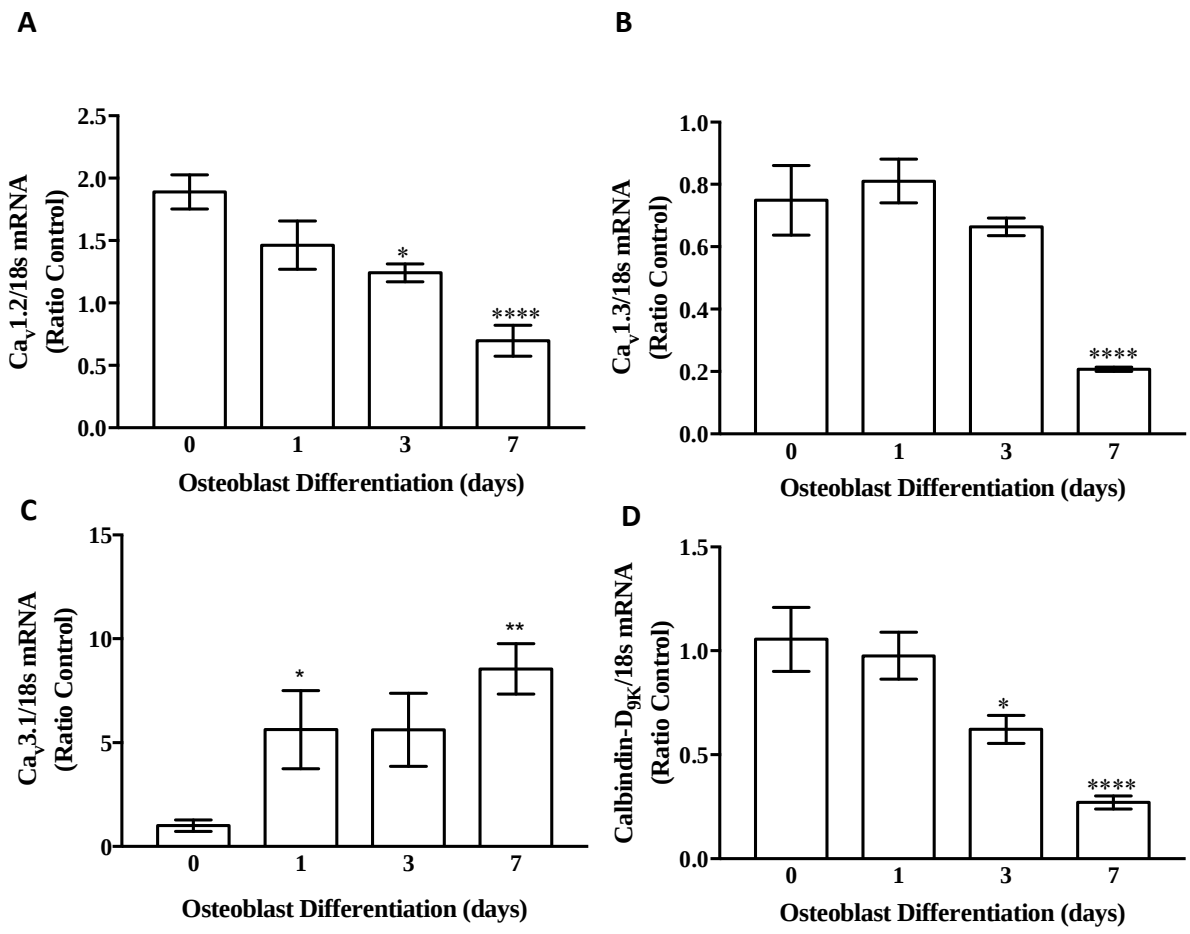

Figure 3. 10 Expression of calcium influx mediators in MC3T3-E1 cells during osteoblast differentiation

(A). $Ca_v1.2$ undergoes a gradual increase from pre-osteoblasts to 7-day differentiated osteoblasts. (B). $Ca_v1.3$ mRNA expression shows a significant reduction in 7-day differentiated osteoblasts (C). $Ca_v3.1$ expression shows a gradual increase as differentiation occurs, exhibiting highest expression levels in 7-day differentiated cells. (D). Calbindin-D_{9K} expression level is significantly reduced in 7-day differentiated osteoblasts.

All gene expression was normalized to 18s expression. n=3 each. Data are presented as means ± SEM. *$p \leq 0.05$, **$p \leq 0.01$, ****$p \leq 0.0001$

3.3.2 Expression of mediators of Ca^{2+} efflux into osteoid

Osteoblasts contain two calcium efflux mechanisms, the Ca^{2+}-ATPase pump (PMCA) and Na^{+}/ Ca^{2+} exchanger (NCX). They both deliver Ca^{2+} ions out of osteoblasts into osteoid, a process important for bone calcification (Shen et al., 1993; Anderson et al., 1984; White et al., 1996). The sodium-calcium exchanger (NCX) is a Ca^{2+}efflux transport protein that sits on the basolateral side of osteoblasts, important for exporting Ca^{2+}into the extracellular matrix (**Figure 4. 1**). NCX is constantly expressed in pre-osteoblasts, and 1-day, 3-day to 7-day differentiated osteoblasts (**Figure 3. 11A**).

There are three isoforms of PMCA, PMCA1, 2, and 4 in osteoblasts, PMCA1 is the major isoform in osteoblastic cells (Meszaros and Karin, 1993; Abramowitz et al., 1995; Stains et al., 2002). Therefore, only PMCA-1b was assessed in the current *in vitro* model. Low expression of PMCA-1b is detected in pre-osteoblasts, and expression level increases as cells undergo differentiation, peaking at 7-day (**Figure 3. 11B**).

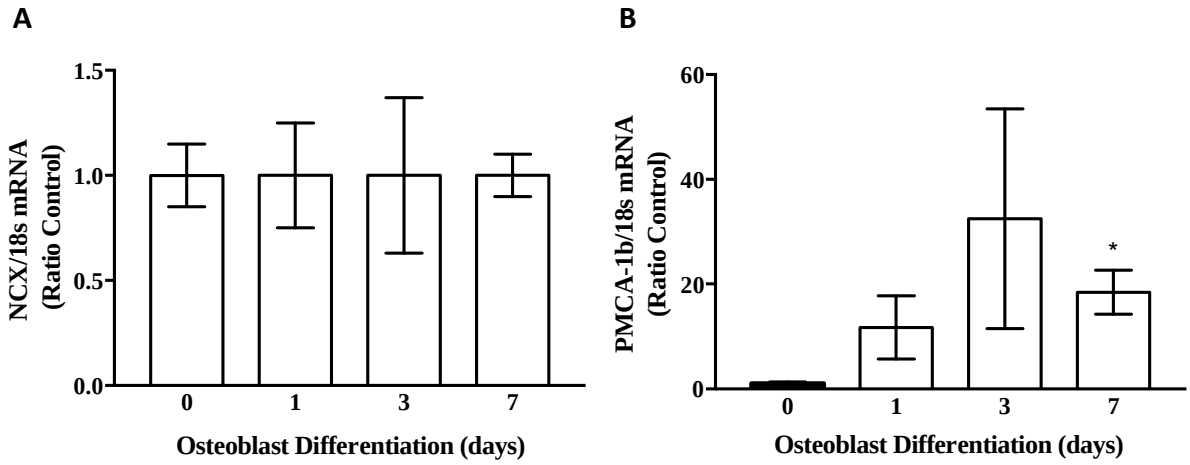

Figure 3. 11 Expression of calcium efflux mediators

(A). NCX expression remains the same during osteoblast differentiation. (B). PMCA-1b exhibited highest expression in 7-day differentiated osteoblasts. All gene expression was normalized to 18s expression. n=3 each. Data are presented as means ± SEM. *p ≤0.05

3.4. Potential interaction between FoxO3a and RXRα in MC3T3-E1 cells

RXRα/VDR heterodimer is an important in vitamin D regulation (Barsony, 2010). RXR is also capable of forming heterodimers with peroxisome-proliferator activator γ (PPAR γ) for the regulation of adipogenesis, cellular differentiation and antioxidant defense mechanism in bone (Chandra et al., 2008; Daitoku et al., 2011; Dowell et al., 2003). Recent study demonstrated PPAR γ cross-talks with FoxO1 in a yeast two-hybrid screen. FoxO1 inhibited transcription of PPAR γ by binding to its promoter, thus reducing PPAR γ activity (Dowell et al., 2003). Co-transfection in 293T cells showed RXR: PPAR γ suppressed FOXO1:PPAR γ expression in a dose-dependent manner (Daitoku et al., 2011; Dowell et al., 2003). In a yeast two-hybrid system, RXRα was suppressed by FoxO activity, suggesting potential direct interaction between RXR and FOXO (Dowell et al., 2003). Therefore, we queried in increasing levels of FoxOs triggered by high levels of ROS-induced oxidative stress would enhance retention of FoxO3a in the nucleus and would then bind to RXRα, leading to competitive reduction in available RXRα. We hypothesized reduction of available RXRα would result to ultimate vitamin D resistance.

To determine FoxO3a: RXRα interaction, we employed co-immunoprecipitation (Co-IP) in 7-day differentiated osteoblasts. Co-IP uses target protein-specific rabbit monoclonal anti-FoxO3a antibodies to capture FoxO3a proteins indirectly bound to their specific target. From the previous results in this current *in vitro* model, we found FoxO3a expression reached the highest levels in 7-day differentiated MC3T3-E1 cells. Therefore, Co-IP was performed on 7-day differentiated MC3T3-E1 cells. We set up two approaches: first we employed specific FoxO3a antibodies to capture FoxO3a proteins in 7-day differentiated osteoblasts and then assessed the interaction with RXRα via immunoblotting. Second, specific RXRα antibodies were used to capture RXRα proteins and interaction with FoxO3a was assessed (**Figure 3. 12**).

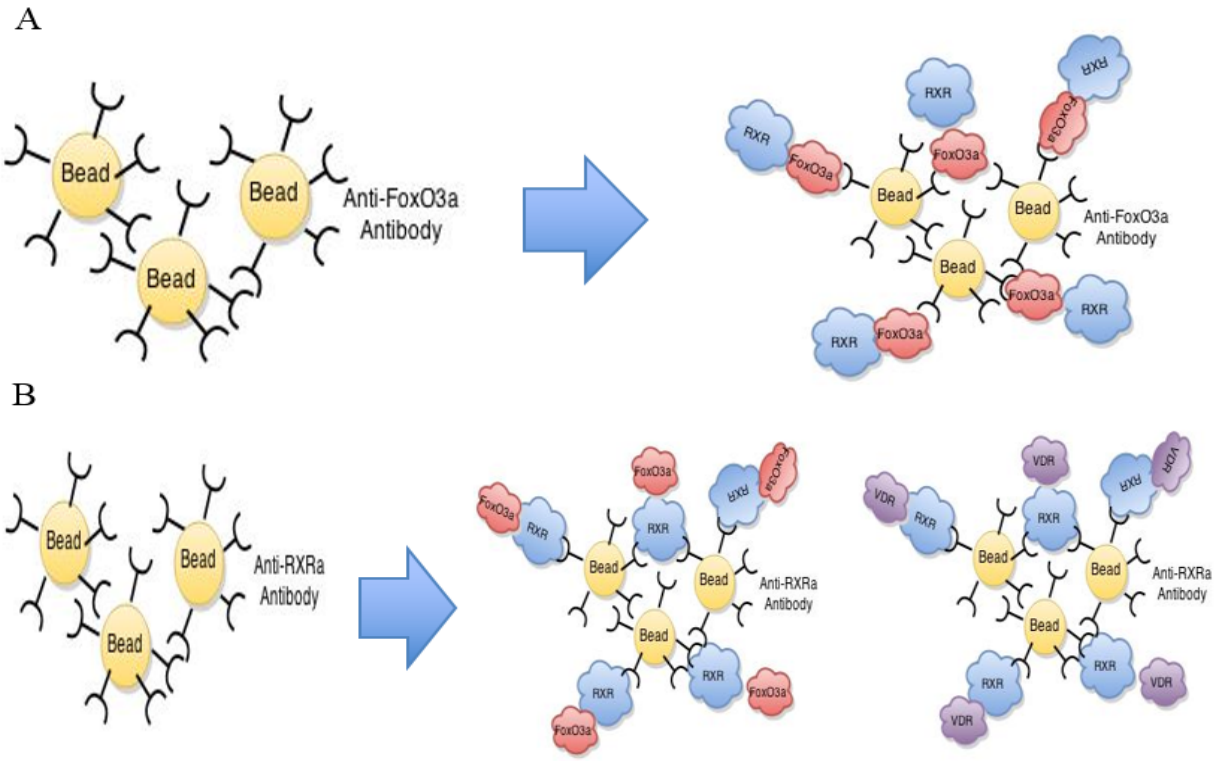

Figure 3. 12 Co-immunoprecipitation (Co-IP) for interaction between FoxO3a and RXRα

(A) FoxO3a is pulled down with rabbit monoclonal FoxO3a primary antibody and then immunoblotted with an anti-rabbit RXRα antibody

(B) RXRα is pulled down with rabbit primary antibody, and then immunoblotted with anti-rabbit FoxO3a antibody

3.4.1 FoxO3a: RXRα interaction was not detected in the current model

Agarose A/G beads coated with rabbit polyclonal anti-FoxO3a antibodies used to pull down FoxO3a proteins from the 7-day differentiated MC3T3-E1 cells. Pull-down of FoxO3a was verified by immunoblotting with rabbit polyclonal anti-FoxO3a antibodies along with negative control of rabbit serum (**Figure 3. 13**). Endogenous FoxO3a was detected at approximately 85 kDa in control, but an unexpected strong band was detected in the negative control in **Figure 3. 13A**. Third lane was loaded with polyclonal rabbit anti-FoxO3a antibody to verify correct molecular weight. Since rabbit serum was used as negative control and immunoblotted with rabbit anti-FoxO3a antibodies, this band could be two heavy chains of rabbit IgG. In order to get around this problem, we then used goat polyclonal anti-FoxO3a antibodies instead of from the rabbit source to pull down FoxO3a. This pull-down of FoxO3a was then immunoblotted with rabbit monoclonal anti-FoxO3a antibodies (**Figure 3. 13B**). FoxO3a protein was not detected in control, suggesting two possibilities. One would be rabbit monoclonal anti-FoxO3a antibodies failed to detect presence of FoxO3a in the lysate, and the other possibility would be goat polyclonal anti-FoxO3a antibodies failed to pull down FoxO3a proteins from the cell lysate. Rabbit monoclonal anti-FoxO3a antibodies have been shown previously to detect FoxO3a proteins in **3.2.1**, thus we investigated the second possibility with the goat antibody. A faint band for FoxO3a was detected with goat polyclonal anti-FoxO3a antibodies in 7-day differentiated osteoblasts, showing this antibody is not the most sensitive compared to other rabbit antibodies, but was able to detect FoxO3a proteins (**Figure 3. 14**). A strong band was also detected at 50 kDa in the negative control, this may be the result of cross-reactivity.

To determine potential FoxO3a:RXRα interaction, FoxO3a protein was pulled down with rabbit polyclonal anti-FoxO3a antibodies in 7-day differentiated osteoblasts and rabbit serum as

negative control, and immunoblotted with rabbit monoclonal anti-RXRα antibodies (**Figure 3. 15A**). A strong band was detected at approximately 54 kDa in the control. A strong dense band was also detected in the negative control and the lane loaded with anti-FoxO3a antibody due to cross-reactivity. We also attempted pulling down FoxO3a with different rabbit monoclonal anti-FoxO3a antibodies from 7-day differentiated osteoblast and rabbit serum as negative control, and immunoblotted with rabbit monoclonal anti-RXRα antibodies. A strong band was detected in the negative control, but no interaction was detected between FoxO3a and RXRα (**Figure 3. 15B**). We were unable to detect an interaction between FoxO3a and RXRα with the current tools available due to problems with cross-reactivity.

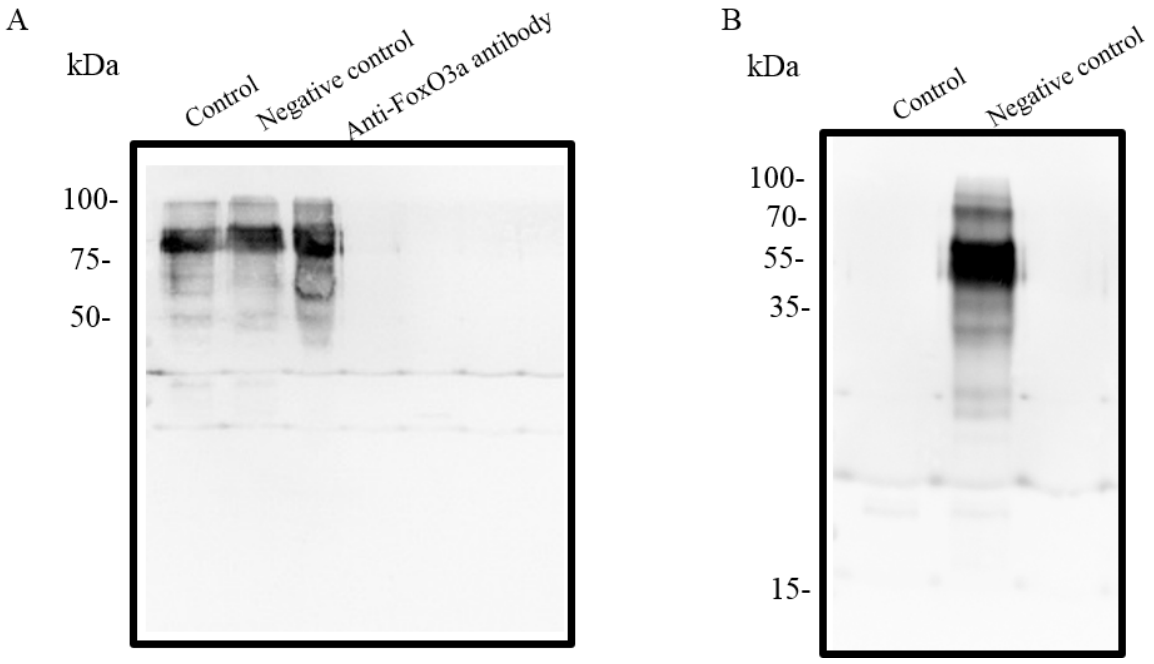

Figure 3. 13 Pull-down of FoxO3a protein from 7-day differentiated MC3T3-E1 cells

(A). FoxO3a was pulled down and immunoblotted with rabbit polyclonal anti-FoxO3a antibodies. A strong band of rabbit IgG was detected in the negative control.

(B). FoxO3a was pulled down with goat polyclonal anti-FoxO3a antibodies and immunoblotted with rabbit monoclonal anti-FoxO3a antibodies.

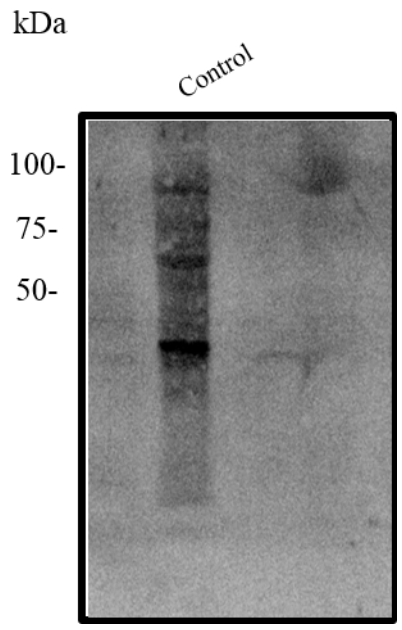

Figure 3. 14 FoxO3a protein expression detected by goat polyclonal anti-FoxO3a antibodies

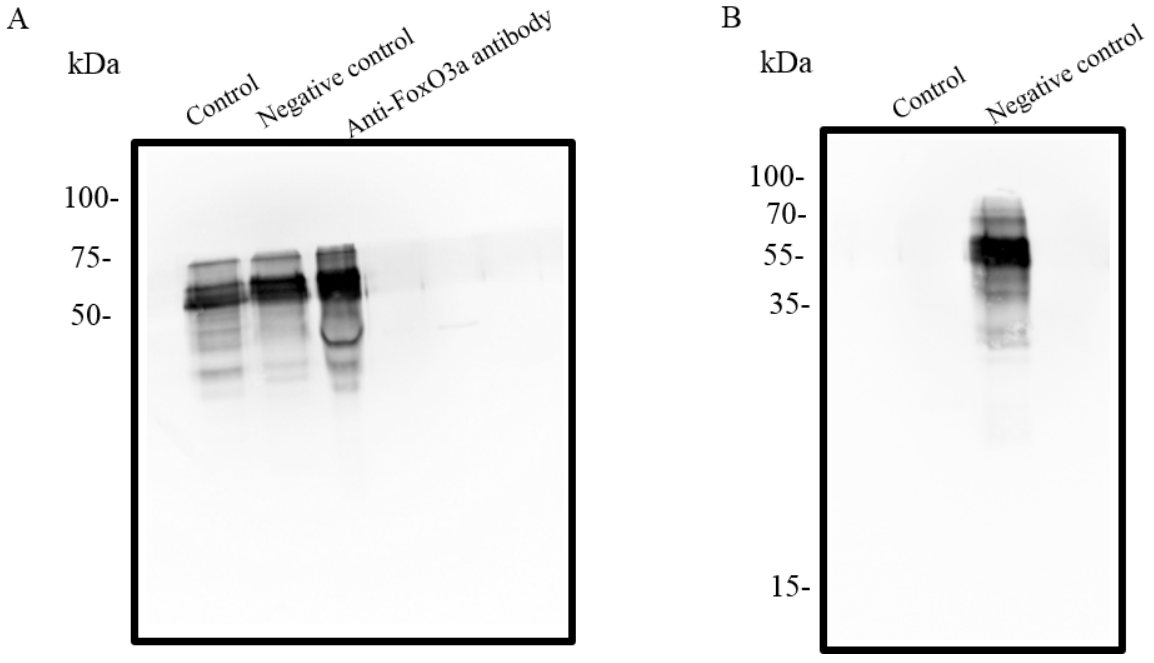

Figure 3. 15 **No FoxO3a:RXRα interaction detected in 7-day differentiated MC3T3-E1 cells**

(A). FoxO3a was pulled down with rabbit polyclonal anti-FoxO3a antibodies and immunoblotted with rabbit monoclonal anti-RXRα antibodies.

(B). No FoxO3a:RXRα interaction was detected when FoxO3a was pulled down rabbit monoclonal anti-FoxO3a antibodies and immunoblotted with rabbit monoclonal anti-RXRα antibodies.

3.5 Discussion

3.5.1. MC3T3-E1 provides a suitable model to study osteoblast differentiation and mineralization

MC3T3-E1 cells incubated with 50 μg/ml ascorbic acid and 10mM β-glycerophosphate exhibited osteoblast phenotype and stage-specific differentiation characteristics. Undifferentiated MC3T3-E1 cells remained cuboidal cell morphology while expressing minimal levels of Runx2 and OCN expression with no visible collagen produced. In the 1-day differentiated MC3T3-E1 cells, cells remained the same morphology as pre-osteoblasts with no collagen produced while expressing significant high levels of Runx2 expression and low OCN levels. These observations indicate cells are immature osteoblasts at this stage. 3-day differentiated MC3T3-E1 cells started to exhibit elongated cell morphology with a skinny cell body that extends dendrites. A thin layer of collagen can be seen in these cells, while Runx2 expression levels decrease dramatically and OCN expression increases significantly. These observations indicate cells have differentiated into osteoblasts at this stage. 7-day differentiated MC3T3-E1 cells showed elongated cells stacked on top of each other, forming a matrix. Cells at this stage displayed the highest amount of collagen produced with the highest expression levels of OCN and the lowest Runx2 expression, indicating cells have differentiated into mature osteoblasts. These combined evidence demonstrated that MC3T3-E1 cells exhibited developmental sequence similar to osteoblasts *in vivo*, thus serving as a suitable *in vitro* model for our study.

3.5.2. FoxO3a's participation during osteoblastogenesis

Both mRNA and protein analysis detected FoxO3a expression at base levels in pre-osteoblasts, and doubled in 1-day immature osteoblasts, which further doubled in 3-day osteoblasts. Finally, FoxO3a expression levels reached the highest levels in 7-day mature osteoblasts, validating FoxO3a's participation during osteoblast differentiation.

Visualization with immunofluorescence and Pearson correlation coefficient (PCC) provided quantified measurements of the linear relationship between FoxO3a and DAPI. FoxO3a was detected with rabbit monoclonal anti-FoxO3a antibodies which then labeled with Cy3-conjugated secondary antibodies. DAPI stained the nucleus.

Pearson's correlation coefficient (PCC) measured co-localization of FoxO3a and DAPI in the nucleus, providing a statistical measurement between FoxO3a and DAPI as a linear relationship using the following equation (**Figure 3. 16**). R_i refers to one channel, FoxO3a, G_i refers to another channel, DAPI. R and G refer to mean intensities of FoxO3a and DAPI across the entire area of image, respectively. PCC values range from 1 when intensities of two images are correlated perfect to -1 when intensities of two images are correlated inversely aligned. PCC measurement subtracts mean intensities from each channel's intensity, thus avoiding unproportioned and background signals (Dunn et al., 2011).

$$\mathrm{PCC} = \frac{\sum_i \left(R_i - \overline{R}\right) \times \left(G_i - \overline{G}\right)}{\sqrt{\sum_i \left(R_i - \overline{R}\right)^2 \times \sum_i \left(G_i - \overline{G}\right)^2}}$$

Figure 3. 16 Pearson's correlation coefficient (PCC) equation for measuring linear association between FoxO3a and DAPI in MC3T3-E1 cells

A P value of 0.002 was measured in pre-osteoblasts and this value increased in a time-dependent manner to 0.068 in 1-day differentiated MC3T3-E1 cells, it further increased to 0.316 in 3-day differentiated cells and to 0.368 in 7-day differentiated MC3T3-E1 cells, reaching the highest nuclear localization in 7-day differentiated mature osteoblasts.

3.5.3. Characterization calcium transport during osteoblast differentiation and mineralization

We performed qPCR and immunoblotting to identify important players in calcium regulation during osteoblastogenesis. $Ca_v1.2$, a subunit belongs to L-type Ca^{2+} channel showed a gradual decrease as cells undergo differentiation, reaching the lowest expression levels in 7-day differentiated mature osteoblasts. Other L-type Ca^{2+} channel subunit $Ca_v1.3$ expression remained constant from pre-osteoblasts to immature then to osteoblasts before significantly down-regulated in 7-day differentiated mature osteoblasts. These observations are consistent with previous findings showing $Ca_v1.2$ being the predominant subunit for Ca^{2+} influx in proliferating pre-osteoblasts which would then decrease in expression during differentiation and switch to T-type in osteocytes (Bergh et al., 2006; Caffrey et al., 1989; Liu et al., 2000).

$Ca_v3.1$, a subunit of the T-type Ca^{2+}channel, showed lowest expression levels in pre-osteoblasts which then increased gradually during differentiation and reached the highest levels in 7-day differentiated osteoblasts. Our next objective was to measure channel activity to determine which channel is the major functioning channel in 7-day differentiated osteoblasts.

Calbindin-D_{9K} expression remained stable in pre-osteoblasts and 1-day immature osteoblasts before declines slightly in 3-day differentiated osteoblasts. Calbindin-D_{9K} reached the lowest levels in 7-day mature osteoblasts, suggesting Calbindin-D_{9K} participation during osteoblastogenesis. We also looked for TRPV channels, TRPV5 and TRPV6 and calcium sensing receptor (CaSR) for mediating extracellular calcium influx into the osteoblasts, and Calbindin-D_{28K} for Ca^{2+} translocation but were not able to detect TRPV5, TRPV 6, CaSR and Calbindin-D_{28K} in the current model.

Two transmembrane proteins in the Ca^{2+} efflux mechanism, NCX and PMCA-1b were assessed for their expression in the current model. NCX showed a stable expression throughout osteoblast differentiation, suggesting it's extruding Ca^{2+} into the ECM steadily. PMCA-1b, which is the primary isoform pf PMCA in osteoblasts, showed a gradual increase in expression from pre-osteoblasts to immature then to osteoblasts before declining in 7-day differentiated mature osteoblasts. This observation is consistent with *in vivo* observation that PMCA expression rises prior to mineralization and decreases as mineralization is initiated (Stains et al., 2002).

3.5.4. FoxO3a:RXRα interaction in osteoblasts?

RXR:PPAR heterodimers play important roles in adipocyte differentiation and emerging roles in stress resistance (Dowell et al., 2003).

Interaction between FoxO3a and RXRα in 7-day differentiated mature osteoblasts

FoxOs have been reported have an inhibitory role in adipocyte differentiation via binding with PPARγ/RXRα (Dowell et al., 2003). Co-transfection with PPARγ:RXRα reduces FoxO1 activity in a dose-dependent manner, suggesting potential interaction between FoxO1 and RXRα. Therefore, we were interested in determining potential FoxO3a:RXRα in osteoblasts. RXR:VDR heterodimer bind to VDRE in the promoter region of target genes such as FoxO3a to modulate gene regulation (Pike et al., 2014). Several lines of literature had suggested expression levels of nuclear FoxO3a can be up-regulated by high levels of oxidative stress. Therefore, we sought to determine if this increased levels of Foxo3a would then bind to RXRα, leading to competitive reduction in available RXRα. We set up two strategies, first to pull down FoxO3a proteins from the cell lysates collected from 7-day differentiated osteoblasts (control). Then immunoblotted with anti-RXRα antibodies to confirm its interaction. We first pulled down and blotted with used

rabbit polyclonal anti-FoxO3a antibodies from control and negative control of rabbit serum, and detected a strong band in the negative control. This problem may be due to rabbit IgG in the serum, therefore, anti-FoxO3a antibodies from goat were used to pull down FoxO3a from control and immunoblotted with anti-FoxO3a from rabbit. Due to our surprise, a dense band was detected in the negative control, suggesting cross-reactivity. We took a different approach, by using goat polyclonal anti-FoxO3a antibodies to pull down FoxO3a from control and immunoblotted with rabbit monoclonal anti-FoxO3a antibodies, but no band was detected. We concluded that due to problems with cross-reactivity, we were unable to identify FoxO3a:RXRα interaction with the current tools available.

CHAPTER 4: VITAMIN D INREASES CALCIUM UPTAKE AND INHIBITS OSTEOBLAST MEDIATED MINERALIZATION

4.1 Effects of vitamin D signaling and ROS on important gene expression in vitro model MC3T3-E1 cells

Vitamin D is a steroid hormone that is important for maintaining calcium homeostasis by increasing calcium absorption in the small intestine, kidneys and bone (Anderson et al., 2012). Active vitamin D enhances bone formation and mineralization and prevents rickets in young children and osteomalacia in adults (DeLuca, 2014; van de Peppel and Leeuwen, 2014). *In vivo* transgenic mice with VDR over-expression driven by osteoblast-specific promoter increased bone mass and volume (Gardiner et al., 2000). Several lines of studies also demonstrated $1,25D_3$ to stimulate proliferating osteoblasts, up-regulate important non-collagenous proteins involved in osteoblast differentiation and mineralization, including osteocalcin, matrix Gla protein and collagen (Driel and Leeuwen, 2014). High levels of ROS can negatively affect vitamin D-mediated bone mineralization (Almeida and O'Brien, 2013; Sethe et al, 2006; Stolzing et al, 2008). Catabolic effects of $1,25D_3$ on bone metabolism have been reported. $1,25D_3$ acts directly on osteoclast progenitor differentiation to osteoclasts by enhancing activation of monocytes, leading to bone resorption (Suda et al., 1992). $1,25D_3$ has also been shown to induce RANKL expression thus stimulates osteoclastogenesis (Anderson et al., 2012). Mice with global knock-out of VDR displayed enhanced bone mass, trabecular volume and thickness (Amling et al., 1999). These reports provide evidence that $1,25D_3$ plays dual roles in osteoblastogenesis. Thus, we sought to investigate the role of FoxO3a's in vitamin D-mediated osteoblast mineralization and matrix calcification using the current *in vitro* model. We hypothesized that FoxO3a is important for both osteoblast differentiation and mineralization. First, we examined the effects of $1,25D_3$ and ROS on FoxO3a and RXR:VDR. Second, we examined expression of calcium mediators and transporters involved in calcium regulation. **Figure 4. 1** is a schematic illustration

of an osteoblast displaying calcium transporters and mediators of calcium homeostasis that were assessed in the previous chapter. L-type calcium channels ($Ca_v1.2$, $Ca_v1.3$) and T-type calcium channel ($Ca_v3.1$) for Ca^{2+} uptake and are present on the plasma membrane facing the bone marrow (Bergh et al., 2006). Calbindin-D_{9K} binds to Ca^{2+} and translocate it to the other side of the cell. NCX is present on the basolateral side of the osteoblast facing osteoid, it deposits Ca^{2+} into the matrix (Bergh et al., 2006). Next, we determined the effects of $1,25D_3$ on Ca^{2+} uptake in osteoblasts via live cell ratiometric calcium imaging. Finally, we investigated the effects of $1,25D_3$ and ROS on Ca^{2+} deposition in osteoblasts via Alizarin Red S staining (ARS).

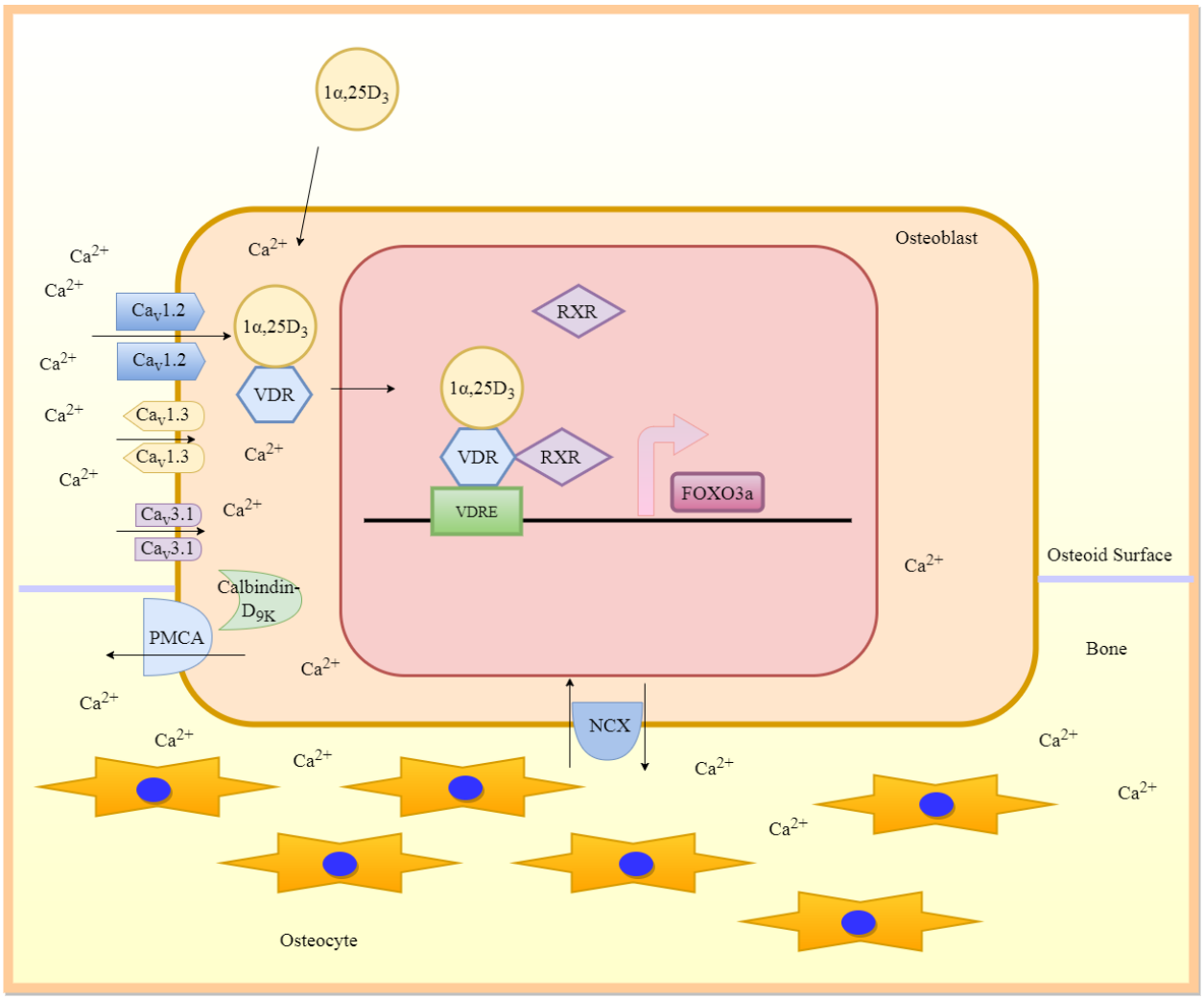

Figure 4. 1 **Schematic illustration of an osteoblast**

L-type Ca^{2+} channels ($Ca_v1.2$, $Ca_v1.3$), T-type Ca^{2+} channel ($Ca_v3.1$) and Plasma membrane Ca^{2+} ATPase isoform 1b (PMCA-1b) are present on the plasma membrane facing the bone marrow. Calbindin-D_{9K} translocates Ca^{2+} to the opposite side, where *s*odium-calcium exchanger (NCX) reside. FoxO3a: Forkhead box O3a, VDR: vitamin D receptor, VDRE: vitamin D response element, RXR: retinoid x receptor.

4.1.1. Assessment of appropriate doses of 1,25D$_3$ and ROS

In order to examine the effects of 1,25D$_3$ on osteoblast mineralization and matrix calcification, 7-day differentiated MC3T3-E1 cells were treated with six concentrations of 1,25D$_3$ with one control of untreated for 24 hours with a dose change every 12 hours. These concentrations include: 10^{-10} M, 10^{-9} M, 10^{-8} M, 10^{-7} M, 10^{-6}M and 10^{-5} M. A suitable concentration would be non-toxic to the cells and be able to stimulate downstream gene expression. Cell viability assessed by MTT assay showed all six concentrations did not cause significant cell death (**Figure 4. 2**). A middle dose of 10^{-7} M 1,25D$_3$ was chosen and used for all measurements.

7-day differentiated MC3T3-E1 cells were incubated with five H_2O_2 concentrations for an hour: 100 μm, 150 μM, 200 μM, 250 μM, and 300 μM, and ROS levels were measured with 2',7' – dichlorofluorescin diacetate (DCFDA). A suitable concentration of H_2O_2 would generate significant ROS levels without causing significant cell apoptosis in 7-day differentiated MC3T3-E1 cells. Treatment with 100 μM H_2O_2 showed a slight increase in ROS levels compared to control (untreated), cells treated with 150 μM and 200 μM showed approximately 0.5-fold increase. A significant increase of almost 2 fold in ROS levels were observed in cells treated with 250 μM H_2O_2. 300 μM H_2O_2 resulted in a slight decline in ROS formation (**Figure 4. 3A**). MTT assay revealed all five H_2O_2 concentrations did not cause significant apoptosis in 7-day differentiated osteoblasts (**Figure 4. 3B**). Therefore, 250 μM H_2O_2 was determined to be the appropriate concentration to use and was therefore used throughout the experiments.

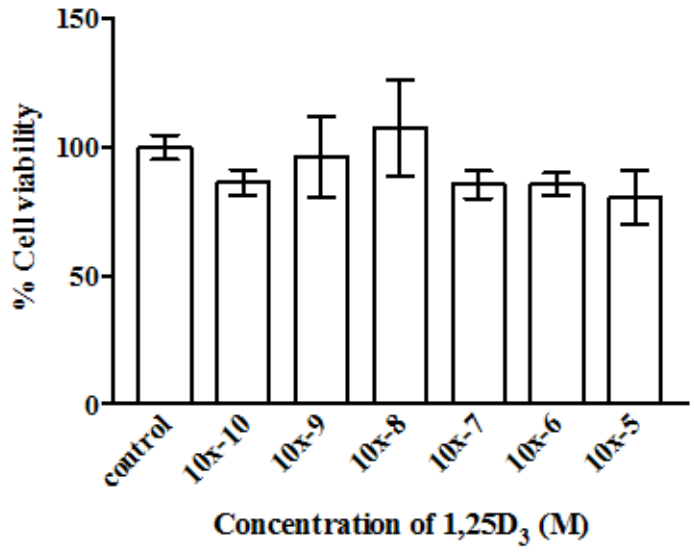

Figure 4. 2 100 nM $1,25D_3$ does not cause cell death in MC3T3-E1 cells

Cell viability was determined in 7-day differentiated MC3T3-E1 cells treated with various concentrations of active vitamin D ($1,25D_3$). n=3 each. Data are presented as means ± SEM.

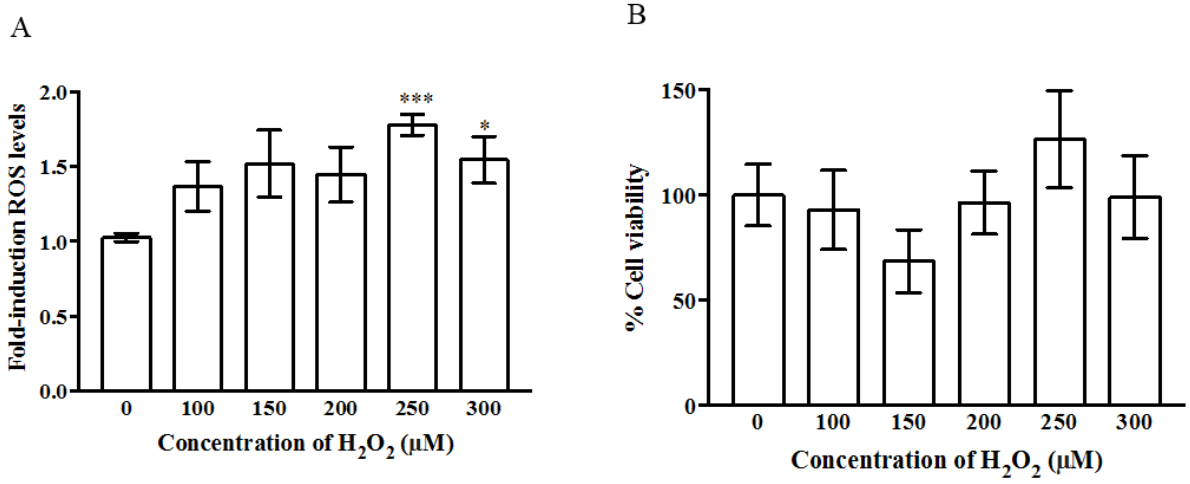

Figure 4. 3 250 µM H_2O_2 causes high levels of ROS in MC3T3-E3 cells

(A) 7-day differentiated MC3T3-E1 cells were treated with various hydrogen peroxide (H_2O_2) concentrations for an hour to generate reactive oxygen species (ROS). n=3 (B) The same

concentrations of hydrogen peroxide (H_2O_2) were also administered to determine cell viability in 7-day differentiated MC3T3-E1 cells after an hour. n=3 each. Data are presented as means ± SEM. *p ≤0.05, ***p ≤0.001

4.1.2 Effects of 1,25D$_3$ an ROS on expression of important transcription factors and genes

7-day differentiated MC3T3-E1 cells were treated with 10^{-7} M of 1,25D$_3$, 250 μM H_2O_2 and the combination treatment of 1,25D$_3$ and H_2O_2. mRNA and protein lysates were harvested for gene expression analysis (**Figure 4. 4**).

Our first objective was to determine effects of 1,25D$_3$ on genes of transcription factors involved in osteoblast differentiation and mineralization, such as Runx2 and OCN. Our second objective was to examine effects of 1,25D$_3$ on FoxO3a, RXRα and VDR in 7-day differentiated osteoblasts.

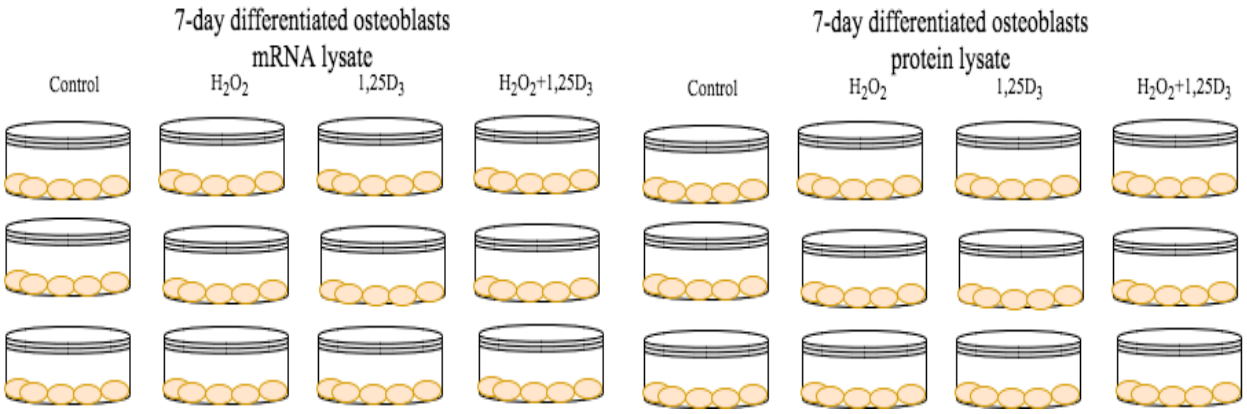

Figure 4. 4 **mRNA and protein collection in 7-day differentiated MC3T3-E1 cells**

(A). mRNA lysate was collected from control, 250 μM H_2O_2, 10^{-7} M 1,25D_3, and combination group.

(B). protein lysate was collected from the same drug matrix. n=3 each

4.1.2.1 Effect of 1,25D$_3$ on osteoblast differentiation and mineralization

10^{-7} M 1,25D$_3$ reduced Runx2 expression significantly, to levels less than half compared to control (**Figure 4. 5A**). An hour treatment with either 250 μM H_2O_2 caused a significant reduction in Runx2 expression in 7-day differentiated MC3T-E1 cells. The combination group of 10^{-7}M 1,25D$_3$ and 250 μM H_2O_2 caused a further reduction in Runx2 expression (**Figure 4. 5A**). 250 μM H_2O_2 had no effect on OCN expression but treatment with 1,25D$_3$ reduced OCN expression significantly. Although a single dose of H_2O_2 did not alter OCN expression, the combination group of 1,25D$_3$ and H_2O_2 caused a significant reduction in OCN expression to comparable levels to just 1,25D$_3$ treatment (**Figure 4. 5B**).

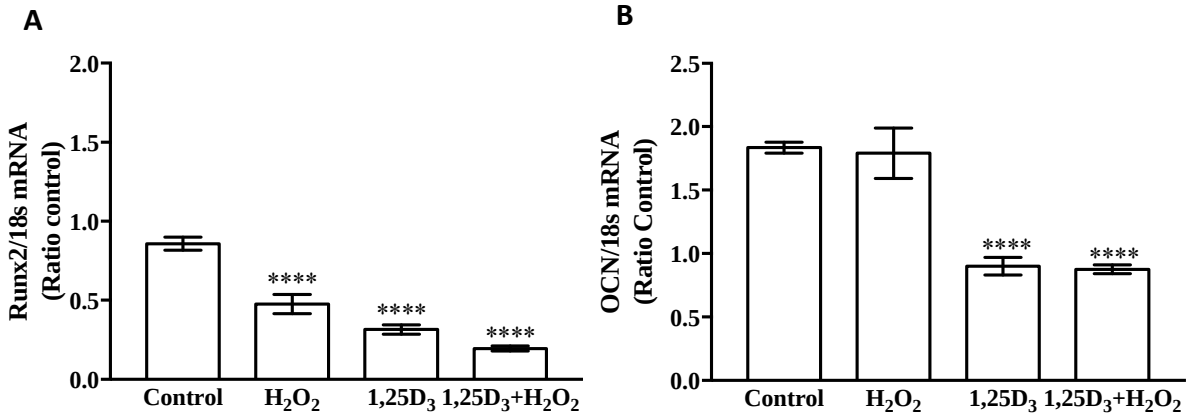

Figure 4. 5 **Effect of ROS and 1,25D$_3$ on markers of osteoblast differentiation**

(A). Significant reduction by H_2O_2 and 1,25D$_3$ on Runx2 expression in 7-day differentiated MC3T3-E1 cells. (B). OCN expression is down-regulated by 1,25D$_3$ and the combination of H_2O_2 and 1,25D$_3$. n=9 each. Data are presented as means ± SEM. n=9 for each group.

****p ≤0.0001

4.1.2.1 1,25D_3 up-regulated FoxO3a expression levels significantly in osteoblasts

To determine the effects of 1,25D_3 on the expression levels of FoxO3a, 7-day differentiated MC3T3-E1 cells were treated with 10^{-7} M of 1,25D_3 for 24 hours, with a dose change every 12 hours. mRNA and protein levels were measured at the end of treatment period.

1,25D_3 up-regulated FoxO3a significantly at both the mRNA and protein levels, reaching an almost 4-fold increase (**Figure 4. 6A and B**).

Immunofluorescence performed in 7-day differentiated MC3T3-E1 cells further demonstrated 1,25D_3-induced increase in FoxO3a expression in **Figure 4. 7C** compared to control in Figure 4. 7**A**. We used DAPI to stain the nucleus, Alexa Fluor 488 to stain the actin cytoskeleton and FoxO3a was detected with rabbit monoclonal FoxO3a antibodies, which were then bound to donkey anti-rabbit Cy3 antibodies. Degree of 1,25D_3-stimulatied FoxO3a nuclear expression could be measured and quantified in comparison with untreated control group via Pearson's correlation coefficient. Untreated 7-day differentiated MC3T3-E1 cells exhibited a PCC value of 0.272 and this increased to 0.395 in 100 nM 1,25D_3 treatment group (**Table 4.3**).

250 μM H_2O_2 alone did no alter FoxO3a mRNA and protein expression levels in 7-day differentiated MC3T3-E1 cells (**Figure 4. 6A and B**). FoxO3a expression detected via immunofluorescence also did not show significant alterations under the treatment of H_2O_2 compared to control (**Figure 4. 7B**). PCC measurement showed a slight increase from 0.272 in control to 0.308 in H_2O_2-treated group (**Table 4.3**). On the other hand, combination treatment of 1,25D_3 and H_2O_2 attenuated the increase mediated by 1,25D_3 alone at mRNA and protein levels (**Figure 4. 6A and B**). Immunofluorescence also showed reduction in FoxO3a expression in the

combination group compared to $1,25D_3$-treated alone (**Figure 4. 7D**). PCC measurement showed H_2O_2 did not cause significant FoxO3a nuclear localization compared to control. $1,25D_3$ significantly increased FoxO3a nuclear localization to 0.395 and the combination treatment of $1,25D_3$ and H_2O_2 attenuated the increase to 0.371 (**Figure 4. 8**).

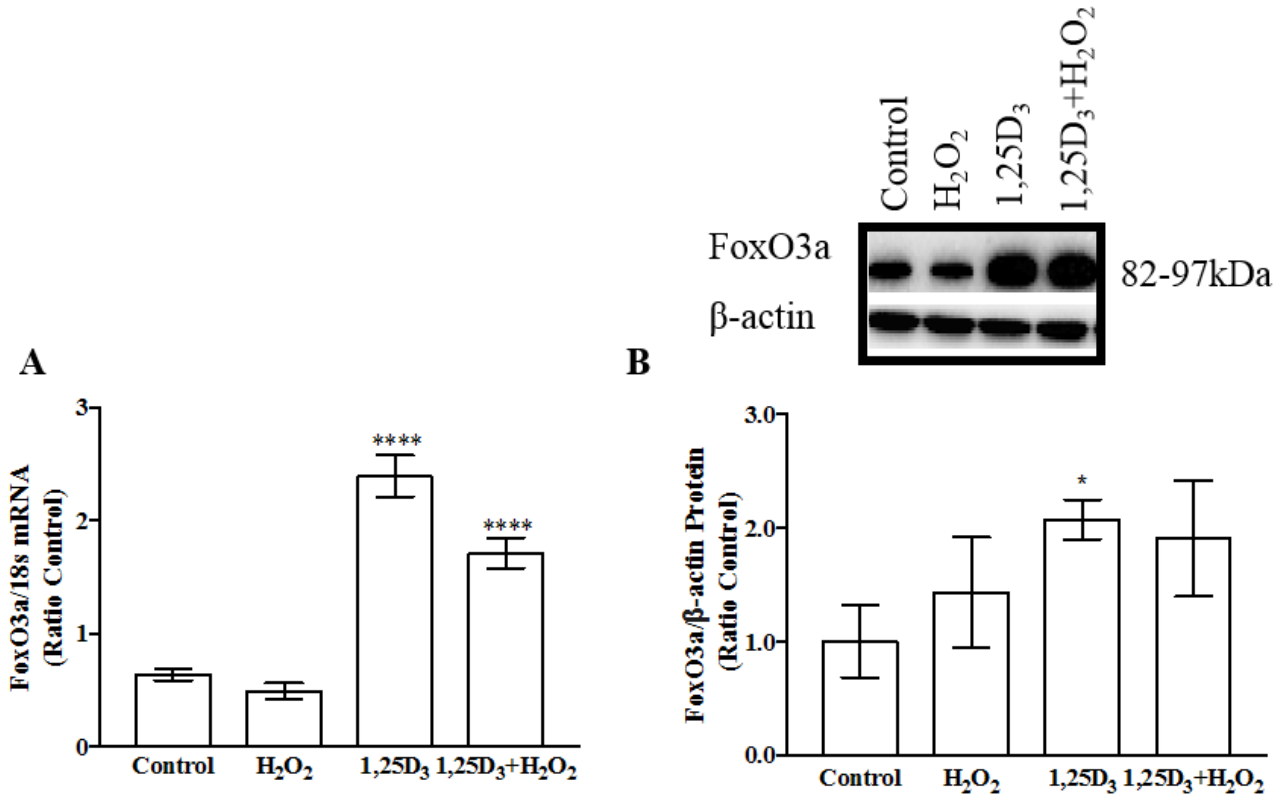

Figure 4. 6 **1,25D$_3$ up-regulates FoxO3a mRNA and protein expression significantly in 7-day differentiated MC3T3-E1 cells**

(A). 1,25D$_3$ up-regulated FoxO3a mRNA expression and this increase was attenuated by treating 7-day differentiated MC3T3-E1 cells with H_2O_2 and 1,25D$_3$.

(B). 1,25D$_3$ increased FoxO3a protein expression, and this increase was attenuated in the combination treatment group, n = 21 each. Data are presented as means ± SEM. *p≤0.05, **p ≤0.01, ****p ≤0.0001

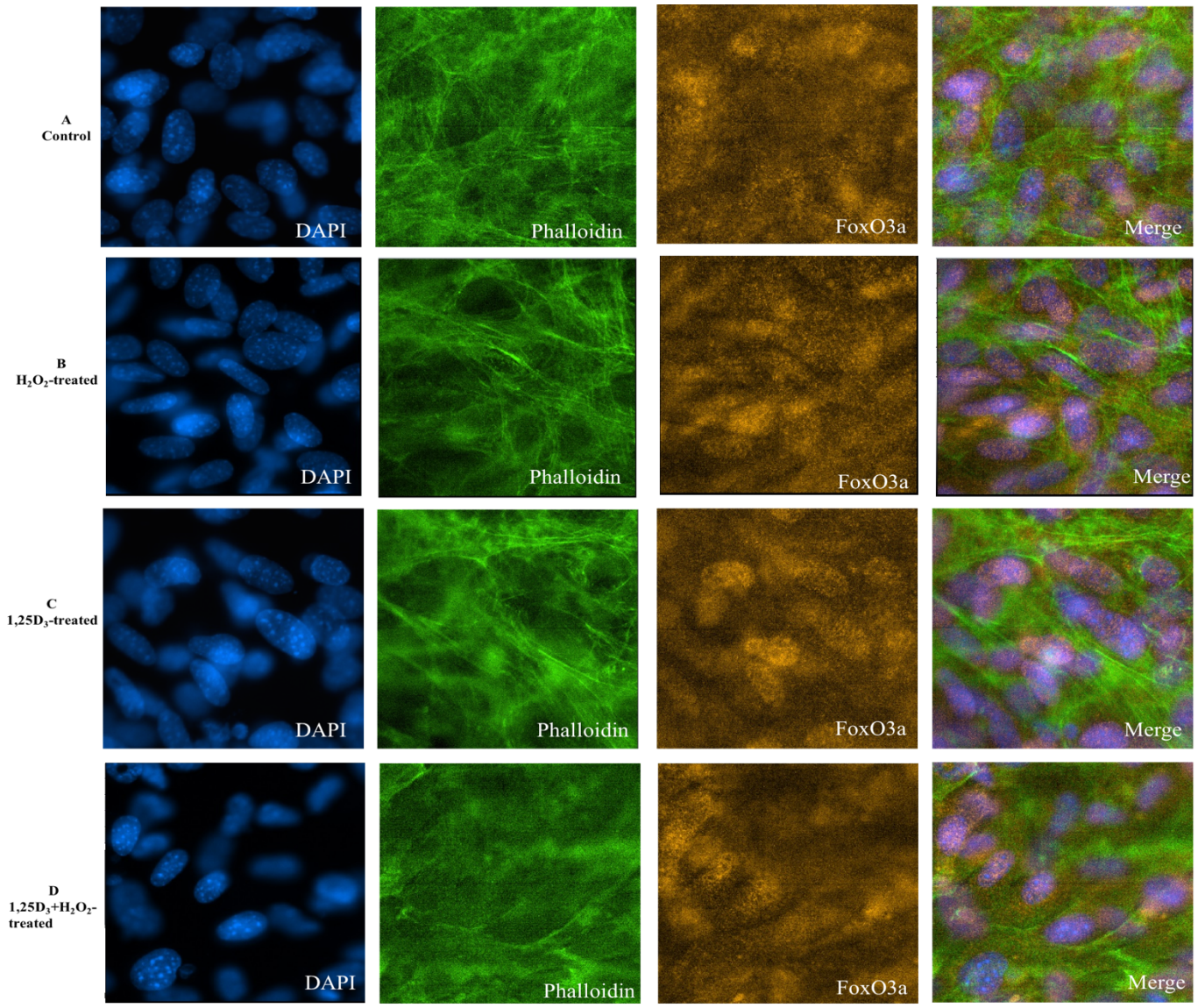

Figure 4. 7 Immunofluorescence showed enhanced nuclear FoxO3a expression in 7-day differentiated MC3T3-E1 cells treated with $1,25D_3$

(A). Untreated (control) group of 7-day differentiated MC3T-3E1 cells showed base levels of nuclear FoxO3a expression.

(B). $1,25D_3$-treated osteoblasts showed a significant increase in nuclear FoxO3a expression.

Table 4.3 Measurement of FoxO3a nuclear localization after treatment with 1,25D3

Drug Treatment	Pearson's correlation coefficient ± SEM	P-values
Control	0.272 ± 0.010	-
250 µM H_2O_2	0.308 ± 0.011	0.0988
10^{-7} M $1,25D_3$	0.395 ± 0.011	< 0.0001
10^{-7} M $1,25D_3$ + 250 µM H_2O_2	0.371 ± 0.011	< .0001

Degree of FoxO3a in the nucleus was measured with DAPI and quantified with Pearson's correlation coefficient in 7-day differentiated MC3T3-E1 cells. n=25 each.

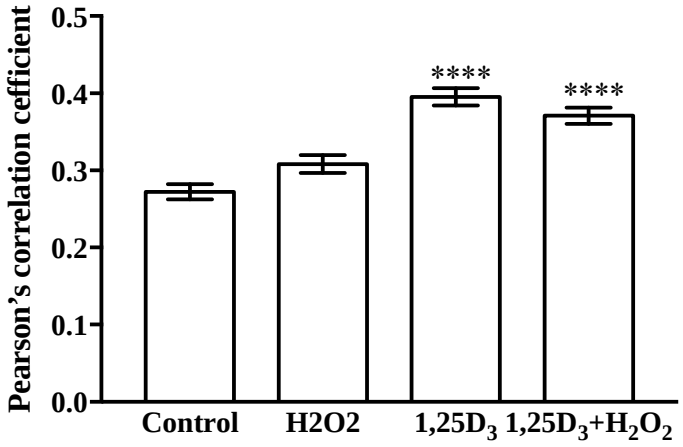

Figure 4. 8 $1,25D_3$ increased FoxO3a nuclear localization in 7-day differentiated osteoblasts and H_2O_2 attenuated this $1,25D_3$-induced localization

Pearson's correlation coefficient measures FoxO3a nuclear localization via co-localization with DAPI. H_2O_2 treatment alone did not alter FoxO3a nuclear localization, $1,25D_3$ enhanced FoxO3a

nuclear localization significantly while the combination reduced the enhancement caused by $1,25D_3$ alone.

Data are presented as means ± SEM. n=25 each. ****p ≤0.0001

Effect of $1,25D_3$ and ROS on RXRα expression in 7-day differentiated MC3T3-E1 cells

Treatment with 250 μM H_2O_2 did not alter RXRα mRNA and protein expression in 7-day differentiated MC3T3-E1 cells. $1,25D_3$ increased RXRα mRNA and protein expression significantly. The combination group of $1,25D_3$ and H_2O_2 attenuated the increase caused by $1,25D_3$ alone in both mRNA and protein expression (**Figure 4. 9A and B**).

The effect of $1,25D_3$ and ROS on VDR expression in 7-day differentiated MC3T3-E1 cells

Treatment with 250 μM H_2O_2 did not alter VDR mRNA and protein expression in 7-day differentiated MC3T3-E1 cells.$1,25D_3$ increased VDR mRNA and protein expression significantly. The $1,25D_3$-mediated increase was attenuated in the combination group of $1,25D_3$ and H_2O_2 (**Figure 4. 10A and B**).

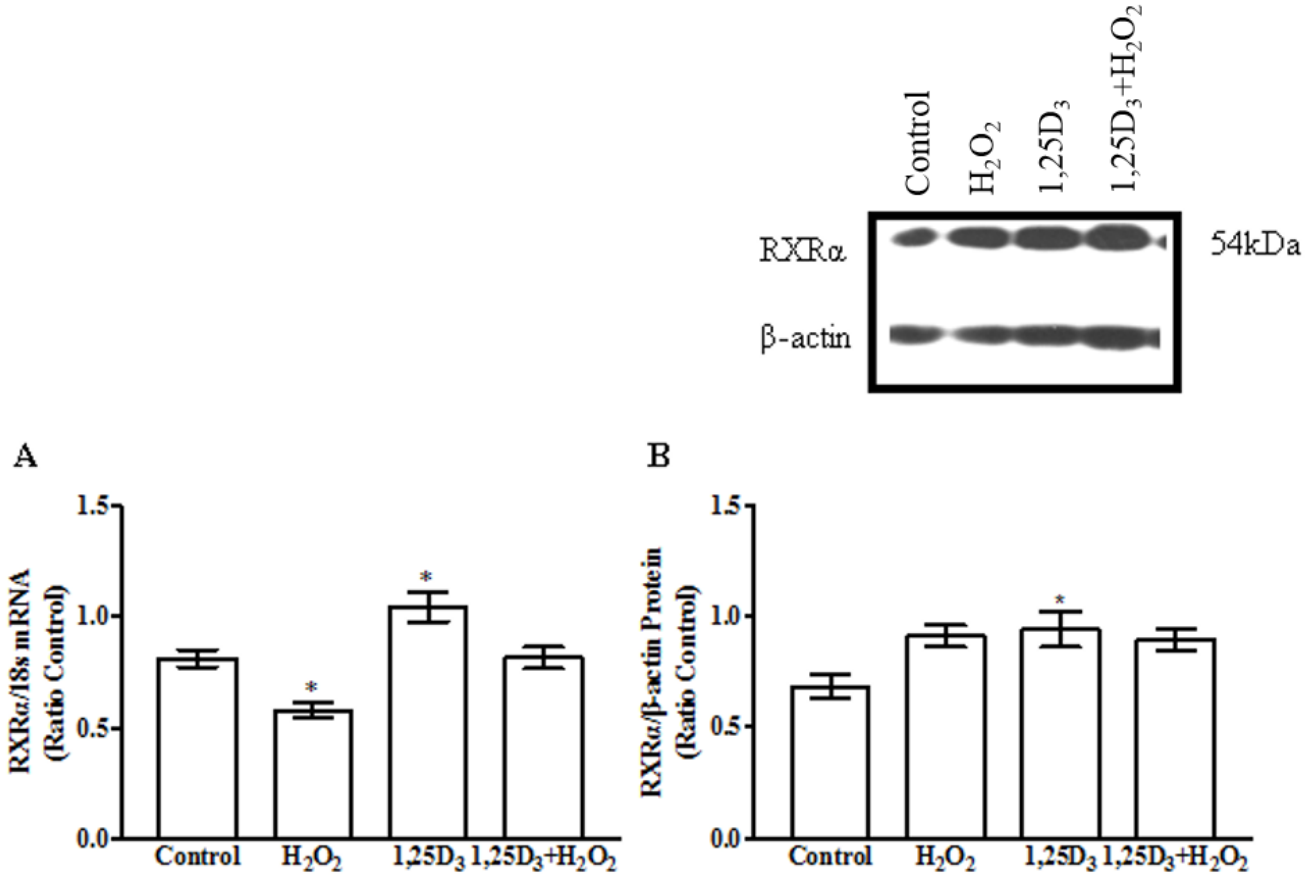

Figure 4. 9 RXRα expression is up-regulated by 1,25D$_3$ in osteoblasts

(A). 1,25D$_3$ up-regulated RXRα mRNA expression but H_2O_2 did not alter it (B) RXRα protein expression showed a similar pattern.

n=9 mRNA samples and n=14 β-actin samples. Data are presented as means ± SEM. *p≤0.05.

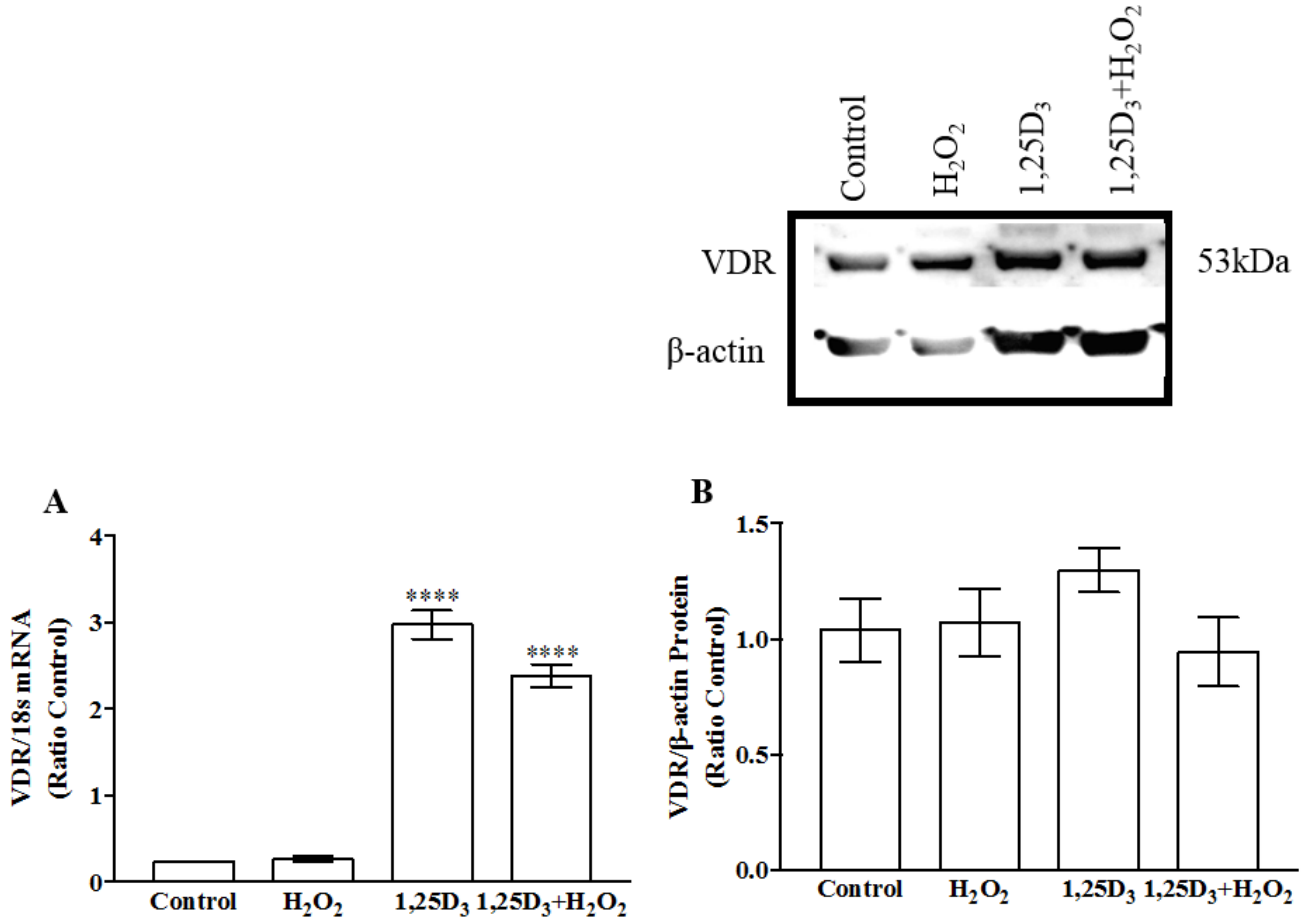

Figure 4. 10 Vitamin D Receptor (VDR) expression was increased by $1,25D_3$ in osteoblasts

(A). $1,25D_3$ up-regulated VDR mRNA expression but H_2O_2 did not alter it (B) VDR protein expression showed a similar pattern. n=6 each. Data are presented as means ± SEM.

****$p \leq 0.0001$

4.2 Effects of 1,25D$_3$ on calcium regulation in vitro MC3T3-E1 cells

In order to assess the effect of 1,25D$_3$ on calcium regulation into our model system, 7-day differentiated MC3T3-E1 cells underwent drug treatment shown in **Figure 4. 4** and RNA was harvested for analysis. We first analyzed Ca^{2+} channels, including L-type ($Ca_v1.2$, $Ca_v1.3$), and T-type ($Ca_v3.1$) that reside on the plasma membrane of the osteoblasts, regulating calcium uptake. We then analyzed Ca^{2+} mediators and transports such as Calbindin-D_{9K}, NCX and PMCA-1b for translocating Ca^{2+} to the opposite side to be deposited in the mineralizing matrix.

4.2.1 Effects of 1,25D$_3$ on expression on Ca^{2+} channels in 7-day differentiated osteoblasts

We first examined effects of 1,25D$_3$ on expression of Ca^{2+} channels involved in regulating Ca^{2+} entry. 1,25D$_3$ did not alter expression levels L-type ($Ca_v1.2$, $Ca_v1.3$) and T-type ($Ca_v3.1$) Ca^{2+} channels significantly. H_2O_2 treatment alone also did not alter $Ca_v1.2$, $Ca_v1.3$ and $Ca_v3.1$ expression levels. However, the combination treatment of 1,25D$_3$ and H_2O_2 reduced $Ca_v1.2$, $Ca_v1.3$ and $Ca_v3.1$ expression significantly (**Figure 4. 11A, B and C**). The expression of calbindin-D_{9K} was up-regulated significantly by 1,25D$_3$ and this increase was reduced by the combination treatment (**Figure 4. 11D**).

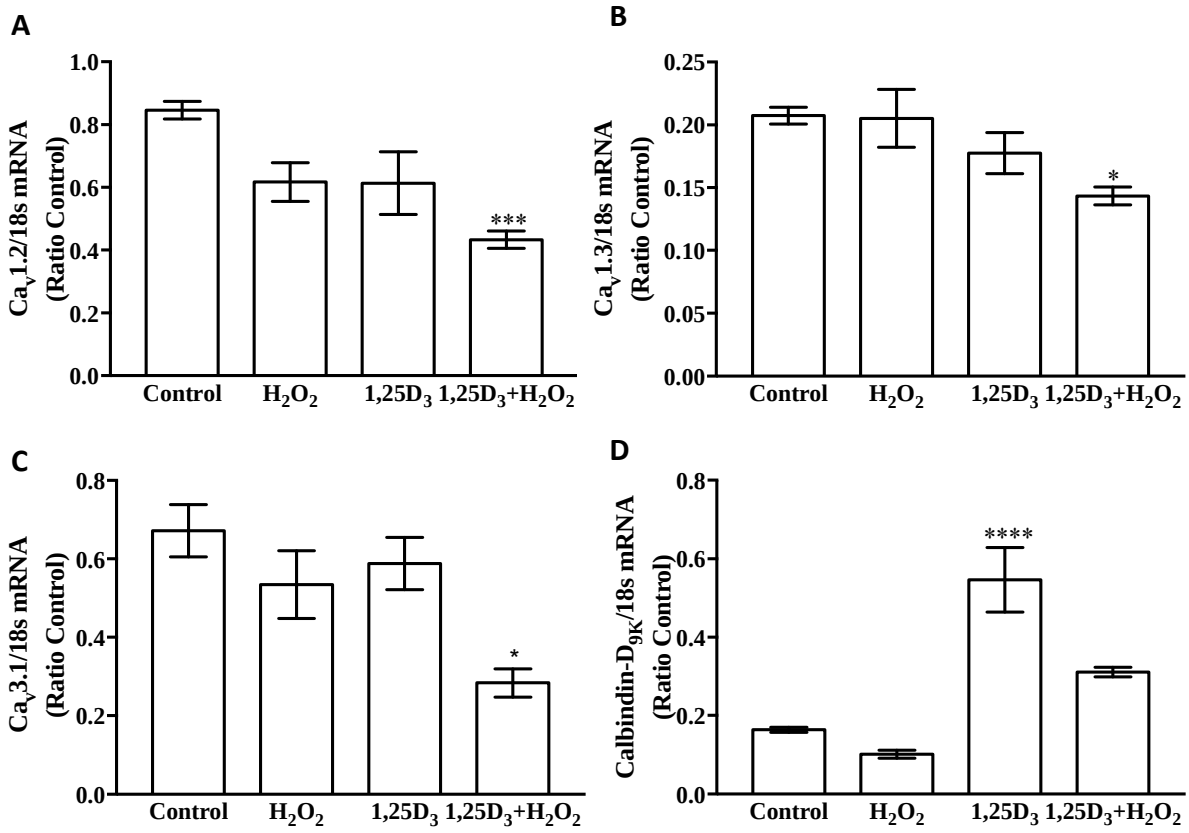

Figure 4. 11 Effects of $1,25D_3$ on L-type and T-type calcium channels in osteoblasts

mRNA expression of (A). $Ca_v1.2$ (B). $Ca_v1.3$ (C) $Ca_v3.1$ and (D) Calbindin-D_{9K}. All gene expression was normalized to 18s expression. n=9 each group for statistical analysis. Data are presented as means ± SEM. *p≤0.05, ***p ≤0.001, ****p ≤0.0001

4.2.2. Effects of 1,25D$_3$ on channel activity in 7-day differentiated osteoblasts

To measure [Ca^{2+}] uptake regulation through L-type and T-type Ca^{2+} channels, we employed ratiometric calcium imaging with Fura-2 AM technique in 7-day differentiated osteoblasts. Calcium uptake was measured in two parameters, Δ peak that indicates how much [Ca^{2+}] enters the cell and Δ slope that measures the rate of [Ca^{2+}] entry. Our first objective was to identify the functional channels in 7-day differentiated MC3T3-E1 cells by inhibiting calcium channel activity with specific channel blockers listed in **Table 4.4**. By inhibiting channel activity, we were able to measure the magnitude of Ca^{2+} entry by specific channel and further determine which channel(s) were responsible for the majority of calcium influx into osteoblasts.
Our second objective was to treat 7-day differentiated osteoblasts with 10^{-7} M 1,25D$_3$ and examined the effects of 1,25D$_3$ on channel activity.

Table 4.4 Channel blockers used for specific channels in 7-day differentiated osteoblasts

Calcium Channel	Calcium channel blockers	References
Divalent cation channels	100 μM Lanthanum Chloride ($LaCl_3$)	Paradis et al., 1974
TRPV channels	100 μM Ruthenium Red	Hoenderop et al., 2001
$Ca_v3.1$ (T-type)	10 μM NNC 55-0396	Huang et al., 2004
L-type	10 μM Felodipine	Hattori et al., 2001

4.2.2.1 Lanthanum chloride reduced calcium uptake in 7-day differentiated MC3T3-E1 cells

Lanthanum chloride ($LaCl_3$), a non-specific cationic channel blocker was expected to reduce all calcium channel activity, including L-type ($Ca_v1.2$, $Ca_v1.3$) and T-type ($Ca_v3.1$) shown in **Figure 4. 12**. $LaCl_3$ was first prepared by dissolving in deionized water as 1 M stock, and a working concentration of 100 μM was prepared freshly on the day of the experiment. For the control group, equal volume of 3.5 μL autoclaved deionized water was added to 35 mL 0.5 mM Ca^{2+} buffer as vehicle and calcium uptake was measured.

100 μM $LaCl_3$ reduced both magnitude (Δ peak) of calcium uptake by half compared to untreated control (**Figure 4. 13A**) and the rate (Δ slope) of calcium uptake was also reduced to less than half by $LaCl_3$ (**Figure 4. 13B**).

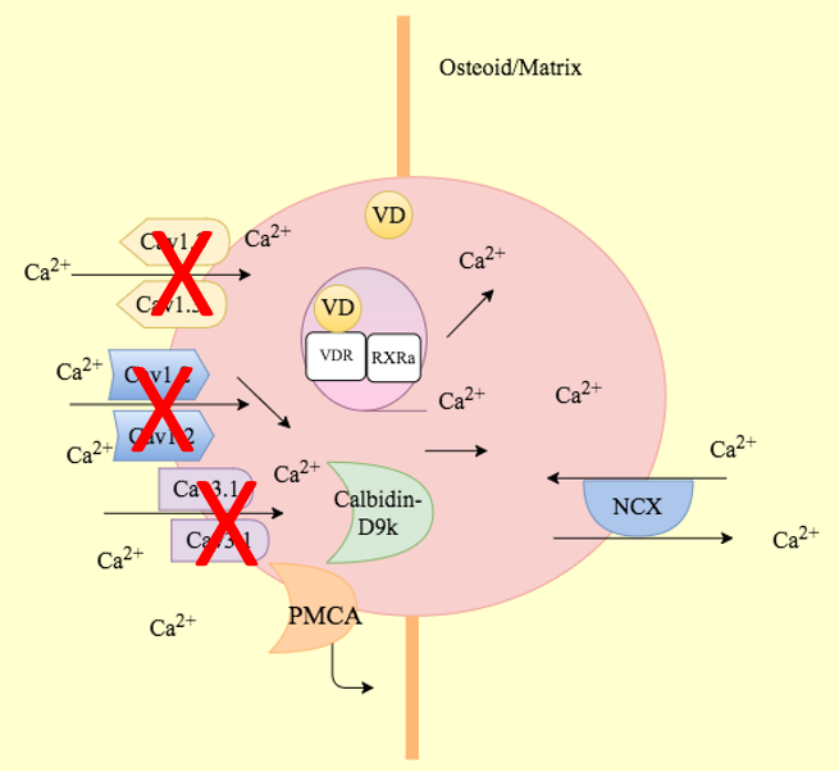

Figure 4. 12 100 µM lanthanum chloride ($LaCl_3$) was expected to reduce all cationic channel activity in osteoblasts

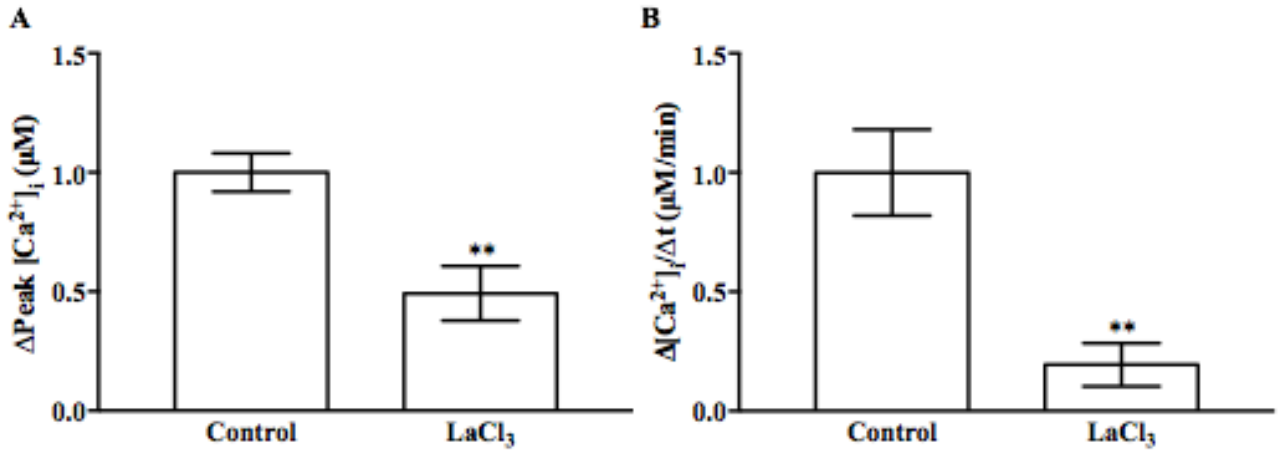

Figure 4. 13 Significant reduction in calcium influx by lanthanum (III) chloride in osteoblasts

(A). Total magnitude of calcium uptake in the presence and absence of $LaCl_3$ and (B). Rate of calcium uptake in the presence and absence of $LaCl_3$. n=6 control and n=4 $LaCl_3$-treated. All measurements were normalized to the day of the experiment, and data are presented as means ± SEM. **p ≤0.01.

4.2.2.2 Low-threshold (T-type) calcium channel is a minor functioning channel in osteoblasts

We next sought to examine whether there are functional T-type calcium channels in MC3T3-E1 cells. To do so we used 10 μM NNC 55-0396 which inhibits low-threshold (T) type calcium channel (**Figure 4. 14**). NNC 55-0396 was prepared by dissolving in autoclaved deionized water to make 10 mM stocks and stored at 4 °C. On the day of the experiment, 10 mM stocks of NNC 55-0396 was diluted to 10 μM which was applied to the 7-day differentiated MC3T3-E1 cells. For the control group, equal volume of 35 μL of autoclaved deionized water was added to 35 mL 0.5 mM Ca^{2+} buffer as vehicle and calcium uptake was measured.

10 μM NNC 55-0396 did not cause a significant alteration of either Δmagnitude or Δslope of calcium uptake into our model osteoblasts, indicating that low threshold T-type calcium channel is a minor functioning channel in osteoblasts (**Figure 4. 15A and B**).

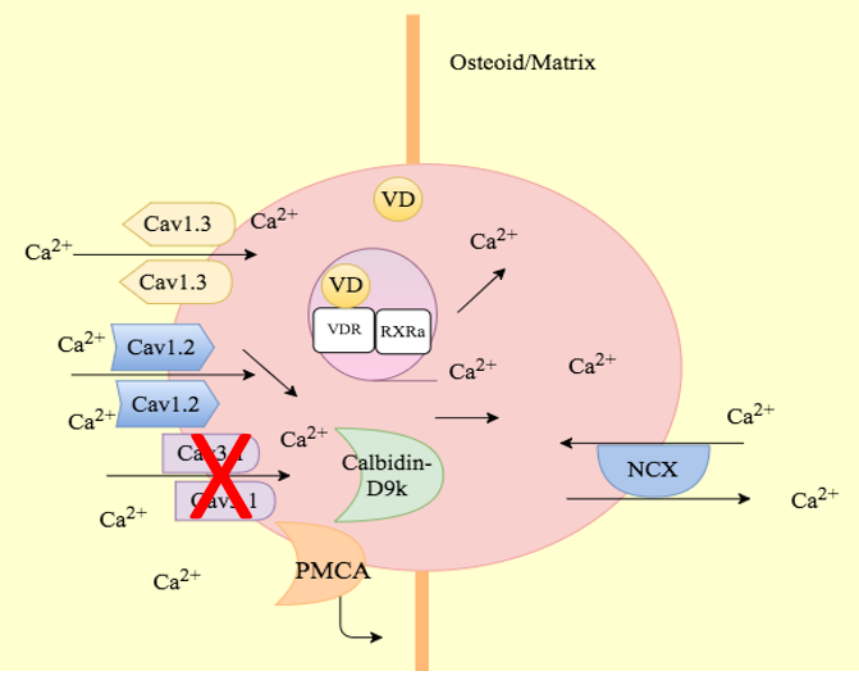

Figure 4. 14 **NNC 55-0396 is a T-type calcium channel blocker**

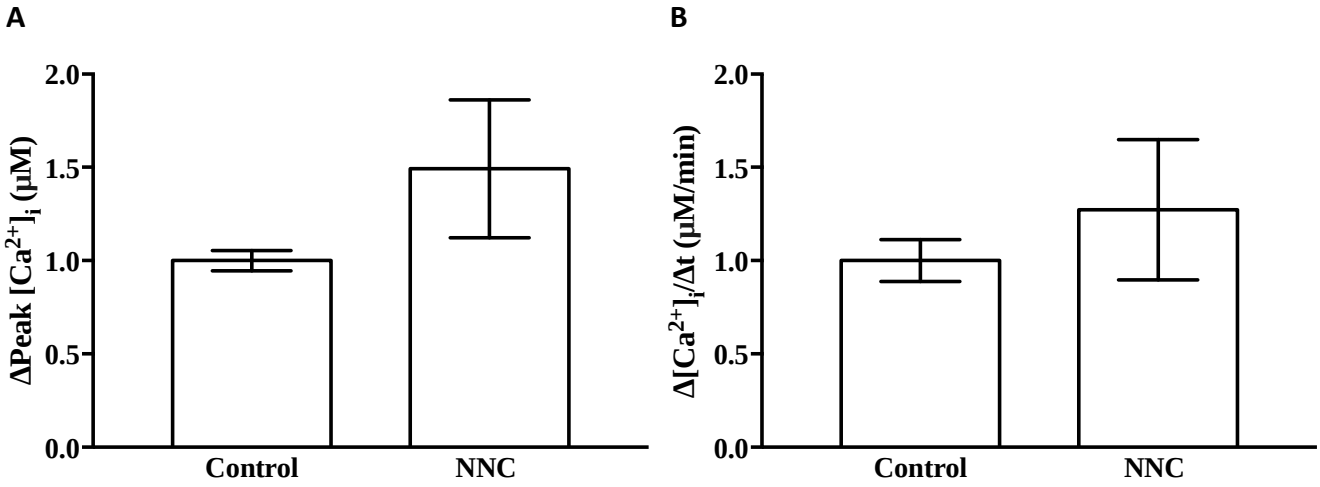

Figure 4. 15 Low threshold (T-type) calcium channel are not a major calcium channel mediating calcium uptake

(A). Magnitude of calcium uptake in 7-day differentiated MC3T3-E1 cells and (B) rate of calcium uptake in the presence and absence of NNC, n=9 control and n=6 NNC 55-0396-treated.

All measurements were normalized to the day of the experiment, and data are presented as means ± SEM.

4.2.2.3 L-type calcium channel is the major functioning calcium channel.

10 μM Felodipine was applied to 7-day differentiated MC3T3-E1 cells to inhibit L-type Ca^{2+} channel activity, including $Ca_v1.2$ and $Ca_v1.3$ (**Figure 4. 16**). For the controls, equal amount of 35μL of DMSO was added to the 35 mL 0.5mM Ca^{2+} buffer and calcium uptake was measured. Felodipine caused a significant reduction in Δ magnitude and Δ rate, almost abolished calcium uptake (**Figure 4. 17A and B**). Felodipine also caused significant calcium efflux (**Figure 4. 17A and B**). In **Figure 4. 18**, Felodipine-treated in red showed a significant reduction in 340/380 Ca^{2+} ratio intensity in comparison with control shown in blue, causing significant Ca^{2+} depletion.

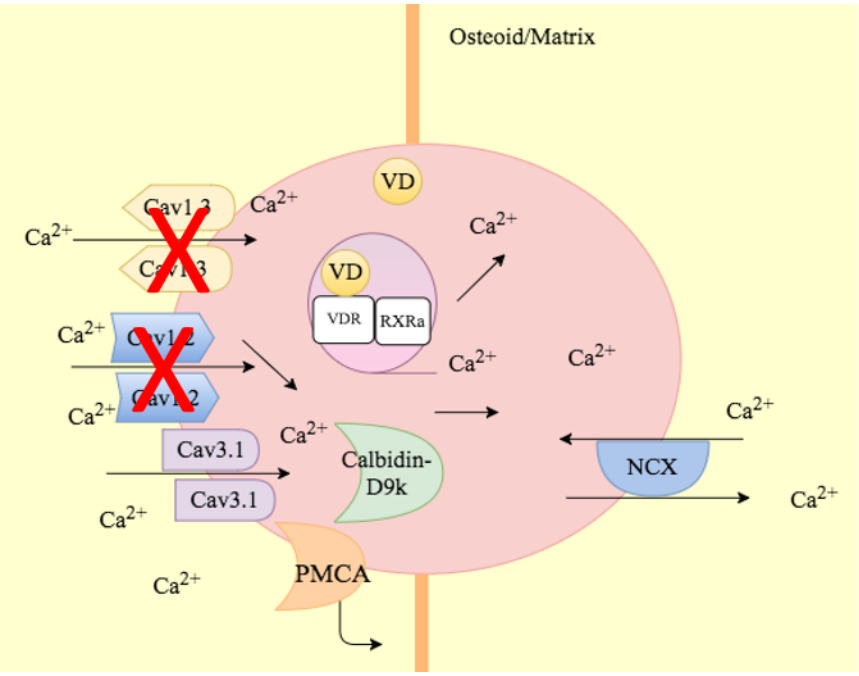

Figure 4. 16 L-type ($Ca_v1.2$, Ca_v 1.3) channels can be blocked with Felodipine in osteoblasts

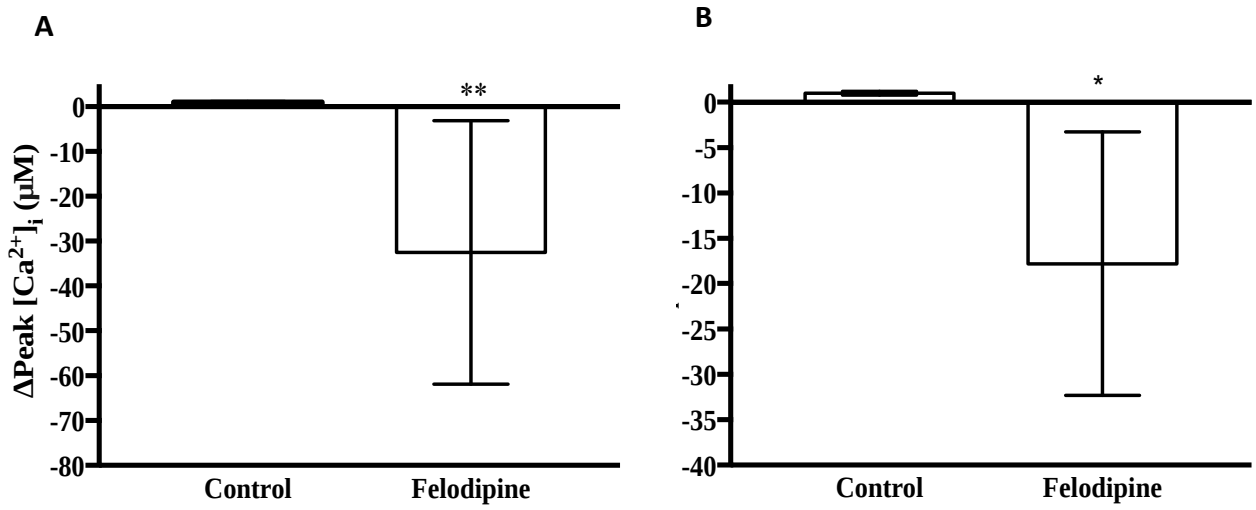

Figure 4. 17 **Felodipine caused significant calcium efflux in 7-day differentiated MC3T3-E1 cells**

(A). Magnitude of calcium uptake and (B) rate of calcium uptake in the presence and absence of Felodipine, n=7 control and n=8 Felodipine-treated. All measurements were normalized to the day of the experiment, and data are presented as means ± SEM, *p≤0.05, **p ≤0.01.

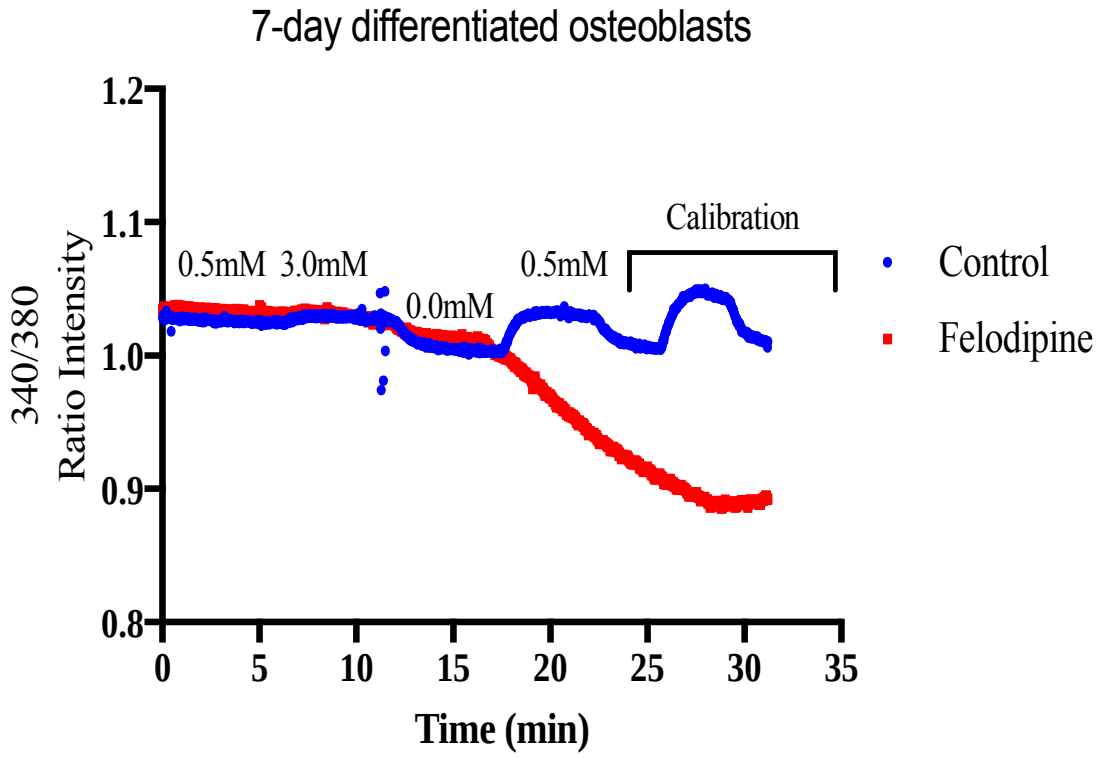

Figure 4. 18 **Felodipine caused calcium efflux in osteoblasts**

Representative traces from the experiment in 21. The control group is shown in blue, and Felodipine-treated group shown in red. Calcium uptake was measured during the first 30 seconds of perfusion with the 0.5 mM Ca^{2+} buffer where DMSO was applied as vehicle in the control group and 10 μM Felodipine was applied to 7-day differentiated MC3T3-E1 cells. The control group showed calcium uptake in the 340/which was prevented by Felodipine leading to significant efflux.

4.2.2.4 Absence of TRPV channels verified in 7-day differentiated MC3T3-E1 cells

Next we assessed the effect of ruthenium red on calcium uptake into 7 day differentiated MC3T3-E1 cells with an inhibitor of TRPV channels. Ruthenium red was dissolved in autoclaved deionized water to make a10 mM stock and prepared freshly on the day of the experiment. It was diluted to 100 μM and applied to 7-day differentiated MC3T3-E1 cells. Ruthenium red did not alter calcium uptake in our model system (**Figure 4. 19**), consistent with the absence of functional TRPV channel in osteoblasts.

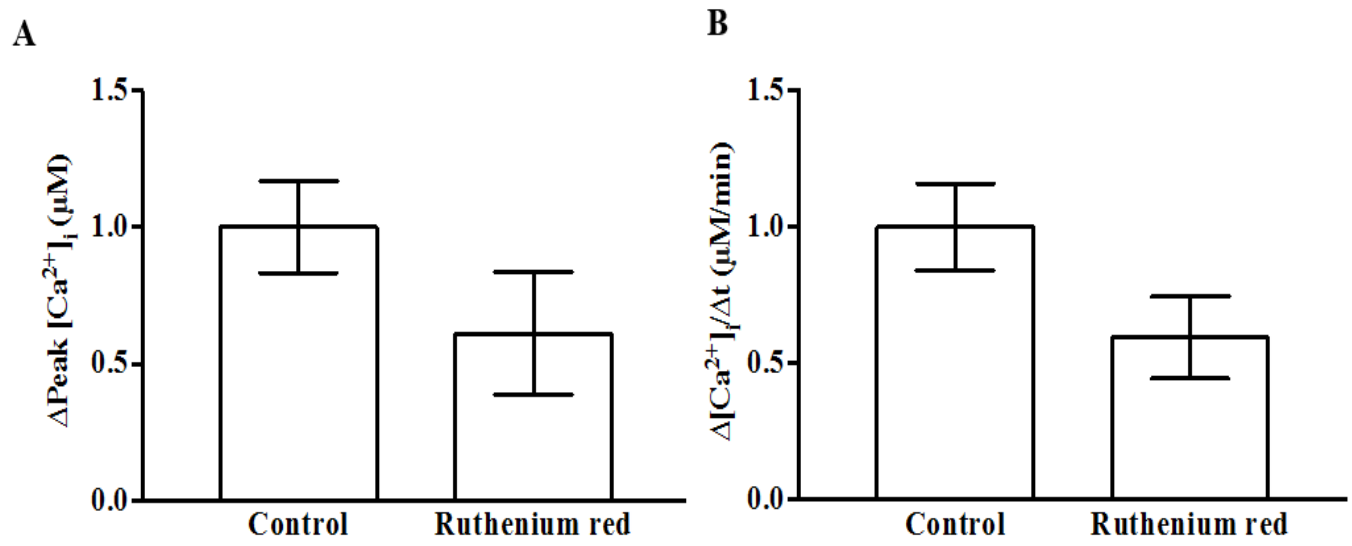

Figure 4. 19 **Ruthenium Red did not cause significant reduction in calcium uptake**

(A). Magnitude of calcium uptake in control vs. ruthenium red-treated group and (B) rate of calcium influx in control vs. ruthenium red-treated group, n=11 each. All measurements were normalized to the day of the experiment, and data are presented as means ± SEM.

4.2.3 1,25D$_3$ increased calcium uptake in 7-day differentiated osteoblasts significantly

To determine effects of 1,25D$_3$ on regulating Ca^{2+} uptake in 7-day differentiated osteoblasts, cells were treated with 10^{-7} M 1,25D$_3$ for 24 h and Ca^{2+} uptake was measured by ratiometric calcium imaging. 10^{-7} M 1,25D$_3$ caused significant increase in Ca^{2+} uptake, showing a 2-fold increase in the magnitude and rate of Ca^{2+} entry (**Figure 4. 20**). Next, Ca^{2+} channel antagonists were applied to 7-day differentiated MC3T3-E1 cells treated with 1,25D$_3$ 24 h prior, in order to identify which channel is responsible for regulating this 1,25D$_3$-mediated Ca^{2+} increase.

4.2.3.1 1,25D$_3$-medaited Ca^{2+} uptake via L-type channel

100 μM $LaCl_3$ was first applied to 7-day differentiated MC3T3-E1 cells treated with 10^{-7} M 1,25D$_3$ and $LaCl_3$ $LaCl_3$ caused significant reduction in Δ peak and Δ slope, rate of calcium entry (**Figure 4. 21**).

10 μM Felodipine was applied to 1,25D$_3$-treated 7-differentiated osteoblasts and almost abolished Ca^{2+} uptake and caused significant Ca^{2+} efflux. This observation suggests 1,25D$_3$-mediated Ca^{2+} uptake is regulated through L-type Ca^{2+} channel (**Figure 4. 22A and B**).

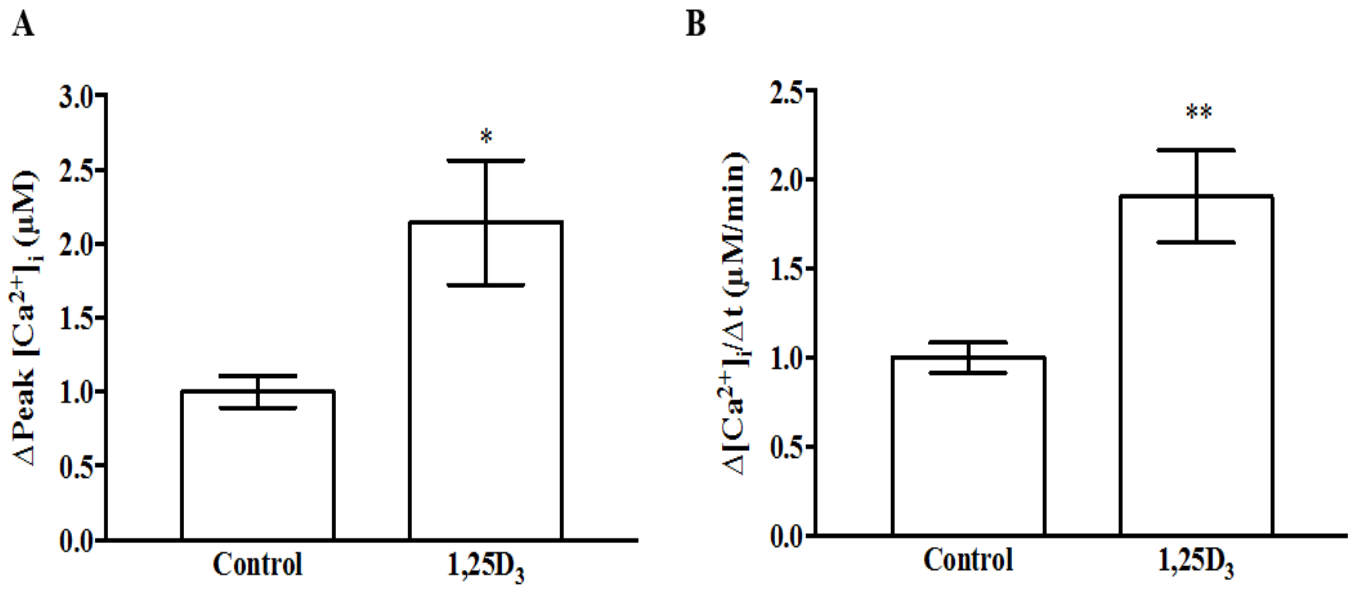

Figure 4. 20 Active vitamin D enhance calcium influx in osteoblasts

(A). Magnitude of calcium uptake (B) and rate of calcium uptake in the presence and absence of $1,25D_3$ treatment, n=8 control, n=10 $1,25D_3$-treated group. All measurements were normalized to the day of the experiment, and data are presented as means ± SEM. *p ≤0.05, ** p ≤0.01.

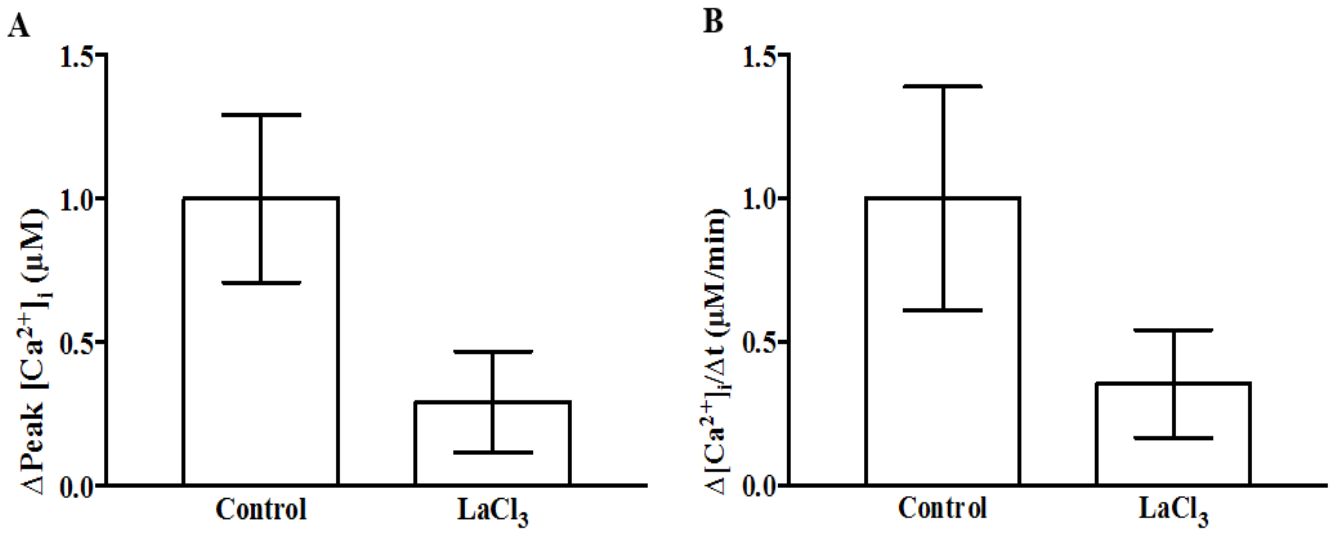

Figure 4. 21 $LaCl_3$ reduced calcium uptake in 1,25-D_3 treated osteoblasts

(A). Magnitude of calcium uptake and (B) rate of calcium uptake in osteoblasts treated with 1,25D_3 in the presence and absence of $LaCl_3$. n=5 each. All measurements were normalized to the day of the experiment, and data are presented as means ± SEM.

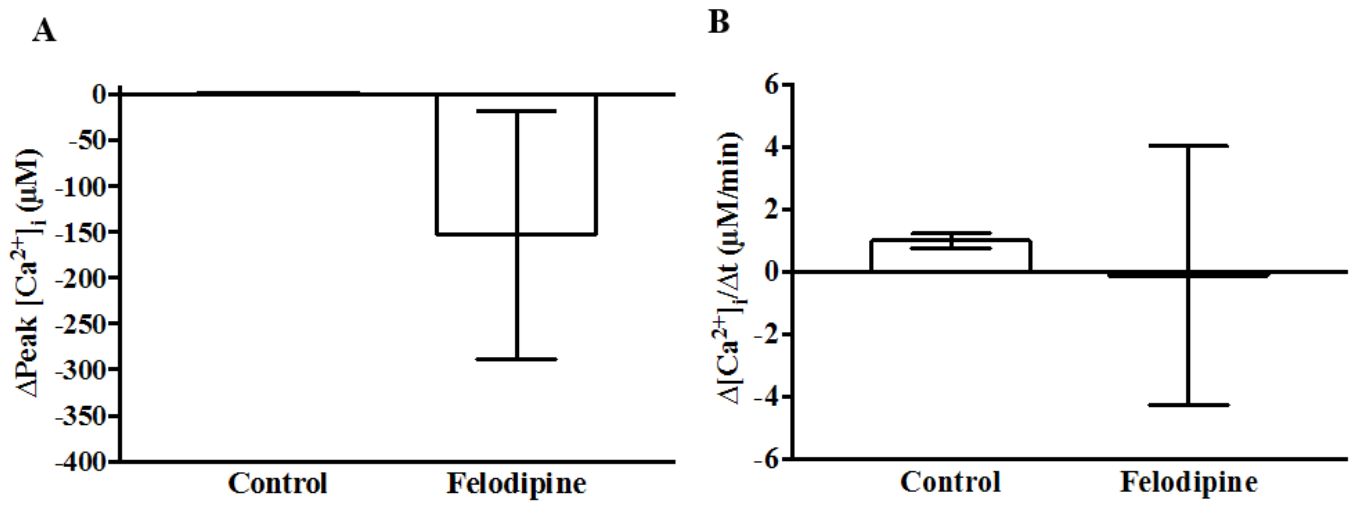

Figure 4. 22 **L-type calcium channels are the major functioning channel after 1,25D$_3$ treatment of 7-day differentiated MC3T3-E1 cells**

(A). Magnitude of calcium uptake and (B). rate of calcium uptake into 1,25D$_3$ treated MCT3-E1 cells in the presence and absence of Felodipine. n=4 control and n=3 Felodipine-treated. All measurements were normalized to the day of the experiment, and data are presented as means ± SEM.

4.2.4 Effects of 1,25D$_3$ on Ca^{2+} mediators/transporter gene expression in efflux regulation

NCX expression was up-regulated by 1,25D$_3$, but this 1,25D$_3$-mediated increase was attenuated by the combination group of 1,25D$_3$ and H_2O_2. 250 μM H_2O_2 alone did not alter NCX expression in 7-day differentiated MC3T3-E1 cells (**Figure 4. 23A**). H_2O_2 or 1,25D$_3$ did not alter PMCA-1b mRNA expression levels in 7-day differentiated cells, but the combination treatment of 1,25D$_3$ and H_2O_2 caused reduce NCX expression significantly (**Figure 4. 23B**).

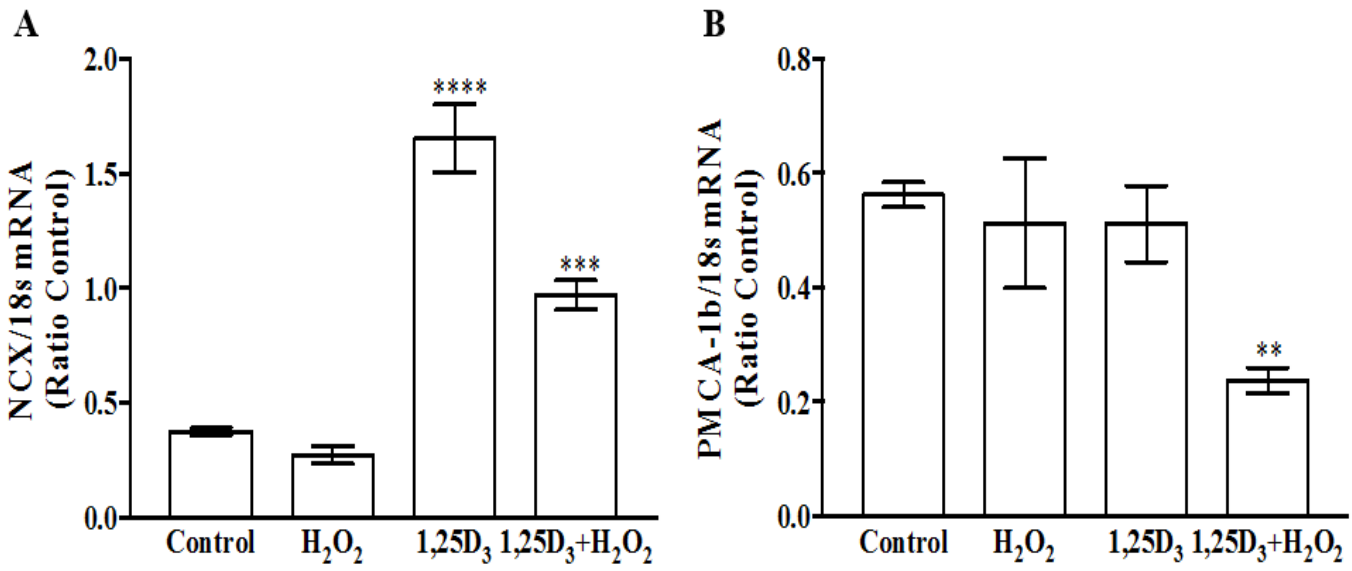

Figure 4. 23 **Effects of 1,25D$_3$ and ROS on mediators for calcium deposition**

(A). 1,25D$_3$ enhanced NCX mRNA expression, which was reduced by combination treatment with H_2O_2 (B). 1,25D$_3$ and ROS did not alter PMCA-1b expression, but combination of 1,25D$_3$ and H_2O_2 significantly reduced expression, n=9 each and data are presented as means ± SEM. **p ≤0.01, ***p ≤0.001, ****p ≤0.0001

4.3 Effects of 1,25D$_3$ on calcium deposition into the mineralizing matrix

To determine Ca^{2+} deposition into the matrix, alizarin red staining (ARS) was employed. Our first objective was to measure Ca^{2+} levels in the matrix of pre-osteoblasts and 7-day differentiated osteoblasts. Our next objective was to examine the effects of 1,25D$_3$ on matrix calcification in both pre-osteoblasts and 7-day differentiated osteoblasts.

4.3.1 Osteoblasts deposited calcium in the matrix during osteoblast differentiation

Pre-osteoblasts stained with ARS showed faint pink staining (**Figure 4. 24A**). Quantification of ARS demonstrated calcium levels in the matrix of approximately 150 μM (**Figure 4. 24C).**
In contrast, 7-day differentiated MC3T3-E1 cells stained with ARS showed a much darker red colour (**Figure 4. 24B**). Quantification of ARS showed an almost 2-fold increase in calcium level to approximately 300 μM (**Figure 4. 24C**).

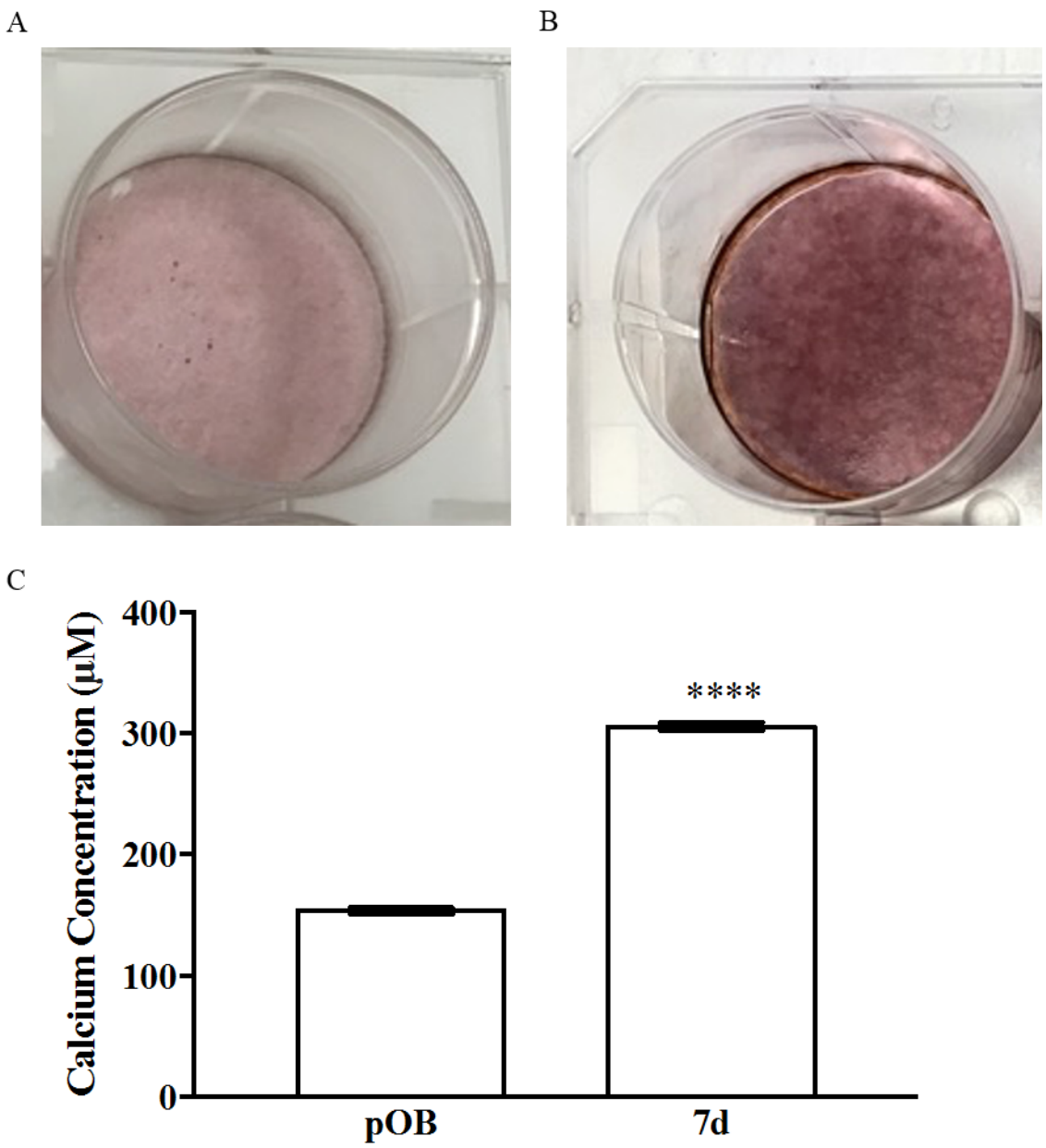

Figure 4. 24 **Significant calcium deposition in 7-day differentiated MC3T3-E1 cells assessed by Alizarin red staining**

(A). Pre-osteoblasts exhibited approximately 150 μM calcium in the matrix in contrast to (B) 7-day differentiated osteoblasts. (C) Quantification of calcium levels comparing pre-osteoblasts with 7-day differentiated osteoblasts. Data are presented as means ±SEM. n=3 each. ****p ≤0.0001.

4.3.2 Effects of 1,25D$_3$ and H$_2$O$_2$ on calcium deposition in pre-osteoblasts

Untreated pre-osteoblasts showed approximately 150 μM calcium levels in the matrix and cells layer showed a faint pink colour (**Figure 4. 25A).** Treatment with H_2O_2 and $1,25D_3$ showed the same levels of intensity in ARS staining compared to control (**Figure 4. 25A**). Quantification of Ca^{2+} levels in the matrix showed that treatment groups did not cause significant alterations in calcium levels (**Figure 4. 25B**).

A

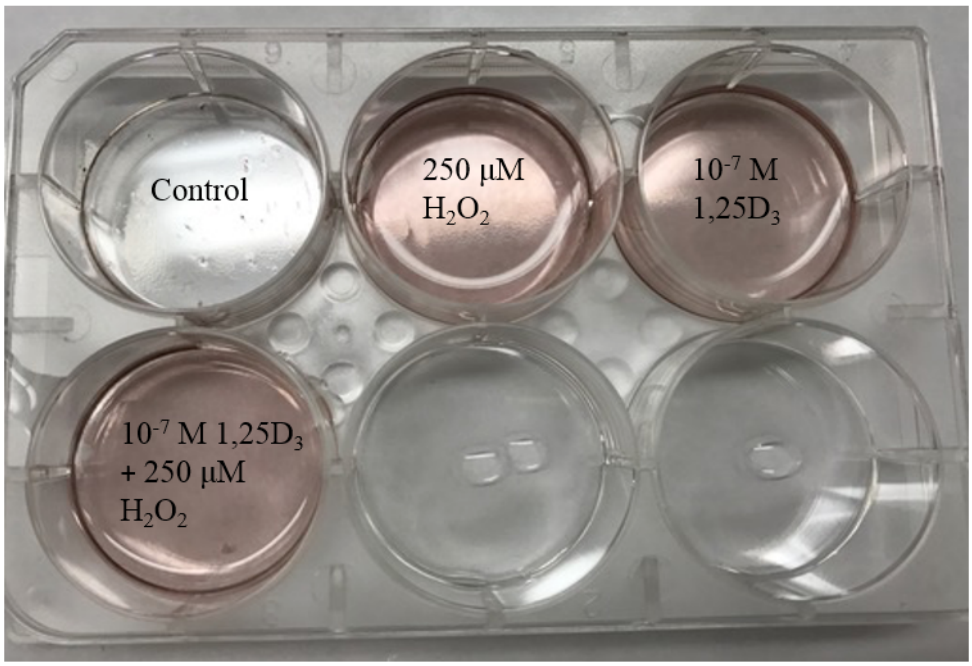

B

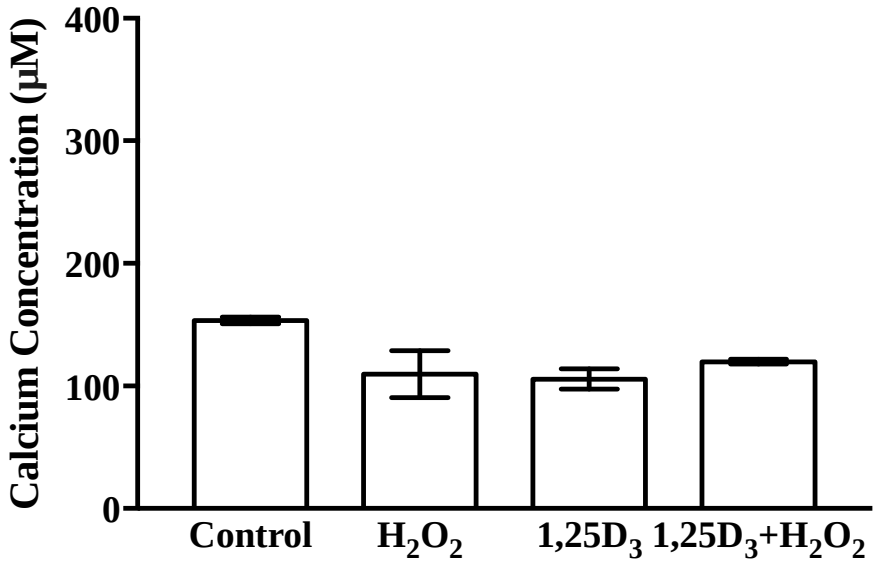

Figure 4. 25 H_2O_2 and $1,25D_3$ did not alter calcium deposition in pre-osteoblasts

(A). Pre-osteoblast cells grown to confluent and treated with $1,25D_3$ and H_2O_2 and (B). Quantification of calcium levels in the treatment groups compared to control. Data are presented

as means ±SEM. n=3 each. The stained cell layer seen in control (A) had been removed from the well for measurement at the time the picture was taken.

4.3.3 High doses of 1,25D$_3$ reduced calcium deposition in 7-day differentiated osteoblasts

7-day differentiated MC3T3-E1 cells showed the same intensity of ARS staining in control and the treatment groups (**Figure 4. 26A**).

Untreated 7-day differentiated MC3T3-E1 cells showed approximately 300 μM Ca^{2+} levels in the matrix. Treatment with H_2O_2 caused an increase to 330 μM but 1,25D_3 significantly reduced calcium levels deposited in the matrix to 270 μM (**Figure 4. 26B**).

A lower dose of 10^{-5} M 1,25D_3 increased Ca^{2+} deposition significantly in the 7-day differentiated MC3T3-E1 cells (**Figure 4. 27**).

A

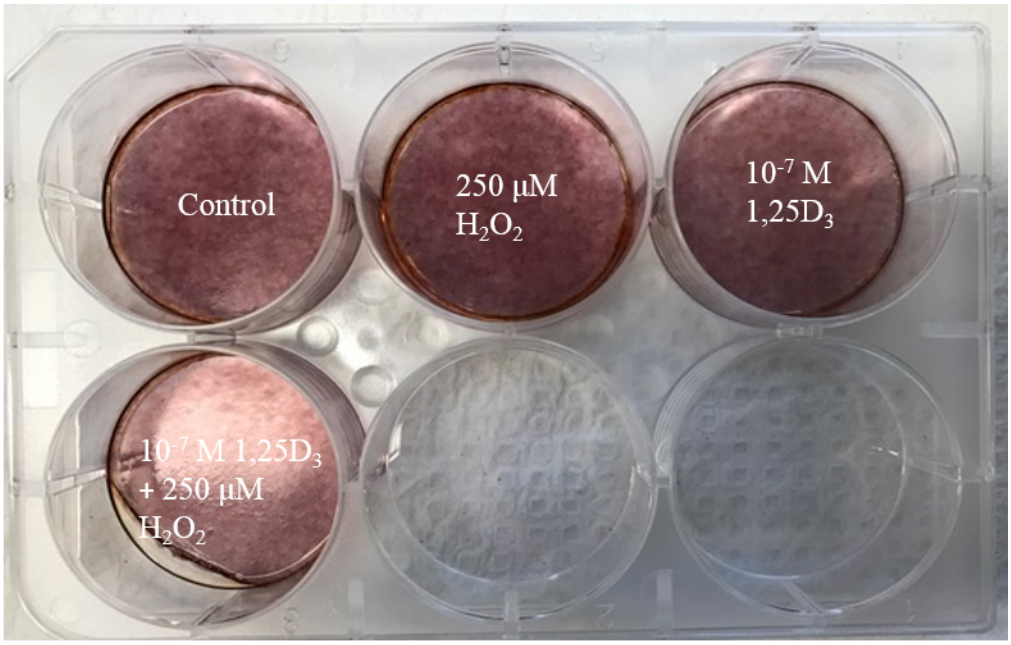

B

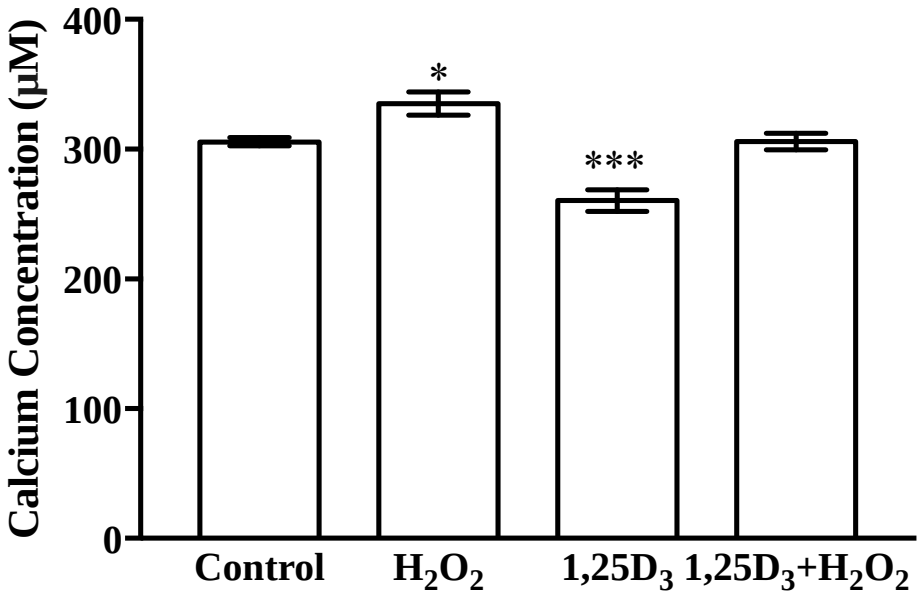

Figure 4. 26 Altered calcium deposition in 7-day differentiated MC3T3-E1 cells by H_2O_2 and $1,25D_3$

(A). Cells grown to confluence and treated with $1,25D_3$ for 24 hours and H_2O_2 for an hour. And combination group of $1,25D_3$ and H_2O_2 (B) quantification of calcium levels in the treatment

groups compared to control. Data are presented as means ±SEM. n=3 each. *p ≤0.05, ***
p ≤0.001.

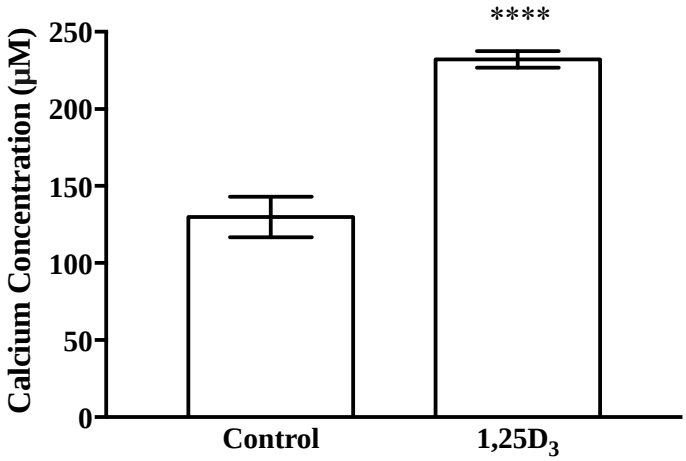

Figure 4. 27 Treatment with 10^{-5} M $1,25D_3$ increased Ca^{2+} deposition significantly in 7-day differentiated osteoblasts

Data are presented as means ±SEM. n=3 each. **** p ≤0.0001.

4.3.4 Matrix calcification was enhanced by increasing external calcium concentration

We next sought to determine if matrix calcification could be further enhanced by increasing the external calcium concentration, thus we cultured both pre-osteoblasts and osteoblasts in culture media supplemented with additional $CaCl_2$ to the existing 0.2 g/L $CaCl_2$ supplemented in the αMEM culture media. Three concentrations of $CaCl_2$ were added: 3 mM, 6 mM and 9 mM. Cells were incubated for 7 days and calcium deposited in the matrix was stained with ARS and quantified.

4.3.4.1 Additional $CaCl_2$ increased Ca^{2+} deposition in pre-osteoblasts

Pre-osteoblasts showed a pink ARS staining in the control (0 mM $CaCl_2$) group. Additional 3 mM $CaCl_2$ did not increase ARS staining intensity. Incubation with additional 6 mM and 9 mM $CaCl_2$ increased ARS staining colour compared to control (**Figure 4. 28A**). Quantification showed 3mM $CaCl_2$ did not alter calcium deposition in the matrix. Incubation with 6 mM $CaCl_2$ resulted in the highest calcium deposition in the matrix, reaching a 12-fold increase. 9 mM $CaCl_2$ also showed significantly higher calcium deposition compared to control, reaching a 7-fold increase (**Figure 4. 28B**).

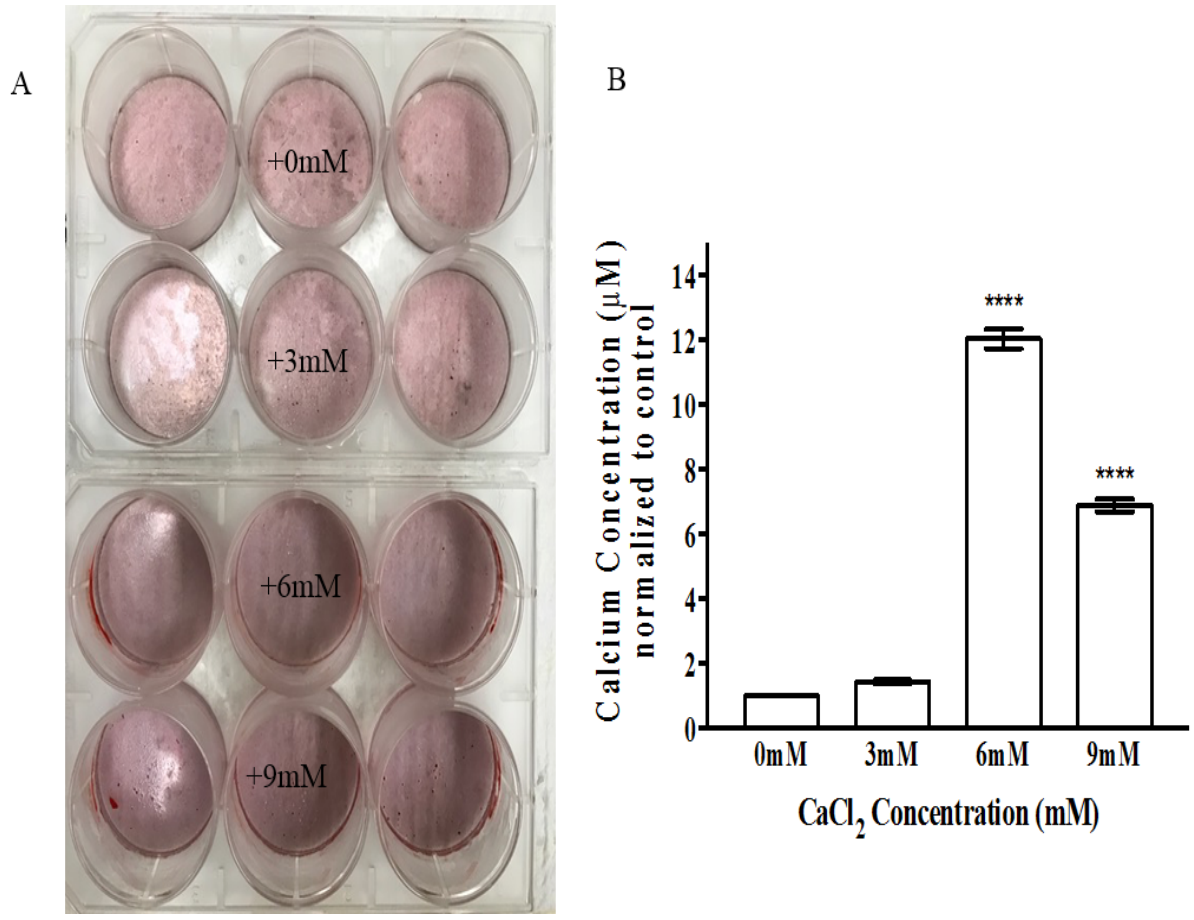

Figure 4. 28 **Pre-osteoblasts incubated with additional 0 mM, 3 mM, 6 mM and 9 mM calcium chloride ($CaCl_2$) for 7 days and calcium deposition in the matrix was assessed with ARS**

(A). Pre-osteoblasts incubated with the stated extra calcium in the medium and (B). quantification of the calcium deposition in the treated pre-osteoblasts

Data are presented as means ±SEM. n=3 each. ****p ≤0.0001.

4.3.4.2 Matrix calcification was further enhanced in 7-day differentiated osteoblasts

7-day differentiated MC3T3-E1 cells showed a darker pink ARS staining in the control group (0 mM $CaCl_2$) group. Incubation with additional 3 mM $CaCl_2$ did not increase ARS intensity but incubation with 6 mM and 9 mM $CaCl_2$ resulted in a darker ARS colour compared to control (**Figure 4. 29A**).

Quantification of ARS showed that incubation with an additional 3 mM and 6 mM $CaCl_2$ caused a significant increase in calcium levels deposited in the matrix, and incubation with 9 mM $CaCl_2$ led to the highest Ca^{2+} deposition in the matrix. (**Figure 4. 29B**).

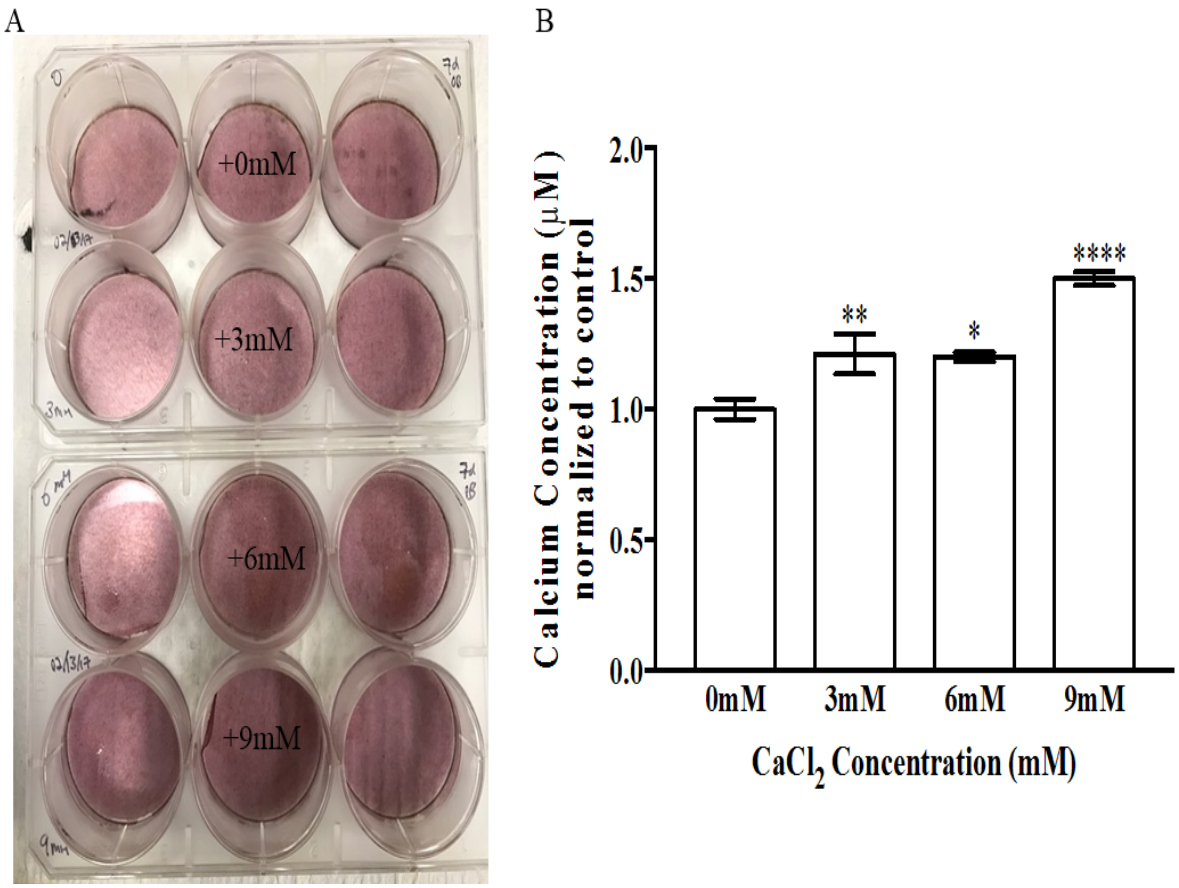

Figure 4. 29 7-day differentiated osteoblasts incubated with 0 mM, 3 mM, 6 mM and 9 mM calcium chloride ($CaCl_2$) for 7 days and calcium deposition in the matrix was assessed with ARS

(A). 7-day differentiated osteoblasts incubated with the stated extra calcium in the medium and (B) quantification of the calcium deposition in the treated osteoblasts from A.

Data are presented as means ±SEM. n=3 each. * $p \leq 0.05$, ** $p \leq 0.01$, **** $p \leq 0.0001$.

4.4 Discussion

4.4.1. 1,25D$_3$-mediated osteoblast differentiation and mineralization

1,25D$_3$ significantly reduced expression levels of Runx2 and OCN in 7-day differentiated osteoblasts. Both Runx2 and OCN are important noncollagenous proteins in osteoblastogenesis and have VDRE in the promoter region that can be activated by RXR:VDR heterodimer. Runx2 is a key regulator in differentiation and stimulates OCN expression in mature osteoblasts. Accumulating data showing 1,25D$_3$ suppresses Runx2 and OCN expression in murine osteoblastic cells including MC3T3-E1 cells (Drissi et al., 2002; Yamaguchi and Weitzmann, 2012). Several studies reported varying Runx2 and OCN expression in human and rat (Prince et al., 2001; Maehata et al., 2006). At this point, detailed explanation for the difference in species is absent. We also measured Ca^{2+} in the 7-day differentiated osteoblasts to determine if 1,25D$_3$-mediated inhibition on Runx2 and OCN would hinder matrix calcification.

4.4.2. Effects of 1,25D$_3$ on expression of transcription factors and genes

1,25D$_3$ increased FoxO3a mRNA and protein expression levels significantly in 7-day differentiated osteoblasts.1,25D$_3$ stimulated both RXRα and VDR mRNA and protein expression in 7-day differentiated mature cells, suggesting 1,25D$_3$ participates directly in osteoblast mineralization. Immunofluorescence further confirmed 1,25D$_3$ augmented FoxO3a nuclear expression. Pearson correlation coefficient (PCC) measured nuclear translocation of FoxO3a, and showed a higher correlation between FoxO3a and DAPI upon treatment with 1,25D$_3$, indicating 1,25D$_3$ increased nuclear translocation of FoxO3a.

4.4.3. Effects of 1,25D$_3$ on calcium regulation in 7-day differentiated osteoblasts

To investigate direct effects of 1,25D$_3$-mediated calcium regulation in osteoblasts, 7-day differentiated MC3T3-E1 cells were treated with 10^{-7} M 1,25D$_3$ for 24 hours. Expression of plasma membrane Ca^{2+} channels for Ca^{2+} influx and Ca^{2+} mediators and transporters for Ca^{2+} efflux was assessed. No significant alterations were found in expression of L-type ($Ca_v1.2$ and $Ca_v1.3$), T-type ($Ca_v3.1$) and PMCA-1b, but significantly up-regulated expression of Calbindin-D_{9K} and NCX. Bergh and colleagues treated pre-osteoblast MC3T3-E1 cells with 10^{-7} M 1,25D$_3$ for 24 hours and found $Ca_v1.2$ and $Ca_v3.1$ to be significantly down-regulated but not $Ca_v1.3$. They interpreted this observation due to anti-apoptosis mechanism to protect the cell from elevated [Ca^{2+}] (Bergh et al., 2006). They also reported 1,25D$_3$ switched predominant Ca^{2+} channel from L-type to T-type in pre-osteoblast MC3T3-E1 cells (Bergh et al., 2006).

4.4.3.1 Identifying Ca^{2+} channel activity in MC3T3-E1 cells

We identified functioning channels in 7-day differentiated mature osteoblast by live cell ratio metric calcium imaging using fluorescent Ca^{2+} indicator, Fura-2 AM. Calcium uptake was determined by measuring two parameters, delta slope and delta peak in control 7-day differentiated mature osteoblasts which was then compared with cells treated with five calcium antagonists. Delta peak, measured how much [Ca^{2+}] was entering the cell in μM and delta slope measured the rate, how fast [Ca^{2+}] was entering in in μM per minute during the first 30 seconds of the uptake.

Calcium uptake can be significantly reduced by $LaCl_3$, indicating activity of non-specific calcium channel that are actively allowing calcium entry. L-type calcium channel was identified to be the major functioning channel as calcium uptake was almost abolished by felodipine. This result supports that L-type calcium channel is responsible for majority of calcium entry into the

cytosolic during mineralization. Felodipine also caused calcium efflux, unmasking calcium efflux via NCX or PMCA-1b. Ruthenium red did not alter calcium uptake, confirming absence of TRPV channels. NNC 55-0396 was used to block T-type calcium channel ($Ca_v3.1$)

4.4.3.2 1,25D$_3$-mediated calcium influx regulated by L-type calcium channels

Treatment with 100 nM 1,25D_3 significantly increased calcium uptake, both in the magnitude and the rate of uptake. In order to determine which channel was mediating this influx, both felodipine and $LaCl_3$ were applied to 7-day differentiated MC3T3-E1 cells treated with 100 nM 1,25D_3 for 24 hours prior. $LaCl_3$ reduced calcium uptake significantly but felodipine completely shut down channel activity, indicating 1,25D_3-mediated increase is regulated through L-type calcium channels.

4.4.3.3 Calcium deposition during matrix calcification in MC3T3-E1 cells

Pre-osteoblasts exhibited calcium levels of approximately 150 μM determined by ARS, an anionic dye that binds to cationic ions such as Ca^{2+}, and staining with ARS showed a faint pink colour. 7-day differentiated osteoblasts showed a 2-fold increase to 300 μM and a dark red colour by ARS, showing calcium deposition into the ECM via NCX or PMCA-1b.

100 nM 1,25D_3 reduced mineralization in 7-day differentiated mature osteoblasts while it didn't have any effect in pre-osteoblasts. Treatment with a lower dose of 10^{-5} M 1,25D_3 increased calcium deposition significantly in matrix, suggesting high doses of 1,25D_3 exerted negative impact on mineralization and a lower dose is beneficial. Previous report by Matsumoto showed a low dose of 3 x 10^{-10} M 1,25D_3 stimulated mineralization in MC3T3-E1 cells, but a higher dose of 10^{-7} M 1,25D_3 inhibited mineralization in MC3T3-E1 cells (Matsumoto et al., 1991; Yamaguchi and Weitzmann, 2012).

4.4.3.4 Matrix calcification was enhanced by increasing external [Ca^{2+}]

Calcium deposition is a critical process in bone formation and in pre-osteoblasts approximately 150 μM [Ca^{2+}] in the matrix was measured while 7-day differentiated osteoblasts showed a 2-fold increase to approximately 300 μM [Ca^{2+}] in the matrix. We queried whether calcium deposition can be further enhanced by culturing pre-osteoblasts and 7-day differentiated mature osteoblasts with additional $CaCl_2$ added to original α-MEM culture media which contains 1.2 g/L $CaCl_2$ and the levels of calcium deposition were measured by ARS. Maeno and colleagues soaked two- and three-dimensional collagen gels coated with primary osteoblast cells in various [Ca^{2+}] to create artificial hydroxyapatite and they found that three ranges of [Ca^{2+}] to be critical in bone mineralization. 2-4 mM Ca^{2+} to be suitable for proliferation and survival of osteoblasts, 6-8 mM Ca^{2+} is suitable for osteoblast differentiation and matrix mineralization, and [Ca^{2+}] higher than 10 mM to be cytotoxic (Maeno et al., 2005). Based on their findings, we chose three concentrations for evaluating osteoblast mineralization and matrix calcification. A low concentration of 3 mM, middle concentration of 6 mM and a high concentration of 9 mM were picked and cells were incubated with these additional [$CaCl_2$] for 7 days.

3 mM [Ca^{2+}] did not stimulate calcium deposition in pre-osteoblasts, this result supports the observation made by Maeno that slightly elevated [Ca^{2+}] stimulates osteoblast proliferation but does not contribute to mineralization. 6 mM [$CaCl_2$] showed the highest calcium deposition in pre-osteoblasts, supporting the observation made by Maeno. Incubation with 9 mM [$CaCl_2$] reduced calcium deposition in pre-osteoblasts and this may be due to toxic effects and that cells were undergoing apoptosis.

In the 7-day differentiated mature osteoblasts, gradual increase in calcium deposition was seen with increasing external [Ca^{2+}]. Incubation with 9 mM [$CaCl_2$] led to 1.5-fold increase compared

to control suggesting cells that have already differentiated are actively involved in mineralization.

These results also support that efflux of [Ca^{2+}] to the bone surface is regulated through NCX or PMCA-1b pump.

CHAPTER 5: OVER-EXPRESSION OF FOXO3A PREVENTS OSTEOBLAST DIFFERENTIATION AND MATRIX CALCIFICATION

5.1 Effects of FoxO3a over-expression on osteoblast differentiation and matrix calcification

In this chapter, FoxO3a overexpression was generated in the current *in vitro* model of MC3T3-E1 cells to examine the effects of FoxO3a on osteoblast differentiation and matrix calcification (**Figure 5. 1**). Using the over-expression model, the following objectives were set up: first objective was to investigate the effects of FoxO3a on osteoblast differentiation and matrix calcification. This objective is addressed by three specific aims. The first specific aim was to assess changes in cell morphology during osteoblast differentiation in the over-expressors. Second specific aim was to examine the expression of important transcription factors and genes, including Runx2, OCN, FoxO3a, RXRα, and VDR. Third specific aim was to address FoxO3a over-expression on calcium transport machinery during osteoblast differentiation and mineralization, including L-type ($Ca_v1.2$ and $Ca_v1.3$) and T-type ($Ca_v3.1$), calcium mediators and transporters, such as Calbindin-D_{9K}, PMCA-1b and NCX.

The second objective was to study involvement of vitamin D signaling during osteogenesis in the over-expression model. First specific aim was to examine effects of $1,25D_3$ on expression of transcription factors and genes, including Runx2, OCN, FoxO3a, RXRα, and VDR. Second specific aim was to investigate vitamin D signaling on expression of calcium transport during osteoblast differentiation and matrix calcification.

Third objective was to examine effects of FoxO3a over-expression on calcium regulation. This objective is divided into three specific aims, first specific aim was to examine Ca^{2+} channel activity regulating influx by live cell radiometric calcium imaging. Second specific aim was to measure calcium deposition through NCX and PMCA-1b into the mineralizing matrix by ARS. The final specific aim was to determine whether matrix calcification could be augmented by increasing external [$CaCl_2$] in both pre-osteoblasts and 7-day differentiated osteoblasts.

5.1.1. Generation of MC3T3-E1 cells over-expressing FoxO3a

Undifferentiated MC3T3-E1 cells grown in culture were transfected with a pCMV6-Entry vector carrying a FoxO3a cDNA with a C-terminal Myc-DDK tag engineered at the 3' end of the gene. Therefore, both endogenous and exogenous FoxO3a expression driven by the CMV promoter were expressed in the model system (**Figure 5. 1**). In order to generate a stable cell line expressing exogenous FoxO3a, it is necessary to determine the minimum concentration of antibiotic required to kill non-transfected cells. A kill curve was therefore generated by treating undifferentiated MC3T3-E1 with seven concentrations of Geneticin and a control of untreated cells for selection. 500 μM Geneticin was sufficient to kill un-transfected cells and consequently this dose was used throughout experiments.

Transfection conditions were optimized by first transfecting undifferentiated MC3T3-E1 cells with green fluorescent protein (GFP) expression (**Figure 5. 2A**). GFP was detected by fluorescent microscopy with an excitation wavelength at 488 mm and excitation wavelength at 510 mm. The highest transfection efficiency resulted in approximately 30% transfected cells (**Figure 5. 2B**). The FoxO3a containing vector, and the empty vector control were then transfected into MC3T3-E1 cells separately by lipofection with Fugene. Immediately after transfection, cells were maintained in non-selective medium for 2 days until the next media change. Fresh culture media with 500 μM Geneticin was replenished every other day for a period of seven days. Only individual clones carrying the transfected FoxO3a DNA would propagate in the cell culture media containing Geneticin. These cells were checked for FoxO3a over-expression via western blotting. In **Figure 5. 1A**, the first lane on the left was loaded with FoxO3a over-expressing protein lysates, noted as FoxO3a (+). The next land on the right was loaded with control cells transfected with an empty vector, noted as FoxO3a (-). These proteins

were blotted for Myc expression using mouse monoclonal anti-Myc antibodies. Endogenous FoxO3a can be detected at approximately 85 kDa, therefore, the band detected at approximately 95 kDa would indicate presence of myc-tagged FoxO3a expression (**Figure 5. 3A**). FoxO3a (+) and FoxO3a (-) were also blotted for FoxO3a with rabbit monoclonal anti-FoxO3a antibodies (**Figure 5. 3B**). A heavily intensified band was detected at 85 kDa, indicating over-expression of FoxO3a in FoxO3a (+). A skinny and lighter band was detected at the same molecular weight in FoxO3a (-), indicating endogenous FoxO3a expression (**Figure 5. 3B**).

Immunofluorescence also detected high nuclear expression levels of FoxO3a in the over-expression model (**Figure 5. 3B**).

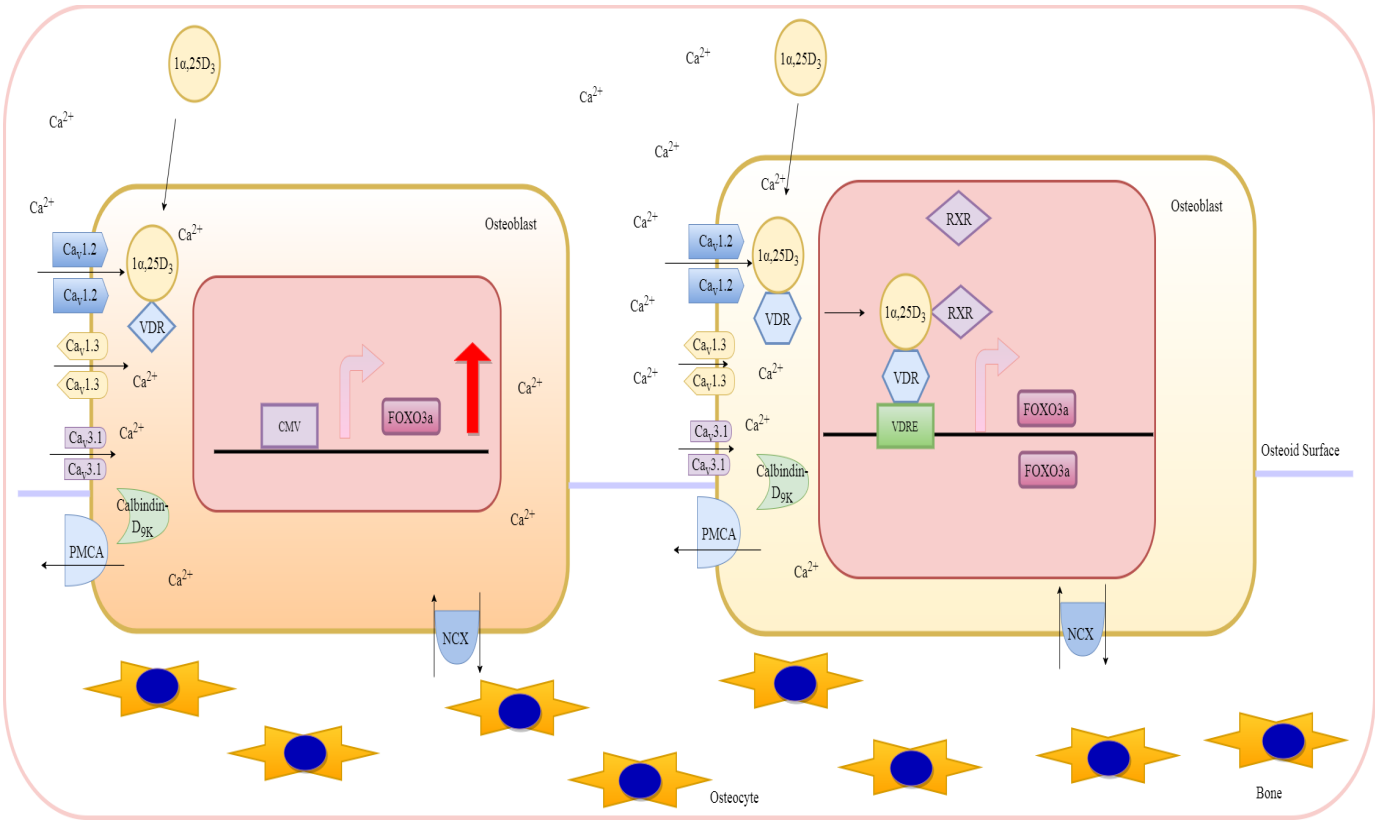

Figure 5. 1 Schematic illustration of an *in vitro* model system with FoxO3a over-expression in MC3T3-E1 cells

By over-expressing FoxO3a in this *in vitro* model, we were able to study the effects of FoxO3a on $1,25D_3$-mediated osteoblast mineralization, calcium uptake via L-type ($Ca_v1.2$, $Ca_v1.3$) and T-type ($Ca_v3.1$) calcium channels, and calcium deposition via NCX and PMCA-1b. FoxO3a: Forkhead box O 3a, NCX: sodium-calcium exchanger, PMCA: plasma membrane Ca^{2+} ATPase, RXRα: retinoid x receptor α, VDR: vitamin D receptor, VDRE: vitamin D response element.

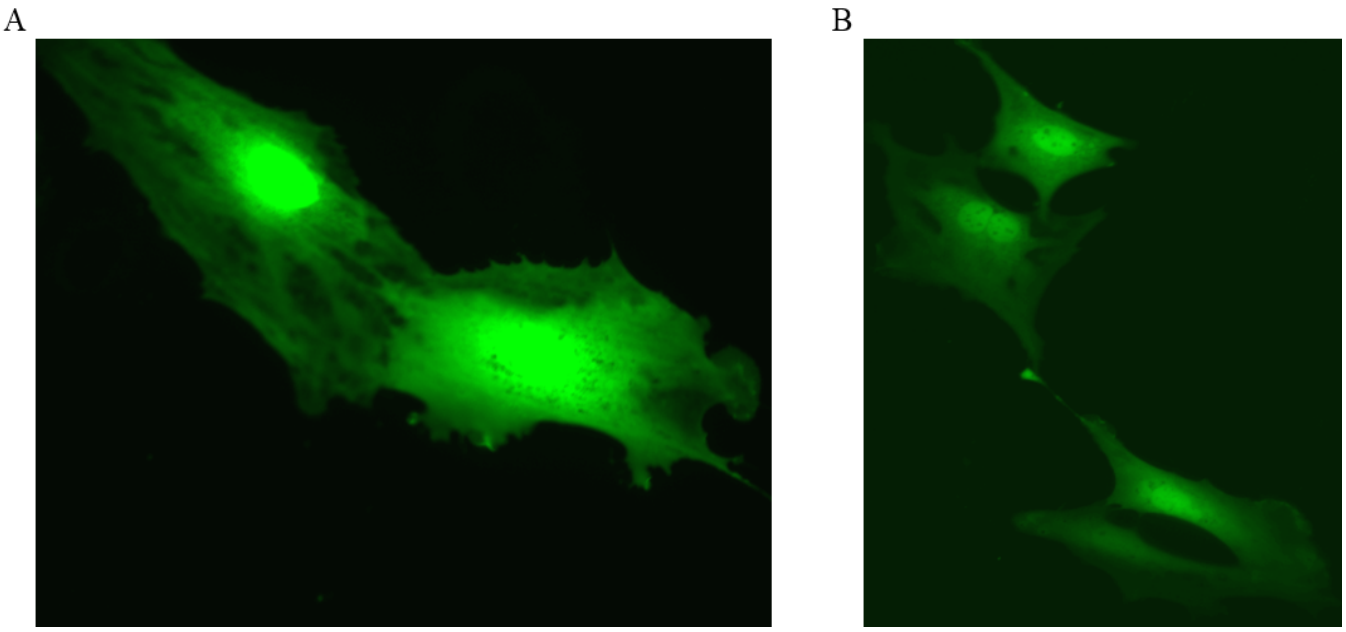

Figure 5. 2 MC3T3-E1 cells transfected with GFP

(A) Strong GFP signal was detected in the nucleus

(B) Neighbouring cells also exhibited GFP

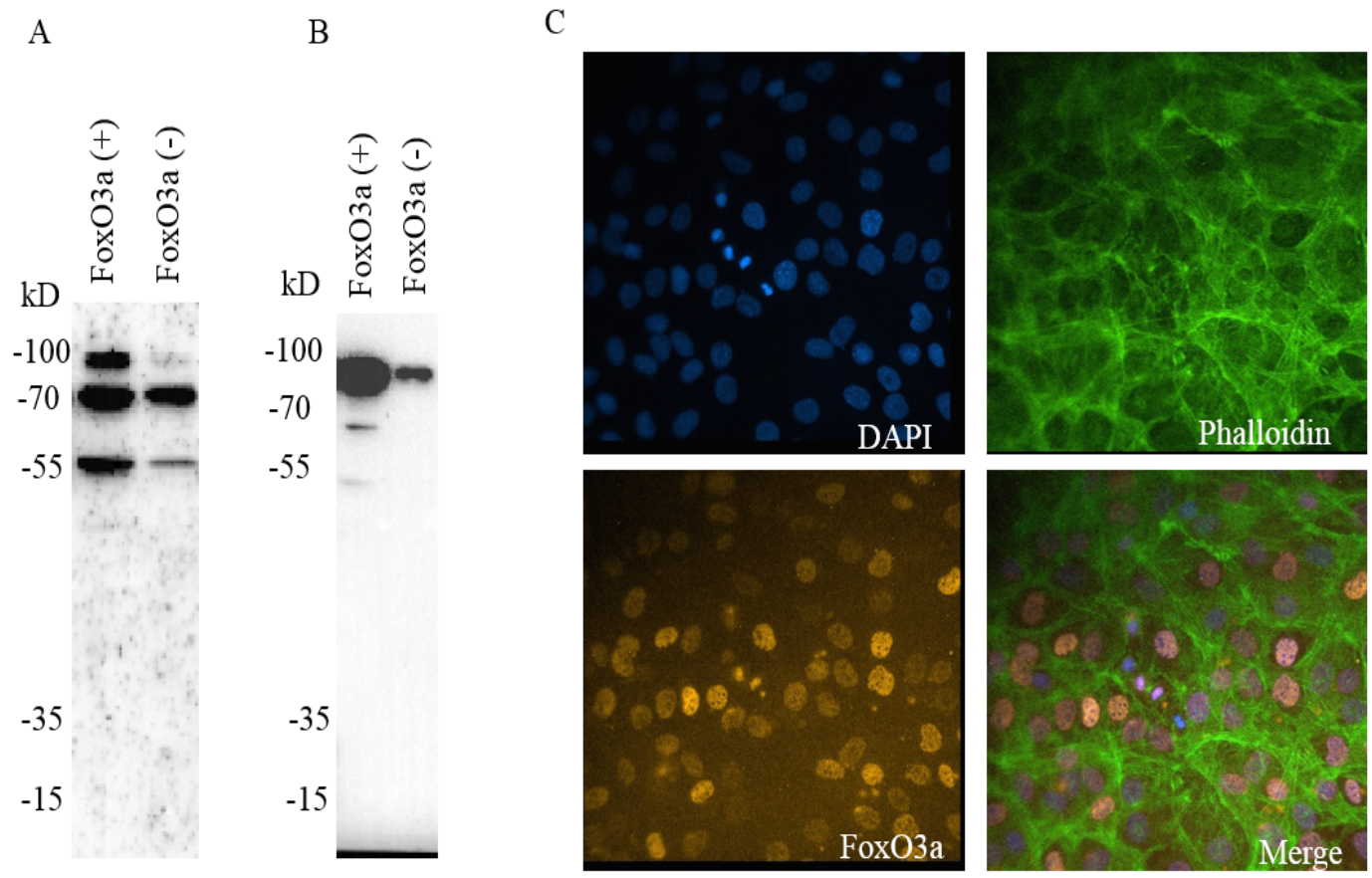

Figure 5. 3 Verification of successful FoxO3a transfection with rabbit monoclonal antibodies

(A) Protein expression of Myc-tag was verified via blotting with mouse monoclonal anti-Myc antibodies

(B). Over-expression of FoxO3a was verified via immunoblotting with rabbit monoclonal anti-FoxO3a antibodies

(C). Immunofluorescence exhibited high levels of FoxO3a and mostly localized in the nucleus. Nucleus was stained with DAPI, actin was stained with Alexa Fluor 488 phalloidin and Myc was stained with rabbit monoclonal anti-Myc antibodies.

5.1.2 Morphology of pre-osteoblasts and osteoblasts over-expressing FoxO3a

After over-expression of FoxO3a had been verified, cell morphology was examined at various stages as pre-osteoblasts underwent differentiation to become 7-day differentiated osteoblasts. Pre-osteoblast MC3T3-E1 cells were seeded sparsely in culture dishes and then observed by bright-field microscopy (**Figure 5. 4A**). Pre-osteoblast cells exhibited adherent and fibroblast-like morphology (**Figure 5. 4B**). These cells proliferated rapidly and reached confluency after staying in culture for 48 hours shown in **Figure 5. 4C** and differentiation was initiated with ascorbic acid and β-glycerophosphate. MC3T3-E1 cells started to exhibit an elongated cell body with extensions one-day post differentiation (**Figure 5. 5A**). The cell body became slimmer in 3-day differentiated MC3T3-E1 cells, exhibiting morphology similar to osteocytes (**Figure 5. 5B**). 7-day differentiated MC3T3-E1 cells exhibited thin and long cell body with formation of extracellular matrix and some cells became embedded in the matrix (**Figure 5. 5C**).

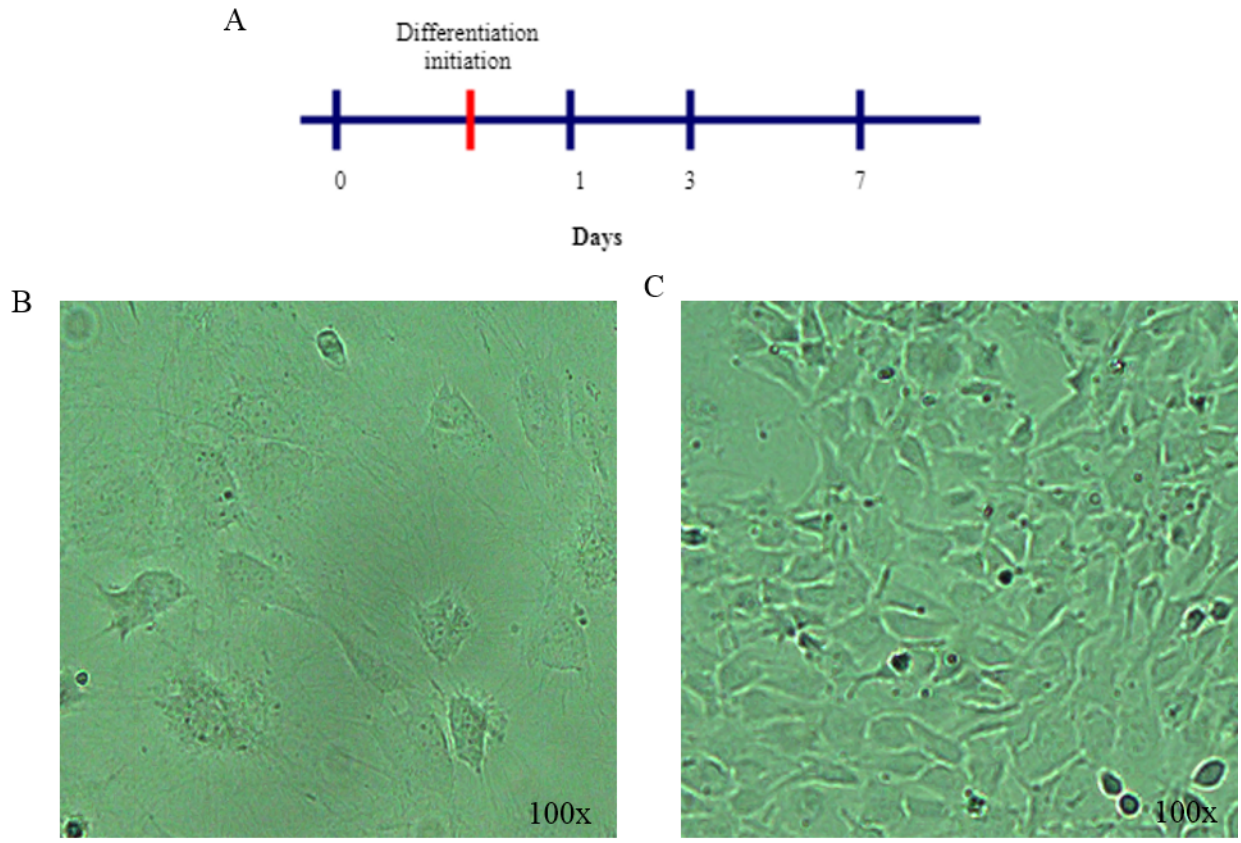

Figure 5. 4 Morphology of pre-osteoblasts with FoxO3a over-expressed visualized under bright field

(A). Timeline for osteoblast differentiation. Cells were examined at day 0 (pre-osteoblasts), day 1, 3 and 7.

(B). Cells were seeded sparsely and resembled fibroblast-like morphology

(C) Cells proliferated rapidly and reached confluency after 48 h in culture

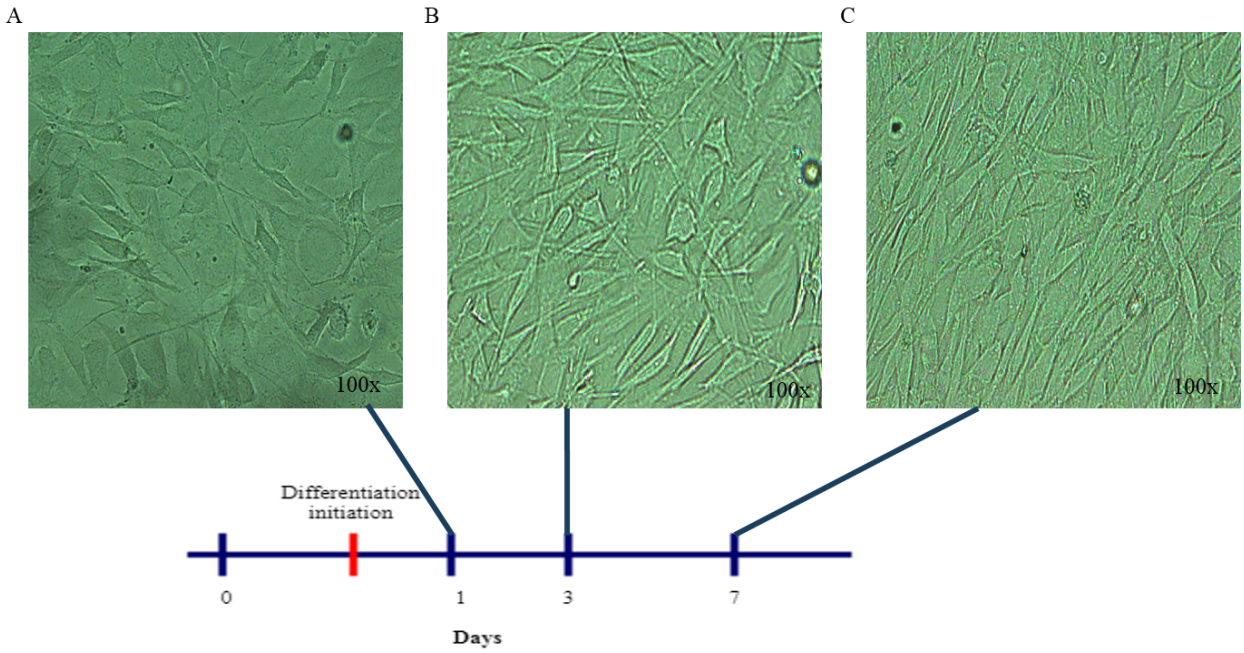

Figure 5. 5 Cell morphology during osteoblast differentiation visualized under bright field image

(A). 1-day post differentiation, cells started to exhibit long elongated cell shape

(B). 3-day post differentiation, cell exhibited morphology similar to osteocyte

(C). 7-day differentiated MC3T3-E1 cells became embedded in the matrix.

5.1.3 Assessment of osteoblast differentiation and mineralization

In the FoxO3a over-expressing cells, the levels of osteoblast differentiation and mineralization were assessed by two biomarkers, Runx2 and OCN. In the over-expressors, Runx2 mRNA expression remained at base levels in pre-osteoblasts which increased significantly in 1-day differentiated MC3T3-E1 cells followed by a dramatic decline in 3-day differentiated MC3T3-E1 cells. Runx2 expression then maintained at the same level in 7-day differentiated MC3T3-E1 cells (**Figure 5. 6A**). Compared to non-transfected control cells, Runx2 expression showed a significant decline after 3 days post differentiation in over-expressors.

OCN mRNA expression levels is significantly reduced in 1-day differentiated MC3T3-E1 cells followed by a dramatic increase, reaching the highest level in 3-day differentiated MC3T3-E1 cells when FoxO3a was over-expressed. OCN expression levels declined dramatically in 7-day differentiated MC3T3-E1 cells to the identical levels as pre-osteoblasts (**Figure 5. 6B**). OCN mRNA expression levels showed a gradual increase as differentiation was initiated in the non-transfected control cells, and reached the highest expression levels in 7-day differentiated MC3T3-E1 cells.

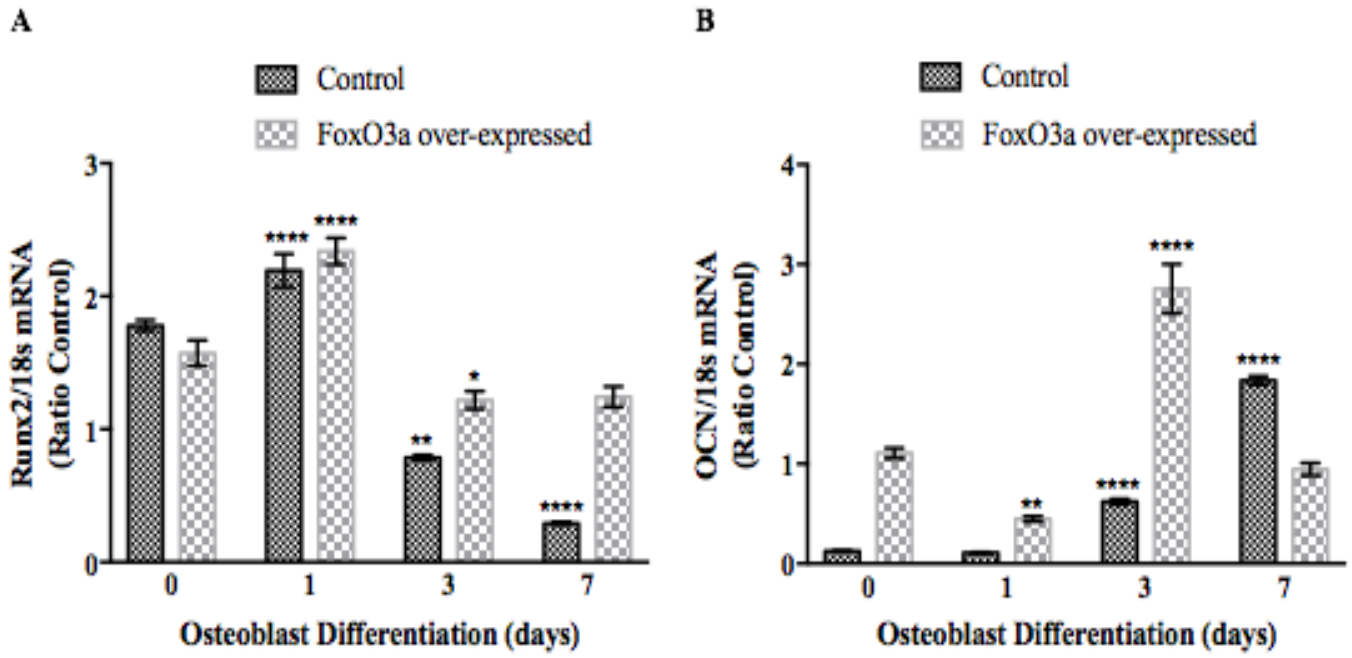

Figure 5. 6 **Runx2 and OCN mRNA expression as an assessment of osteoblast differentiation in FoxO3a over expressing cells**

(A). Runx2 showed highest expression levels in one-day differentiated MC3T3-E1 cells and the same levels as pre-osteoblasts in 7-day differentiated cells.

(B). OCN showed highest expression levels in 3-day differentiated MC3T3-E1 cells, and the same level as pre-osteoblasts in 7-day differentiated cells.

All gene expression was normalized to 18s expression. n=3 FoxO3a over-expressed at each time point.

Data are presented as means ± SEM. *p≤0.05, **p ≤0.01, ****p ≤0.0001

5.1.4 Effects of FoxO3a over-expression on expression of transcription factors and genes

FoxO3a mRNA expression stayed uniform in pre-osteoblasts, 1-day and 3-day differentiated MC3T3-E1 cells. Significantly higher FoxO3a expression levels were detected in 7-day differentiated osteoblasts (**Figure 5. 7A**). FoxO3a protein levels stayed high and uniform throughout osteoblast differentiation (**Figure 5. 7B**). Uniform RXRα mRNA expression was detected in pre-osteoblasts, 1-day, 3-day and 7-day differentiated MC3T3-E1 cells (**Figure 5. 8A**). A gradual, but not significant, increase was detected in RXRα protein expression levels during osteoblast differentiation (**Figure 5. 8B**). Vitamin D Receptor (VDR) mRNA expression levels stayed constant in pre-osteoblasts and 1-day differentiated MC3T3-E1 cells. VDR mRNA expression levels underwent an increase in 3-day and a slightly further increase in 7-day differentiated MC3T3-E1 cells (**Figure 5. 9A**). VDR protein expression levels remained constant in pre-osteoblasts, 1-day differentiation before significantly up-regulated in 3-day differentiated osteoblasts. VDR protein expression levels returned back to base levels in 7-day differentiated osteoblasts (**Figure 5. 9B**).

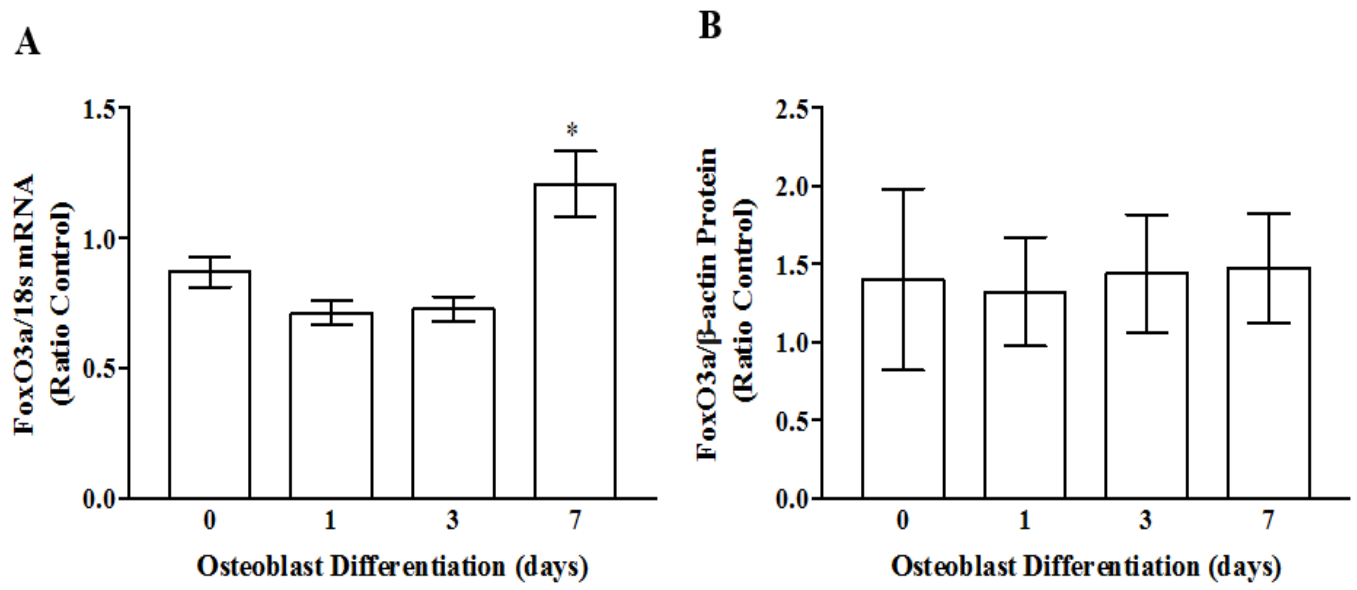

Figure 5. 7 FoxO3a expression in MC3T3-E1 cells during osteoblast differentiation

(A). FoxO3a mRNA expression reached a significantly higher level in 7-day differentiated MC3T3-E1 cells.

(B). FoxO3a protein expression levels stayed uniform throughout osteoblast differentiation

All gene expression was normalized to 18s expression, n=3 mRNA samples and n=9 protein samples.

Data are presented as means ± SEM. *$p \leq 0.05$

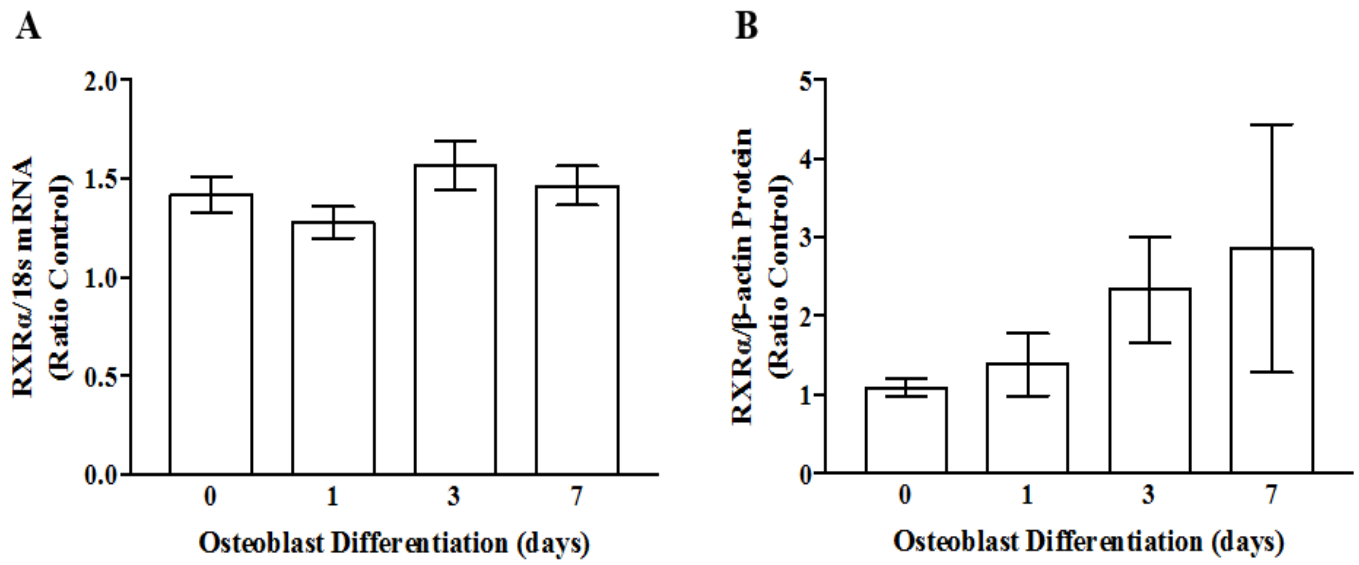

Figure 5. 8 RXRα expression in MC3T3-E1 cells during osteoblast differentiation

(A). RXRα mRNA expression level was maintained constant throughout osteoblast differentiation. (B). RXRα protein expression exhibited a gradual increase as osteoblast differentiation progressed. All gene expression was normalized to 18s expression, n=3 mRNA samples and n=9 protein samples. Data are presented as means ± SEM

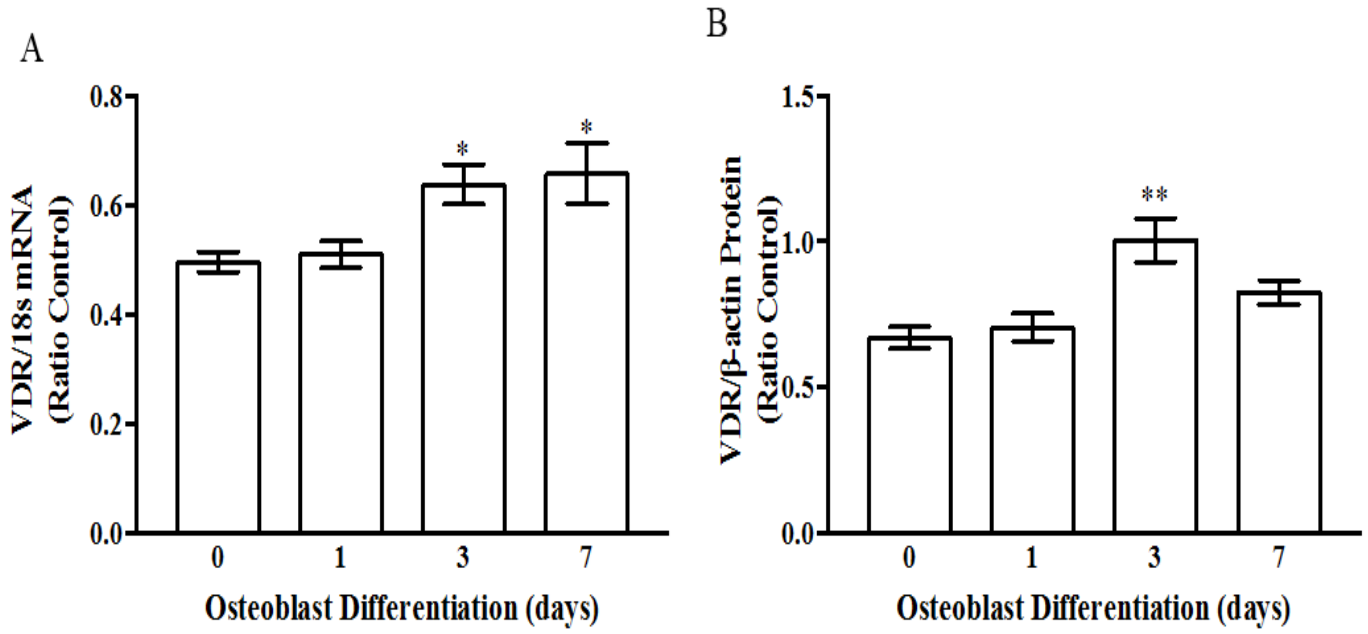

Figure 5. 9 Vitamin D Receptor (VDR) expression levels in FoxO3a over-expression model during osteoblast differentiation

(A). VDR mRNA expression levels increased significantly in 3-day and 7-day differentiated MC3T3-E1 cells (B). VDR protein expression levels increased significantly in 3-day but not 7-day differentiated MC3T3-E1 cells. All gene expression was normalized to 18s expression, n=3 mRNA samples and n=9 protein samples. Data are presented as means ± SEM. *$p \leq 0.05$, **$p \leq 0.01$

5.1.5 Expression of calcium transport machinery in FoxO3a over-expressors

RNA lysate was harvested at four osteoblast differentiation stages, including pre-osteoblasts, 1-day, 3-day and 7-day differentiated MC3T3-E1 cells over-expressing FoxO3a and expression levels of L-type calcium channels ($Ca_v1.2$, $Ca_v1.3$), T-type calcium channel ($Ca_v3.1$), Calbindin-D_{9K}, NCX, and PMCA-1b were assessed.

5.1.5.1 Expression of L-type and T-type calcium channels during osteoblast differentiation

We first examined expression levels of plasma membrane Ca^{2+} channels involved in Ca^{2+} uptake during differentiation. L-type Ca^{2+} channel, $Ca_v1.2$ and $Ca_v1.3$ showed uniform mRNA expression throughout osteoblast differentiation in the over-expressors (**Figure 5. 10A and B**). $Ca_v1.2$ mRNA expression showed the highest levels in pre-osteoblasts, followed by a gradual decrease, reaching the lowest levels in the non-transfected 7-day differentiated osteoblasts. $Ca_v1.3$ mRNA expression also reduced significantly in the non-transfected 7-day differentiated osteoblasts.

T-type Ca^{2+} channel, $Ca_v3.1$ mRNA expression levels showed a significant reduction in 1-day differentiated MC3T3-E1 cells over-expression FoxO3a, which returned to the same levels as pre-osteoblasts in 3-day and 7-day differentiated MC3T3-E1 cells (**Figure 5. 10C**). $Ca_v3.1$ mRNA expression increased gradually during differentiation, reaching the highest levels in the non-transfected 7-day differentiated osteoblasts.

Calbidin-D_{9K} exhibited uniform expression levels throughout osteoblast differentiation over-expressing FoxO3a (**Figure 5. 10D**). On the other hand, Calbidin-D_{9K} mRNA expression underwent a gradual decrease during differentiation, and reached the lowest levels in the non-

transfected 7-day differentiated osteoblasts.

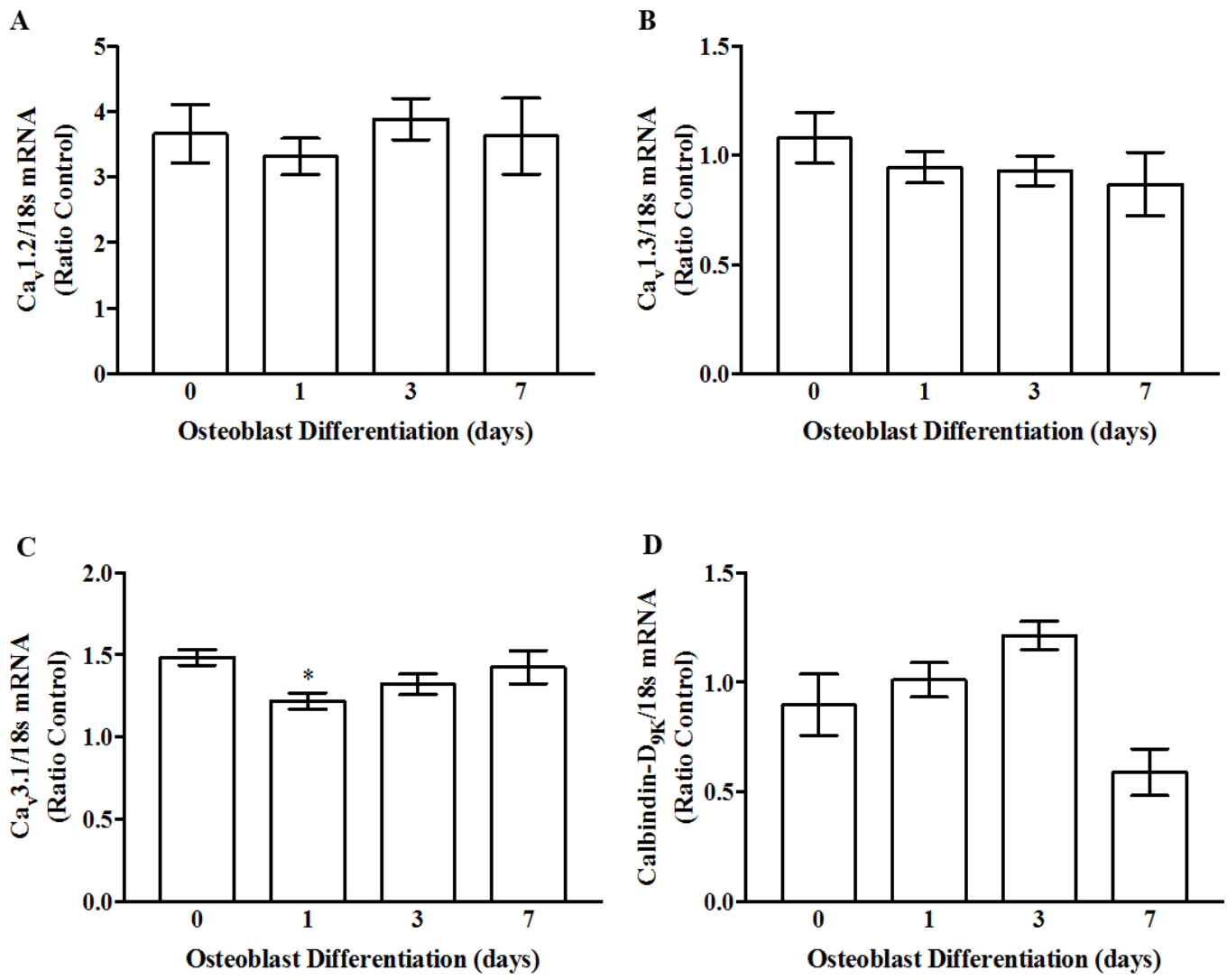
A
$Ca_v1.2$/18s mRNA (Ratio Control)
5
4
3
2
1
0
0
1
3
7
Osteoblast Differentiation (days)
B
$Ca_v1.3$/18s mRNA (Ratio Control)
1.5
1.0
0.5
0.0
0
1
3
7
Osteoblast Differentiation (days)
C
$Ca_v3.1$/18s mRNA (Ratio Control)
2.0
1.5
1.0
0.5
0.0
*
0
1
3
7
Osteoblast Differentiation (days)
D
Calbindin-D_{9K}/18s mRNA (Ratio Control)
1.5
1.0
0.5
0.0
0
1
3
7
Osteoblast Differentiation (days)

Figure 5. 10 **Expression of L-type and T-type calcium channels during osteoblast differentiation** mRNA expression of (A). $Ca_v1.2$ (B). $Ca_v1.3$ (C). $Ca_v3.1$ (D). Calbidin-D_{9K}. All gene expression was normalized to 18s expression. n=9 each.

Data are presented as means ± SEM. *$p \leq 0.05$

5.1.5.2 Expression of Ca^{2+} efflux mediators and transporters during osteoblast differentiation

In the FoxO3a over-expressors, NCX mRNA expression remained constant in pre-osteoblasts, 1-day and 3-day differentiated MC3T3-E1 cells with a slight but not significant increase in 1-day differentiated MC3T3-E1 cells. NCX mRNA expression reduced significantly in 7-day differentiated osteoblasts over-expressing FoxO3a (**Figure 5. 11A**). In contrast, mRNA expression of NCX stayed at the same levels throughout differentiation in the non-transfected cells.

Uniform PMCA-1b expression was detected throughout osteoblast differentiation in the over-expressors (**Figure 5. 11B**). In contrast, mRNA expression of PMCA-1b in the non-transfected cells increased gradually during differentiation and reached the highest levels in 7-day differentiated MC3T3-E1 cells.

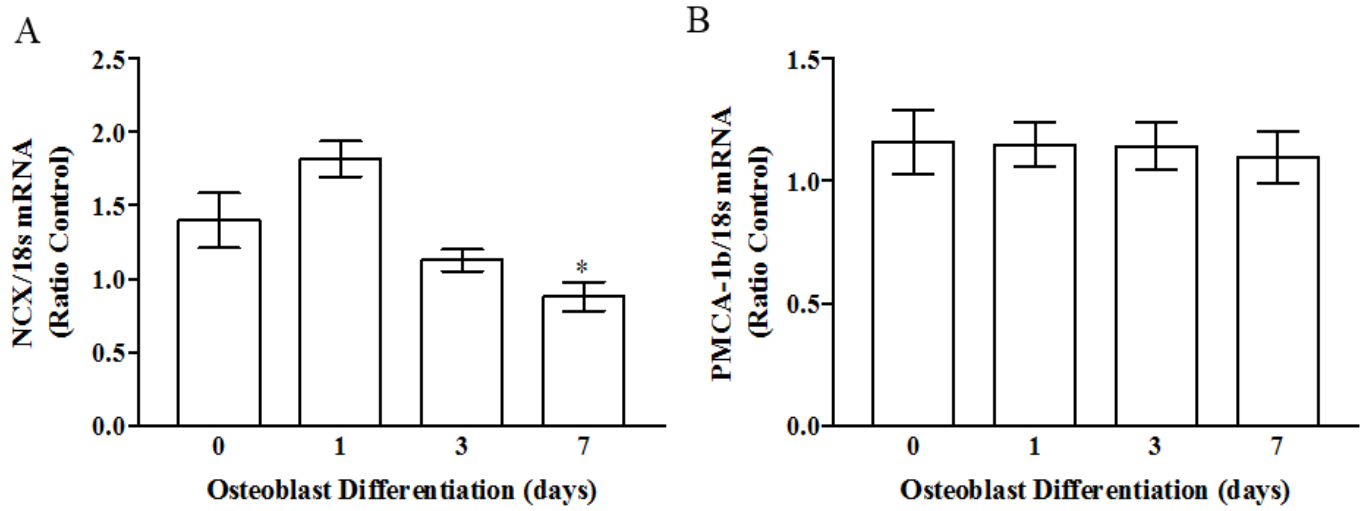

Figure 5. 11 Expression of mediators for calcium deposition during osteoblast differentiation

(A). NCX exhibited a significant reduction in 7-day differentiated MC3T3-E1 cells (B). PMCA-1b showed uniform expression levels throughout osteoblast differentiation. All gene expression was normalized to 18s expression, n=9 each.

Data are presented as means ± SEM. *$p \leq 0.05$

5.2 Effects of 1,25D$_3$ and ROS on FoxO3a over-expressors during osteoblast differentiation and matrix calcification

5.2.1 Assessment of 1,25D$_3$ and ROS on osteogenesis in FoxO3a over-expressors

7-day differentiated MC3T3-E1 cells over-expressing FoxO3a were treated with H_2O_2, 1,25D$_3$ and a combination of 1,25D$_3$ and H_2O_2 and the expression of Runx2 and OCN mRNA was evaluated. H_2O_2 did not have an effect on Runx2 mRNA expression, but treatment with 1,25D$_3$ reduced Runx2 expression significantly. The combination treatment of both 1,25D$_3$ and H_2O_2 also led to significant reduction in Runx2 mRNA expression (**Figure 5. 12A**). In comparison, Treatment with H_2O_2 up-regulated OCN expression levels, but treatment with 1,25D$_3$ and the combination of treatments did not alter OCN expression (**Figure 5. 12B**).

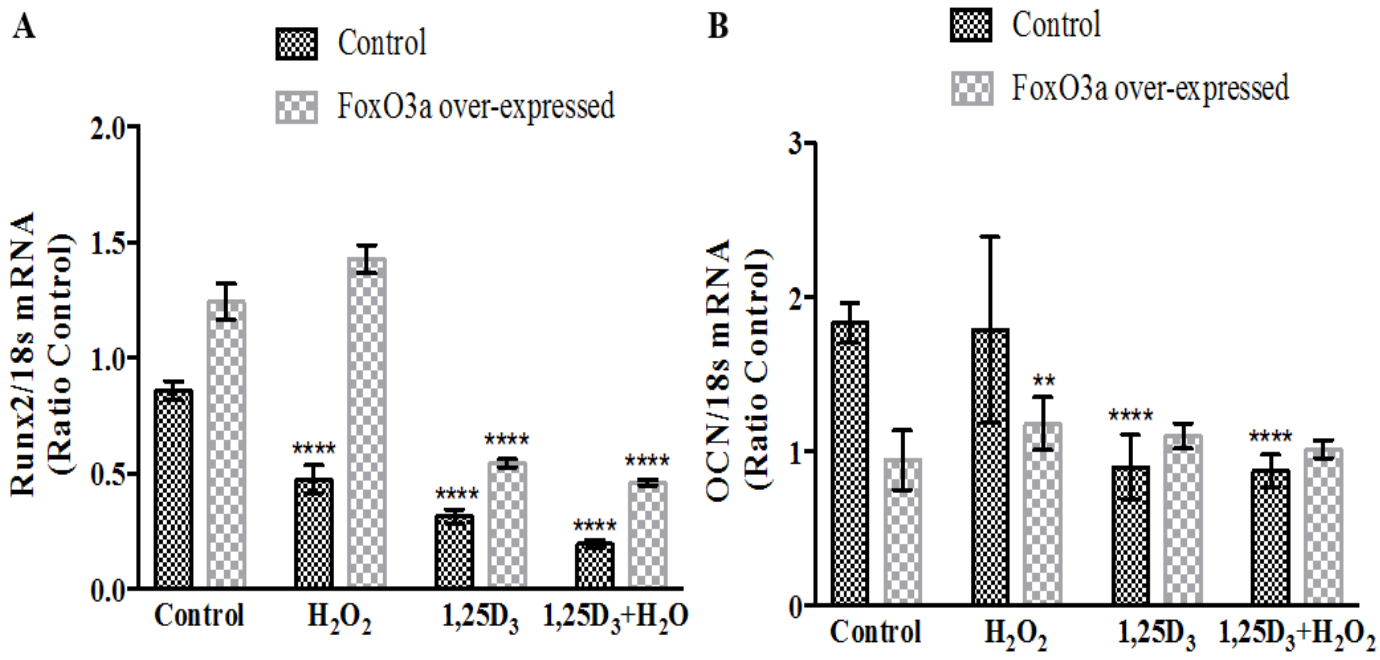

Figure 5. 12 Effects of $1,25D_3$ and H_2O_2 on Runx2 and OCN expression in 7-day differentiated wild type and FoxO3a over-expressors

(A). $1,25D_3$ reduced Runx2 mRNA expression levels, but H_2O_2 did not alter its expression

(B). $1,25D_3$ did not alter OCN mRNA expression levels, while H_2O_2 increased its expression

All gene expression was normalized to 18s expression, n=9 per condition.

Data are presented as means ± SEM. **p ≤0.01, ****p ≤0.0001

5.2.2 Effects of 1,25D$_3$ and ROS on expression of transcription factors and genes in FoxO3a over-expressors

Pre-osteoblast MC3T3-E1 cells were differentiated with ascorbic acid and β-glycerophosphate for seven days and RNA and protein lysates collected for analysis. 1,25D$_3$ increased FoxO3a mRNA expression, but H_2O_2 did not nor did the combination group of 1,25D$_3$ and H_2O_2 (**Figure 5. 13A**). FoxO3a protein expression levels were not altered by H_2O_2, 1,25D$_3$ or the combination of 1,25D$_3$ and H_2O_2 (**Figure 5. 13B**). Gene expression involved in vitamin D signaling, such as RXRα and VDR was also evaluated. RXRα mRNA expression was not affected by H_2O_2 or 1,25D$_3$, but the combination drug treatment of 1,25D$_3$ and H_2O_2 reduced RXRα expression significantly (**Figure 5. 14A**). RXRα protein expression levels were not altered by H_2O_2, 1,25D$_3$ or the combination treatment (**Figure 5. 14B**). VDR mRNA expression was up-regulated significantly up 1,25D$_3$ and the combination treatment of 1,25D$_3$ and H_2O_2 (**Figure 5. 15A**). However, VDR protein expression was not affected by H_2O_2, 1,25D$_3$ or the combination of both (**Figure 5. 15B**).

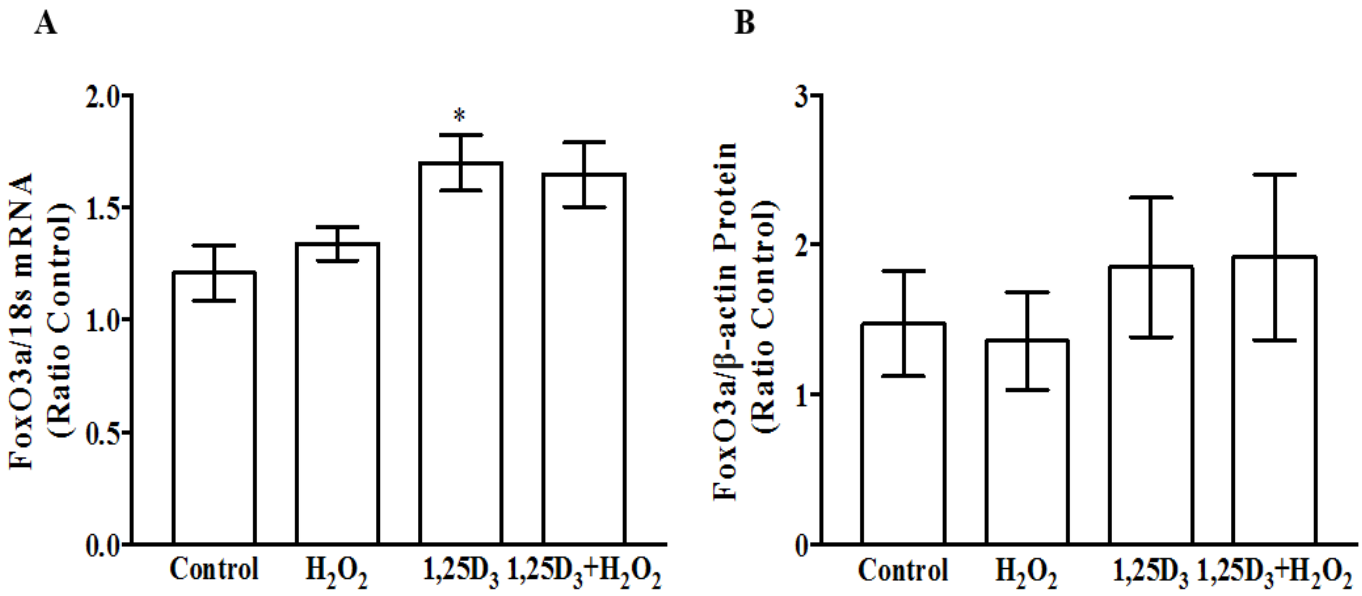

Figure 5. 13 $1,25D_3$ up-regulated FoxO3a mRNA expression in 7-day differentiated FoxO3a over-expressors

(A). FoxO3a mRNA expression was enhanced by $1,25D_3$ but not H_2O_2. (B). Treatments with H2O2 and $1,25D_3$ did not alter FoxO3a protein expression levels. All gene expression was normalized to 18s expression, n=9 mRNA samples and n=4 protein samples. Data are presented as means ± SEM. *$p \leq 0.05$

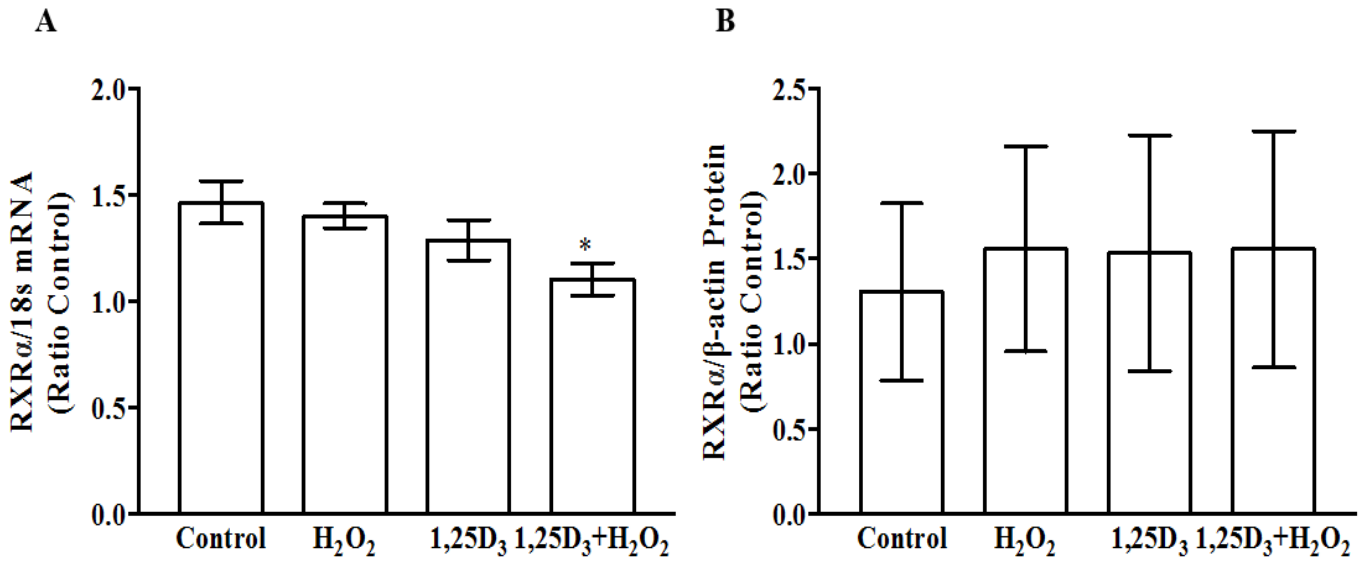

Figure 5. 14 RXRα expression not altered by 1,25D$_3$ in 7-day differentiated FoxO3a over-expressors

(A). RXRα mRNA expression was significantly reduced by combination treatment of 1,25D$_3$ and H_2O_2. (B). RXRα protein expression was not altered by treatments. All gene expression was normalized to 18s expression, n=9 mRNA samples and n=3 protein samples. Data are presented as means ± SEM. *p≤0.05

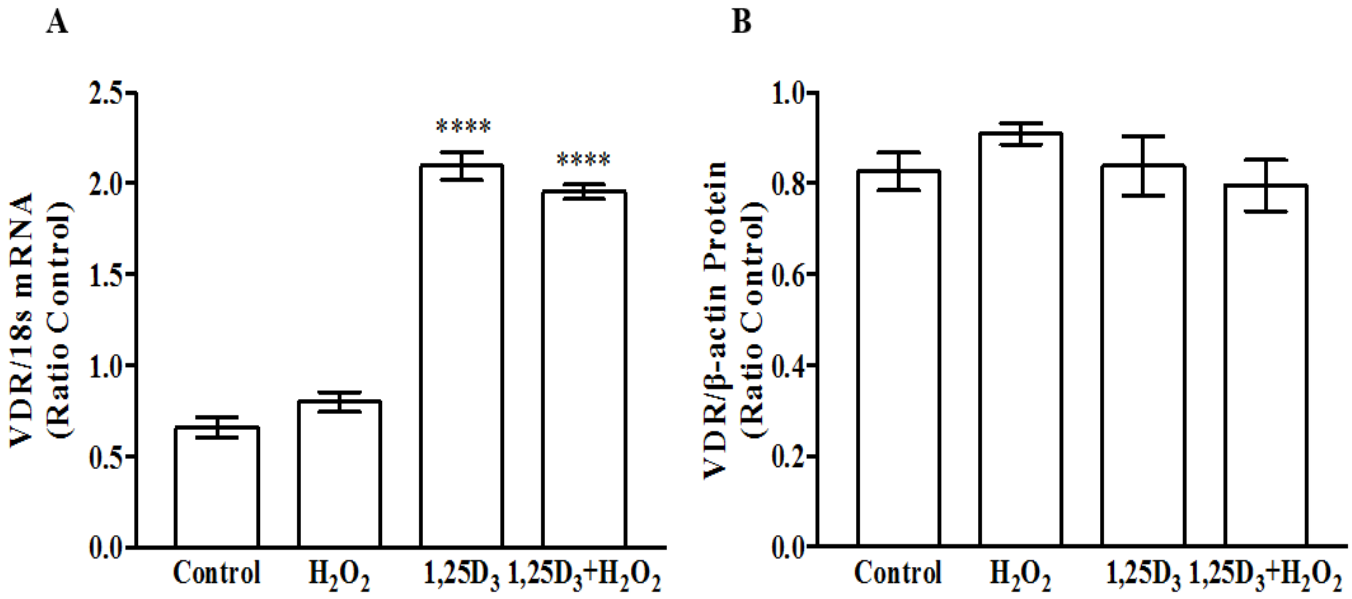

Figure 5. 15 Effects of $1,25D_3$ and H_2O_2 on vitamin D receptor (VDR) expression in 7-day differentiated FoxO3a over-expressors

(A). VDR mRNA expression was up-regulated by $1,25D_3$ and the combination group. (B). VDR protein expression was not altered by $1,25D_3$ or H_2O_2

All gene expression was normalized to 18s expression, n=9 mRNA samples and n=3 protein samples. Data are presented as means ± SEM. ****p ≤0.0001

5.2.3 Effects of vitamin D signaling and ROS on calcium transport machinery during osteoblast mineralization

Treatment with 250 μM H_2O_2 did not alter mRNA expression of L-type ($Ca_v1.2$, $Ca_v1.3$), and T-type ($Ca_v3.1$) calcium channels. $1,25D_3$ up-regulated $Ca_v1.2$ mRNA expression (**Figure 5. 16A**), but not $Ca_v1.3$ mRNA expression (**Figure 5. 16B**). $1,25D_3$ down-regulated $Ca_v3.1$ mRNA expression (**Figure 5. 17C**). $1,25D_3$ up-regulated Calbindin-D_{9K} mRNA expression (**Figure 5. 16D**). The combination group of $1,25D_3$ and H_2O_2 attenuated the $1,25D_3$ effect on $Ca_v1.3$ and $Ca_v3.1$ (**Figure 5. 16B and C**). Treatment with 250 μM H_2O_2 did not alter mRNA expression of NCX and PMCA-1b. $1,25D_3$ up-regulated NCX mRNA expression, and the combination group of $1,25D_3$ and H_2O_2 attenuated the increase caused by $1,25D_3$ alone (**Figure 5. 17A**). $1,25D_3$ down-regulated PMCA-1b mRNA expression (**Figure 5. 17B**). In the non-transfected 7-day differentiated MC3T3-E1 cells, treatment with $1,25D_3$ or H_2O_2 did not alter expression of $Ca_v1.2$, $Ca_v1.3$ and $Ca_v3.1$ but up-regulated Calbindin-D_{9K}. Combination treatment of $1,25D_3$ and H_2O_2 significantly reduced expression of all these genes.

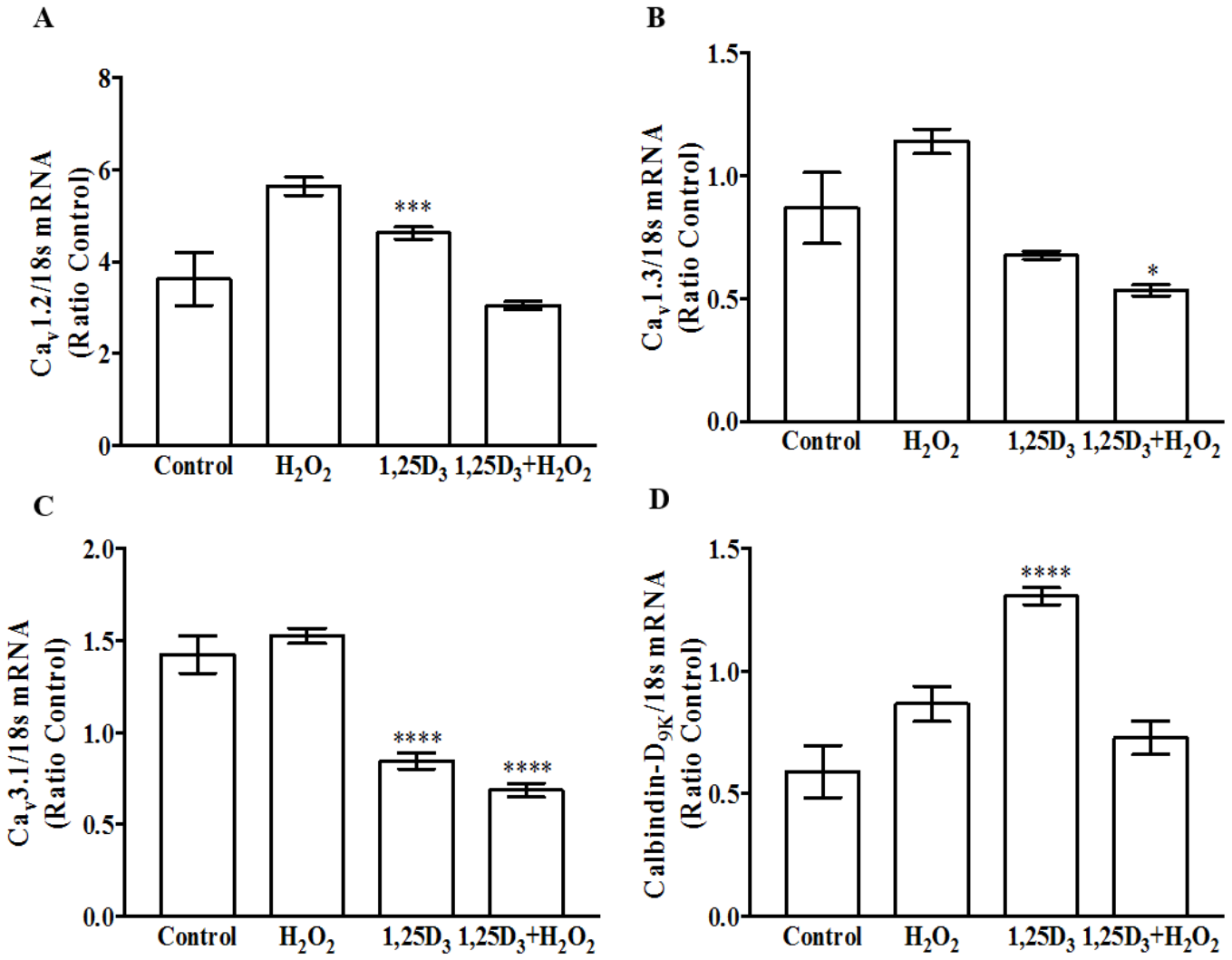

Figure 5. 16 **Effects of 1,25D_3 on L-type and T-type calcium channels in 7-day differentiated MC3T3-E1 cells over expressing FoxO3a** mRNA expression of (A) $Ca_v1.2$, (B) $Ca_v1.3$, (C) $Ca_v3.1$ and (D) Calbindin-D_{9K}. All gene expression was normalized to 18s expression. n=9 each. Data are presented as means ± SEM. *p≤0.05, ***p ≤0.001, ****p ≤0.0001

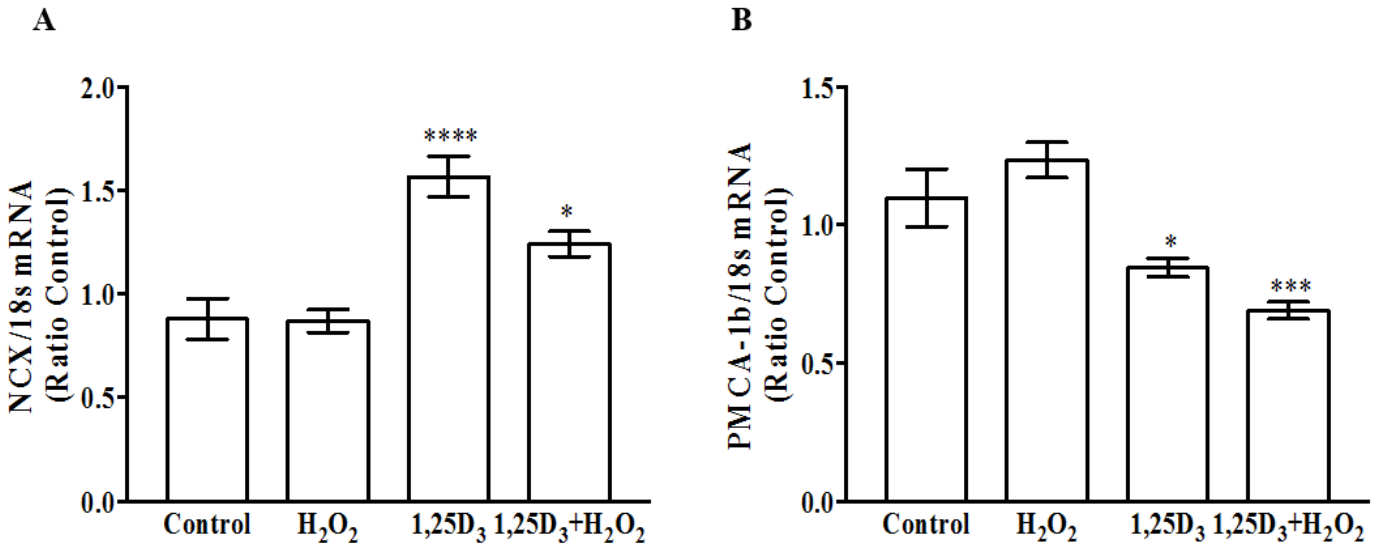

Figure 5. 17 Effects of 1,25D_3 and H_2O_2 on mediators for calcium deposition in 7-day differentiated MCT3-E1 cells over-expressing FoxO3a

(A)1,25D_3 up-regulated NCX mRNA expression significantly which was attenuated by the combination treatment with H_2O_2 (B).1,25D_3 down-regulated PMCA-1b mRNA expression significantly which was further reduced by combination treatment with H_2O_2. All gene expression was normalized to 18s expression, n=9 each.

5.3 Effects of FoxO3a over-expression on calcium influx

Expression of Ca^{2+} channels, mediators and transporters have been characterized previously. Our next specific aim was to determine the effect of FoxO3a on Ca^{2+} uptake into pre-osteoblasts and 7-day differentiated osteoblasts by ratiometric calcium imaging with Fura-2 AM. Three channel antagonists listed in **Table 4.4** were applied to these over-expressors to inhibit activity of specific channels, and [Ca^{2+}] uptake was measured. 100 μM lanthanum chloride ($LaCl_{3)}$ was used to inhibit activity of cationic channels, 10 μM NNC 55-0396 was used to inhibit $Ca_v3.1$ of T-type Ca^{2+} channel activity and 10 μM felodipine was used to inhibit activity of L-type Ca^{2+} channel, including $Ca_v1.2$ and $Ca_v1.3$.

5.3.1 FoxO3a over-expression caused significant reduction in calcium uptake

We first measured [Ca^{2+}] uptake in both pre-osteoblasts and 7-day differentiated osteoblasts over-expressing FoxO3a. L-type ($Ca_v1.2$ and $Ca_v1.3$) calcium channel was identified to be the major functioning channel in the current cell model, thus we sought to examine the degree of reduction in calcium uptake compared to wild type. Both magnitude and rate of calcium uptake were significantly reduced compared with wild type (**Figure 5. 18**). The magnitude of calcium uptake in wild type 7-day differentiated MC3T3-E1 cells was approximately 6.5 nM calcium, in contrast to less than 1 nM calcium in the FoxO3a over-expressed model (**Figure 5. 18A**). Similarly, the rate of calcium uptake was also significantly reduced, at approximately 4.7 nM/min in wild type to less than 1 nM/min in the FoxO3a over-expressed model (**Figure 5. 18B**). Together this data demonstrates that FoxO3a over-expression attenuates the ability for osteoblasts to mediate calcium uptake.

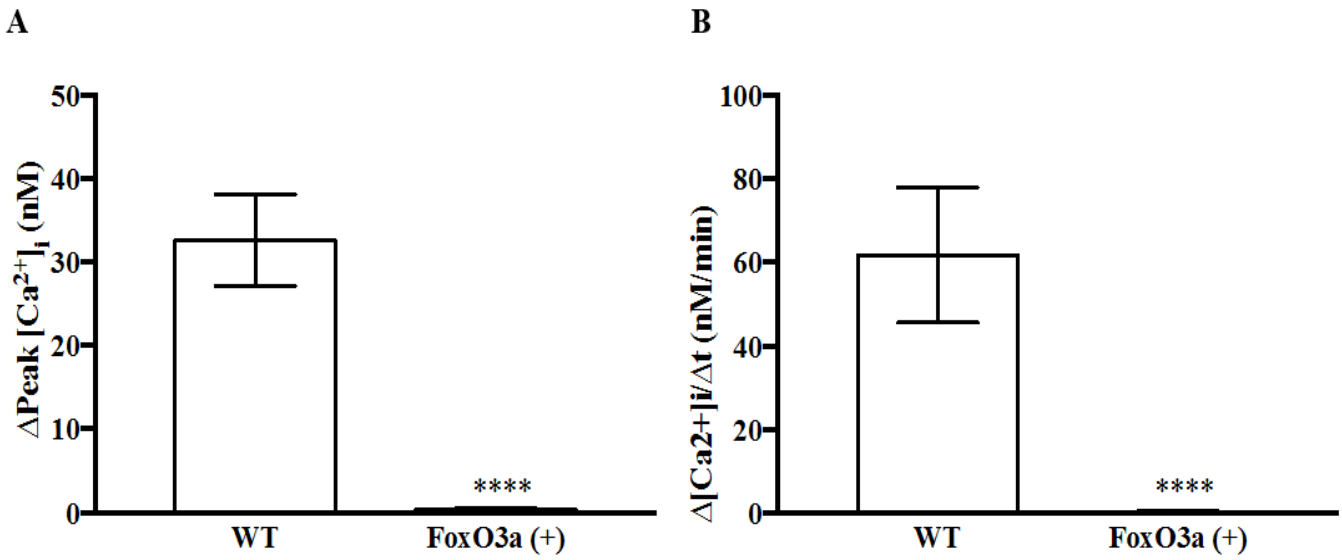

Figure 5. 18 FoxO3a over-expression inhibited calcium influx in 7-day differentiated osteoblasts

(A). Magnitude of calcium uptake. (B) Rate of calcium uptake in wild type (WT) and FoxO3a over-expressing cells. n=18 wild type/control and n=8 FoxO3a (+). All measurements were normalized to the day of the experiment, and data are presented as means ±SEM. ****p ≤0.0001.

5.3.2 L-type Ca^{2+} channel is the major functioning Ca^{2+} channel in pre-osteoblasts

FoxO3a over-expression reduced Ca^{2+} uptake significantly in pre-osteoblasts and 7-day differentiated osteoblasts. We sought to determine which specific Ca^{2+} channel was affected by high levels of FoxO3a, thereby inhibiting Ca^{2+} influx.

We first examined the activity of L-type calcium channel in undifferentiated MC3T3-E1 cells over-expressing FoxO3a by inhibiting activity with Felodipine, which blocks both $Ca_v1.2$ and $Ca_v1.3$ channels. 10 μM Felodipine caused a significant reduction in calcium influx, both Δpeak of Ca^{2+} influx magnitude and rate of calcium uptake, Δslope. This result suggests L-type to be the major functioning Ca^{2+} channel in pre-osteoblasts, responsible for majority of calcium uptake (**Figure 5. 19A and B**).

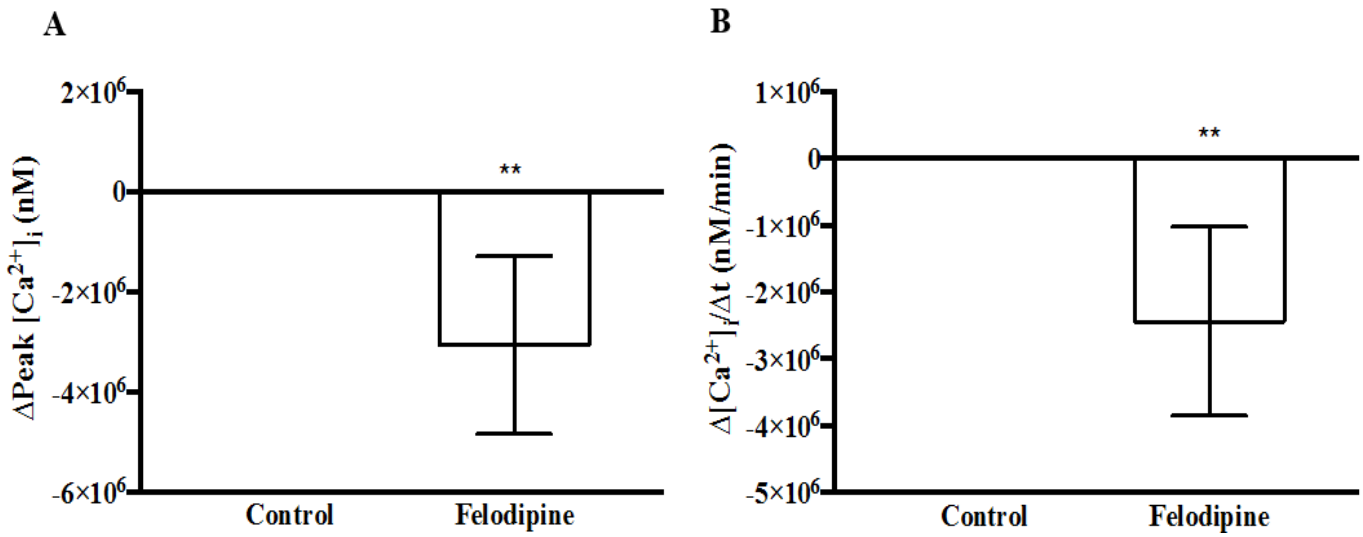

Figure 5. 19 Significant reduction in calcium uptake with Felodipine treatment in pre-osteoblasts MC3T3-E1 cells over expressing FoxO3a

(A). Magnitude of calcium uptake (B). Rate of calcium uptake in the presence and absence of Felodipine, n=6 control, n=5 Felodipine-treated. All measurements were normalized to the day of the experiment, and data are presented as means ±SEM. **p ≤0.01.

5.3.3 1,25D$_3$ increased calcium uptake in the undifferentiated MC3T3-E1 cell model

L-type ($Ca_v1.2$ or $Ca_v1.3$) calcium channels were identified to be the major functioning channels in pre-osteoblast cells. We therefore wanted to determine the effects of 1,25D$_3$ on this channel activity. Pre-osteoblast cells were treated with 100 nM 1,25D$_3$ for 24 hours and then calcium uptake was measured. 1,25D$_3$ increased both magnitude and rate of calcium uptake into our model, confirming the effects of 1,25D$_3$ were through a L-type calcium channel in pre-osteoblasts (**Figure 5. 20A and B**).

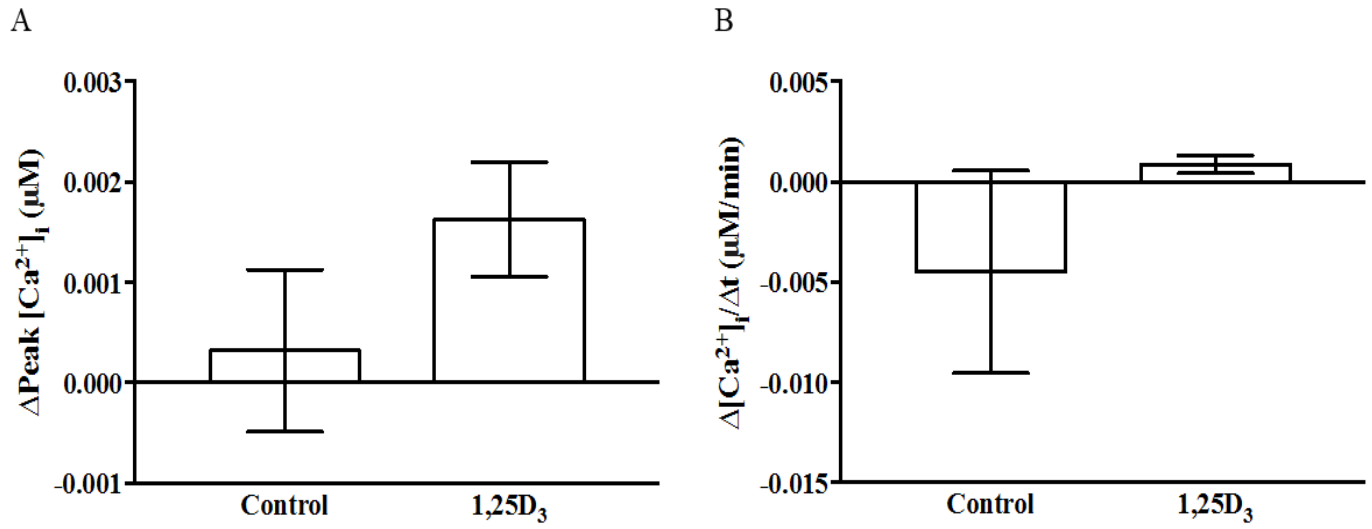

Figure 5. 20 Active vitamin D increased calcium uptake in pre-osteoblast MC3T3-E1 cells over expressing FoxO3a

(A). Magnitude of calcium uptake. (B). Rate of calcium uptake in the presence and absence of $1,25D_3$ treatment, n=3 each. All measurements were normalized to the day of the experiment, and data are presented as means ±SEM.

5.3.4 Lanthanum chloride reduced Ca^{2+} uptake in 7-day differentiated osteoblasts

100 μM lanthanum chloride ($LaCl_3$) was used to inhibit cationic calcium channel activity including both L-type ($Ca_v1.2$, $Ca_v1.3$) and T-type ($Ca_v3.1$) calcium channels in 7-day differentiated MC3T3-E1 cells. Both the magnitude of calcium uptake into and rate of calcium uptake were reduced by this treatment (**Figure 5. 21A and B**).

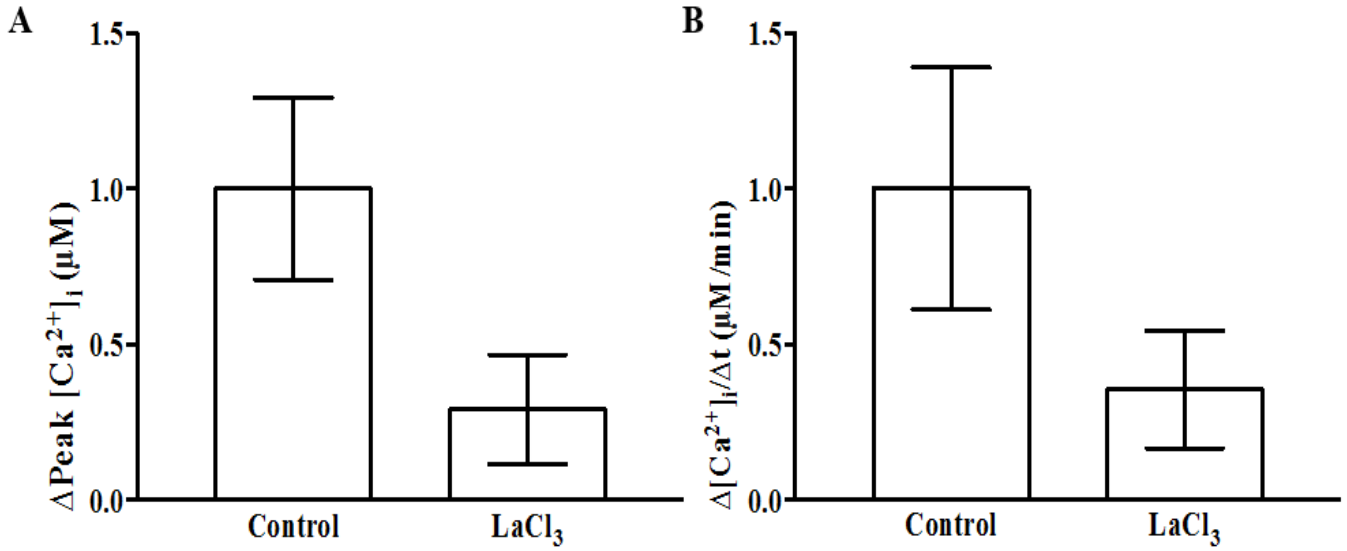

Figure 5. 21 $LaCl_3$ caused reduction in calcium uptake in 7-day differentiated MC3T3-E1 cells over expressing FoxO3a

(A). Magnitude of calcium uptake. (B). Rate of calcium uptake in the presence and absence of $LaCl_3$, n=5 each. All measurements were normalized to the day of the experiment, and data are presented as means ±SEM.

5.3.5 L-type calcium channels are the major functioning channel in 7-day differentiated MC3T3-E1 cell model

10 μM felodipine was employed to inhibit L-type ($Ca_v1.2$ and $Ca_v1.3$) calcium channel activity in 7-day differentiated MC3T3-E1 cells with FoxO3a over-expressed. Felodipine caused a significant reduction in both magnitude and rate of calcium uptake (**Figure 5. 22B and C**). Felodipine also caused significant calcium efflux (**Figure 5. 22A**), likely by significantly blocking calcium influx while not altering the efflux mechanism. This data further confirms ongoing efflux mechanisms likely through a calcium pump or NCX.

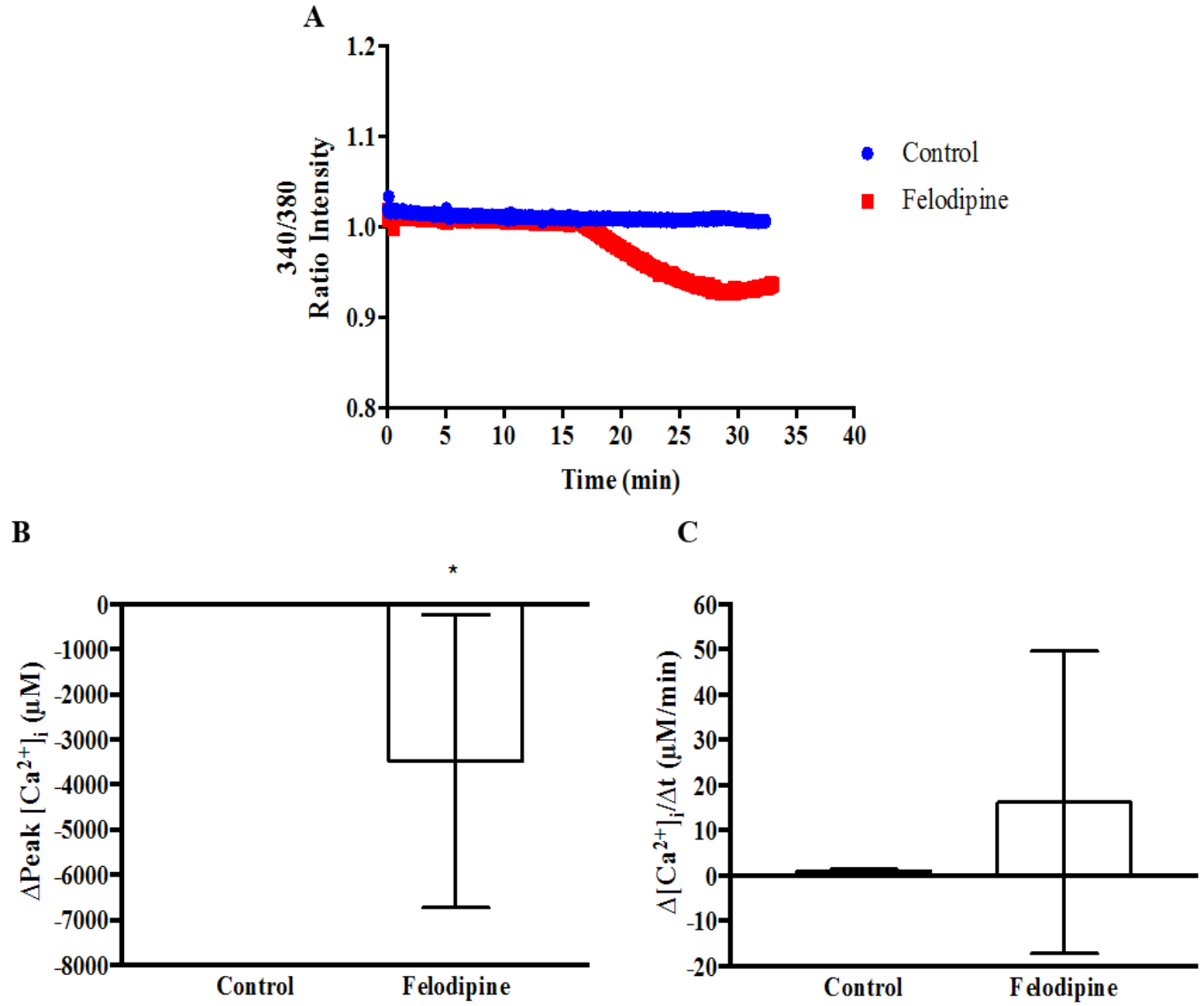

Figure 5. 22 Felodipine caused calcium efflux in 7-day differentiated MC3T3-E1 cells over expressing FoxO3a

(A). Representative traces of 340/380 ratio intensity, felodipine treatment caused calcium efflux. Control group is shown in blue and Felodipine-treated group in red

(B). Magnitude of calcium uptake (C). Rate of calcium uptake in the presence and absence of Felodipine. n=5 each. Data are presented as means ± SEM.

5.4 Active vitamin D increased calcium uptake in 7-day differentiated MC3T3-E1 cells over-expressing FoxO3a

7-day differentiated MC3T3-E1 cells were treated with 100 nM $1,25D_3$ for 24 hours and then calcium uptake measured. $1,25D_3$ increased both the magnitude and rate of calcium uptake significantly in the current cell model (**Figure 5. 23A and B**). When the$1,25D_3$-mediated increase in calcium uptake in the FoxO3a over-expression model differentiated for 7 days was compared to $1,25D_3$-mediated increase in 7-day differentiated MC3T3-E1 wild type controls cells, FoxO3a over-expressing cells exhibited1000 times less calcium uptake than wild type control cells both treated with $1,25D_3$ (**Figure 5. 24A and B**). This data demonstrates that FoxO3a over-expression attenuates calcium uptake into osteoblasts as well as the $1,25D_3$-induced increase in calcium uptake.

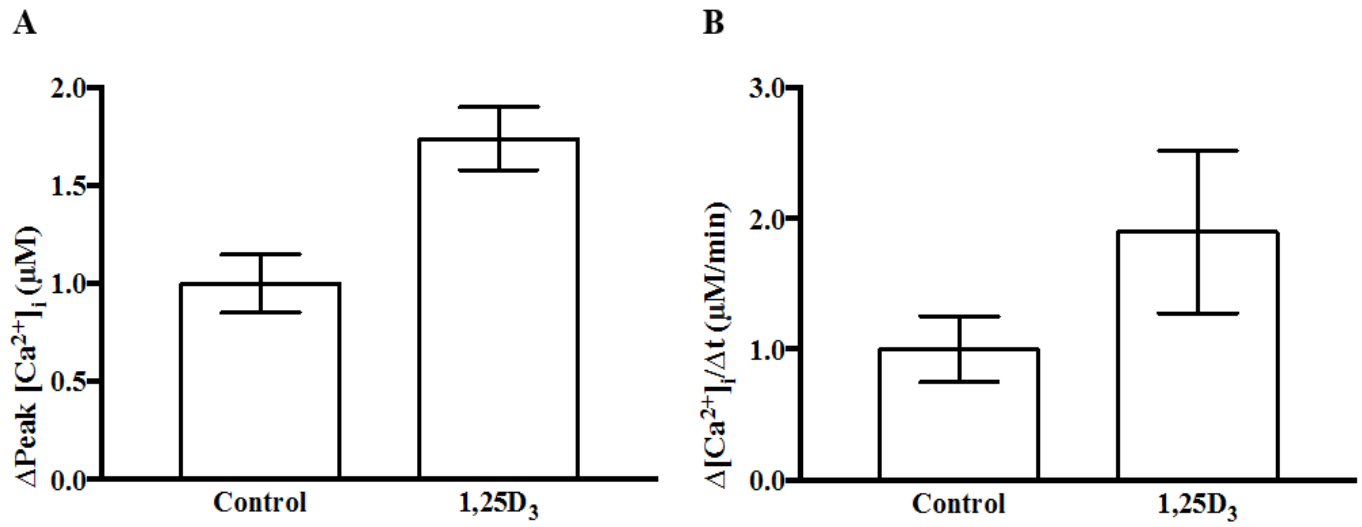

Figure 5. 23 $1,25D_3$ increased calcium uptake significantly in 7-day differentiated MC3T3-E1 cells over expressing FoxO3a

(A) Magnitude of calcium uptake. (B). Rate of calcium uptake in the presence and absence of $1,25D_3$ treatment. All measurements were normalized to the day of the experiment, and data are presented as means ±SEM. n=3 each *p ≤0.05.

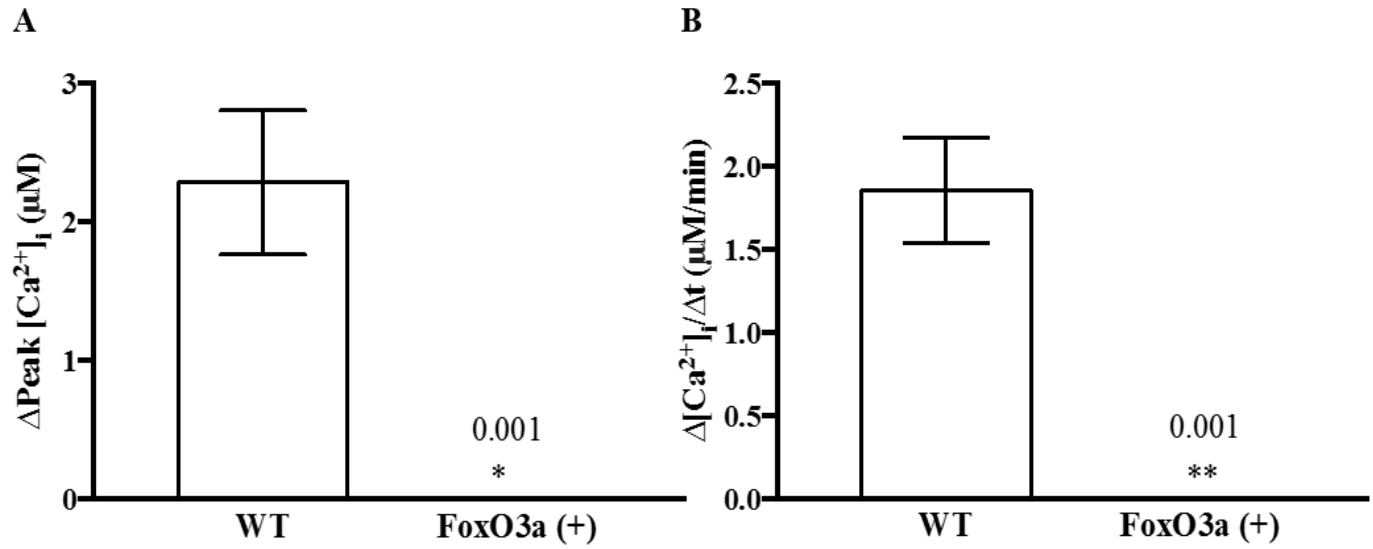

Figure 5. 24 **$1,25D_3$-mediated increase in calcium uptake is 1000-times less in FoxO3a over expressing cells relative to wild type cells**

(A). Magnitude of calcium uptake. (B). Rate of calcium uptake. n=8 wild type, n=3 FoxO3a over-expressed. Data are presented as means ± SEM. *p≤0.05, **p ≤0.01.

5.5 Calcium deposition in FoxO3a over-expressing cells assessed by Alizarin Red staining (ARS)

ARS was employed to visualize and quantify calcium levels in our model system. We first determined calcium levels in pre-osteoblasts and then in 7-day differentiated MC3T3-E1 cells. We finally examined the effects of $1,25D_3$ and ROS on calcium deposition.

5.5.1 Pre-osteoblast over-expressing Foxo3a fail to deposit calcium during osteoblast differentiation

Pre-osteoblasts stained with ARS exhibited faint ARS staining (**Figure 5. 25A**), which was surprisingly similar to 7-day differentiated MC3T3-E1 cells over-expressing FoxO3a (**Figure 5. 25B**). Staining in both cultures were quantified. Pre-osteoblasts showed calcium levels to be of approximately 80 nM and 7-day differentiated osteoblasts to be approximately 75 nM (**Figure 5. 25C**). Calcium deposition in pre-osteoblasts with FoxO3a over-expression was compared to wild type pre-osteoblasts. Wild type pre-osteoblasts exhibited calcium levels of 150 μM in contrast to calcium level of less than 40 μM in the FoxO3a over-expression model (**Figure 5. 26A**), showing an almost four-fold reduction in calcium levels (**Figure 5. 26B**). Wild type 7-day differentiated osteoblasts were also compared with 7-day differentiated osteoblasts with FoxO3a over-expressed. Wild type 7-dy differentiated osteoblasts exhibited calcium levels of 300 μM, in contrast to approximately 50 μM in 7-day differentiated osteoblasts with FoxO3a over-expressed (**Figure 5. 27A**), demonstrating approximately a six-fold decrease in calcium deposition (**Figure 5. 27B**). Together this data demonstrates that FoxO3a over-expression attenuates calcium deposition in pre-osteoblasts and severely prevents calcium deposition in differentiated osteoblasts.

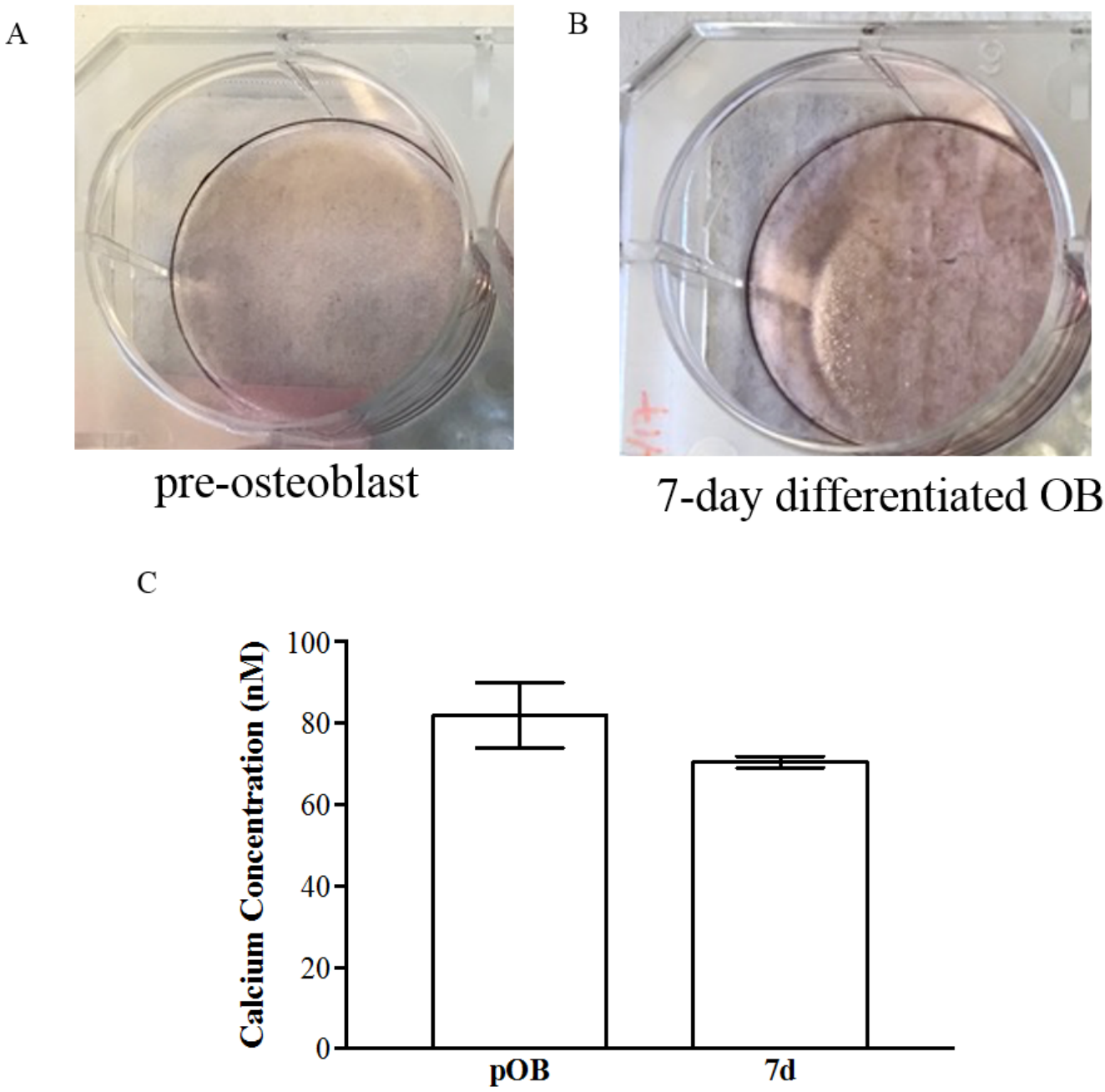

Figure 5. 25 7-day differentiated osteoblasts over expressing FoxO3a failed to incorporate calcium into the extracellular matrix

(A). Pre-osteoblasts exhibited approximately 80 nM calcium in the matrix. (B). 7-day differentiated osteoblasts exhibited approximately 75 nM calcium in the matrix. (C).

Quantification of calcium levels comparing pre-osteoblasts with 7-day differentiated MC3T3-E1 cells. n=6 each. Data are presented as means ± SEM.

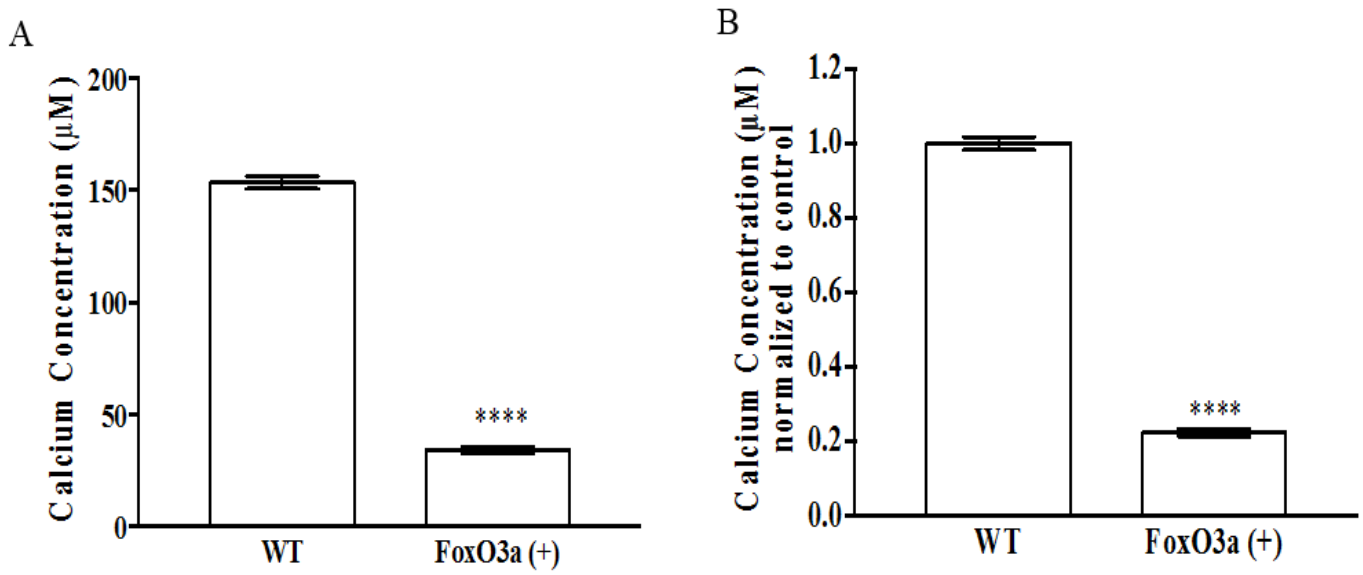

Figure 5. 26 Significantly reduced calcium deposition in pre-osteoblasts over expressing FoxO3a assessed by Alizarin red staining

(A). Wild type pre-osteoblasts exhibited approximately 150 µM calcium in contrast to 50 µM in the FoxO3a over-expressed model. (B). Wild type exhibited 5 times more calcium in the matrix. Data are presented as means ±SEM. n=3 each, ****p ≤0.0001.

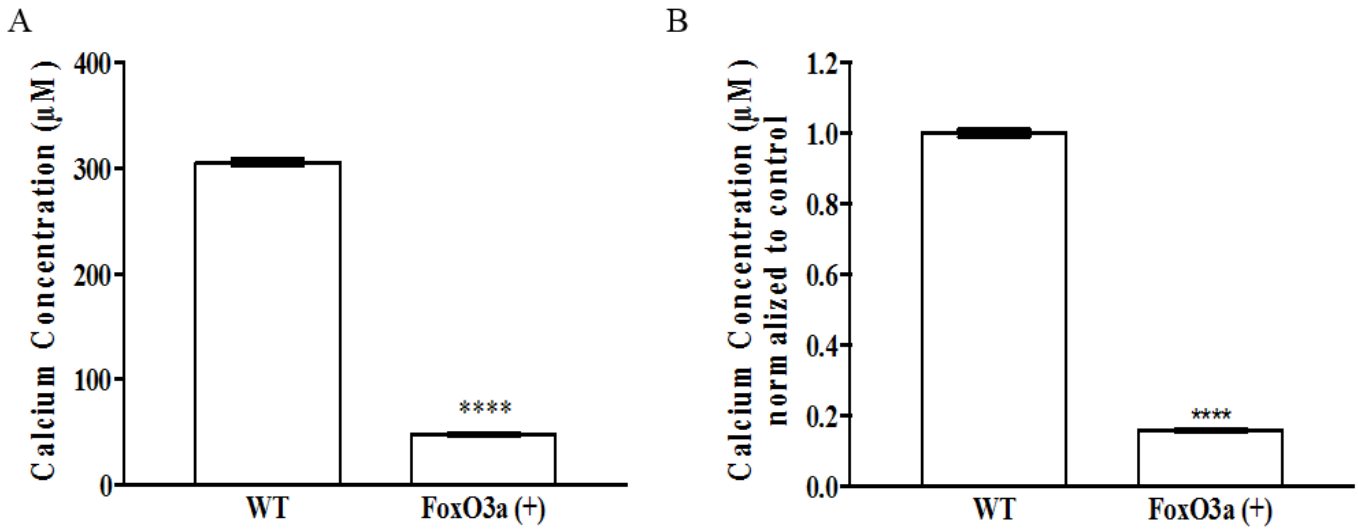

Figure 5. 27 Significantly reduced calcium deposition in 7-day differentiated MC3T3-E1 cells over expressing FoxO3a assessed by Alizarin red staining

(A). Wild type cells exhibited approximately 300 µM calcium in contrast to 50 µM in the FoxO3a over-expressed model. (B). Wild type cells exhibited 5 times more calcium in the matrix. Data are presented as means ±SEM. n=3 each, ***p ≤0.001.

5.5.2 Effects of H_2O_2 and 1,25D_3 on calcium deposition in pre-osteoblasts and 7-day differentiated MC3T3-E1 cells

Pre-osteoblasts stained with ARS displayed a faint staining in control and treatment groups (**Figure 5. 28A**). Untreated pre-osteoblasts exhibited 21 μM calcium levels in the matrix and treatment with H_2O_2 caused an increase to 32 μM but 1,25D_3 caused no alterations (**Figure 5. 28B**).

7-day differentiated osteoblasts stained with ARS also displayed faint ARS staining in control and treatment groups (**Figure 5. 29A**). Untreated 7-day differentiated MC3T3-E1 cells showed calcium levels of approximately 49 μM and treatments with 1,25D_3 and H_2O_2 did not cause significant alterations (**Figure 5. 29B**).

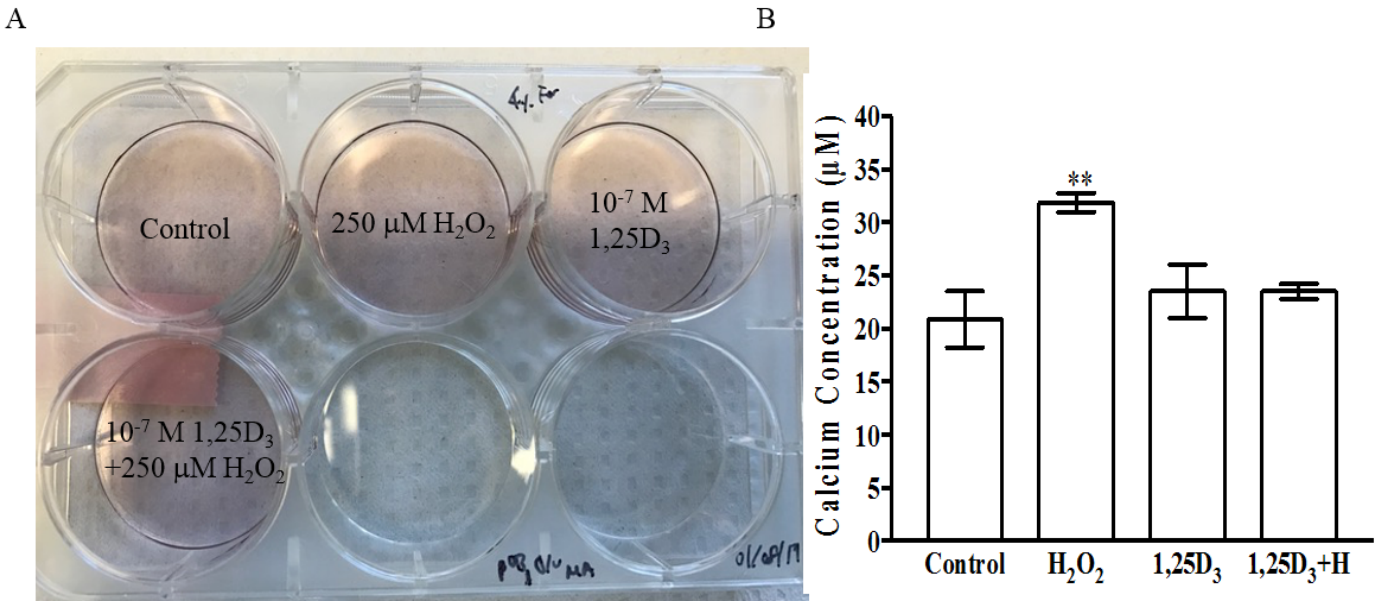

Figure 5. 28 Altered calcium deposition in pre-osteoblasts by H_2O_2

(A). Pre-osteoblast cells grown to confluent and treated with 1,25D_3 and H_2O_2 and (B). Quantification of calcium levels in the treatment groups compared to control. Data are presented as means ±SEM. n=3 each. **p ≤0.01.

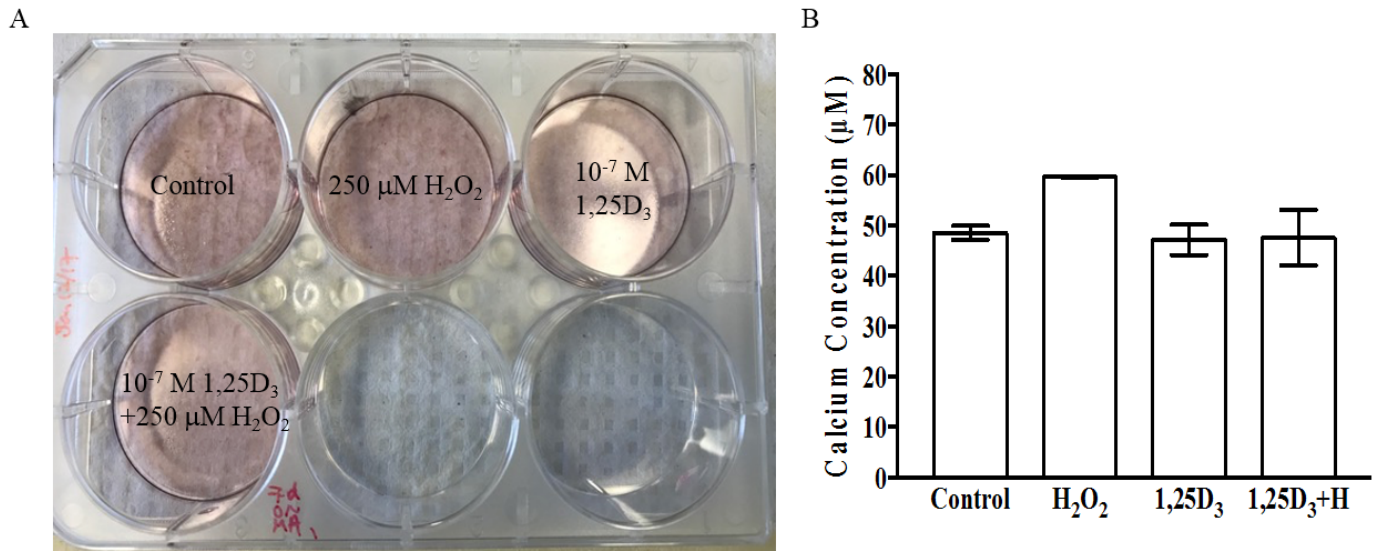

Figure 5. 29 1,25D_3 and H_2O_2 did not alter calcium deposition in 7-day differentiated MC3T3-E1 cells over expressing FoxO3a

(A). Osteoblast cells gown to confluence and treated with H_2O_2 for an hour, 1,25D_3 for 24 hours.

(B). Quantification of calcium levels in the treatment groups compared to control. Data are presented as means ±SEM. n=3 each.

5.5.3 Matrix calcification cannot be rescued by increasing external calcium concentration in the FoxO3a over-expressing cells

We sought to determine if matrix calcification could be rescued by increasing the external calcium concentration in the current FoxO3a over-expression model. To this end, pre-osteoblasts and 7-day differentiated MC3T3-E1 cells were incubated with media supplemented with additional $CaCl_2$ for seven days. The three differentiation concentrations of $CaCl_2$ employed included: 3 mM, 6mM and 9 mM. Calcium deposited into the matrix were stained with ARS and quantified. Untreated pre-osteoblasts exhibited faint staining as did other groups supplemented with 3 mM, 6 mM and 9 mM $CaCl_2$ (**Figure 5. 30A**) In pre-osteoblasts, 3 mM $CaCl_2$ increased calcium deposition significantly to 1.4-fold, 6 mM $CaCl_2$ increased 2-fold and 9 mM $CaCl_2$ increased 3-fold in calcium deposition (**Figure 5. 30B**). 7-day differentiated osteoblasts exhibited faint staining in the untreated group as did other groups supplemented with 3 mM, 6 mM and 9mM $CaCl_2$ (**Figure 5. 31A**). Incubation with 3 mM, 6 mM and 9 mM $CaCl_2$ did not alter levels of calcium deposition, suggesting additional medium calcium fail to rescue matrix calcification when FoxO3a was over-expressed 7-day differentiated osteoblasts (**Figure 5. 31B**).

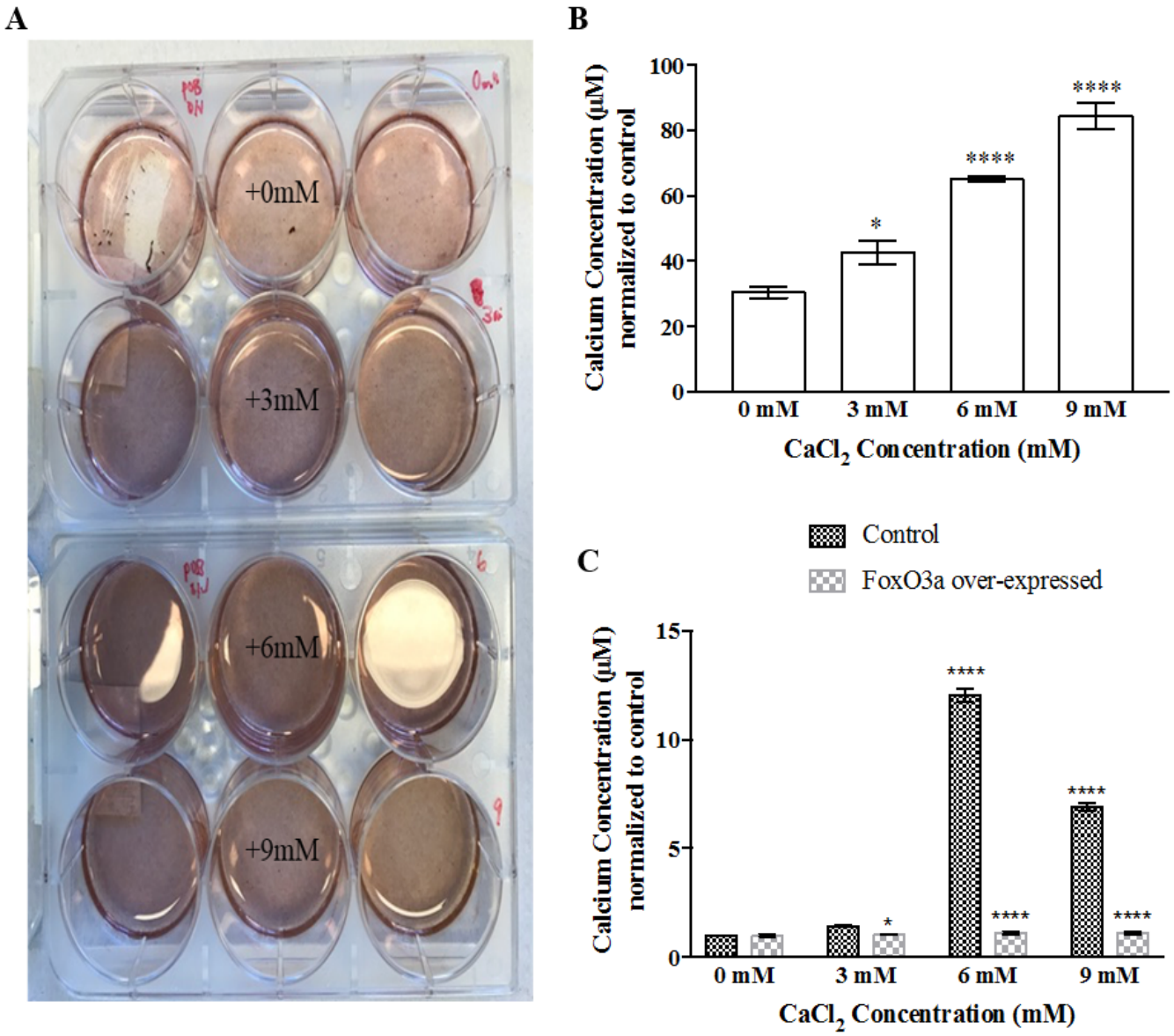

Figure 5. 30 Pre-osteoblasts incubated with additional 0 mM, 3 mM, 6 mM and 9 mM calcium chloride ($CaCl_2$) for 7 days and then calcium deposition in the matrix was assessed with ARS

(A) Pre-osteoblasts incubated with the stated extra calcium in the medium in the medium and (B). Quantification of the calcium deposition in the treated pre-osteoblast. Data are presented as means ±SEM, n=9 each *p ≤0.05, ****p ≤0.0001.

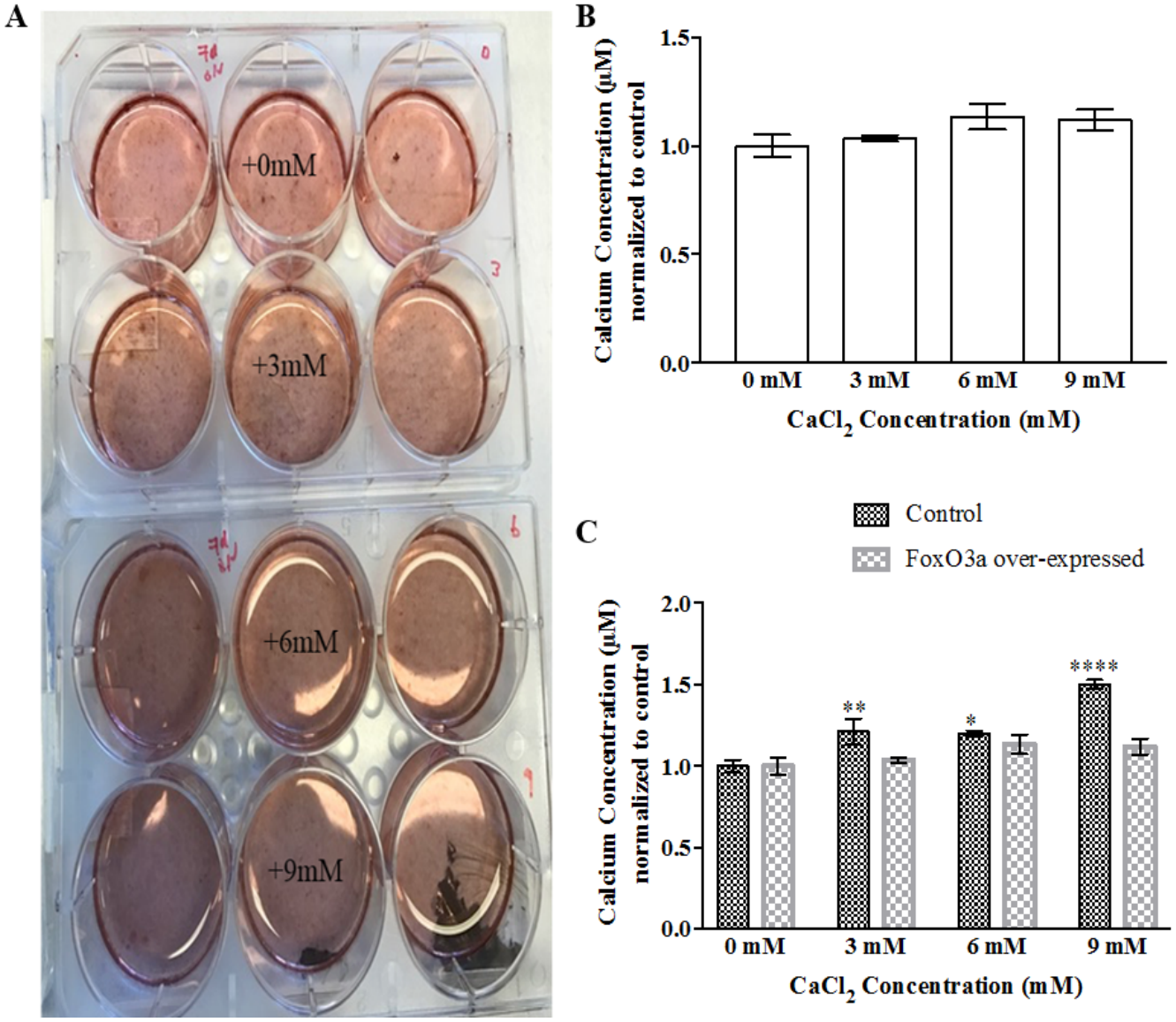

Figure 5. 31 7-day differentiated osteoblasts incubated with 0 mM, 3 mM, 6 mM and 9 mM calcium chloride ($CaCl_2$) for 7 days and calcium deposition in the matrix was assessed with ARS

(A). 7-day differentiated osteoblasts incubated with the stated amount of additional calcium in the medium and (B). Quantification of the calcium deposition in the treated osteoblasts from A. Data are presented as means ±SEM. n=9 each.

5.6 Discussion

5.6.1 FoxO3a over-expression in vitro system used to study osteoblast differentiation and matrix calcification

To study how FoxO3a influences osteoblast differentiation and matrix calcification, FoxO3a over-expression *in vitro* system was successfully generated in MC3T3-E1 cells. FoxO3a was inserted between restriction sites SgfI and MluI in pCMV6-entry vector under the control of CMV promoter with a Myc tag in the C-terminal. This construct was transfected into pre-osteoblast MC3T3-E1 cells and successfully transfected colonies were selected by incubating cells in 500 μM Geneticin.

Pre-osteoblast MC3T3-E1 cells showed a cuboidal morphology similar to non-transfected control cells. Transfected cell started to show long and elongated cell body with extensions as early as 1-day into differentiation. 3-day differentiated cells lost most of their Golgi content and extensions became longer, exhibited similar morphology as osteocytes. 7-day differentiated MC3T3-E1 cells exhibited long cell bodies and embedded in the extracellular matrix. Collagen production was reduced compared to control non-transfected 7-day differentiated cells.

FoxO3a protein levels reached the maximum levels throughout differentiation under the control of CMV promoter. Differ from non-transfected control cells where FoxO3a expression undergoes a gradual increase in expression from pre-osteoblasts to 1-day immature, 3-day differentiated osteoblasts, reaching the highest expression levels in 7-day differentiated mature osteoblasts.

Retinoid x receptor (RXRα) and vitamin D receptor, important regulator in vitamin D-signaling, also reached the maximum levels in the system. Differ from non-transfected control cells where RXRα and VDR expression gradually increase during osteoblast differentiation, RXRα and

VDR expression in these transfected overexpressors remained constant during this process. Treatment with $1,25D_3$ also did not alter RXRα and VDR protein expression levels in 7-day differentiated osteoblasts.

5.6.2 FoxO3a over-expression altered expression of Ca^{2+} mediators

L-type ($Ca_v1.2$ and $Ca_v1.3$) and T-type ($Ca_v3.1$) Ca^{2+} channels are expressed constantly during osteoblast differentiation. This result is very different compared to non-transfected control cells where $Ca_v1.2$ mRNA expression decreases gradually as cells undergo differentiation, reaching the lowest expression in 7-day differentiated mature osteoblasts. $Ca_v1.3$ mRNA expression in the non-transfected control cells maintained the same levels from pre-osteoblasts to 1-day immature osteoblasts, to 3-day differentiated osteoblasts, then declined significantly in 7-day differentiated mature osteoblasts. $Ca_v3.1$ mRNA expression in the over-expressors shows a significant reduction in 1-day differentiated immature osteoblasts and this decline is recovered to the same levels as pre-osteoblasts in 3-day and 7-day mature osteoblasts. In contrast, $Ca_v3.1$ expression levels remained uniform in pre-osteoblasts, 1-day immature and 3-day osteoblasts in the non-transfected control cells before reaching the lowest levels in 7-day differentiated mature osteoblasts. Calbindin-D_{9K} expression remained constant throughout differentiation in the over-expressors, showing Ca^{2+} ions are delivered to the other side of osteoblast steadily, similar to the non-transfected control cells.

5.6.3 High levels of FoxO3a inhibited calcium uptake

Live cell ratiometric calcium imaging showed L-type calcium channels still being the major functioning channels in the transfected 7-day differentiated mature osteoblasts. Use of felodipine inhibited calcium uptake and caused calcium efflux. In the transfected over-expressors, cells

were not sensitive to changes in extracellular $CaCl_2$ concentrations. Unlike non-transfected control cells which give a stronger signal when raising the external [Ca^{2+}] to 10 mM during calibration, changes in external [Ca^{2+}] did not alter Fura-2 AM signals in the over-expressors. Furthermore, cells with FoxO3a over-expression showed significant reduction in calcium influx and rate of calcium uptake in comparison with non-transfected control cells. Treatment with $1,25D_3$ increased calcium uptake in 7-day differentiated over-expressors. However, this $1,25D_3$-mediated increase is a-thousand times less compared to $1,25D_3$-mediated increase in non-transfected control cells and still failed to raise cytosolic [Ca^{2+}].

5.6.4 High levels of FoxO3a almost abolished calcium deposition

Calcium efflux mediator NCX mRNA expression remained constant in pre-osteoblasts, 1-day immature osteoblasts and 3-day differentiated osteoblasts before declining in 7-day differentiated mature osteoblasts. This observation is different from non-transfected control cells, where NCX expression remained constant throughout osteoblast differentiation. Another calcium efflux mediator, PMCA-1b expression in the over-expressors remained unchanged throughout differentiation. In contrast, PMCA-1b expression in the non-transfected control cells showed a gradual increase from pre-osteoblasts to 1-day immature osteoblasts, 3-day osteoblasts and reaching the highest levels in 7-day differentiated mature osteoblasts. These alterations in NCX and PMCA-1b expression showed Ca^{2+} efflux regulation is impaired.

Alizarin red staining found calcium levels in the matrix of pre-osteoblasts to be less than half in the over-expressors compared to non-transfected control cells. These transfected pre-osteoblasts also failed to incorporate calcium into the matrix during osteoblast differentiation. Pre-osteoblasts exhibited [Ca^{2+}] at approximately 80 nM in the matrix and this level remained

unchanged in 7-day differentiated mature osteoblasts. In contrast, non-transfected control cells exhibited 150 μM [Ca^{2+}] in pre-osteoblasts, and this level went up 2-fold to 300 μM in 7-day differentiated MC3T3-E1 cells.

$1,25D_3$ failed to increase matrix calcification in the 7-day differentiated mature osteoblasts

Treatment with 100 nM $1,25D_3$ raised mRNA expression of $Ca_v1.2$ significantly in the 7-day differentiated mature osteoblasts but had no effects on $Ca_v1.3$ and down-regulated $Ca_v3.1$, suggesting $Ca_v1.2$ is the primary site for $1,25D_3$-mediated increase determined by ratiometric calcium imaging. $1,25D_3$ increased expression of Calbindin-D_{9K} similar to that in the non-transfected control cells. $1,25D_3$ also increased expression of NCX, suggesting more Ca^{2+} may be exported out of the osteoblast and deposited in the matrix. Conversely, $1,25D_3$ reduced expression of PMCA-1b, suggesting [Ca^{2+}] increase by NCX may be counteracted by PMCA-1b. Therefore, $1,25D_3$ failed to stimulate matrix calcification in the transfected 7-day differentiated mature osteoblasts determined by ARS.

250 μM H_2O_2 stimulated calcium deposition in pre-osteoblasts while 100 nM $1,25D_3$ and the combination treatment with H_2O_2 did not have any effects. This observation is consistent with previous studies demonstrating low non-toxic [H_2O_2] induces cell differentiation and matrix mineralization *in vitro* (Lee et al., 2006).

5.6.5 Rescue matrix calcification in FoxO3a over-expression?

High levels of FoxO3a prevents osteoblast differentiation and matrix calcification, resulting in low cytosolic [Ca^{2+}] and almost abolished Ca^{2+} deposition in the matrix. Therefore, we wondered if this phenotype can be rescued by supplementing cells with additional $CaCl_2$ in the culture media. Pre-osteoblasts and 7-day differentiated osteoblasts were cultured with additional 3 mM, 6 mM and 9 mM for 7 days. Pre-osteoblasts demonstrated a gradual increase with increasing

concentration, reaching the highest calcium levels with 9 mM. However, 7-day differentiated MC3T3-E1 cells did not incorporate more calcium into the matrix with elevated external $CaCl_2$. Cultures incubated with additional $CaCl_2$ exhibited the same levels of $[Ca^{2+}]$ in the matrix as to control. Therefore, we concluded that reduced matrix calcification in 7-day differentiated mature osteoblasts cannot be rescued.

5.6.6 FoxO3a over-expression impaired osteoblast differentiation and eventual matrix calcification

Expression of Runx2 and OCN was used to assess levels of osteoblast differentiation and mineralization in the over-expressors that found altered Runx2 and OCN expression during osteoblast differentiation and mineralization. Runx2 expression increased significantly in 1-day differentiated cells, indicating pre-osteoblasts have differentiated to immature osteoblasts. Runx2 expression then showed a dramatically decline in 3-day differentiated osteoblasts, lower than in pre-osteoblasts, and this level remained the same in 7-day differentiated mature osteoblasts.

In contrast, non-transfected control cells showed that Runx2 expression augmented in 1-day differentiated immature osteoblasts, then declined progressively before reaching the lowest levels in 7-day differentiated mature osteoblasts.

In the over-expressors, OCN expression reached the lowest levels in 1-day immature osteoblasts, and increased significantly to the highest levels in 3-day osteoblasts and reduced back to baseline levels in mature osteoblasts. On the other hand, OCN expression gradually increased as cells underwent differentiation, reaching the highest levels in mature osteoblasts in non-transfected control cells. Analysis of these two biomarkers indicated that FoxO3a over-expressors failed at osteoblast differentiation and eventual mineralization.

In summary, FoxO3a prevents osteoblast differentiation, mineralization and matrix calcification. We provide evidence that high levels of FoxO3a altered expression of calcium mediators, decreased calcium uptake and deposition significantly. In the FoxO3a over-expressors, treatment with $1,25D_3$ increased calcium uptake but this increase is negligible in comparison to the non-transfected control cells and did not increase calcium deposition in the ECM.

Incubating FoxO3a over-expressors with additional external [$CaCl_2$] failed to rescue matrix calcification. Assessment with Runx2 and OCN, revealed that high levels of FoxO3a prevented osteoblast differentiation, mineralization and eventual matrix calcification.

CHAPTER 6: DISCUSSION

6.1 Characterization of an in vitro model in MC3T3-E1 cells to study osteoblast differentiation and matrix calcification

Current available studies primarily focus on FoxOs's ability to defend against oxidative stress in bone (Ambrogini et al., 2011; Almeida et al., 2007). Initial interest in FoxOs emerged when FoxOs were shown to extend longevity and promote stress resistance in *C.elegans* and *Drosophila* (Arden, 2008). Recent genetic studies in mice also demonstrated FoxOs are capable of reducing age-related damage, further establishing FoxOs' role in stress defense mechanism (Ambrogini et al., 2011; Almeida et al.,2007). Oxidative stress has been associated with age-related bone diseases. In a recent study, osteoporotic women exhibited a significant reduction in plasma antioxidants, suggesting decline in oxidative stress defense mechanism contributes to osteoporosis (Maggio et al., 2003). In another study, assessment of 8-iso-$PGF_{2\alpha}$, a biomarker for ROS, showed a negative correlation between BMD and the biomarkers, indicating high levels of oxidative stress are associated with a decline in BMD (Basu et al., 2001). Animal studies demonstrated high levels of oxidative stress leads to premature skeletal aging in mice and caused reduction in bone mass, bone formation rate, osteoblast number while increasing osteoblast apoptosis, thus leading to osteoporitic fractures in aging mice (Almeida, 2007; Ambrogini et al., 2010; Arai et al., 2007). Osteoblast differentiation was inhibited by increasing levels of oxidative stress in various bone cells including pre-osteoblasts MC3T3-E1 cells (Arai et al., 2007), marrow stromal cells M2-10B4 (Mody et al., 2001), rabbit osteoblastic calvaria cells and bone marrow stromal cells (BMSC) (Bai et al., 2004). All these combined evidence suggest high levels of ROS contribute to age-related osteoporosis.

Ambrogini and colleagues demonstrated FoxOs are capable of defending against oxidative stress by up-regulating anti-oxidant enzymes including superoxide dismutase (SOD), glutathione

peroxidase (GSH-Px) and lipid peroxidation end-product malondialdehyde (MDA) to counteract these high levels of ROS (Ambrogini et al., 2010). Transgenic mice generated with deletion of FoxO3a in differentiated osteoblasts led to significant loss in bone mass and osteoblast number. Similarly, mice with FoxO3a over-expression exhibited significant increase in bone mass, bone formation rate and osteoblast number. In addition, these animals also showed a decrease in ROS assayed by phosphorylation of $p66^{shc}$ and osteoblast apoptosis. These authors also found loss of FoxOs led to an increase in osteoblasts apoptosis, a decrease in osteoblast number and bone formation rate and bone mass (Ambrogini et al., 2010).

However, conflicting observation was reported suggesting FoxOs attenuate bone formation independent of oxidative stress by altering Wnt signaling pathways. Mice with FoxO3a deletion in progenitor cells of osteoblasts and adipocytes exhibited increase in bone mass and osteoblast number (Iyer et al., 2013). Thus far, exact function of FoxOs, particularly FoxO3a, on bone formation remains unclear.

Based on these above *in vivo* studies, we then queried whether FoxO3a participates in osteoblast differentiation and matrix calcification independent of ROS. We hypothesized that FoxO3a plays a fundamental role in regulating osteoblast differentiation and matrix calcification.

We tested our hypothesis by carefully setting up specific objectives and designing experiments to answer these research questions. Our first specific objective was to find a suitable *in vitro* model to study osteoblast differentiation and mineralization discussed in **Chapter 3**. Although *in vivo* models in small and large animals may be the closest representation of bone remodeling to humans and these *in vivo* models may provide less variation than *in vitro* models, it is difficult to study osteoblast activity and functions *in vivo* due to cost, availability reproducibility and manageability, especially in large animals (Suda et al., 2012; Turner, 2011). i*n vitro* cell model

provide the advantage to focus on only osteoblast cells rather than heterogeneity mixed cell population including osteoclasts, osteoblasts and osteocytes. Also, in vitro culture models represent a distinct stage of development including morphology, phenotype and biosynthetic activity (Kartsogiannis and Ng, 2004). Various cultured cell lines have been used to study osteoblast differentiation, gene expression and hormonal responses (Kartsogiannis and Ng, 2004). These cell cultures provide many advantages including basic culture environments and maintenance, relative homogeneity, reproducibility, and retain key aspects of osteoblastic behaviours of particular stage of differentiation (Karin and Farach-Carson, 2004). *In vitro* cell lines are derived from species such as mouse, rat and human. Rat cell lines ROS 17/2.8 (Rodan et al., 1983) and UMR 106-01 (Partridge et al., 1983; 1987) are both derived from osteosarcomas that undergo transformation frequently and may have altered gene expression (Karin and Farach-Carson, 2004). Human cell lines, MG-63 (Billiau et al., 1977) and Saos-2 (Rodan et al., 1987; Fogh et al., 1977) are also derived from osteosarcoma cells. Mouse cell line such as KS-4, MMC2 and MC3T3-E1 cells are pre-osteoblast cells derived from calvaria (Yamashita et al., 1990; Nakayama et al., 1997; Franceschi et al., 1994; Sudo et al., 1983). MBA-15 and 2T3 are pre-osteoblast cells derived from bone marrow and calvaria from SV40 transgenic mice, respectively (Karin and Farach-Carson, 2004). We wanted a model system that fit the following requirement: retains key features of osteoblast phenotype, can be differentiated and mineralized *in vitro*, and can be easily manipulated. Murine pre-osteoblast MC3T3-E1 subclone 4 cells have been reported to exhibit similar characteristics as woven bone *in vivo* by express genes specific to a particular differentiation stage, including Runx2, osteocalcin, type I collagen, osteonectin and osteopontin (Sudo et al., 1983; Quarles et al., 1992). MC3T3-E1 cells have also been

reported to differentiate and form a mineralized matrix *in vitro* by adding ascorbic acid and β-glycerophosphate (Quarles et al., 1992; Wang et al., 1999).

Stage-specific gene expression was assessed by real-time qPCR in the current *in vitro* model. Runx2 mRNA expression was first detected in pre-osteoblasts and significantly up-regulated and reached the highest expression levels in 1-day differentiated MC3T3-E1 cells, indicating cells at this stage are immature osteoblasts. Runx2 mRNA expression decreased in 3-day differentiated osteoblasts and reached the lowest expression levels in 7-day differentiated MC3T3-E1 cells, indicating cells at this stage are mature osteoblasts. Our observation confirms Runx2 initiates the direction of immature bone formation in cells 1-day post differentiation, and triggers expression of major bone matrix genes (Komori, 2010). Down-regulation of Runx2 in differentiated osteoblasts suggests inhibition of osteoblast maturation and bone formation (Komori, 2006). OCN mRNA expression was used to assess late stage differentiation. Minimal levels of OCN were detected in per-osteoblasts and 1-day differentiated immature osteoblasts. Significant up-regulation of OCN was detected in 3-day differentiated osteoblasts, indicating osteoblast maturation occurs at this stage. OCN mRNA expression reached the highest levels in 7-day differentiated mature osteoblasts. Alkaline phosphatase is an another important pre-osteoblastic marker for differentiation and bone-specific ALP is used clinically to assess bone formation. In the current model of MC3T3-E1 subclone 4, this cell line has been reported to not express ALP mRNA expression (Wang et al., 1999). Wang and colleagues isolated 10 subclones, and their ability to mineralize *in vitro* was assessed. Subclone 4 was found to exhibit the highest mineralizing potential in comparison with other subclones despite the lack of ALP expression. Wang and colleagues also measured ability of subclone 4 to form bone in vivo by designing a Collagraft sponge with subclone 4 and implanted in immune-deficient mice. Animals retained

the implant for 6 weeks and area of the implant was examined with histologic staining. Subclone was reported to have the highest in vivo bone formation ability. These data suggested ALP expression may not be essential for ECM formation, and subclone 4 provides a suitable model for studying osteoblast differentiation and mineralization (Wang et al., 1999).

Cell morphology was examined for validating osteoblast differentiation. Pre-osteoblast cells looked fusiform with a large Golgi content and produced minimal levels of collagen. Morphology of 1-day differentiated MC3T3-E1 cells did not differ much from pre-osteoblasts and production of collagen was at basal levels, but they started to exhibit slimmer and longer cell body with extensions 3 days into differentiation, suggesting these cells are osteoblasts at this stage. 7-day differentiated MC3T3-E1 cells exhibited morphology similar to osteocytes, skinny cell body and long extensions. Some cells become embedded in the matrix, showing overlapping cells in the matrix. A white thick collageoues extracellular matrix layer was observed in 7-day differentiated MC3T3-E1 cells. Combined evidence of morphology observations with Runx2 and OCN expression demonstrate MC3T3-E1 cell line can be differentiated and mineralized *in vitro* with ascorbic acid and β-glycerophosphate, thus serves a suitable model to study osteoblast differentiation and bone matrix formation.

6.2 Calcium transport machinery in MC3T3-E1 cells

In **Chapter 3**, we identified expression important calcium channels, transporters and mediators in the transport system in the current model, including influx and efflux. We then measured channel activity regulating Ca^{2+} influx by live cell ratiometric calcium imaging with Fura-2 AM in **Chapter 4**. Finally, calcium deposition via Ca^{2+}-ATPase pump and Na^{+}/ Ca^{2+} exchanger into the ECM was measured with a staining method ARS during matrix calcification.

6.2.1. Identify expression of calcium channels, mediators and transporters

Real-time qPCR identified plasma membrane channels including L-type ($Ca_v1.2$ and $Ca_v1.3$) and T-type ($Ca_v3.1$) Ca^{2+} channels involved in calcium influx. $Ca_v1.2$ expression underwent a gradual decrease from pre-osteoblasts to the lowest levels in 7-day differentiated osteoblasts. Recent works showed $Ca_v1.2$ to be the major isoform with highest expression levels compared to other Ca_v channels, such as $Ca_v1.1$ and $Ca_v1.3$ (Bergh et al., 2003; Caffrey and Farach-Carson, 1989; Meszaros et al., 1996). Shao and colleagues performed immunostaining in MC3T3-E1 cells, and detected intense $Ca_v1.2$ expression in pre-osteoblasts but the signal dramatically reduces by 75% as cells undergo differentiation to almost non-existence in fully differentiated MC3T3-E1 cells (Shao et al., 2005). These authors also found absence of $Ca_v1.2$ in osteocytes by performing immunostaining in MLO-Y4 cells. These combined observations indicate $Ca_v1.2$ exhibits the strongest expression levels in pre-osteoblasts, which decreases gradually during differentiation, to almost non-detectable in osteocytes, consistent with our finding (Shao et al., 2005; Kato et al., 1997). However, functional studies showed $Ca_v1.2$ to be the primary site for Ca^{2+} influx in osteoblasts (Bergh et al., 2006; Caffrey and Farach-Carson, 1989; Liu et al., 2000). These observations suggest low amount of $Ca_v1.2$ still contribute greatly to calcium influx in

osteoblasts, therefore, we measured of L-type ($Ca_v1.2$) Ca^{2+} channel activity in **Chapter 4** which would be discussed in the next section.

Another L-type Ca^{2+} channel, $Ca_v1.3$ mRNA expression was detected in pre-osteoblasts and remained constant in 1-day immature osteoblasts and 3-day differentiated osteoblast cells before reaching a significant reduction in 7-day differentiated MC3T3-E1 cells. Other reports investigating Ca^{2+} transport did not find $Ca_v1.3$ to regulate majority of Ca^{2+} influx (Bergh et al., 2006). Mice with $Ca_v1.3$ deletion did not cause significant alterations in bone metabolism with only slight decline in bone mass in male mice (Li et al., 2010). Under the absence of $Ca_v1.3$, these mice demonstrated an increase in $Ca_v1.2$ expression suggested to compensate for bone homeostasis (Li et al, 2010). These combined observations suggested $Ca_v1.3$ is not the major isoform of L-type Ca^{2+} channel.

In contrast, the lower activated T-type Ca^{2+} channel, $Ca_v3.1$ mRNA expression increased gradually during differentiation and reached the highest levels in 7-day differentiated osteoblasts. To determine whether T-type Ca^{2+}channel is a major functioning channel in 7-day differentiated osteoblasts, we measured T-type Ca^{2+}channel activity in **Chapter 4** and is discussed in the next section.

Calbindin-D_{9K}, calcium-binding protein responsible for translocating Ca^{2+} ions in the cytosol across the cell to the basolateral side to be deposited into the bone, underwent a reduction during differentiation and reached the lowest levels in 7-day differentiated osteoblasts. This observation suggests Calbindin-D_{9K} may be transporting only partial of Ca^{2+}, and there may be another transporter involved. However, Calbindin-D_{28K} mRNA expression was not detectable in the current model, suggesting presence of other calcium-binding proteins such as calmodulin.

Calmodulin has been reported to be involved in osteoblast proliferation and differentiation in MC3T3-E1 cells (Zayzafoon et al., 2004).

Calcium-sensing receptor (CaSR) and TRPV channels (TRPV 5 and TRPV 6) had been reported to be present in MC3T3-E1 cells and play important roles in regulating calcium influx (Lieben and Carmeliet, 2009; Marie, 2010; Yamaguchi et al., 1998; 2005). However, we were not able to detect calcium-sensing receptor (CaSR) or TRPV 5/TRPV 6 in the current model. Quarles and colleagues reported by treating MC3T3-E1 cells with a CaSR agonist, cells were able to generate a G protein-dependent activation and DNA synthesis was increased, suggesting behaviour of CaSR (Quarles et al., 1997). Yamaguchi and colleagues also suggested involvement of CaSR in osteoblast differentiation as MC3T3-E1 cells treated with NPS-R467, a specific CaSR activator, resulted in significantly enhanced mineralization (Yamaguchi et al., 2005). Similar to our observation, Quarles and colleagues were not able to detect CaSR in qPCR (Quarles et al., 1997). Yamaguchi and colleagues identified kidney-specific CaSR for identification in osteoblasts (Yamaguchi et al., 1998). Presence of TRPV 5 and TRPV 6 have been reported in *in vivo* osteoblastic cells, but so far no available evidence shows their presence in MC3T3-E1 cells (Lieben and Carmeliet, 2012).

6.2.2 Ca^{2+} influx channel activity in 7-day differentiated osteoblasts

Chapter 4 discussed the identification of Ca^{2+} channels that are actively allowing Ca^{2+} entry into 7-day differentiated osteoblasts using ratiometric calcium imaging with Fura-2 AM. Specific channel antagonists were applied and each channel activity was determined. Non-specific channel blocker, 100 μM $LaCl_3$ caused significant reduction in calcium uptake, it decreased both

the magnitude (Δ peak), and the rate (Δ slope) of calcium uptake, indicating regulation of Ca^{2+} influx by VSCCs.

Report by Bergh and colleagues demonstrating $Ca_v1.2$ being the primary site for Ca^{2+} influx (Bergh et al., 2006). We tested this hypothesis by the application of 10 μM felodipine, a L-type Ca^{2+} channel antagonist to 7-day differentiated osteoblasts. Felodipine completely abolished calcium uptake into the cells and even caused significant calcium efflux. This evidence shows L-type VSCC is the major functioning channel and regulates the majority of Ca^{2+} into the cells. This observation is consistent with study demonstrating chronic treatment of nifedipine, another L-type Ca^{2+} channel antagonist, caused significant reduction in cancellous and cortical bone formation, mineral apposition, and epiphyseal growth plate activity in rabbits (Duriez et al., 1993). Treatment with verapamil and diltiazem, other classes of L-type Ca^{2+} inhibitors showed direct inhibition on osteoblastic function in MC3T3-E1 cells by decreasing collagen production significantly (Kim et al., 1991). Ion flux experiment with $^{45}Ca^{2+}$ further confirmed L-type channel being the primary channel for calcium influx into osteosarcoma cells (Caffrey and Farach-Carson, 1989).

We were unable to distinguish $Ca_v1.2$ from $Ca_v1.3$, both isoforms of L-type calcium channels by Fura-2 AM imaging because there are no selective channel antagonists targeting $Ca_v1.2$ or $Ca_v1.3$ specifically. One approach to confirm the predominant isoform would be to knock-down $Ca_v1.2$ in MC3T3-E1 cells. If $Ca_v1.2$ regulated Ca^{2+} influx largely, ablation of $Ca_v1.2$ would cause significant reduction in Ca^{2+} influx in MC3T3-E1 cells. This observation had been reported previously in osteosarcoma cells (Hofmann et al., 2014).

T-type Ca^{2+} channel activity was investigated by inhibiting calcium uptake with 10 μM NNC 55-0396 dihydrochloride, a $Ca_v3.1$ selective VSCC antagonist. NNC did not cause significant reduction, suggesting $Ca_v3.1$ calcium channel is not the major contributor to bone formation in 7-day differentiated osteoblasts, consistent with studies by others (Bergh et al., 2006; Zhao et al., 2010). Our qPCR analysis showed a switch in expression from L-type to T-type calcium channels during osteoblast differentiation in **Chapter 3**. $Ca_v1.2$ mRNA expression showed a gradual increase as differentiation was initiated, and the lowest levels of expression was reached in 7-day differentiated osteoblasts. $Ca_v1.3$ mRNA expression also declined significantly in 7-day differentiated osteoblasts. Whereas $Ca_v3.1$ mRNA expression showed a gradual increase during differentiation, and reached the highest levels in 7-day differentiated osteoblasts. Channel activities determined with felodipine and NNC 55-0396 confirmed L-type, including $Ca_v1.2$ and $Ca_v1.3$, are the major functioning channel in 7-day differentiated osteoblasts, regulating majority of calcium uptake into the cells despite significant reduction in mRNA levels.

Our results are consistent with other reports showing immunoblotting detecting both L-type and T-type Ca^{2+} channels in osteoblasts and osteocytes *in vivo*, with highest expression of $Ca_v1.2$ in regions of rapid growth of long bone and $Ca_v3.2$ in osteocytes embedded in mineralized matrix (Shao et al., 2005). This observation supports L-type Ca^{2+} channel is actively involved in Ca^{2+} uptake. Further immunoblotting detected both L-and T-type Ca^{2+} channels in MC3T3-E1 cells, but very low levels of expression was detected in L-type were detected in MLO-Y4 osteocyte cells in comparison to high expression levels of T-type detected (Shao et al., 2005).

Localization studies with dual antibodies demonstrated the predominant channel switches from L-type $Ca_v1.2$ to T-type $Ca_v3.2$ when osteoblasts differentiate to osteocytes. This switch would lead to less calcium permeability in the osteocytes due to transient nature of T-type channels

(Shao et al., 2005). Deletion of a T-type Ca^{2+} channel $Ca_v3.2$ resulted in significant reduction in bone mineral density (BMD) and bone mineral content (BMC) in animals (Srinivasan et al., 2015).

mRNA expression and channel activity of TRPV5 or TRPV6 were absent in the current model. Human and murine bone samples showed TRPV5 to be one of the most selective TRP channels in osteoclast and localized in ruffled border membrane but absent in osteoblasts, agreeable with our observation (van der Eerden et al., 2005). TRPV6 expression was found in human and mouse osteoblasts on the apical side and in human osteoclasts on the osteoid-facing side (van der Eerden et al., 2012). TRPV6 exhibited the highest expression in mineralizing human osteoblasts, but over-expression of TRPV6 did not affect mineralization and transgenic mice with a mutation in TRPV6 gene did not cause functional change to the degree of bone mineralization. Therefore, although TRPV6 is dynamically expressed in the bone, it is not essential for bone mineralization (van der Eerden et al., 2012).

6.2.3 Calcium efflux regulation during osteoblast differentiation in the current model

Ca^{2+} translocated from the apical side via L-and T-type Ca^{2+} channels to the osteoid-facing side of osteoblasts would then be deposited in the matrix via NCX and PMCA-1b. Real-time qPCR analysis showed uniform NCX1 mRNA expression throughout osteoblast differentiation, suggesting constant Ca^{2+} efflux during osteoblastogenesis. Several lines of studies showed that NCX3 to be the predominate isoform in osteoblasts (Stains et al., 2002; Sosnoski and Gay, 2008). This may explain the stable expression of NCX1 and we may need to assess expression of NCX3 during osteoblastogenesis in this current model. We applied 10 μM benzamil hydrochloride, an antagonist for NCX in 7-day differentiated mature osteoblasts to study NCX

activity. We reasonably expected an increase in cytosolic [Ca^{2+}] when NCX activity were to be inhibited since calcium ions would not able to leave the cells. Contrary to our expectation, benzamil hydrochloride did not cause increase in cytosolic calcium concentration, but it led to significant calcium efflux in the osteoblasts. This is because benzamil hydrochloride is an analog of amiloride, which also inhibited L-type Ca^{2+} channel activity (Garcia et al., 1990). Benzamil structurally resembles phenylalkyalmines such as verapamil by two aromatic rings connected by a flexible chain with a nitrile substitute (Cheng et al., 2009; Hockerman et al., 1997). Other NCX specific blockers such as bepridil and KB-R7943 an isothiourea derivative (2-[2-[4-94-nitrobenzyloxy]phenyl]ethyl)isothiourea) have also been shown to pose inhibitory effects on L-type calcium channels, causing a reduction in mineralization (Blair et al., 2010; Stains and Gay, 2001; Birinyi et al., 2005; Hockerman et al., 1997). Other approach such as knockdown of NCX1 using siRNA in MC3T3-E1 cells showed no alteration in the calcifying matrix, but knockdown of NCX3 demonstrated significant reduction in Ca^{2+} efflux (Sosnoski and Gay, 2008). PMCA-1b, an ATP-dependent pump, mRNA expression is detected at low levels in pre-osteoblasts, gradually increases in immature osteoblasts and osteoblasts, reaching the highest levels in mature osteoblasts. We were unable to measure PMCA-1b activity using radiometric calcium imaging technique because we were unable to find PMCA-specific antagonist at the present time to test its activity. Another approach we could take is to knock-down PMCA in the current model to measure [Ca^{2+}] in the matrix by ARS. This has been done *in vivo* where PMCA knockout mice showed a decrease in bone mass measured by von Kossa staining and micro-CT scanning (Kim et al., 2012).

6.4 FoxO3a participates in osteoblast differentiation and mineralization

Our next specific aim was to examine participation and determine the role of FoxO3a in this current *in vitro* model system during osteogenesis. We focused on FoxO3a instead of other FoxO isoforms because of its predominance with an almost 2-fold increase in calvaria and vertebrae in wild type mice compared to FoxO 1 and FoxO 4 (Ambrogini et al., 2011). In our current culture, FoxO3a mRNA and protein expression could be induced significantly as cells underwent differentiation, and reached the highest levels in 7-day differentiated osteoblasts. In their transgenic animals with FoxO3a deletion exhibited reduced expression of Runx2, suggesting FoxO3a plays a regulatory role in osteoblastogenesis (Ambrogini et al., 2011).

FoxO3a expression via immunofluorescence with fluorescent microscopy showed approximately 70% of FoxO3a expressed in the nucleus, leaving 30% expressed in the cytoplasm in the 1-day differentiated immature osteoblasts. This percentage went up dramatically showing approximately 90% of FoxO3a is expressed in the nucleus, with 10% expressed in the cytoplasm in 3-day differentiated osteoblasts. This nuclear FoxO3a expression increased further to approximately 95% of FoxO3a in the nucleus, leaving only 5% expressed in the cytoplasm in 7-day differentiated mature osteoblasts. All the above data suggest FoxO3a is involved in the regulation of osteoblast differentiation and mineralization in the current *in vitro* model, consistent with observations made by Ambrogini and colleagues.

6.5 Effects of vitamin D on bone

Contribution of vitamin D on bone mineralization and formation is under active investigation. Up-to-date literature suggest the effects of $1,25D_3$ on bone formation are primarily due to indirect regulation on increasing intestinal Ca^{2+} absorption and renal Ca^{2+} re-absorption and only

partially is due to direct action on osteoblasts (van de Peppel and Leeuwen, 2014). In the current thesis, we investigated the direct effects of $1,25D_3$ on osteoblast differentiation and mineralization by analyzing expression of Runx2, a master regulator in osteoblast differentiation and OCN, matrix proteins in mineralization. Second, we measured $1,25D_3$-mediated effects on expression of Ca^{2+} transport machinery. Thirdly, we measured channel uptake activity and eventual deposition were determined in **Chapter 4**.

6.5.1 Vitamin D signaling in osteoblast differentiation and mineralization

Real-time qPCR and immunoblotting confirmed vitamin D signaling participation. Both RXRα and VDR participate in osteoblast differentiation, reaching the highest levels of expression in 7-day differentiated osteoblasts.

In our current *in vitro* model $1,25D_3$- negatively regulated mRNA expression of Runx2 in 7-day differentiated osteoblasts, an important regulator in triggering major bone matrix genes during early stage of osteoblast differentiation, but does not play a critical role in differentiated osteoblasts suggesting Runx2 does not impact osteoblast mineralization directly (Komori, 2010; Takarada et al., 2013). Conflicting results have been reported where $1,25D_3$ enhanced Runx2 expression in human osteoblasts but reduced its expression in murine and rat osteoblastic cells (Viereck et al., 2002; van Driel and van Leeuwen, 2014). Runx2 has been found to stimulate osteopontin expression, an ECM protein that expresses highest levels in mineralized bone-tissue (Stein et al, 1996). We did not assess expression of osteopontin in the current model because it was found to inhibit osteogenesis in MC3T3-E1 cells despite opposite findings in *in vivo* models (Huang et al., 2004). Therefore, we assessed another ECM protein, OCN, for the $1,25D_3$-mediated effects in 7-day differentiated osteoblasts. OCN mRNA expression is also negatively

regulated by $1,25D_3$. Additional experiment would be needed to determine the effects of $1,25D_3$-mediated inhibition on osteoblast mineralization in the current model. Varying observations on $1,25D_3$-mediated OCN expression have been reported (van Driel and van Leeuwen, 2014; Zhang et al., 1997). In human osteoblasts, $1,25D_3$ has been shown to enhance bone matrix proteins including collagen, osteocalcin, osteopontin and Gla matrix proteins. $1,25D_3$ also has been reported to up-regulate alkaline phosphatase activity and ALP-positive matrix vesicles (van Driel and van Leeuwen, 2014; Woeckel et al., 2012). All these contribute to enhanced osteoblast differentiation and mineralization. In contrast, in murine models, $1,25D_3$ has been reported to inhibit osteoblast differentiation by reducing Runx2 and osteocalcin expression, consistent with our observation (van Driel and van Leeuwen, 2014). Detailed explanation for this species-specific discrepancy is lacking (van Driel and van Leeuwen, 2014). Many factors have been suggested, such as extracellular environment such as phosphate concentration and presence of growth factors and cytokines have been suggested. Another factor may be cell origin, mode of osteogenesis and function, for instance, cells from calvaria origin such as MC3T3-E1 cells formed by intramembranous bone formation in comparison with long bones formed by endochondral formation (van Driel and van Leeuwen, 2014).

6.3 Matrix calcification in the current model

Amount of Ca^{2+} deposited in the matrix was measured with ARS. Pre-osteoblasts exhibited calcium levels of approximately 150 μM and cells stained a faint pink colour. Calcium levels increased 2-fold to approximately 300 μM calcium levels as pre-osteoblasts differentiated to 7-day osteoblasts and cells exhibited a dark red colour. These observations suggest MC3T3-E1 cells' ability to calcify mineralizing matrix *in vitro*. By increasing external $[Ca^{2+}]$, both pre-

osteoblasts and 7-day differentiated osteoblasts exhibited a dose-dependent increase in Ca^{2+} deposition in the matrix. Our model system showed osteoblast mineralization mechanism at the molecular level where entry of Ca^{2+} via mostly L-type and partly of T-type channels. [Ca^{2+}] was then translocated partially via Calbindin-D_{9K} to the membrane domain facing the osteoid and to be deposited through NCX exchanger and PMCA-1b pump. By increasing external [Ca^{2+}], pre-osteoblasts and osteoblasts demonstrated a physiological significance of Ca^{2+} deposition mechanism. Additional experiments would be needed to further investigate the distribution of nucleation of collagen fibrils or formation of matrix vesicles (MVs). One approach we can take is to isolate MVs and evaluate calcium content inside and transmission electron microscopy (TEM) to visualized osteoblasts in the process of secreting collagen during matrix formation. Cytochemical calcium detection methods such as energy-dispersive X-ray spectroscopy can also provide elemental mapping at the molecular levels, to distinguish between calcium and phosphate distribution (Hasegawa et al., 2017).

Another limitation of our current approach with ARS is that this staining method measures the total calcium levels including [Ca^{2+}] in the cells and in the ECM with the assumption that majority of [Ca^{2+}] reside within ECM. Combined the use of TEM and elemental mapping technique, we can focus only on [Ca^{2+}] in the ECM. Another approach we can take is measure $^{45}Ca^{2+}$ in the matrix, however, our problem would be to isolate external Ca^{2+} and Ca^{2+} in the matrix.

6.5.2 Vitamin D negatively regulated ECM calcification

Calcium deposition in making of hydroxyapatite [$Ca_{10}(PO4)_6(OH)_2$] is a vitamin D-dependent process. Therefore, we were interested in investigating $1,25D_3$-stimulated calcium deposition in

differentiated osteoblasts. This objective was broken down into specific objectives, first we analyzed $1,25D_3$-medaited effects on Ca^{2+} uptake via L-and T-type Ca^{2+} channels, then Ca^{2+} transport via Calbindin-D_{9K}. Finally, $1,25D_3$-mediated effects on Ca^{2+} extrusion into mineralizing osteoid via NCX or PMCA-1b.

Real-time qPCR analysis revealed that $1,25D_3$ did not alter expression of both L-type ($Ca_v1.2$ and $Ca_v1.3$) and T-type ($Ca_v3.1$) Ca^{2+} channels in 7-day differentiated MC3T3-E1 cells. However, $1,25D_3$ significantly increased Ca^{2+} uptake into differentiated osteoblasts measured with Fura-2 AM. By blocking with felodipine, it was demonstrated this $1,25D_3$-mediated Ca^{2+} influx was through L-type Ca^{2+} channel. This result is consistent with observations made by other researchers, showing $1,25D_3$ shifted the threshold for activation of in- ward calcium current to more negative potentials, thus allowing more Ca^{2+} entry (Caffrey and Farach-Carson, 1989). Uchida and colleagues reported that $1,25D_3$ induced transient increase in $[Ca^{2+}]_i$ in pre-osteoblast MC3T3-E1 cells after 40 seconds of treatment (Uchida et al., 2010).

Calbindin-D_{9K} mRNA expression is significantly enhanced upon treatment with $1,25D_3$, falls in line with translocating $1,25D_3$-mediated increased Ca^{2+} uptake to the basolateral side to be extruded, confirming its role in mineralization (Balmain, 1991). We further assessed effects of $1,25D_3$ on Ca^{2+} deposition into the mineralizing osteoid. $1,25D_3$ enhanced expression NCX mRNA expression but not PMCA-1b in 7-day differentiated mature osteoblasts, suggesting NCX may play a more important role in bone mineralization. Further experiments would be needed to measure contribution significance of NCX and PMCA-1b, respectively. Since benzamil hydrochloride failed to inhibit NCX activity and we could not find an specific antagonist for PMCA, one approach would be to delete NCX or PMCA in MC3T3-E1 cells and determine $[Ca^{2+}]$ deposition. Primary osteoblastic cells demonstrated PMCA proteins to be localized on the

plasma membrane and NCX proteins to reside on the opposite side suggested NCX is involved in Ca^{2+} efflux directly while PMCA contributes to a lesser extent (Stains et al., 2002).

6.5.3 High dose 1,25D$_3$ reduces calcium deposition in 7-day differentiated osteoblasts

Measurement of Ca^{2+} levels in the matrix by ARS revealed 100 nM of 1,25D$_3$ reduced Ca^{2+} deposition significantly in differentiated osteoblasts despite Ca^{2+} uptake was raised. Vitamin D has been suggested to play dual roles in ECM calcification. High concentrations of 1,25D$_3$ has been shown to inhibit osteoblast function and induce osteoclast activity *in vivo*, inducing bone resorption (Anderson et al., 2006; Sanders et al., 2010; Takahashi et al., 2014). High doses of 1,25D$_3$ suppressed osteoblast mineralization was reported in MC3T3-E1 cells, as a result of inhibition on Smad signaling pathway, an important pathway for osteoblasts (Yamaguchi and Weitzmann, 2012). Bergh and colleagues reported high concentration of 100 nM 1,25D$_3$ has an inhibitory effect on calcium regulation in pre-osteoblasts. Specifically, $Ca_v1.2$, major isoform in L-type Ca^{2+} channel and T-type $Ca_v3.1$ while not affecting $Ca_v1.3$ and $Ca_v1.1$ of L-type Ca^{2+} channel (Bergh et al., 2006). We also treated these 7-day differentiated osteoblasts with a lower dose of 10^{-5}M 1,25D$_3$ and significant increase in Ca^{2+} deposition was observed.

6.6 Effect of oxidative stress on osteoblast differentiation and mineralization

FoxOs have been reported to play an important role in defending against oxidative stress in bone (Ambrogini et al., 2011). We first needed to choose an appropriate [H_2O_2] that generated high levels of ROS without cells going into apoptosis. Study by Fatokun found H_2O_2 to reduce cell viability in a dose- and time-dependent manner, and [H_2O_2] of 200 μM or more substantially for an hour reduced cell viability in differentiated MC3T3-E1 cells (Fatokun et al., 2006).

Based on their finding, we used 200 μM H_2O_2 as the middle concentration, and chose two lower concentrations of 100 μM and 150 μM and two higher concentrations of 250 μM and 300 μM. 7-day differentiated MC3T3-E1 cells were treated with these five concentrations of H_2O_2 plus one untreated control for an hour and levels of ROS formation were measured. Intracellular ROS levels were determined by 2',7'-dichlorodihydrofluorescein diacetate (DCFDA). DCFDA is a popular probe for biological assays due to stability, permeability, low background, homogeneous distribution inside the cell and low cytotoxicity (Chen et al., 2010). The non-fluorescent lipophilic $DCFH_2$-DA is able to diffuse through the membrane. Once inside the cell, intracellular esterases deacetyles $DCFH_2$-DA to form $DCFH_2$, making it unable to diffuse across the membrane but retain in the cytoplasm. $DCFH_2$ reacts with ROS, excites at wavelength of approximately 492-495 nm and emits at wavelength of approximately 517-527 nm, resulting in intense fluorescent compound (Chen et al, 2010). In our *in vitro* model, 250 μM was found to cause significant ROS formation without cell apoptosis. Thus, 250 μM H_2O_2 was used throughout experiments.

This dose of H_2O_2 caused significant reduction in early-stage differentiation marker, Runx2 expression, implicating H_2O_2-induced oxidative stress negatively affects osteoblast differentiation. Another biomarker, OCN expression was assessed to elucidate the effect of oxidative stress on osteoblast mineralization. Treatment of 250 μM H_2O_2 did not alter OCN expression in 7-day differentiated osteoblasts, but combination treatment with $1,25D_3$ reduced OCN expression significantly.

H_2O_2-induced ROS also did not alter mRNA and protein expression of FoxO3a in mature osteoblasts, suggesting effect of FoxO3a is independent of ROS. ROS did not affect vitamin D

signaling players, RXRα and VDR expression as well. $1,25D_3$-mediated increase in RXRα and VDR expression was attenuated by combination treatment with $1,25D_3$.

ROS did not alter gene expression of calcium mediators, suggesting they are independent of ROS. Combination treatment with $1,25D_3$ decreased mRNA expression levels of L-type ($Ca_v1.2$ and $Ca_v1.3$) and T-type ($Ca_v3.1$) calcium channels and efflux NCX and PMCA-1b.

Effect of ROS on calcium deposition was measured in both pre-osteoblasts 7-day differentiated mature osteoblasts. Calcium levels in ECM were not altered in pre-osteoblasts by H_2O_2, but H_2O_2 elicited an increase in 7-day differentiated mature osteoblasts.

6.7 FoxO3a over-expression prevents osteoblast differentiation and matrix calcification

We sought to determine effects of FoxO3a on osteoblast differentiation and calcium handling during matrix calcification by generating an *in vitro* system to drive FoxO3a over-expression under the control of CMV promoter.

In order to find the optimal transfection conditions, pre-osteoblast MC3T3-E1 cells were transfected with a green fluorescent protein (GFP) expression vector. Cells were allowed to grow to confluency and excited with UV light to give off to give a bright green fluorescent light and the culture with the highest transfection ratio was selected. Immunofluorescence also detected high levels of FoxO3a in the transfected MC3T3-E1 cells.

Stable transfection of FoxO3a was generated and FoxO3a expression remain high throughout osteoblast differentiation and differentiation stage did not further alter its expression. Similarly, RXRα and VDR expression also remained high throughout osteoblast differentiation. qPCR analysis also revealed important calcium transporters such as L-type ($Ca_v1.2$ and $Ca_v1.3$), T-type

($Ca_v3.1$), and mediators, Calbindin-D_{9K}, NCX and PMCA-1b to be constantly expressed during osteoblast differentiation.

We first assessed what effect does FoxO3a over-expression on calcium deposition in the ECM by ARS and found calcium deposition to be reduced dramatically. Pre-osteoblasts had calcium levels of approximately 80 nM and cell layers showed a faint pink color. These pre-osteoblast cells failed to incorporate calcium into the matrix during osteogenesis as 7-day differentiated mature osteoblasts demonstrated almost the same levels of calcium in the ECM. Both pre-osteoblasts and 7-day differentiated mature osteoblasts showed a 3-fold decrease in calcium levels compared to non-transfected control cells. These transfected cells also failed to respond to $1,25D_3$. We then queried if this reduction in deposition is due to less calcium entering the cells, leading to less cytosolic [Ca^{2+}]. We employed live cell ratiometric calcium imaging in mature osteoblasts and found mature osteoblasts to be not as sensitive to changes in external [Ca^{2+}] in comparison with non-transfected control cells. Although L-type Ca^{2+} channels were still the major functioning channels in the over-expressors, calcium influx was significantly reduced, resulting in lower [Ca^{2+}] to be deposited via NCX or PMCA-1b pump into the osteoid.

Even though treatment with $1,25D_3$ was able to elicit an increase in calcium uptake, this $1,25D_3$-induced calcium influx did not raise [Ca^{2+}] high enough to alter calcium deposition.

Measurement of Runx2 expression in the over-expressors demonstrated significant reduction in 3-day but stalls at 7-day differentiated MC3T3-E1 cells, at the same levels as pre-osteoblasts. In contrast, non-transfected control cells showed gradual reduction in Runx2 since 3-day post differentiation, reaching the lowest expression levels in 7-day differentiated mature osteoblasts. 7-day differentiated mature osteoblasts exhibited even lower Runx2 expression than pre-osteoblasts. Assessment of OCN expression in the over-expressors revealed disorganization in

expression, reduced in immature 1-day differentiated cells, followed by a significantly up-regulation in 3-day differentiated osteoblast. This increased expression then drops significantly to the same level as detected in pre-osteoblasts. On the other hand, non-transfected cells showed gradual increase in OCN expression as cells undergo differentiation, reaching the highest level in mature osteoblasts, indicating formation of extracellular matrix (ECM). These results indicated high levels of FoxO3a led to failure at osteoblast differentiation and eventual matrix calcification during mineralization.

Since OCN is an important matrix protein, we thought of supplementing 7-day differentiated over-expressors with high levels of osteocalcin to rescue osteoblast mineralization. Unexpectedly, *in vivo* animal study with deletion in OCN did not have detectable defects in ECM (Ducy et al., 1996; Ducy et al., 1997). Also, expression of other non-collagenous proteins including ostepontin, matrix gla proteins, bone sialo protein was not affected by the deletion of OCN (Ducy et al., 1996; Ducy et al., 1997).

Another approach to rescue decreased in calcium deposition in ECM was to supplement pre-osteoblasts and 7-day differentiated mature osteoblasts with additional 3 mM, 6mM and 9 mM [$CaCl_2$] to the culture media. Differ from the non-transfected control cells where matrix calcification increased in a dose-dependent manner, these over-expressors failed to increase calcium deposition with increasing external [$CaCl_2$].

6.8 Conclusion

This dissertation examined FoxO3a participation during osteoblast differentiation and matrix calcification in an *in vitro* murine model system. Since the identification of FoxOs in mammalian systems, extensive research has been actively exploring the role of FoxOs in a wide range of human diseases, especially in stress resistance and longevity. FoxOs have been heavily studied in skeletal homeostasis maintenance via oxidative stress defense mechanism. We queried whether FoxOs, especially FoxO3a, also plays a fundamental role in regulating calcium handling for maintaining skeletal homeostasis independent of ROS. First part of the thesis, we have successfully validated FoxO3a's participation in osteoblast differentiation and matrix calcification in MC3T3-E1 cells. Both FoxO3a mRNA an protein expression increases during osteoblast differentiation, indicating FoxO3a's involvement during the process. FoxO3a can be further enhanced by 100 nM $1,25D_3$ in 7-day differentiated mature osteoblasts, showing it's a downstream target of $1,25D_3$. Important calcium mediators and transporters have been identified, including L-type ($Ca_v1.2$ and $Ca_v1.3$) and T-type ($Ca_v3.1$), Calbindin-D_{9K}, NCX and PMCA-1b. L-type calcium channels have found to be the major functioning channel in mature osteoblasts, responsible for majority of calcium uptake into the cytosol. Use with L-type calcium channel antagonist, felodipine, almost abolished calcium uptake into the cell and caused calcium efflux. This observation supports calcium deposition through NCX or PMCA-1b pump into the mineralizing osteoid during matrix calcification. $1,25D_3$ increased calcium uptake through L-type calcium channels, but this regulation is independent of FoxO3a. Stable transfection of FoxO3a in pre-osteoblast MC3T3-E1 cells was generated to investigate the role FoxO3a during osteogenesis. In the FoxO3a over-expression model, calcium uptake and efflux are inhibited, resulting in significant reduction in matrix calcification. Osteogenesis biomarkers, Runx2 and

OCN revealed high levels of FoxO3a negatively regulate osteoblast differentiation and eventual matrix calcification.

6.9 Future Directions

Future work will be addressing some of the short-comings of the current work and extending the ideas to further explore role of FoxO3a in maintaining skeletal homeostasis.

Our current results showed high levels of FoxO3a negatively regulated calcium handling, leading to significant reduction in calcium influx and efflux. Another approach to confirm our findings is to generate a FoxO3a-deficient model, which can be achieved via CRISPR/Cas 9 technology. CRISPR/Cas 9 stands for clustered regularly interspaced short palindromic repeats (CRISPR) adaptive immune system, and is a powerful tool for mediating genome alterations with high accuracy (Ran et al., 2013). RNA-guided nucleases will be used to cleave endogenous FoxO3a in cells, and cells will undergo a selection process. Once a stable cell line has been generated, we can then gain insights into stage-wise regulation of important genes during osteogenesis. We can also use it to study calcium handling in differentiated osteoblasts. We hypothesized that deletion of FoxO3a will lead to increase in calcium uptake, and this raise in cytosolic [Ca^{2+}] will lead to enhanced calcium deposition into the calcifying matrix, resulting in higher bone mass.

Another extension of the work is to study if FoxO3a regulates calcium handling the same way in human osteoblast cells. An ideal cell line would be immortalized human fetal osteoblast-like (hFOB 1.19) cells or adult human osteoblast-like (hOB) cell line. These cell lines exhibit osteoblastic phenotype including collagen, osteopontin, alkaline phosphatase, osteocalcin, osteonectin, BSP and respond to steroid-stimulation such as $1,25D_3$. These cell line are also capable of forming mineralized ECM (Kartsogiannis and Ng, 2004). Thus, these cell lines would be a suitable model for studying osteogenesis.

REFERENCES

1. Ajibade D, Benn BS, Christakos S. "Mechanism of action of 1,25-dihydroxyvitamin D3 on intestinal calcium absorption and renal calcium transport." *Vitamin D: physiology, molecular biology, and clinical applications*, edited by Michael F. Holick, Humana, 2010, pp. 175-187.

2. Almeida M, O'Brien CA. Basic Biology of Skeletal Aging: Role of Stress Response Pathways. Journals Gerontol Ser A Biol Sci Med Sci. 2013; 68(10):1197-1208.

3. Almeida M. Unraveling the role of FoxOs in bone-Insights from mouse models. Bone. 2011;49(3):319-327.

4. Almeida M, Han L, Martin-Millan M, Plotkin LI, Stewart SA, Roberson PK, Kousteni S, O'Brien CA, Bellido T, Parfitt AM, Weinstein RS, Jilka RL, Manolagas SC. Skeletal involution by age-associated oxidative stress and its acceleration by loss of sex steroids. J Biol Chem. 2007;282(37):27285-27297.

5. Altindag O, Erel O, Soran N, Celik H, Selek S. Total oxidative/anti-oxidative status and relation to bone mineral density in osteoporosis. Rheumatol Int. 2008;28(4):317-321.

6. Ambrogini E, Almeida M, Martin-Millan M, Paik JK, Depinho RA, Han L, Goellner J, Weinstein RS, Jilka RL, O'Brien CA, Manolagas SC. FoxO-mediated defense againist oxidative stress in osteoblasts is indispensable for skeletal homeostasis in mice. Cell Metab. 2010;11(2):136-146.

7. Amling MI, Priemel M, Holzmann T, Chapin K, Rueger JM, Baron R, Demay MB. Rescue of the skeletal phenotype of vitamin D receptor- ablated mice in the setting of normal mineral ion homeostasis: formal histomorphometric and biomechanical analyses. Endocrinology. 1999;140(11):4982-4987.

8. Anderson HC. Matrix vesicles and calcification. Curr Rheumatol Rep. 2003;5(3):222-226.

9. Anderson HC. Molecular biology of matrix vesicles. Clin Orthop Relat Res. 1995; (314):266-280.

10. Anderson RE, Kemp JW, Jee WS, Woodbury DM. Ion-transporting ATPase and matrix mineralization in cultured osteoblastlike cells. In Vitro. 1984;20(11):837-846.

11. Anderson PH, Turner AG, Morris HA. Vitamin D actions to regulate calcium and skeletal homeostasis. Clin Biochem. 2012;45(12):880-886.

12. Andresen C, Olson E, Nduaka CI, Pero R, Bagi CM. Action of Calciotropic Hormones on Bone Metabolism – Role of Vitamin D_3 in Bone Remodeling Events. American Journal of Immunology. 2006;2(2):40-51.

13. Anderson HC, Garimella R, Tague SE. The role of matrix vesicles in growth plate development and biomineralization. Front Biosci. 2005;1(10):822-37.

14. Arai M, Shibata Y, Pugdee K, Abiko Y, Ogata Y. Effects of reactive oxygen species (ROS) on antioxidant system and osteoblastic differentiation in MC3T3-E1 cells. IUBMB Life. 2007;59(1):27-33.

15. Arden K. FOXO animal models reveal a variety of diverse roles for FOXO transcription factors. Oncogene. 2008;27(2008):2345-2350.

16. Aubin JE, Liu F, Malaval L, Gupta AK. Osteoblast and chondroblast differentiation. Bone. 1995;17(2 Suppl):77S-83S.

17. Bai XC, Lu D, Bai J,Zheng H, Ke ZY, Li XM, Luo SQ. Oxidative stress inhibits osteoblastic differentiation of bone cells by ERK and NF-kappaB. Biochem Biophys Res Commun. 2004;314(1):197-207.

18. Balmain N. Calbindin-D9k. A vitamin D-dependent, calcium-binding protein in mineralized tissues. Clin Orthop Relat Res. 1991;265:265-76.

19. Balmain N, Berdal A, Hotton D, Cuisinier-Gleizes P, Mathieu H. Calbindin-D9K immunolocalization and vitamin D-dependence in the bone of growing and adult rats. Histochemistry. 1989;92(5):359-365.

20. Banfi G, Iorio EL, Corsi MM. Oxidative stress, free radicals and bone remodeling. Clin Chem Lab Med. 2008;46(11):1550-1555.

21. Barsony J. "VDR and RXR subcellular trafficking." *Vitamin D: physiology, molecular biology, and clinical applications*, edited by Michael F. Holick, Humana, 2010, pp. 153-173.

22. Bellido T, Plotkin LI, Bruzzaniti A. Bone Cells. Basic Appl Bone Biol. 2014;14:27-45.

23. Bergh JJ, Shao Y, Puente E, Duncan RL, Farach-Carson MC. Osteoblast Ca(2+) permeability and voltage-sensitive Ca(2+) channel expression is temporally regulated by 1,25-dihydroxyvitamin D(3). Am J Physiol Cell Physiol. 2006; 290(3):C822-31.

24. Berridge MV, Tan AS. Characterization of the Cellular Reduction of 3-(4,5-dimethylthiazol-2-yl)-2,5-diphenyltetrazolium bromide (MTT): Subcellular Localization, Substrate Dependence, and Involvement of Mitochondrial Electron Transport in MTT Reduction. Arch Biochem Biophys. 1993;303(2):474-482.

25. Bikle DD. Vitamin D and Bone. Curr Osteoporos Rep. 2013;10(2):151-159.

26. Billiau A, Edy VG, Heremans H, Damme JV, Desmyter J, Georgiades JA, Somer PD. Human interferon: mass production in a newly established cell line, MG-63. Antimicrob Agents Chemother. 1977;12 (1):11-15.

27. Binkley N, Ramamurthy R, Krueger D. Low vitamin D status: definition, prevalence, consequences, and correction. Endocrinol Metab Clinc North Am. 2010;39(2):287.301.

28. Birinyi P, Acsai K, Bányász T, Tóth A, Horváth B, Virág L, Szentandrassy N, Magyar J, Varró A, Fülöp F, Nánási PP. Effects of SEA0400 and KB-R7943 on Na+/Ca2+ exchange current and L-type Ca2+ current in canine ventricular cardiomyocytes. Naunyn Schmiedebergs Arch Pharmacol. 2005;372(1):63-70.

29. Bonewald LF. The Amazing Osteocyte. Journal of Bone and Mineral Research. 2011; 26(2):229-238

30. Boonrungsiman S. The role of intracellular calcium phosphate in osteoblast-mediated bone apatite formation. Proc Natl Acad Sci. 2012;109(35):14170-14175.

31. Boyce RW, Weisbrode SE. Histogenesis of hyperosteoidosis in 1,25(OH)2D3-treated rats fed high levels of dietary calcium. Bone. 1985;6(2):105-112.

32. Brini M, Carafoli E. The Plasma Membrane Ca2+ ATPase and the plasma membrane Sodium Calcium exchanger cooperate in the regulation of cell Calcium. Cold Spring Harb Perspect Biol. 2011;3(2):1-15.

33. Briot K, Roux C. Glucocorticoid-induced osteoporosis. RMD Open. 2015;1(1): e0000014.

34. Brunet A, Bonni A, Zigmond MJ, Lin MZ, Juo P, Hu LS, Anderson MJ, Arden KC, Blenis J, Greenberg ME. Akt Promotes Cell Survival by Phosphorylating and Inhibiting a Forkhead Transcription Factor. Cell. 1999;96:857-868.

35. Buckwalter JA, Glimcher MJ, Cooper RR, Recker R. Bone biology. I: Structure, blood supply, cells, matrix, and mineralization. Instr Course Lect. 1996;45:371-386.

36. Bukka P, McKee M.D, Karaplis A.C. "Molecular Regulation of Osteoblast Differentiation." *Bone Formation* edited by Felix Bronner and Mary C, Springer, 2004, pp.1-17.

37. Burdon RH. Superoxide and hydrogen peroxide in relation to mammalian cell proliferation. Free Radic Biol Med. 1995;18(4):775-794.

38. Burr DB, Akkus O. Bone "Morphology and Organization." *Basic and Applied Bone Biology,* edited by David B. Burr and Matthew R. Allen, Academic Press Inc, 2014, pp.3-25. https://www.sciencedirect.com/science/book/9780124160156

39. Caffrey JM, Farach-Carson MC. Vitamin D3 metabolites modulate dihydropyridine-sensitive calcium currents in clonal rat osteosarcoma cells. J Biol Chem. 1989;264 (34):20265-20274.

40. Callaway DA, Jiang JX. Reactive oxygen species and oxidative stress in osteoclastogenesis, skeletal aging and bone diseases. J Bone Miner Metab. 2015;33(4):359-370

41. Calnan DR, Brunet A. The FoxO code. Oncogene. 2008;27(16):2276-2288.

42. Carlsson A, Lindqvist M, Magnusson T. Tracer Experiments on the Effect of Vitamin-D on the Skeletal Metabolism of Calcium and Phosphorus. Acta Physiol Scand. 1952;26:212-220.

43. Chandra V, Huang P, Hamuro Y, Raghuram S, Wang Y, Burris TP, Rastinejad F. Structure of the intact PPAR-γ–RXR-α nuclear receptor complex on DNA. Nature. 2008;456(7220):350-356.

44. Chen G, Deng C, Li YP. TGF-β and BMP signaling in osteoblast differentiation and bone formation. Int J Biol Sci. 2012;8(2):272-288.

45. Chen JH, Stoeber K, Kingsbury S, Ozanne SE, Williams GH, Hales CN. Loss of proliferative capacity and induction of senescence in oxidatively stressed human fibroblasts. J Biol Chem. 2004;279(47):49439-49446.

46. Chen X, Zhong Z, Xu Z, Chen L, Wang Y. 2',7'-Dichlorodihydrofluorescein as a fluorescent probe for reactive oxygen species measurement: Forty years of application and controversy. Free Radic Res. 2010;44(6):587-604.

47. Chen TC, Lu Z, Holick MF. "Photobiology of Vitamin D." *Vitamin D: physiology, molecular biology, and clinical applications*, edited by Michael F. Holick, Humana, 2010, pp.35-60.

48. Cheng RCK, Tikhonov DB, Zhorov BS. Structural model for phenylalkylamine binding to L-type calcium channels. J Biol Chem. 2009;284(41):28332-28342.

49. Christakos S, Ajibade DV, Dhawan P, Fechner AJ, Mady LJ. Vitamin D: Metabolism. Endocrinol Metab Clin North Am. 2010;39(2):243-253.

50. Christakos S, Dhawan P, Porta A, Mady LJ, Seth T. Vitamin D and intestinal calcium absorption. Mol Cell Endocrinol. 2011;347(1-2):25-29.

51. Christakos S, Liebsbet L, Masuyama R, Carmeliet G. Vitamin D endocrine system and the intestine. Bonekey Rep. 2014;3:496.

52. Clarke B. Normal bone anatomy and physiology. Clin J Am Soc Nephrol. 2008;3 Suppl 3:131-139.

53. Daitoku H, Sakamaki J, Fukamizu A. Regulation of FoxO transcription factors by acetylation and protein-protein interactions. Biochim Biophy Acta. 2011;1813(11):1954-1960.

54. Dallas SL, Bonewald LF. Dynamics of the Transition from Osteoblast to Osteocyte. Ann N Y Acad Sci. 2010;(816):437-443.

55. Day TF, Guo X, Garrett-Beal L, Yang Y. Wnt/β-catenin signaling in mesenchymal progenitors controls osteoblast and chondrocyte differentiation during vertebrate skeletogenesis. Dev Cell. 2005;8(5):739-750.

56. Deluca HF. History of the discovery of vitamin D and its active metabolites. Bonekey Rep. 2014;3:479.

57. Dennison E, Mohamed MA, Cooper C. Epidemiology of Osteoporosis. Rheum Dis Clin North Am. 2006;32(4):617-629.

58. Desbois C, Hogue DA, Karsenty G. The Mouse Osteocalcin Gene-Cluster Contains 3 Genes with 2 Separate Spatial and Temporal Patterns of Expression. J Biol Chem. 1994;269(2):1183-1190.

59. Dimke H, Desai P, Borovac J, Lau A, Pan W, Alexander RT. Activation of the Ca(2+)-sensing receptor increases renal claudin-14 expression and urinary Ca(2+) excretion. Am J Physiol Renal Physiol. 2013;304(6):F761-9.

60. Dowd DR, MacDonald PN. "The molecular biology of vitamin D receptor." *Vitamin D: physiology, molecular biology, and clinical applications*, edited by Michael F. Holick, Humana, 2010, pp. 135-152.

61. Dowell P, Otto TC, Adi S, Lane MD. Convergence of Peroxisome Proliferator-activated Receptor gamma and Foxo1 Signaling Pathways. J Biol Chem. 2003;278(46):45485-45491.

62. Drissi H. 1,25-(OH)2-Vitamin D3 Suppresses the Bone-Related Runx2/Cbfa1 Gene Promoter. Exp Cell Res. 2002;274(2):323-333.

63. Ducy P, Desbois C, Boyce B, Pinero G, Story B, Dunstan C, Smith E, Bonadio J, Goldstein S, Gundberg C, Bradley A, Karsenty G. Increased bone formation in osteocalcin-deficient mice. Nature. 1996;382(6590):448-452.

64. Ducy P, Zhang R, Geoffroy V, Ridall AL, Karsenty G. Osf2/Cbfa1: A Transcriptional Activator of Osteoblast Differentiation. Cell. 1997;89(5):747-754.

65. Duncan RL, Akanbi KA, Farach-Carson MC. Calcium signals and calcium channels in osteoblastic cells. Semin Nephrol. 1998;18(2):178-90.

66. Duren DL, Seselj M, Froehle AW, Nahhas RW, Sherwood RJ. Skeletal growth and the changing genetic landscape during childhood and adulthood. Am J Phys Anthropol. 2013;150(1):48-57.

67. Duriez J, Flautre B, Blary MC, Hardouin P. Effects of the calcium channel blocker nifedipine on epiphyseal growth plate and bone turnover: a study in rabbit. Calcif Tissue Int. 1993;52(2):120-124.

68. Ecarot-Charrier B, Shepard N, Charette G, Grynpas M, Glorieux FH. Mineralization in osteoblast cultures: A light and electron microscopic study. Bone. 1988;9(3):147-154.

69. Ecarot-charrier B, Glorieux FH, Rest MVANDER, Pereira G. Osteoblasts isolated from mouse calvaria initiate matrix mineralization in culture. J. cell Biol 1983;96:639-643.

70. Eelen G, Verlinden L, Meyer MB, Gijsbers R, Pike JW, Bouillon R, Verstuyf A. 1,25-Dihydroxyvitamin D3 and the aging-related Forkhead Box O and Sestrin proteins in osteoblasts. J Steroid Biochem Mol Biol. 2013;136:112-119.

71. Eisman JA, Bouillon R. Vitamin D: direct effects of vitamin D metabolites on bone: lessons from genetically modified mice. Bonekey Rep. 2014;3:499.

72. Erben RG. Vitamin D analogs and bone. J Musculoskelet Neuronal Interact. 2001;2(1):59-69.

73. Erben RG, Bromm S, Stangassinger M. Therapeutic efficacy of 1alpha,25-dihydroxyvitamin D3 and calcium in ostepenic ovariectomized rats: evidence for a direct anabolic effect of 1alpha,25-dihydroxyvitamin D3 on bone. Endocrinology. 1998;139(10):4319-4328.

74. Erben RG, Soegiarto DW, Weber K, Zeitz U, Lieberherr M, Gniadecki R, Moller G, Adamski J, Balling R. Deletion of deoxyribonucleic acid binding domain of the vitamin D receptor abrogates genomic and nongenomic functions of vitamin D. Mol Endocrinol. 2002;16(7):1524-1537.

75. Eriksen EF, Axelrod DW, Melsen F. Bone Histomorphometry, New York, Raven Press,1994., pp.1 –12.

76. Everts V, Delaisse JM, Korper W, Jansen DC, Tigchelaar-Gutter W, Saftig P, Beertsen W. The Bone Lining Cell: Its Role in Cleaning Howships' Lacunae and Initiating Bone formation. J Bone Miner Res. 2002;17(1):77-90.

77. Fatokun AA, Stone TW, Smith RA. Hydrogen peroxide-induced oxidative stress in MC3T3-E1 cells: The effects of glutamate and protection by purines. Bone. 2006;39(3):542-551.

78. Fogh J, Wright WC, Loveless JD. Absence of HeLa cell contamination in 169 cell lines derived from human tumors. Journal of the National Cancer Institute. 1997;58(2):209-214.

79. Franceschi RT, Iyer BS, Cui Y. Effects of ascorbic acid on collagen matrix formation and osteoblast differentiation in murine MC3T3-E1 cells. J Bone Miner Res. 1994;9(6):843-854.

80. Fratzl P, Fratzl-Zelman N, Klaushofer K, Vogl G, Koller K. Nucleation and growth of mineral crystals in bone studied by small-angle X-ray scattering. Calcif Tissue Int. 1991;48(6):407-413.

81. Friedenstein AJ, Chailakhyan RK, Gerasimov U V. Transplantation in Diffusion Chambers. 1987:263-272.

82. Garabedian M, Holick MF, Deluca HF, Boyle IT. Control of 25-hydroxycholecalciferol metabolism by parathyroid glands. Proc Natl Acad Sci U S A. 1972;69(7):1673-1676.

83. Garcia ML, King VF, Shevell JL, et al. Amiloride analogs inhibit L-type calcium channels and display calcium entry blocker activity. J Biol Chem. 1990;265(7):3763-3771.

84. Gardiner EM, Baldock PA, Thomas GP, Sims NA, Henderson NK, Hollis B, White CP, Sunn KL, Morrison NA, Walsh WR, Eisman JA. Increased formation and decreased resorption of bone in mice with elevated vitamin D receptor in mature cells of the osteoblastic lineage. Faseb J. 2000;14(13):1908-1916.

85. Garrett IR, Boyce BF, Oreffo RO, Bonewald L, Poser J, Mundy GR. Oxygen-derived free radicals stimulate osteoclastic bone resorption in rodent bone in vitro and in vivo. J Clin Invest. 1990;85(3):632-639.

86. Glimcher MJ. Recent studies of the mineral phase in bone and its possible linkage to the organic matrix by protein-bound phosphate bonds. Philos Trans R Soc Lond B Biol Sci. 1984;304(1121):479-508.

87. Gregory CA, Gunn WG, Peister A, Prockop DJ. An Alizarin red-based assay of mineralization by adherent cells in culture: Comparison with cetylpyridinium chloride extraction. Anal Biochem. 2004;329(1):77-84.

88. Grynkiewicz G, Poenie M, Tsien RY. A new generation Ca2+ indicators with greatly improved fluorescence properties. J Biol Chem. 1985;260(6):3440-3450.

89. Haussler MR, Haussler CA, Bartik L, Whitfield GK, Hsieh JC, Slater S, Jurutka PW. Vitamin D receptor: molecular signaling and actions of nutritional ligands in disease prevention. Nutr Rev. 2008;66(10 Suppl 2):S98-112.

90. Haussler MR, Whitfield GK, Haussler CA, Hsieh JC, Jurutka PW. Chapter 8-Nuclear vitamin D receptor: natural ligands, molecular structure-function, and transcriptional control of vital genes. Vitamin D (3rd ED). 2011;1:137-170.

91. Hockerman GH, Johnson BD, Abbott MR, Scheuer T, Catterall WA. Molecular determinants of high affinity phenylalkylamine block of L-type calcium channels in transmembrane segment IIIS6 and the pore region of the alpha1 subunit. J Biol Chem. 1997;272(30):18759-18765.

92. Hoenderop JGJ, Vennekens R, Muller D, Prenen J, Droogmans G, Bindels RJM, Nilius B. Function and expression of the epithelial Ca^{2+} channel family: comparison of mammalian ECaC1 and 2. J Physiol. 2001;537(Pt3):747-761.

93. Hofbauer LC, Heufelder AE. Role of receptor activator of nuclear factor-kappaB ligand and osteoprotegerin in bone cell biology. J Mol Med (Berl). 2001;79(5-6):243-253.

94. Hofmann F, Flockerzi V, Kahl S, Wegener JW. L-Type CaV1.2 calcium channels: from in vitro findings to in vivo function. Physiol Rev. 2014;94(1):303-326.

95. Holick MF. Vitamin D Deficiency. The New England Journal of Medicine. 2007;357: 266-281.

96. Holick MF, Chen TC. Vitamin D deficiency: a worldwide problem with health consequences. Am J Clin Nutr. 2008;87:1080S-6S.

97. Holtrop ME, Cox KA, Calrk MB, Holick MF, Anast CS. 1,25-dihydroxycholecalciferol stimulates osteoclasts in rat bones in the absence of parathyroid hormone. Endocrinology. 1981;108(6):2293-22301.

98. Hopkins RB, Burke N, Von Keyserlingk C, Leslie WD, Morin SN, Adachi JD, Papaioannou A, Bessette L, Brown JP, Pericleous L, Tarride J. The current economic burden of illness of osteoporosis in Canada. Osteoporos Int. 2016;27(10):3023-3032.

99. Howell DS, Pita JC, Marquez JF, Madruga JE. Partition of calcium, phosphate, and protein in the fluid phase aspirated at calcifying sites in epiphyseal cartilage. J Clin Invest. 1968;47(5):1121-1132.

100. Howell, D.S. Review Article. Current concepts of calcification. J. Bone Joint Surg. Am. 1971;53A(2):250-7.

101. Huang L, Keyser BM, Tagmose TM, Hansen JB, Taylor JT, Zhuang H, Zhang M, Ragsdale DS, Li M. NNC 55-0396 [(1S,2S)-2-(2-(N-[(3-benzimidazol-2-yl)propyl]-N-methylamino)ethyl)-6-fluoro-1,2,3,4-tetrahydro-1-isopropyl-2-naphtyl cyclopropanecarboxylate dihydrochloride]: a new selective inhibitor of T-type calcium channels. J Pharmacol Exp Ther. 2004;309(1): 193-199.

102. Ikeda K, Matsumoto T, Morita K, Kurokawa K, Ogata E. Inhibition of in vitro mineralization by aluminum in a clonal osteoblastlike cell line, MC3T3-E1. Calcif Tissue Int. 1986;39(5):319-323.

103. Imai K, Neuman MW, Kawase T, Saito S. Calcium in osteoblast-enriched bone cells. Bone. 1992;13(3):217-223.

104. Imel EA, DiMeglio LA, Burr DB. Metabolic Bone Diseases. Basic and Applied Bone Biology Elsevier Inc.; 2014.

105. Ioannidis G, Papaioannou A, Hopman WM, Akhtar-Danesh N, Anastassiades T, Pickard L, Kennedy CC, Prior JC, Olszynski WP, Davison KS, Goltzman D, Thabane L, Gafni A, Papadimitropoulous EA, Brown JP, Josse RG, Hanley DA, Adachi JD. Relation between fractures and mortality: results from the Canadian Multicentre Osteoporosis Study. CMAJ. 2009;181(5):265-271.

106. Iyer S, Ambrogini E, Bartell SM, Han L, Roberson PK, de Cabo R, Jilka RL, Weinstein RS, O'Brien CA, Manolagas SC, Almeida M. FOXOs attenuate bone formation by suppressing Wnt signaling. J Clin Invest. 2013;123(8):3409-3419.

107. Jacobs FMJ, Van der Heide LP, Wijchers PJEC, Burbach JPH, Hoekman MFM, Smidt MP. FoxO6, a novel member of the FoxO class of transcription factors with distinct shuttling dynamics. J Biol Chem. 2003;278(38):35959-35967.

108. Jilka RL. Biology of the basic multicellular unit and the pathophysiology of osteoporosis. Med Pediatr Oncol. 2003;41(3):182-185.

109. Jones G. "Metabolism and catabolism of vitamin D, its metabolites and clinically relevant analogs." *Vitamin D: physiology, molecular biology, and clinical applications*, edited by Michael F. Holick, Humana, 2010, pp. 99-134.

110. Jung SY, Park YJ. Na+-Ca2+ exchanger moedulates Ca2+ content in intracellular Ca2+ stores in rat osteoblasts. Exp Mol Med. 2007;39(4):458-468.

111. Kaestner KH, Knochel W, Martinez DE. Unified nomenclature for the winged helix/forkhead transcription factors. Genes Dec. 2000;14(2): 142-146.

112. Kanis JA, Odén A, McCloskey E V., Johansson H, Wahl DA, Cooper C. A systematic review of hip fracture incidence and probability of fracture worldwide. Osteoporos Int. 2012;23(9):2239-2256.

113. Karin N.J., Farach-Carson M.C. "*In Vitro* Regulation of Osteoblast Activity." *Bone Formation* edited by Felix Bronner and Mary C. Farach-Carson, Springer, 2004, pp.18-43.

114. Kartsogiannis V, Ng KW. Cell lines and primary cell cultures in the study of bone cell biology. Mol Cell Endocrinol. 2004;228(1-2):79-102.

115. Kato Y, Windle JJ, Koop BA, Mundy GR, Bonewald LF. Establishment of an osteocyte-like cell line, MLO-Y4. J Bone Miner Res. 1997;12(12):2014-2023.

116. Kim HJ, Prasad V, Hyung SW, Lee ZH, Lee SW, Bhargava A, Pearce D, Lee Y, Kim HH. Plasma membrane calcium ATPase regulates bone mass by fine-tuning osteoclast differentiation and survival. J Cell Biol. 2012;199(7):1145-1158.

117. Kim YS, Yang IM, Kim SW, Kim JW, Kim KW, Choi YK. Responses of osteoblastic cell line MC3T3-E1 cell to the calcium channel blocker diltiazem and verapamil. Contrib Nephrol. 1991;91:43-49.

118. Klein-Nulend J, Nijweide PJ, Burger EH. Osteocyte and bone structure. Curr Osteoporos Rep. 2003;1(1):5-10.

119. Kodama H, Amagai Y, Sudo H, Kasai S, Yamamoto S. Establishment of a clonal osteogenic cell line from newborn mouse calvaria. J Oral Biol. 1981;23:899-901.

120. Kogawa M, Findlay DM, Anderson PH, Ormsby R, Vincent C, Morris HA, Atkins GJ. Osteoclastic metabolism of 25(OH)-vitamin D3: a potential mechanism for optimization of bone resorption. Endocrinology. 2010;151(10):4613-4625.

121. Komori T. Regulation of osteoblast differentiation by transcription factors. J Cell Biochem. 2006;99(5):1233-1239.

122. Komori T. Regulation of osteoblast differentiation by Runx2. Adv Exp Med Biol. 2010;658:43-49.

123. Komori T, Yagi H, Nomura S, Yamaguchi A, Sasaki K, Deguchi K, Shimizu Y, Bronson RT, Gao YH, Inada M, Sato M, Okamoto R, Kitamura Y, Yoshiki S, Kishimoto T. Targeted disruption of Cbfa1 results in a complete lack of bone formation owing to maturational arrest of osteoblasts. Cell. 1997;89(5):755-764.

124. Kopic S, Geibel JP. Gastric acid, calcium absorption, and their impact on bone health. Physiol Rev. 2013;93:189-268.

125. Kops GJ, Dansen TB, Polderman PE, Saarloos I, Wirtz KW, Coffer PJ, Huang TT, Bos JL, Medema RH, Burgering BM. Forkhead transcription factor FOXO3a protects quiescent cells from oxidative stress. Nature. 2002;419(6904):316-321.

126. Kops GJ, de Ruiter ND, De Vries-Smits AM, Powell DR, Bos JL, Burgering BM. Direct control of the Forkhead transcription factor AFX by protein kinase B. Nature. 1999;398(6728):630-634.

127. Lam EWF, Brosens JJ, Gomes AR, Koo CY. Forkhead box proteins: tuning forks for transcriptional harmony. Nature. 2013;13(7):482-495.

128. Lanteri P, Lombardi G, Colombini A, Banfi G. Vitamin D in exercise: Physiologic and analytical concerns. Clin Chim Acta. 2013;415:45-53.

129. Lean JM, Davies JT, Fuller K, Jagger CJ, Kirstein B, Partington GA, Urry ZL, Chambers TJ. A crucial role for thiol antioxidants in estrogen-deficiency bone loss. J Clin Invest. 2003;112(6):915-923.

130. Lee DH, Lim BS, Lee YK, Yang HC. Effects of hydrogen peroxide (H2O2) on alkaline phosphatase activity and matrix mineralization of odontoblast and osteoblast cell lines. Cell Biol Toxicol. 2006;22(1):39-46.

131. Lentle B, Cheung AM, Hanley DA, Leslie WD, Lyons D, Papaioannou A, Atkinson S, Brown JP, Feldman S, Hodsman AB, Jamal AS, Josse RG, Kaiser SM, Kvern B, Morin S, Siminoski K. Osteoporosis Canada 2010 guidelines for the assessment of fracture risk. Can Assoc Radiol J. 2011;62(4):243-250.

132. Li J, Zhao L, Ferries IK, Jiang L, Desta MZ, Yu X, Yang Z, Duncan RL, Turner CH. Skeletal phenotype of mice with a null mutation in Cav 1.3 L-type calcium channel. J Musculoskelet Neuronal Interact. 2010;10(2):180-187.

133. Lian JB, Stein GS. Concepts of osteoblast growth and differentiation: basis for modulation of bone cell development and tissue formation. Crit Rev Oral Biol Med. 1992;3(3):269-305.

134. Lian JB, Stein GS, Stein JL, van Wijnen AJ. Transcriptional control of osteoblast differentiation. Biochem Soc Trans. 1998;26(1):14-21.

135. Lian JB, Stein GS, Montecino M, Stein JL, van Wijnen AJ. Chatper 16-Genetic and epigenetic control of the regulatory machinery for skeletal development and bone formation: contributions of vitamin D3. Vitamin D (3rd Ed). 2011;1:301-319.

136. Lieben L, Carmeliet G. The delicate balance between vitamin D, calcium and bone homeostasis: Lessons learned from intestinal-and osteocyte-specific VDR null mice. J Steroid Biochem Mol Biol. 2013;136(1):102-106.

137. Lieben L, Carmeliet G. The involvement of TRP channels in bone homeostasis. Front Endocrinol (Lausanne). 2012;3:99.

138. Lieberherrs M. Effects of Vitamin D metabolites on cytosolic free calcium in confluent mouse osteoblasts. J Biol Chem. 1987;262(27):13168-13173.

139. Lieben L, Matsuyama R, Torrekens, S, Looveren, RV, Schrooten J, Baatsen P, Lafage-Proust MH, Dresselaers T, Feng JQ, Bonewald, LF, Meyer MB, Pike JW, Bouillon R, Carmeilet G. Normocalcemia is maintained in mice under conditions of calcium malabsorption by vitamin D-induced inhibition of bone mineralization. J Clin Invest. 2012; 122(5):1803-15.

140. Maehata Y, Takamizawa S, Ozawa S, et al. Both direct and collagen-mediated signals are required for active vitamin D3-elicited differentiation of human osteoblastic cells: Roles of osterix, an osteoblast-related transcription factor. Matrix Biol. 2006;25(1):47-58.

141. Maeno S, Niki Y, Matsumoto H, Morioka H, Yatabe T, Funayama A, Toyama Y, Taguchi T, Tanaka J. The effect of calcium ion concentration on osteoblast viability, proliferation and differentiation in monolayer and 3D culture. Biomaterials. 2005;26(23):4847-4855.

142. Maggio D, Barabani M, Pierandrei M, Polidori MC, Catani M, Mecocci P, Senin U, Pacifici R, Cherubini A. Marked decrease in plasma antioxidants in aged osteoporotic women: results of a cross-sectional study. J Clin Endocrinol Metab. 2003;88(4):1523-1527.

143. Mahamid J, Addadi L, Weiner S. Crystallization pathways in bone. Cells Tissues Organs. 2011;194(2-4):92-97.

144. Manolagas SC. Birth and death of bone cells : basic regulatory mechanisms and implications for the pathogenesis and treatment of osteoporosis. Endocr Rev. 2015;21(2):115-137.

145. Marie PJ. The calcium-sensing receptor in bone cells; a potential therapeutic target in osteorporosis. Bone. 2010;46(3):571-576.

146. Martins R, Lithgow GJ, Link W. Long live FOXO: Unraveling the role of FOXO proteins in aging and longevity. Aging Cell. 2016;15(2):196-207.

147. Massaro, E., and Rogers, J. The Skeleton: Biochemical, Genetic, and Molecular Interactions in Development and Homeostasis. 2004. Totowa, NJ: Humana Press.

148. Matsumoto T, Igarashi C, Takeuchi Y, Harada S, Kikuchi T, Yamato H, Ogata E. Stimulation by 1,25-dihydroxyvitamin D3 of in vitro mineralization induced by osteoblast-like MC3T3-E1 cells. Bone. 1991;12(1):27-32.

149. Meszaros JG, Norman JK, Akanbi K, Farach-Carson MC. Down-regulation of L-type Ca2+ channel transcript levels by 1,25-dihydroxyivitamin D3 osteoblast cells express L-type α1C Ca2+ channel isoforms. J Biol Chem. 1996; 271 (51): 32981-32985.

150. Meyer MB, Goetsch PD, Pike JW. Genome-wide analysis of the VDR/RXR cistrome in osteoblast cells provides new mechanistic insights into the actions of the Vitamin D hormone. J Sterroid Biochem Mol Biol. 2010;121(1-2):136-141.

151. Meyer MB, Benkusky NA, Lee CH, Pike JW. Genomic determinants of gene regulation by 1,25-dihydroxyvitamin D 3 during osteoblast-lineage cell differentiation. J Biol Chem. 2014;289(28):19539-19554.

152. Miederer A-M, Alansary D, Schwär G, Lee PH, Jung M, Helms V, Niemeyer BA. A STIM2 splice variant negatively regulates store-operated calcium entry. Nat Commun. 2015;6:6899.

153. Mody N, Pargami F, Sarafian T, Demer L. Oxidative stress modulates osteoblastic differentiation of. Vascular and bone cells. Free Radic Biol Med. 2001;31(4):509-519.

154. Murshed M, Schinke T, McKee MD, Karsenty G. Extracellular matrix mineralization is regulated locally; different roles of two gla-containing proteins. J Cell Biol. 2004;165(5):625-630.

155. Myatt SS, Lam EW. The emerging roles of forkhead box (Fox) proteins in cancer. Nat Rev Cancer. 2007. 7(11):847-859.

156. Nakae J, Kitamura T, Kitamura Y, Biggs WH 3rd, Arden KC, Accili D. The forkead transcription factor Foxo1 regulates adipocytet differentiation. Dev Cell. 2003;4(1):119-129.

157. Nakano Y, Addison WN, Kaartinen MT. ATP-mediated mineralization of MC3T3-E1 osteoblast cultures. Bone. 2007;41(4):549-561.

158. Nakano Y, Beertsen W, Vandenbos T, Kawamoto T, Oda K, Takano Y. Site-specific localization of two distinct phosphatases along the osteoblast plasma membrane: Tissue non-specific alkaline phosphatase and plasma membrane calcium ATPase. Bone. 2004;35(5):1077-1085.

159. Nemoto S, Finkel T. Redox regulation of forkhead proteins through a p66shc-dependent signaling pathway. Science. 2002;295(5564):2450-2452.

160. Nijweide PJ, Burger EH, Feyen JH. Cells of bone: proliferation, differentiation, and hormonal regulation. Physiol Rev. 1986;66(4):855-886.

161. Otto F, Thornell a P, Crompton T, Denzel A, Gilmour KC, Rosewell IR, Stamp GW, Beddington RS, Mundlos S, Olsen BR, Selby PB, Owen MJ. Cbfa1, a candidate gene for cleidocranial dysplasia syndrome, is essential for osteoblast differentiation and bone development. Cell. 1997;89(5):765-771.

162. Ozgocmen S, Kaya H, Fadillioglu E, Aydogan R, Yilmaz Z. Role of antioxidant systems, lipid peroxidation, and nitric oxide in postmenopausal osteoporosis. Mol Cell Biochem. 2007;295(1-2):45-52.

163. Pan W, Borovac J, Spicer Z, Hoenderop JG, Bindels RJ, Shull GE, Doschak MR, Cordat E, Alexander RT. The epithelial sodium/proton exchanger, NHE3, is necessary for renal and intestinal calcium (re)absorption. Am J Physiol Renal Physiol. 2012;302(8):F943-956.

164. Papaioannou A, Morin S, Cheung AM, Atkinson S, Brown JP, Feldman S, Hanley DA, Hodsman A, Jamal SA, Kaiser SM, Kvern B, Siminoski K, Leslie WD. 2010 clinical practice guidelines for the diagnosis and management of osteoporosis in Canada: Summary. CMAJ. 2010;182(17):1864-1873.

165. Paradis GR, Bassingthwaighte BB, Kelly PJ. Inhibition of transport of ^{47}Ca and ^{85}Sr by lanthanum in canine cortical bone. J Appl Physiol. 1974;36(2): 221-225.

166. Partridge NC, Alcorn D, Michelangeli VP, Ryan G, Martin TJ. Morphological and biochemical charactierzation of four clonal osteogenic sarcoma cell lines of rat origin. Cancer Res. 1983;43(9):4308-4314.

167. Partridge NC, Jeffrey JJ, Ehlich LS, Teitelbaum SL, Fliszar C, Welgus HG, Kahn AJ. Hormonal regulation of the production of collagenease and a collagenase inhibitor activity by rat osteogenic sarcoma cells. Endocrinology. 1987;120(5):1956-1962.

168. Partridge L, Bruning JC. Forkhead transcription factors and ageing. Oncogene. 2008;27(16):2351-2363.

169. Peress NS, Anderson HC, Sajdera SW. The lipids of matrix vesicles from bovine fetal epiphyseal cartilage. Calcif Tissue Res. 1974;14(1):275-281.

170. Pike JW, Lee SM, Meyer MB. Regulation of gene expression by 1,25-dihydroxyvitamin D3 in bone cells: exploiting new approaches and defining new mechanisms. Bonekey Rep. 2014;3:482.

171. Pike JW, Meyer MB. The vitamin D receptor: new paradigms for the regulation of gene expression by 1,25-dihydroxyvitamin D(3). Endocrinol. Metab. Clin. North Am. 2010;39:255–269.

172. Pike JW, Meyer MB, Lee SM. Chapter 7-The Vitamin D Receptor: Biochemical, Molecular, Biological, and Genomic Era Investigations. Vitamin D (3rd Ed). 2011;1:97-135.

173. Plum LA, DeLuca HF. "The functional metabolism and molecular biology of vitamin D action." *Vitamin D: physiology, molecular biology, and clinical applications*, edited by Michael F. Holick, Humana, 2010, pp.61-97.

174. Prentice A. Vitamin D deficiency: A global perspective. Nutr Rev. 2008;66(10 Suppl 2):S153-164.

175. Prentice A. Micronutrients and the bone mineral content of the mother, fetus and newborn. J Nutr. 2003;133(5 Suppl 2):1693S-1699S.

176. Prince M, Banerjee C, Javed A, Green J, Lian JB, Stein GS, Bodine PV, Komm BS. Expression and regulation of Runx2/Cbfa1 and osteoblast phenotypic markers during the growth and differentiation of human osteoblasts. J Cell Biochem. 2001;80(3):424-440.

177. Puig O, Mattila J. Understanding Forkhead box class O function: lessons from Drosophila melanogaster. Antioxid Redox Signal. 2011;14(4):635-647.

178. Puzas J.E. "Site-specific Mineralized Matrix Formation by Osteoblasts". *Bone Formation,* edited by Felix Bronner and Mary C. Farach-Carson, Springer, 2004, pp.71-78.

179. Quarles LD, Yohay DA, Lever LW, Caton R, Wenstrup RJ. Distinct proliferative and differentiated stages of murine MC3T3-E1 cells in culture: an in vitro model of osteoblast development. J Bone Miner Res. 1992;7(6):683-692.

180. Raisz LG, Trummel CL, Holick MF, DeLuca HF. 1,25-dihydroxycholecalciferol: a potent stimulator of bone resorption in tissue culture. Science. 1972;175(4023):768-769.

181. Ran FA, Hsu PD, Wright J, Agarwala V, Scott DA, Zhang F. Genome engineering using the CRISPR-Cas9 system. Nat Protoc. 2013;8(11):2281-2308.

182. Richards JS, Sharma SC, Falender AE, Lo YH. Expression of FKHR, FKHRL1, and AFX genes in the rodent ovary: evidence for regulation by IGF-1, estrogen, and the gonadotropins. Mol Endocrinol. 2002;16(3): 580-599.

183. Riggs L, Melton LJ 3rd. The worldwide problem of osteoporosis: insights afforded by epidemiology. Bone. 1995;17(5 Suppl):505S-511S.

184. Riggs BL, Khosla S, Melton III LJ. A unitary Model for Involutional Osteoporosis: Estrogen Deficiency Causes Both Type I and Type II Osteoporosis in Postmenopausal

Women and Contributes to Bone Loss in Aging Men. Journal of Bone and Mineral Research. 1998;13(5):763-773.

185. Riggs BL, Melton LJ 3rd. The prevention and treatment of osteoporosis. The New England Journal of Medicine. 1992;327(9):620-627.

186. Ringbom-Anderson T, Jantti J, Akerman KE. Production and release of matrix vesicles in the cell processes of TPA-treated human osteoblast-like cells. J Bone Miner Res. 1994;9(5):661-670.

187. Rochel N, Moras D. Chapter 9-Structural basis for ligand activity in VDR. Vitamin D (3rd Ed). 1:171-191.

188. Rodan GA, Noda M. Gene expression in osteoblastic cells. Crit Rev Eukaryot Gene Expr. 1991;1(2):85-98.

189. Rodan SB, Imai Y, Thiede MA, Wesolowski G, Thompson D, Bar-Shavit Z, Shull S, Mann K, Rodan GA. Characterization of a human osteosarcoma cell line (Saos-2) with osteoblastic properties. Cancer Res. 1987;47(18):4961-4966.

190. Rodríguez-Martínez M a, García-Cohen EC. Role of Ca(2+) and vitamin D in the prevention and treatment of osteoporosis. Pharmacol Ther. 2002;93(1):37-49.

191. Ronnebaum SM, Patterson C. The FoxO Family in Cardiac Function and Dysfunction. Annu Rev Physiol. 2010; 72: 81-94.

192. Roodman GD. Advances in bone biology: the osteoclast. Endocr Rev. 1996;17(4):308-332.

193. Sahin E, DePinho RA. Linking functional decline of telomeres, mitochondria and stem cells during ageing. Nature. 2010;464(7288):520-528.

194. Sakaki T, Sugimoto H, Hayashi K, Yasuda K, Munetsuna E, Kamakura M, Ikushiro S, Shiro Y. Bioconversion of vitamin D to its active form by bacterial or mammalian cytochrome P450. Biochim Biophys Acta. 2011;1814(1):249-256.

195. Salih DA, Brunet A. FoxO transcription factors in the maintenance of cellular homeostasis during aging. Curr opin Cell Biol. 2008;20(2):126-36.

196. Sethe S, Scutt A, Stolzing A. Aging of mesenchymal stem cells. Ageing Res Rev. 2006;5(1):91-116.

197. Shao Y, Alicknavitch M, Farach-Carson MC. Expression of voltage sensitive calcium channel (VSCC) L-type Ca v1.2 (α1C) and T-type Cav3.2 (α 1H) subunits during mouse bone development. Dev Dyn. 2005;234(1):54-62.

198. Shevde NK, Bendixen AC, Dienger KM, Pike JW. Estrogens suppress RANK ligand-induced osteoblast differentiation via a stromal cell independent mechanism involving c-Jun repression. Proc Natl Acad Sci USA. 2000;97(14): 7829-7834.

199. Shevde NK, Plum LA, Clagett-Dame M, Yamamoto H, Pike JW, DeLuca HF. A potent analog of 1alpha,25-dihydroxyvitamin D3 selectively induces bone formation. Proc Natl Acad Sci USA. 2002;99(21):13487-13491.

200. Sosnoski DM, Gay CV. NCX3 is a major functional isoform of the sodium-calcium exchanger in osteoblasts. J Cell Biochem. 2008;103(4):1101-1110.

201. Souberbielle JC, Friedlander G, Kahan A, Cormier C. Evaluating vitamin D status. Implications for preventing and managing osteoporosis and other chronic diseases. Jt Bone Spine. 2006;73(3):249-253.

202. Srinivasan PP, Parajuli A, Price C, Wang L, Duncan RL, Kirn-Safran CB. Inhibition of T-Type Voltage Sensitive Calcium Channel Reduces Load-Induced OA in Mice and Suppresses the Catabolic Effect of Bone Mechanical Stress on Chondrocytes. PLoS One. 2015;10(5):1-18.

203. Staal A, van Wijnen AJ, Birkenhäger JC, Pols HA, Prahl J, DeLuca H, Gaub MP, Lian JB, Stein GS, van Leeuwen JP, Stein JL. Distinct conformations of vitamin D receptor/retinoid X receptor-alpha heterodimers are specified by dinucleotide differences in the vitamin D-responsive elements of the osteocalcin and osteopontin genes. Mol Endocrinol. 1996;10(11):1444-1456.

204. Stains JP, Gay CV. Inhibition of Na+/Ca2+ exchange with KB-R7943 or bepridil diminished mineral deposition by osteoblasts. J Bone Miner Res. 2001;16(8):1434-1443.

205. Stains JP, Gay CV. Asymmetric distribution of functional sodium-calcium exchanger in primary osteoblasts. J Bone Miner Res. 1998;13(12):1862-1869.

206. Stains JP, Weber JA, Gay CV. Expression of Na+/Ca2+ exchanger isoforms (NCX1 and NCX3) and plasma membrane Ca2+ ATPase during osteoblast differentiation. J Cell Biochem. 2002;84(3):625-635.

207. Stein GS, Lian JB, van Wijnen AJ, Stein JL, Montecino M, Javed A, Zaidi SK, Young DW, Choi JY, Pockwinse SM. Runx2 control of organization, assembly and activity of the regulatory machinery for skeletal gene expression. Oncogene. 2004;23(24):4315-4329.

208. Stein GS, Stein JL, Lian JB, van Wijnen AJ, Montecino M. Functional interrelationships between nuclear structure and transcriptional control: contributions to regulation of cell cycle-and tissue-specific gene expression. J Cell Biochem. 1996;62(2):198-209.

209. Stolzing A, Jones E, McGonagle D, Scutt A. Age-related changes in human bone marrow-derived mesenchymal stem cells: consequences for cell therapies. Mech Ageing Dev. 2008;129(3):163-173.

210. Suda T, Takahashi N, Abe E. Role of vitamin D in bone resorption. J Cell Biochem. 1992;49(1):53-58.

211. Suda T, Takahashi N, Udagawa N, Jimi E, Gillespie MT, Martin TJ. Modulation of osteoclast differentiation and function by the new members of the tumor necrosis factor receptor and ligand families. Endocr Rev. 1999;20(3):345-357.

212. Suda T, Takahashi N, Martin TJ. Modulation of osteoclast differentiation. Endocr Rev. 1992;13(1):66-80.

213. Suda T, Udagawa N, Nakamura I, Miyaura C, Takahashi N. Modulation of osteoblast differentiation by local factors. Bone. 1995;17(2 Suppl):S87-S91

214. Suda T, Takahashi F, Takahashi N. Bone effects of vitamin D - Discrepancies between in vivo and in vitro studies. Arch Biochem Biophys. 2012;523(1):22-29.

215. Sudo H, Kodama H, Amagai Y, Yamamoto S, Kasai S. In vitro differentiation and calcification in a new clonal osteogenic cell line derived from newborn mouse calvaria. J Cell Biol. 1983;96(1):191-198.

216. Takahashi N, Udagawa N, Suda T. Vitamin D endocrine system and osteoclasts. Bonekey Rep. 2014;3:495.

217. Takahashi N, Takuhiko A, Udagawa N, Sasaki T, Yamaguchi A, Moseley JM, Martin TJ, Suda T. Osteoblastic cells are involved in osteoclast formation. Endocrinology. 1988;123(5):2600-2602.

218. Takarada T, Hinoi E, Nakazato R, Ochi H, Xu C, Tsuchikane A, Takeda S, Karsenty G, Abe T, Kiyonari H, Yoneda Y. An analysis of skeletal development in osteoblast-specific and chondrocyte-specific runt-related transcription factor-2 (Runx2) knockout mice. J Bone Miner Res. 2013;28(10):2064-2069.

219. Tsao YT, Huang YJ, Wu HH, Liu YA, Liu YS, Lee OK. Osteocalcin mediates biomineralization during osteogenic maturation in human mesenchymal stromal cells. Int J Mol Sci. 2017;18(1).

220. Tzivion G, Dobson M, Ramakrishnan G. FoxO transcription factors; Regulation by AKT and 14-3-3 proteins. Biochim Biophys Acta. 2011;1813(11): 1938-1945.

221. Uchida Y, Endoh T, Shibukawa Y, Tazaki M, Sueishi K. 1α,25-dihydroxyvitamin D3 rapidly modulates Ca(2+) influx in osteoblasts mediated by Ca(2+) channels. Bull Tokyo Dent Coll. 2010:51(4):221-226.

222. van de Peppel J, van Leeuwen JPTM. Vitamin D and gene networks in human osteoblasts. Front Physiol. 2014;5:137.

223. van der Eerden BC, Weissgerber P, Fratzl-Zelman N, Olausson J, Hoenderop JG, Schreuders-Koedam M, Eijken M, Roschger P, de Vries TJ, Chiba H, Klaushofer K, Flockerzi V, Bindels RJ, Freichel M, van Leeuwen JP. The transient receptor potential channel TRPV6 is dynamically expressed in bone cells but is not crucial for bone mineralization in mice. J Cell Physiol. 2012;227(5):1951-1959.

224. van der Horst A, Burgering BM. Stressing the role of FoxO proteins in lifespan and disease. Nat Rev Mol Cell Biol. 2007;8(6):440-450.

225. van Leeuwen JP, van Driel M, van den Bemd GJ, Pols HA. Vitamin D control of osteoblast function and bone extracelluar matrix mineralization. Crit Rev Eukaryot Gene Expr. 2001; 11(1-3):199-226.

226. Viereck V, Siggelkow H, Tauber S, Raddatz D, Schutze N, Hüfner M. Differential regulation of Cbfa1/Runx2 and osteocalcin gene expression by vitamin-D3, dexamethasone, and local growth factors in primary human osteoblasts. J Cell Biochem. 2002;86(2):348-356.

227. Wang D, Christensen K, Chawla K, Xiao G, Krebsbach PH, Franceschi RT. Isolation and characterization of MC3T3-E1 preosteoblast subclones with distinct in vitro and in vivo differentiation/mineralization potential. J bone Miner Res. 1999;14(6):893-903.

228. Weigel D, Jurgens G, Kuttner F, Seifert E, Jackle H. The homeotic gene fork head encodes a nuclear protein and is expressed in the terminal regions of the Drosophila embryo. Cell. 1989;57(4): 645-658.

229. Weitzmann MN, Pacifici R. Estrogen deficiency and bone loss: an inflammatory tale. J Clin Invest. 2006;116(5): 1186-1194.

230. Wheater G, Elshahaly M, Tuck SP, Datta HK, van Laar JM. The clinical utility of bone marker measurements in osteoporosis. J Transl Med. 2013;11(1):201.

231. White KE, Gesek FA, Friedman PA. Na+/Ca2+ exchange in rat osteoblast-like UMR 106 cells. J Bone Miner Res. 1996;11(11):1666-1675.

232. Woeckel VJ, Alves RD, Swagemakers SM, Eijken M, Chiba H, van der Eerden BC, van Leeuwen JP. 1Alpha,25-(OH)2D3 acts in the early phase of osteoblast differentiation to enhance mineralization via accelerated production of mature matrix vesicles. J Cell Physiol. 2010;225(2):593-600.

233. Woeckel VJ, Koedam M, van de Peppel J, Chiba H, van der Eerden BC, van Leeuwen JP. Evidence of vitamin D and interferon-β cross-talk in human osteoblasts with

1α,25-dihydroxyvitamin D3 being dominant over interferon-β in stimulating mineralization. J Cell Physiol. 2012;227(9):3258-3266.

234. Wu L, Forsling W. Potentiometric and spectrophotometric study of calcium and alizarin red s complexation. Acta Chemica Scandinavica. 1992;46(5):418-422.

235. Yamaguchi M, Weitzmann MN. High dose 1,25(OH)2D3 inhibits osteoblast mineralization in vitro. Int J Mol Med. 2012;29(5):934-938.

236. Yamaguchi T, Chattopadhyay N, Kifor O, Butters RR, Sugimoto T, Brown EM. Mouse osteoblastic cell line (MC3T3-E1) expresses extracellular calcium (Ca2+o)-sensing receptor and its agonists stimulate chemotaxis and proliferation of MC3T3-E1 cells. J Bone Miner Res. 1998;13(10):1530-1538.

237. Yamaguchi M, Yamaguchi T, Kaji H, Sugimoto T, Chihara K. Involvement of calcium-sensing receptor in osteoblastic differentiation of mouse MC3T3-E1 cells. Am J Physiol Endocrinol Metab. 2005;288(3):E608-E616.

238. Yamashita T, Asano K, Takahashi N, Akatsu T, Udagawa N, Sasaki T, Martin TJ, Suda T. Cloning of an osteoblastic cell line involved in the formation of osteoclast-like cells. J Cell Physiol. 1990;145(3):587-595.

239. Zhang R, Ducy P, Karsenty G. 1,25-Dihydroxyvitamin D3 inhibits Osteocalcin expression in mouse through an indirect mechanism. J Biol Chem. 1997;272(1):110-116.

240. Zhang X, Yang M, Lin L, Chen P, Ma KT, Zhou CY, Ao YF. Runx2 overexpression enhances osteoblastic differentiation and mineralization in adipose - derived stem cells in vitro and in vivo. Calcif Tissue Int. 2006;79(3):169-178.